Effects of ageing, calorie restriction and ageing-associated diseases on the mitochondrial proteome

TECHNISCHE UNIVERSITÄT DARMSTADT

Vom Fachbereich Chemie

der Technischen Universität Darmstadt

zur Erlangung des akademischen Grades eines

Doctor rerum naturalium (Dr. rer. nat.)

genehmigte

Dissertation

vorgelegt von

Dipl.-Chem. Manuela Kratochwil

aus Wiesbaden

Referent: Prof. Dr. Norbert A. Dencher

Korreferent: Prof. Dr. Bodo Laube

Tag der Einreichung: 14. September 2015

Tag der mündlichen Prüfung: 09. November 2015

Darmstadt 2016

D 17

Die vorliegende Arbeit wurde unter Leitung von Herrn Prof. Dr. Norbert A. Dencher in der Zeit von August 2010 bis September 2015 im Fachbereich Chemie am Clemens-Schöpf-Institut für Organische Chemie und Biochemie der Technischen Universität Darmstadt angefertigt.

Publications

Parts of this doctoral thesis are published:

R. Koziel, H. Pircher, M. Kratochwil, B. Lener, M. Hermann, N. A. Dencher, P. Jansen-Dürr

Mitochondrial respiratory chain complex I is inactivated by NADPH oxidase Nox4.

Biochemical Journal, 2013, 452, 231-239.

Manuscript submitted:

K. Kuter, M. Kratochwil, K. Berghauzen-Maciejewska, U. Głowacka, M. D. Sugawa, K. Ossowska, N. A. Dencher

Adaptation within mitochondrial oxidative phosphorylation supercomplexes and membranes viscosity during degeneration of dopaminergic neurons in an animal model of early Parkinson's Disease.

Journal of Molecular Biology

Manuscript in preparation:

M. Kratochwil, S.-H. Marx, V. Decker, S. Hartwig, K. Kuter, L. Cavlovic, K. Ossowska, S. Lehr, N. A. Dencher

Identification of mitochondrial proteins from hearts of five different mammals, from kidney of one mammal, from five different rat brain areas and two cell culture samples, all separated by 2D-BN/SDS PAGE.

planned: J. Proteome research

Manuscript planned:

K. Kuter, M. Kratochwil, S.-H. Marx, S. Hartwig, S. Lehr, N. A. Dencher

Determination of changes in mitochondrial protein amount due to degeneration of dopaminergic neurons in an animal model of early Parkinson's disease.

Oral presentations at conferences

N. A. Dencher, A. Atenhan, B. Becker, K. Brahm, M. Frenzel, M. Kratochwil, M. Muschol, E. R. Schäfer, S. Thilmany, M. D. Sugawa

CoQ10-mediated Performance of the Respiratory Chain is Modulated by Age, Diseases and Calorie Restriction via Super-Assembly of OxPhos Complexes

Seventh Conference of the International Coenzyme Q_{10} Association, 8 to 11 November 2012, Sevilla, Spain

N. A. Dencher, M. Frenzel, M. Kratochwil, M. Muschol, E. R. Schäfer, H. Seelert, S. Thilmany, S. Goto, H. D. Osiewacz, I. Shimokawa, M. D. Sugawa

Evolutionary Conserved Alterations by Age and Calorie Restriction of the Organization and Performance of the Respiratory Chain

20th IAGG World Congress of Gerontology and Geriatrics, 23 to 27 June 2013, Seoul, South Korea

Poster presentations

K. Kuter, U. Głowacka, K. Beghauzen-Maciejewska, K. Ossowska, M. Kratochwil, N. A. Dencher

Functional compensation of the dopaminergic nigrostriatal system degeneration. Role of mitochondrial supercomplexes function and assembly.

Konferencja Neurochemiczna, 24 to 25 October 2013, Warsaw, Poland

K. Kuter, M. Kratochwil, U. Głowacka, K. Beghauzen-Maciejewska, M. D. Sugawa, K. Ossowska, N. A. Dencher

Functional compensation of the motor deficits after dopaminergic nigrostriatal system degeneration in relation to early Parkinson's disease. Activity of mitochondrial complex I – as individual and in supercomplexes.

Targeting Mitochondria, 17 to 18 October 2013, Berlin, Germany

M. Kratochwil, K. Kuter, S. Goto, M. D. Sugawa, K. Ossowska, N. A. Dencher

Changes in mitochondrial respiratory chain complexes associated with age, calorie restriction and age-dependent diseases.

Molecular Life Sciences 2013, International Symposium of the German Society for Biochemistry and Molecular Biology, 3 to 6 October 2013, Frankfurt am Main, Germany

K. Kuter, M. Kratochwil, U. Głowacka, K. Beghauzen-Maciejewska, M. D. Sugawa, K. Ossowska, N. A. Dencher.

Functional compensation of the motor deficits after dopaminergic nigrostriatal system degeneration. DIGE analysis of mitochondrial membranes proteins in relation to early Parkinson's disease.

The third World Parkinson Congress, 1 to 4 October 2013, Montreal, Canada

M. Kratochwil, L. Cavlovic, C. Kern, S. Kern, N. A. Dencher

Difference 2D-BN/SDS PAGE – a method to analyse the mitochondrial proteome, especially membrane proteome, of neuronal cells irradiated with ionizing radiation.

GBS Jahrestagung 2013, 24 to 27 September 2013, Darmstadt, Germany

M. Kratochwil, K. Kuter, S. Goto, M. D. Sugawa, K. Ossowska, N. A. Dencher

Changes in mitochondrial respiratory chain complexes associated with age and calorie restriction.

GDCH Wissenschaftsforum Chemie 2013, 1 to 4 September 2013, Darmstadt, Germany

K. Kuter, U. Głowacka, K. Beghauzen-Maciejewska, K. Ossowska, M. Kratochwil, N. A. Dencher

Functional and molecular compensation of the dopaminergic nigrostriatal system degeneration in relation to early Parkinson's disease.

XVIIIth International Congress of the Polish Pharmacological Society, 23 to 25 May 2013, Kazimierz Dolny, Poland

M. Kratochwil, K. Kuter, S. Goto, M. D. Sugawa, K. Ossowska, N. A. Dencher

Age and calorie restriction associated changes in mitochondrial respiratory chain complexes.

64. Mosbacher Kolloquium - "Membranes in Motion" of the German Society for Biochemistry and Molecular Biology, 4 to 6 April 2013, Mosbach (Baden), Germany

M. Kratochwil, K. Kuter, C. Ramallo Guevara, A. Poetsch, N. A. Dencher

Analysis of mitochondrial OxPhos complexes and their post-translational modifications.

5th EU Summer School in "Proteomic Basics", 31 July to 6 August 2011, Brixen, Italy

Acknowledgement

Thank you for scientific exchange:

- Prof. Dr. Norber A. Dencher, my PhD supervisor, for giving me the opportunity to work in this interesting research field, for precious support, discussions and the faith in my work.
- Prof. Dr. Bodo Laube, for spending your time, being my second reviewer.
- Prof. Dr. Gerd Buntkowsky and PD Dr. Tobias Meckel for being members of my thesis committee.
- Prof. Dr. Kristina Ossowska and Dr. Katarzyna Kuter, for collaboration in Parkinson's studies, a lot of interesting discussions, corrections of parts of my thesis and invitation to wonderful Krakow and bringing "pierogi" and "śliwka w czekoladzie" into my life.
- Dr. Stefan Lehr, Dr. Sonja Hartwig and co-workers from DDZ, for MALDI MS/MS analyses and wonderful rainbow workshops and a lot of advice in MS and 2D-PAGE.
- Prof. Dr. Piddar Jansen-Dürr and Dr. Rafal Koziel, for collaboration in ageing research and confidence in my working experience.
- Prof. Dr. Sataro Goto and Dr. Michiru D. Sugawa, for providing the rat brain samples from Japan and important information, as well as Dr. Diksha Dani, for isolation of mitochondria from cerebrum.
- Prof. Dr. Karl-Dieter Entian and Dr. Sunny Sharma, for providing and training on Tyhoon scanning system.
- Dr. Ansgar Poetsch and Dr. Carina Ramallo Guevara, for measurement of PTMs.
- Graduate College 1657, "Molecular and cellular responses to ionizing radiation" for financial and educational support.
- M. Sc. Stefanie Kern, for anisotropy measurements and together with M. Sc. Laura Babel and M. Sc. Anne Atenhan, for testing different recipes of in-gel activity test solutions.
- M. Sc. Olga Ankudin for Western Blot analyses of RBM.
- Dr. Sandra Thilmany, Dr. Eva R. Schäfer, Dipl. Chem. Michaela Söhn and Dipl. Chem. Maria Saager, for introduction in the methods of the laboratory and time spent together.
- Dr. Holger Seelert, Dr. Monika Frenzel, Dr. Nicolas Heidrich and Dr. Michael Muschol, for scientific discussions.
- Dipl. Biochem. Victoria Decker, Dipl. Biochem. Lidija Cavlovic, M. Sc. Tamara Dzinic, for a great time in the "Frauenbüro".
- Christine Schröpfer, Sabine Reinhold, Michaela Fröhlich, Edith Hiemenz, for support.
- Elisabeth Trapp, for good mood and clean surroundings anytime.
- Simone Bartl-Zimmermann, Dr. Monika Hofmann, Dr. Heiko Hofmann, Dr. Thorsten Heinlein, M. Sc. Stefanie Kemski, Dr. Nicole Plohnke, for being there.
- Sheila Snowwhite, for being there from time to time.
- Dr. Kerstin Brand for correction of parts of my thesis.
- Special thanks to my best friend Dipl. Chem. Sven-H. Marx for scientific exchange and support at all times.

Thank you:

- to my parents and to my family, for support at all times and to my beloved niece Mia.
- to my best friend Sarah Walter, for tea-time, X-mas cookies and for being there at all times
- to my friends.
- to all the ones I forgot to mention right now.

"Dass ich erkenne, was die Welt // Im Innersten zusammenhält."

Johann Wolfgang von Goethe:
“Faust - Der Tragödie erster Teil.“
Tübingen: Cotta. 1808, Seite 34

"Imagination is more important than knowledge. For knowledge is limited."

Albert Einstein:
“What Life Means to Einstein”, The Saturday Evening Post,
26. Oktober 1929

Summary

This thesis outlines the effects of ageing, calorie restriction and ageing-associated diseases on the mitochondrial proteome.

Several techniques were tested to study the mitochondrial proteome:
Techniques for visualisation of proteins after two dimensional (2D) blue native (BN) / sodium dodecyl sulphate (SDS) polyacrylamide gel electrophoresis (PAGE) were compared: staining of gels with Coomassie Brilliant Blue G-250 (CBBG), silver and the fluorescent dye SYPRO®Ruby as well as labelling of the proteins before gel run with fluorescent dyes from Refraction-2D™ Labeling Kit (differential gel electrophoresis, DIGE). A recommendation was elaborated either for staining with fluorescent dye, when enough amount of protein is available, or for labelling with fluorescent dye, when analysis of low amount of protein is needed.
Quantitation of the amount of mitochondrial oxidative phosphorylation (OxPhos) complexes after BN PAGE and subsequent CBBG staining was compared to quantitation after 2D-BN/SDS-PAGE and subsequent SYPRO®Ruby staining, using the rat brain tissue samples for the ageing and calorie restriction analyses (cerebellum, hippocampus and cerebrum). The results showed, that quantitation in CBBG stained BN gels is less accurate than in 2D-BN/SDS gels and subsequent SYPRO®Ruby staining, and therefore not applicable for detailed quantitation studies.
The effects of ageing and calorie restriction were studied on the mitochondrial proteome of three different brain tissues of Fischer 344 rats: cerebellum, hippocampus and cerebrum. Animals were fed *ad libitum* (AL) or calorie restricted (CR, intake about 60 % of *ad libitum* fed animals, start point: after the age of 6 weeks) and analysed at two ages: 6.5 months (young, Y) and 27 months (old, O). Mitochondria were isolated and the mitochondrial proteins were separated by 2D-BN/SDS PAGE and identified by peptide mass fingerprint (PMF) with MALDI-MS. The protein amount of the assigned subunits was quantified by SYPRO®Ruby staining. BN PAGE of mitochondrial proteins and subsequent in-gel activity tests were applied to analyse the specific activity of the respiratory chain complexes I and IV. The mitochondrial membrane "fluidity" was determined by measurement of the steady-state fluorescence anisotropy of the intercalated probe diphenyl-1,3,5-hexatriene (DPH).
In general, it was found that animals of young age under CR (YCR) developed a smaller body weight than young AL ones (YAL). Ageing under AL increased the body weight to the same extent as under CR. Commonly for all three tissues, the results of PMF showed that the migration pattern of subunits of mitochondrial proteins from rat brain tissues in 2D-BN/SDS PAGE are highly comparable, also to other mammalian tissue such as bovine heart. Therefore analyses of the proteome of the different tissues could be compared. The mtDNA encoded protein subunits CYB of OxPhos complex III (CIII) and COX2 of complex IV (CIV) did not show specific changes during ageing neither AL nor CR. Their changes followed the trends of total CIII and total CIV. The highest activities of CI were found in supercomplex $I_1III_2IV_3$ and of CIV in supercomplex $I_1III_2IV_2$ for all three brain tissues. However, the changes during ageing and calorie restriction of specific CI and CIV activities were not very pronounced.
In cerebellum ageing of AL fed rats reduced the tissue weight and total mitochondrial protein amount as well as the fluidity of the mitochondrial membranes. The amount of OxPhos complexes and the activity was not altered. Already at young age the tissue weight of

cerebellum decreased under CR and developed in the same way as in AL fed animals during ageing. The total mitochondrial protein amount in young and in old rats under CR was higher compared to AL fed rats, but it decreased during ageing under CR (YCR vs. OCR), thereof were proteins of cellular stress management, energy metabolism and neuronal composition. The amount of OxPhos complexes was decreased in young animals under CR compared to AL but increased during ageing to the same level of protein amount from animals under AL at old age. In general, the mitochondrial membrane fluidity decreased with ageing, even more in cerebellum of animals under CR than under AL. Already at young age under CR the fluidity was decreased compared to AL.
For hippocampus the tissue weight, the total mitochondrial protein amount and CI activity in some (super-)complexes decreased by ageing independently from nutrition. Most of the analysed proteins decreased under AL and in young animals under CR. However, during ageing under CR the amounts of analysed proteins increased to a higher level in aged CR animals than aged AL animals. During ageing under AL the membrane "fluidity" did not change but in young and old animals under CR the membrane fluidity was decreased compared to the AL animals, even though the fluidity increased during age in CR animals. Decreased fluidity could be explained by increased cholesterol amount or increased membrane protein amounts and these could be needed to compensate for the decreased CI activity.
In cerebrum the tissue weight decreased during ageing independently from nutrition. The amount of OxPhos complexes (excl. CV) decreased during ageing under AL while ageing under CR increased the protein amount of OxPhos complexes (excl. CV) in old rats. Ageing decreased the mitochondrial membrane "fluidity" in AL animals. Under CR the fluidity did not change, but was still increased in aged animals under CR compared to AL.
In conclusion, ageing under AL decreased brain tissue weight, total protein amount and fluidity of mitochondrial membrane. The amount of the OxPhos complexes and their activity remained mainly unchanged. During ageing under CR the total protein amount increased and membrane fluidities decreased which, in terms of remained OxPhos complexes activities, seem to be part of compensation processes.

Together with Dr. Koziel (IBA) the effects of ageing (senescence) were studied on a cell culture model, human umbilical vein endothelial cells, in which NADPH oxidase 4 (Nox4), known as producer of reactive oxygen species, was knocked down. The results showed a depleted CI amount and reduced CI activity under the influence of Nox4 which were both increased when Nox4 was knocked down.

In collaboration with Dr. Kuter (IF-PAN) an early stage model of the ageing-associated disease Morbus Parkinson was studied. The effects of neuronal degradation in substantia nigra on the mitochondrial proteome were analysed in Wistar rats. For identification of proteins, 2D-BN/SDS PAGE and subsequent PMF were performed. Quantitation was achieved by application of DIGE. In-gel activities of OxPhos complexes I and IV were measured as well as membrane "fluidity". The evaluation of the obtained results is still in progress. Some of the data were already submitted and are under review and for copyright reasons not described in this thesis.

Zusammenfassung

Diese Arbeit befasst sich mit den Auswirkungen des Alterns, der Kalorienrestriktion und von altersassoziierten Krankheiten auf das mitochondriale Proteom.

Verschiedene Techniken wurden verglichen, um das mitochondriale Proteom zu analysieren: Die Visualisierung der Proteine nach Auftrennung mit der zwei-dimensionalen (2D) blau-nativen (BN) Natriumdodecylsulfat-(SDS) Polyacrylamid-Gelelektrophorese (PAGE) durch die Färbung der Gele mit Coomassie Brilliant Blau G-250 (CBBG), Silber oder dem Fluoreszenzfarbstoff SYPRO®Ruby wurden mit der differentiellen Gelelektrophorese (DIGE) verglichen, bei der vor dem Gellauf die kovalente Markierung der Proteine mit Fluoreszenzfarbstoffen (Refraction-2D™ Labeling Kit) stattfindet. Die Färbung mit Fluoreszenzfarbstoff wurde empfohlen, wenn genug Protein zur Verfügung steht und falls die Menge eingeschränkt ist für die Markierung der Proteine mit Fluoreszenzfarbstoff.
Die Quantifizierung der Menge von mitochondrialen Proteinen der oxidativen Phosphorylierung (OxPhos) nach Auftrennung durch BN PAGE und anschließender CBBG Färbung wurde verglichen mit der Auftrennung mittels 2D-BN/SDS PAGE und SYPRO®Ruby Färbung. Hierfür wurden dieselben Proben verwendet, die auch für die Analyse der Einflüsse von Altern und Kalorienrestriktion auf das mitochondriale Proteom der unterschiedlichen Gehirngewebe verwendet wurden. Die Quantifizierung nach BN PAGE und CBBG Färbung lieferte weniger genaue Resultate als die 2D-BN/SDS PAGE und SYPRO®Ruby Färbung und ist daher nicht geeignet für quantitative Analysen.

Die Einflüsse von Altern und Kalorienrestriktion wurden am mitochondrialen Proteom von den drei Fischer 344 Rattenhirngeweben Cerebellum, Hippocampus und Cerebrum analysiert. Die Tiere wurden *ad libitum* (AL) gefüttert oder unter Kalorienrestriktion (CR, Aufnahmemenge etwa 60 % von AL, wurde nach Alter von 6 Wochen gestartet) gehalten. Zwei Altersgruppen wurden analysiert: 6,5 Monate (jung, Y) und 27 Monate (alt, O). Die Mitochondrien wurden isoliert und deren Gesamtproteinmenge bestimmt. Die Proteine wurden mittels 2D-BN/SDS PAGE aufgetrennt und die Untereinheiten im Gel durch *Peptide Mass Fingerprint* (PMF) mittels MALDI-MS identifiziert. Die Proteinmenge der Untereinheiten wurde nach SYPRO®Ruby Färbung der Gele quantifiziert. Die Auftrennung der mitochondrialen Proteine mittels BN PAGE und anschließender in-Gel Aktivitätstests lieferte die spezifische Aktivität der OxPhos-Komplexe I (CI) und IV (CIV). Durch die *steady-state* Fluoreszenz-Anisotropie Messung der interkalierten Fluoreszenzsonde Diphenyl-1,3,5-hexatrien (DPH) wurde die „Fluidität“ der Mitochondrienmembran bestimmt.
Bereits im jungen Alter hatten die Tiere unter CR ein niedrigeres Körpergewicht, als die AL gefütterten Tiere. Mit dem Altern erhöhte sich das Körpergewicht beider Tiergruppen im gleichen Maße. Nach Identifizierung der Proteinuntereinheiten mittels PMF im 2D-BN/SDS-Gel zeigte sich für Mitochondrien aus allen drei untersuchten Rattenhirngeweben, dass die elektrophoretische Mobilität der Untereinheiten annähernd identisch ist. Dies konnte ebenso für die untersuchten Rinderherzmitochondrien gezeigt werden. Daher konnten die Proteine der verschiedenen Gewebe miteinander verglichen werden. Die durch die mtDNS kodierten Untereinheiten CYB von OxPhos-Komplex III (CIII) und COX2 von CIV zeigten keine spezifischen Veränderungen beim Altern. Sie folgten den Veränderungen der Gesamtkomplexe CIII und CIV. Die höchsten Aktivitäten wurden in allen drei Geweben für die Superkomplexe $I_1III_2IV_3$ (CI-Aktivität) und $I_1III_2IV_2$ (CIV-Aktivität) gefunden. Allerdings

waren die Veränderungen durch Altern und Kalorienrestriktion in den CI- und CIV-Aktivitäten nur sehr geringfügig ausgeprägt.
Das Gewicht des Cerebellum, dessen mitochondriale Gesamtproteinmenge und die Fluidität der Mitochondrienmembran nahm mit dem Altern von AL gefütterten Tieren ab. Die Menge der OxPhos-Komplexe und die Aktivität von CI und CIV waren nicht verändert. Bereits junge Tiere unter CR wiesen ein geringeres Gewicht des Cerebellum verglichen mit AL gefütterten Ratten auf. Mit dem Altern wuchs das Cerebellum beider Tiergruppen im gleichen Maße an. Die mitochondriale Gesamtproteinmenge in jungen und alten Ratten unter CR war jeweils höher als bei den AL gefütterten Tieren, verringerte sich jedoch auch während des Alterns. darunter die Proteine des zellulären Stressmanagements, des Energiemetabolismus und an der neuronalen Zusammensetzung und Funktion beteiligten Proteine. Die Menge der OxPhos-Komplexe war in jungen Tieren unter CR verringert, erhöhte sich aber mit dem Altern unter CR auf dasselbe Niveau wie bei den Tieren unter AL. Die mitochondriale Membranfluidität verringerte sich im Cerebellum während des Alterns bei beiden Formen der Ernährung, allerdings bei den Tieren unter CR sogar stärker und bereits seit dem jungen Alter.
Das Gewicht des Hippocampus, die mitochondriale Gesamtproteinmenge und die CI-Aktivität in einigen OxPhos-(Super-)Komplexen verringerten sich unabhängig von der Ernährung mit dem Altern, genauso wie die meisten analysierten Proteine unter AL und in jungen Tieren unter CR. Jedoch beim Altern unter CR stiegen die Proteinmengen sogar auf ein höheres Maß als bei den vergleichbaren AL Tieren an. Beim Altern unter AL veränderte sich die mitochondriale Membranfluidität nicht, aber bei den jungen und alten Tieren unter CR konnte eine verringerte Membranfluidität verglichen mit den Tieren unter AL festgestellt werden, obwohl sich sogar die Fluidität der Mitochondrienmembranen der jungen CR Tiere mit dem Altern etwas erhöhte. Die verringerte Fluidität könnte durch die erhöhte Proteinmenge erklärt werden oder einen erhöhten Cholesterinanteil und die damit verbundene Reaktion des Gewebes auf die verringerte CI Aktivität.
Das Gewicht des Cerebrum verringerte sich mit dem Altern unabhängig von der Ernährung. Die Menge der OxPhos-Komplexe (exkl. CV) verringerte sich mit dem Altern unter AL aber unter CR erhöhte sich deren Menge. Die mitochondriale Membranfluidität verringerte sich unter dem Einfluss des Alterns und AL Fütterung, jedoch nicht unter CR. Die Fluidität der Membranen der CR gefütterten Tiere war stets höher als die der AL Tiere.
Zusammengefasst verringerte das Altern das Hirngewebegewicht, die Gesamtproteinmenge und die Fluidität der Mitochondrienmembran von AL gefütterten Tieren. Die Menge der OxPhos-Komplexe und ihre Aktivität blieb größtenteils unverändert. Beim Altern unter CR erhöhte sich die Gesamtproteinmenge und die Membranfluidität verringerte sich, was im Zusammenhang mit gleichbleibenden CI- und CIV-Aktivitäten ein Teil von Kompensations-mechanismen zu sein scheinen.

In Zusammenarbeit mit Dr. Koziel (IBA) wurden die Effekte des Alterns anhand eines Zellkulturmodells (HUVEC) analysiert. Hierin wurden die Einflüsse von NADPH Oxidase 4 (Nox4), ein Produzent von reaktiven Sauerstoffspezies, durch genetische Gen-Deaktivierung untersucht. Die Ergebnisse zeigten unter anderem, dass Nox4 für eine verringerte CI Menge und CI-Aktivität sorgte, was durch Gen-Deaktivierung umgekehrt wurde.

Durch die Zusammenarbeit mit Dr. Kuter (IF-PAN) konnte ihr Modell der Parkinson Erkrankung in einem frühen Stadium analysiert werden. Die Effekte der Degeneration in Substantia nigra und Striatum von Wistar Ratten wurden beschrieben. Proteomanalysen

umfassten die Identifikation der mitochondrialen Proteine durch PMF von 2D-BN/SDS Gelen, Quantifizierung der Proteinuntereinheiten durch die DIGE-Technik, CI- und CIV in-Gel Aktivitätstests und Messungen der Membranfluidität. Die Auswertungen sind noch in Bearbeitung. Teile der Daten wurden zur Veröffentlichung eingereicht und sind unter Begutachtung, weshalb unter Beachtung des Urheberrechts diese Daten in dieser Arbeit nicht beschrieben wurden.

Table of contents

List of abbreviations

abbreviation	in full text
% C	total cross-linker concentration
% T	total acrylamide concentration
(v/v)	volume per volume
(w/v)	weight per volume
°C	degree Celsius
µg	microgram
µL	microlitre
µm	micrometre
10x	ten times
2D	two-dimensional
3D	three dimensional
3x	three times
4DL	four days after lesion
4WL	four weeks after lesion
5x	five times
6-OHDA	6-hydroxydopamine
abbrev.	abbreviation
ABC	Ammonium bicarbonate
ACN	Acetonitrile
AcOH	Acetic acid
ADP	Adenosine-5'-diphosphate
$AgNO_3$	Silver nitrate
APS	Ammonium peroxodisulphate
ATP	Adenosine-5'-triphosphate
b. sol.	before solubilisation
BCIP	5-Bromo-4-chloro-3-indoylphosphate
BHM	bovine heart mitochondria
Bis-Tris	*Bis*(2-hydroxyethyl)-imino-*tris*-(hydroxymethyl)-methane
bit	binary digit
BN	blue native
BSA	Bovine serum albumine
CBBG	Coomassie Brilliant Blue G-250
CI	complex I
CII	complex II
CIII	complex III
CIV	complex IV
cm	centimetre
CO_2	carbon dioxide
CR	calorie restriction
CV	complex V
d/p	ratio: digitonin / protein
DA	dopamine
DAB	Diaminobenzidine
DDZ	Deutsches Diabetes Zentrum Düsseldorf
DIGE	differential gel electrophoresis
dist. H_2O	distilled water
DMF	Dimethylformamide
DMSO	Dimethyl sulfoxide
DNA	deoxyribonucleic acid

abbreviation	in full text
DPH	1,6-diphenyl-1,3,5-hexatriene
dpi	dots per inch
DTT	Dithiotreitol
EDTA	Ethylendiamine tetraacetate
EtOH	Ethanol
excl.	excluding
G	G-factor
g	gravitational acceleration
g	gram
GABA	γ–aminobutyric acid
G-Dyes	Refraction-2D™ Labeling Kit
Gel A	Rotiphorese® Gel A
Gel AB	Rotiphorese® Gel 40 (29:1)
Gel B	Rotiphorese® Gel B
H	horizontally
h	hour
H_2O	water
H_2O_2	Hydrogen peroxide
HCCA	α-Cyano-4-hydroxycinnamic acid
HCl	Hydrochloric acid
HEPES	*N*-2-Hydroxy piperazine-*N*′-2-ethanesulfonic acid
HMW	High molecular weight calibration kit for native electrophoresis
HPLC	High-performance liquid chromatography
HUVEC	human umbilical vein endothelial cells
I	Intensity
IBA	Institute for Biomedical Aging Research
ID	inner diameter
IF-PAN	Institute of Pharmacology, Polish Academy of Sciences
incl.	including
IS	internal standard
KCl	Potassium chloride
KD	knocked down
KOH	Potassium hydroxide
L	litre
LDPE	Low-density polyethylene
LMW	Low molecular weight calibration kit for SDS electrophoresis
LT	long-term calorie restriction
M	1 mol/L, molar
mA	milliampere
MALDI	matrix assisted laser desorption / ionisation
max	maximum
MeOH	Methanol
MeSH	β-Mercaptoethanol
MFB	medial forebrain bundle

abbreviation	in full text
mg	milligram
$MgCl_2$	magnesium chloride
min	minute
mL	millilitre
mM	millimolar
mm	millimetre
MS	mass spectrometry
mtDNA	mitochondrial DNA
$N_{2\ (l)}$	liquid nitrogen
Na_2CO_3	Sodium carbonate
$Na_2S_2O_3$	Sodium thiosulphate anhydrous
$Na_2S_2O_3x$ 5 H_2O	Sodium thiosulphate pentahydrate
NaCl	Sodium chloride
NADH	Nicotinamide adenine dinucleotide
NADPH	Nicotinamide adenine dinucleotide phosphate
NaOH	Sodium hydroxide
NBT	Nitrotetrazolium Blue chloride
nDNA	nuclear DNA
NIA	National Institute on Ageing
nm	nanometre
no.	number
Nox4	NADPH oxidase 4
Nox4 KD	Nox4 knocked down
Ø	diameter
O_2	dioxygen
OAL	old ad libitum
OCR	old calorie restriction
OxPhos	oxidative phosphorylation
p.a.	pro analysi
PAC	prespotted AnchorChip
PAGE	polyacrylamide gel electrophoresis
PBS	phosphate buffered saline
PC	personal computer
PD	Parkinson's disease
PE	polyethylene
PIC	Protease inhibitor cocktail
PMF	peptide mass fingerprint
PMMA	Poly(methyl methacrylate)
PP	polypropylene
PTFE	Polytetrafluoroethylene

abbreviation	in full text
PVDF	polyvinylidene difluoride
r	Anisotropy
RBM	rat brain mitochondria
rel.	relative
ROS	reactive oxygen species
RPM	revolutions per minute
rRNA	ribosomal ribonucleic acid
RT	room temperature
SDS	sodium dodecyl sulphate
SH	sham operated
shRNA	small hairpin ribonucleic acid
SN	substantia nigra
SNc	substantia nigra pars compacta
SNr	substantia nigra pars reticulata
SOD	superoxide dismutase
ST	short-term calorie restriction
stat. high. sig.	statistically highly significant
stat. sig.	statistically significant
STR	striatum
TCA	tricarboxylic acid
TEMED	Tetramethylethylenediamine
TFA	Trifluoroacetic acid
tif	Tagged Image File Format
TOF	time of flight
Tricine	*N*-[*Tris*(hydroxymethyl)-methyl]-glycine
Tris	Tris(hydroxymethyl)-aminomethane
tRNA	transfer ribonucleic acid
TUD	Technische Universität Darmstadt
UV/Vis	ultra violet + visible light spectrum
V	volt
V	absolute grey value pixel volume
V	vertically
V %	relative grey value pixel volume
vs.	versus
WB	Western blot
WNPRC	Wisconsin National Primat Research Center
YAL	young ad libitum
YCR	young calorie restriction
λ	wavelength

List of figures

List of tables

1 Introduction

1.1 Ageing and statistics

In the world as well as in Germany, the average age of the population is continuously increasing. The global life expectancy was about 71.5 years for both sexes in 2013 (The Lancet 2015). The prognosis of the age distribution in Germany (given for men and women) for the years 2015 (blue and magenta) and 2050 (green line) is depicted in Fig. 1.1 (Destatis Statistisches Bundesamt 18.07.2015). In 2050 the expected number of people > 65 years old would have increased (+11 %), while 20-64 years old (-9 %) and < 20 years (-2 %) would have decreased (Fig. 1.1, Table 1.1).

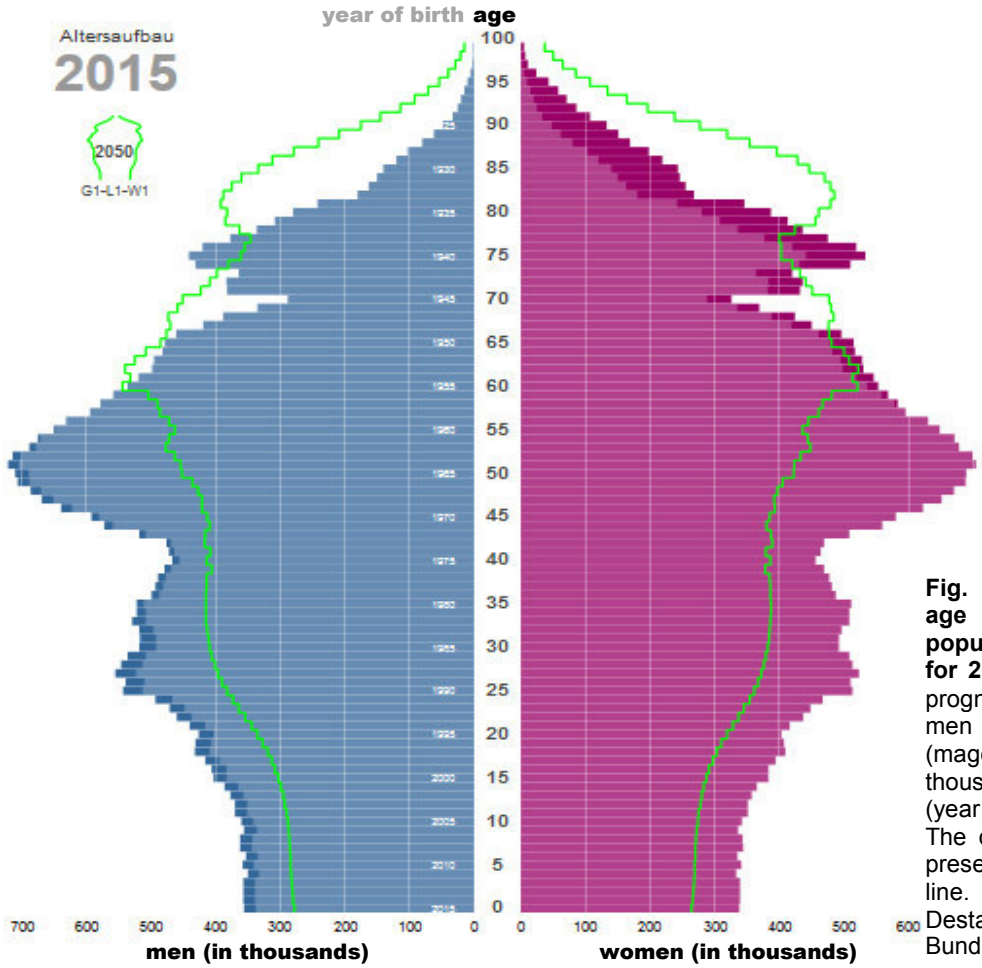

Fig. 1.1: Prognosis of age distribution of population in Germany for 2015 and 2050. The prognosed number of men (blue) and women (magenta) is depicted in thousands for each age (year of birth) for 2015. The quantity for 2050 is presented by the green line. Diagram (modified) Destatis Statistisches Bundesamt (18.07.2015)

Table 1.1: Prognosis for age distribution of the population (men+women) in Germany for the years 2015 and 2050.

	2015		2050	
age	millions	fraction	millions	fraction
65+	17.3	21 %	22.7	32 %
20-64	49.4	61 %	37.7	52 %
< 20	14.6	18 %	11.4	16 %
total	81.3	100 %	71.9	100 %

Table 1.1 (modified) Destatis Statistisches Bundesamt (18.07.2015).

44.4 million people suffered from dementia worldwide in 2013, 1.5 million people in Germany in 2014. Two third of them are older than 80 years while only 20,000 (less than 2 %) are younger than 65 years. It is supposed that the incidence rate will be in average 300,000 each year, and about three million people will be affected in Germany in 2050, and about 135 million people worldwide (Wortmann et al. 2014). It is estimated that about 250,000 people, who have developed dementia, die in Germany each year (Deutsche Alzheimer Gesellschaft e.V. Selbsthilfe Demenz 2014). Of 54.9 million deaths worldwide in 2013 about 2.0 million were caused by neurological disorders, thereof 1.7 million by Alzheimer's disease and other dementias, and 102,500 by Parkinson's (The Lancet 2015).

The main cause of dementia with about two third is supposed to be caused by Morbus Alzheimer followed by vascular dementia (Deutsche Alzheimer Gesellschaft e.V. Selbsthilfe Demenz 2014). In Germany about 250,000 to 400,000 people were affected with Morbus Parkinson in 2007. The incidence rate is supposed 12,500 each year (Gerlach et al. 2007). The Rotterdam study by Ott et al. (1995) gives an overview about the distribution of several forms of dementia. 7,528 persons in the age of 55 to 106 years from a suburb of Rotterdam, NL, participated. Of this cohort, 6.3 % were demented. From all demented, 72 % suffered from Alzheimer's disease, 16 % from vascular dementia, 6 % from Parkinson's disease and 5 % from other forms of dementia.

Health-care cost for dementia affected people were about 5.6 billion Euro in Germany in 2002 (Weyerer 2005). In 2008 they already increased to 9.3 billion Euro (Destatis Statistisches Bundesamt 19.07.2015). Global cost was estimated at US$ 604 billion in 2010 and estimated to rise to US$ 1 trillion by 2030 (Wortmann et al. 2014).

Because of these facts, it is of great interest to study the effects of ageing and causes of ageing-associated diseases, as well as possibilities to influence the process of ageing in a positive way, for example by calorie restriction.

1.2 “The free radical theory of ageing” and “The mitochondrial theory of ageing”

Reactive oxygen species (ROS) are indispensable for life. For example, they are released by phagocytic cells in the context of the immune defence and they play an important role in cell signalling and apoptosis or necrosis (Hancock et al. 2001). ROS are produced by enzymes as NADPH oxidases or glycerol-3-phosphate dehydrogenase or are released as byproducts from the respiratory chain, by complex I (CI) , complex II (CII) or complex III (CIII) (Hamanaka and Chandel 2010).

In Fig. 1.2, the chemical equations of formation and reaction of biologically relevant ROS are depicted. Oxygen reacts with a free electron to the superoxide radical anion (a), which is protonated to form the hydroperoxyl radical (b), which is more reactive than the superoxide radical anion. The superoxide radical anion can also react with hydrogen peroxide to form oxygen, water and the hydroxyl radical (c). Another generation of the hydroxyl radical is the oxidation of a metal cation by hydrogen peroxide. Hydroxyl anion is generated as side product (d). ROS are extremely reactive and therefore short-lived. They can interact with biomolecules like lipids from membranes, deoxyribonucleic acid (DNA) or proteins. Because of their point of origin in the mitochondria, it is supposed that mainly the mitochondrial lipids and proteins, as well as mitochondrial DNA (mtDNA) are oxidised by ROS. Degenerative diseases like Morbus Alzheimer, Morbus Huntington or Morbus Parkinson are supposed to be linked with oxidative modified mitochondria. (Voet et al. 2002, Murphy 2009)

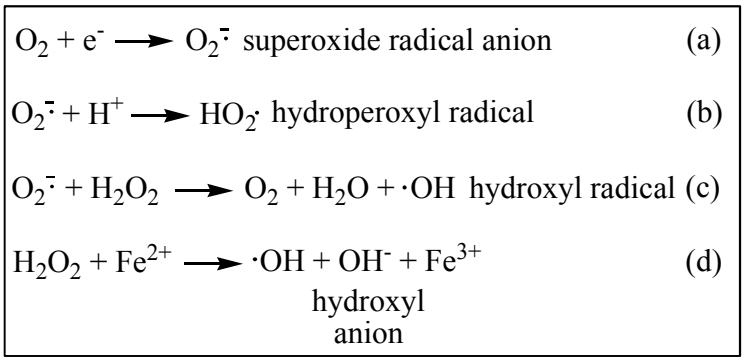

Fig. 1.2: Biologically active reactive oxigen species (ROS). Formation and reaction equations (modified: Voet et al. (2002))

Harman (1956) proposed that free radicals could be the cause of ageing and ageing-related diseases. The “free radical theory of ageing” was founded. He expanded his theory in 1972 and proposed that mitochondria are the main source and target of ROS at the same time (Harman 1972). Several subsequent publications lead to the findings that damage in mitochondria could accumulate. For example lipid (per-)oxidation leads to oxidised mitochondrial membranes, oxidation of mtDNA causes accumulated mutations changing the biosynthesis of mitochondrial proteins or proteins could be modified posttranslationally. The result could be that the oxidative phosphorylation (OxPhos) pathway produces a higher output of ROS or a declined output of adenosine triphosphate (ATP). The “mitochondrial theory of ageing” was postulated. Mitochondria were supposed to be the main trigger for ageing and age-related diseases (Lenaz 2012).

However, there are also mechanisms to reduce the amount of ROS in the cell, like reaction with antioxidants (vitamins) or scavenging enzymes, like superoxide dismutases (SOD) (Voet et al. 2002).

To study the effects of ROS in ageing, nicotinamide adenine dinucleotide phosphate (NADPH) oxidases (Nox), as source of superoxide radicals and other ROS, can be analysed. They are involved in posttranslational modification of proteins, cellular signalling, regulation of gene expression, differentiation of cells, and in immunological defense (Bedard and Krause 2007). Within the framework of this thesis the influence of Nox4 on the mitochondrial function was analysed with BN PAGE, 2D-BN/SDS PAGE and in-gel enzyme activity tests as part for the publication with Dr. R. Koziel (Institute for Biomedical Research (IBA), Innsbruck University, Austria) and other authors (Koziel et al. 2013). We could demonstrate that Nox4 inhibits CI of the respiratory chain.

1.3 Mitochondria

Mitochondria are the organelles in the cells which provide chemical energy in form of ATP by the respiratory chain. They are also involved in degradation of fatty acids, heat production, calcium storage, provide second messengers e.g. ROS or Ca^{2+} for cellular signalling, trigger apoptosis, are location for the TCA cycle, and involved in heme and hormone synthesis (Voet et al. 2002). A large number of mitochondria are usually located in tissues, where high energy supply is necessary as in muscles and in the central nervous system (E and Swerdlow 2012).

ATP synthesis

For ATP synthesis, five OxPhos complexes are embedded in the inner mitochondrial membrane. A schematic of a mitochondrion as well as the OxPhos complexes are depicted in Fig. 1.3. OxPhos complexes exist as functional individual complexes, homooligomers and in so called supercomplexes, which are assemblies of different OxPhos complexes. Only complex III occurs not as individual complex, the smallest entity found is the homodimer. The supercomplex formation leads to increased stability, activity and less dysfunction (Schäfer et al. 2006). Two theories have been discussed in literature for long time. The fluid or random collision model proposed that the complexes are individual entities that freely diffuse in the inner mitochondrial membrane, while the solid model proposed that all complexes except ATP synthase are organised in supercomplexes for increased efficiency of electron transport. The plasticity model unifies both theories and suggests a balanced dynamic distribution of individual complexes and supercomplexes (Acin-Perez and Enriquez 2014).

In the respiratory chain electrons are translocated by redox reactions. Complex I (CI, NADH ubiquinone oxidoreductase) oxidises NADH to NAD^+ and transfers protons and electrons to ubiquinone and reduces it to ubiquinol. Additional electrons are transferred by complex II (CII, succinate dehydrogenase) from succinate to ubiquinone. CII serves therefore as a link between tricarboxylic acid (TCA) cycle and OxPhos. Ubiquinol transfers the electrons to complex III (CIII, cytochrome c oxidoreductase), which reduces cytochrome c. From there electrons are transferred to complex IV (CIV, cytochrome c oxidase), where molecular oxygen is reduced to water. Connected to this, a proton gradient is build up by translocation of protons from the matrix into the intermembrane space by CI (4 e^-), CIII (4 e^-, 2 from matrix and 2 from re-oxidation of ubiquinone) and CIV (4 e^-, 4 additional protons are transferred to O_2). This gradient is used by the ATP synthase (CV) to phosphorylate adenosine diphosphate (ADP) to the energy-rich ATP. (Voet et al. 2002)

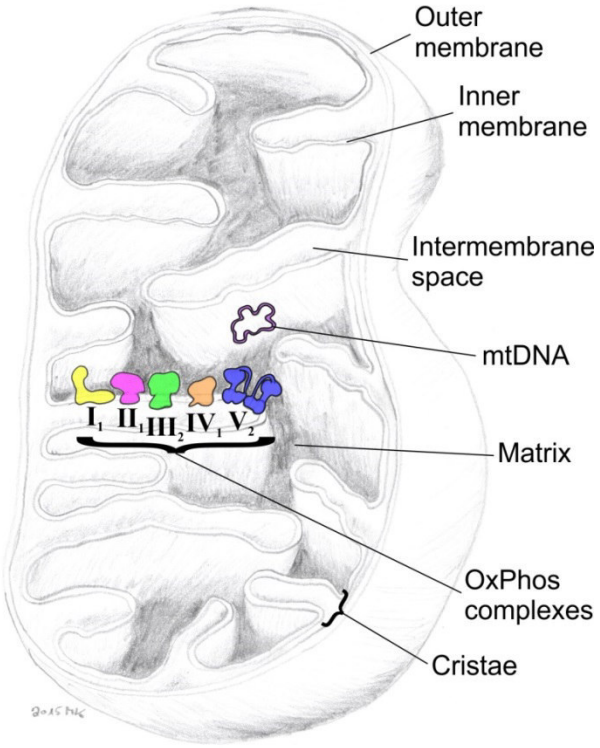

Fig. 1.3: Sketch of a mitochondrium with OxPhos complexes. Mitochondrium was drawn and OxPhos complexes were sketched in. Membranes and compartments were assigned, as well as circular mtDNA. Mitochondrium: (modified) Voet et al. (2002), OxPhos: (modified) Dudkina et al. (2010)

Mitochondrial DNA

Mitochondria have their own doublestranded circular DNA (mtDNA), organised in so called nucleoids. 13 peptides of the OxPhos complexes are encoded in the mtDNA, seven subunits of CI, one of CIII, three of CIV and two of CV. Additionally 22 transfer ribonucleic acids (tRNAs) and two ribosomal ribonucleic acids (rRNAs), which are involved in mitochondrial protein synthesis, are encoded. A control region, called D-loop, is also included. It contains the mtDNA replication origin and promotors for mtRNA transcription. Mitochondria are maternally inherited, hence mtDNA originates from the mother. Several copies of mtDNA can exist in each mitochondrium. They are mixed from wild-type and mutant mtDNA at the same time (heteroplasmy). It is supposed that a threshold of mutant mtDNA must be reached, before dysfunction appears. (Li et al. 2012)

mtDNA even encodes for proteins, which do not belong to the OxPhos system. For example, additonal protein-coding genes were found for corals, cnidarians, sponges and even in human mtDNA: humanin encodes a neuroprotective peptide (Breton et al. 2014).

Mitochondria underlie continuous fusion and fission processes. In this respect, the inner and outer membranes fuse and membrane lipids and matrix including content are exchanged, before fission takes place. Thereby circular mtDNA is exchanged as well (Chan 2006).

mtDNA repair system

Repair mechanisms for mtDNA depend on the kind of damage which occurred. For example, complex damages, which involve the whole double strand of the mtDNA like cross links, double strand breaks or formation of large adducts, are not repaired as known from nuclear DNA (nDNA) repair mechanisms (as nucleotide excision repair or homologous recombination). These repair mechanisms seem to be missing in mitochondria. But damages due to deamination, alkylation or oxidation of single bases are repaired by a conserved base excision repair mechanism. This makes mtDNA even more stable against oxidation from ROS than nDNA (Shokolenko et al. 2007). But it is known that genes of mtDNA have a higher mutation rate than of nDNA. It is supposed that the species only invests energy for maintaining the mtDNA for successful reproduction (Wallace 2010).

Mitochondria in the neural network

Neurons have a high energy demand, therefore mitochondria are found in axons, dendrites and mainly at the synapses. The energy is needed for maintain ionic gradients across the cell membranes, for transmission of signals through the synaptic cleft of neighbouring nerve cells, and for active axonal transport. (Schwarz 2013)

1.4 Ageing influences the brain structures

Ageing makes the brain tissue shrink especially in the areas prefrontal cortex (front part of frontal lobe, Fig. 1.4) and hippocampus (Fig. 1.5). Neurons and neurotransmitters are changed. Axons (white matter, compare 1.4.1) are degraded. The blood vessels change as well. Tangles or plaques of protein deposition appear. Oxidation by ROS increase as well as inflammation processes. The consequences are that attention, memory and learning processes decline with age. In some cases so called “plasticity” is increased, which means brain areas are activated for compensation, when other parts degenerate (Brown Rodgers 2008).

The changes in the brain can lead to cognitive impairment in different stages, up to neurodegenerative diseases as dementia. The changed properties of blood vessels increase the probability for development of vascular disease. To study the effects of ageing on the brain, cerebellum (Fig. 1.4), hippocampus and cerebrum of rats were analysed (4.1). In this thesis, cerebrum consisted of cerebral cortex (Fig. 1.4), basal ganglia (Fig. 1.6) and the limbic system (Fig. 1.5) from which the hippocampus was separated (for details see 2.6.1).

1.4.1 Brain areas

Description about anatomic structure and function of the areas of the human brain is based on Thews et al. (1999). Fig. 1.4, Fig. 1.5 and Fig. 1.6 show the sagittal plane of the human brain (drawn by hand, M. K., based upon webpage of Columbia University (15.07.2015)). In Fig. 1.4 the areas of cerebral cortex and corpus callosum (red), midbrain (turquoise) and hindbrain (cerebellum, medulla oblongata, pons varolii, grey) are marked. In Fig. 1.5 parts of the limbic system (as from diagonally sagittal cut) have been sketched in front of the sagittal plane of projection (Thews et al. 1999) as well as in Fig. 1.6 parts of the basal ganglia (Buratovich 15.07.2015).

The brain consists mainly of grey matter and white matter, together with capillary blood vessels. The white appearance of white matter derives from the myelin sheath of the axons, while grey matter is formed by neuronal cell bodies or unmyelinated neurons. Grey matter is found on the surface of cerebral cortex and cerebellum, as well as inside cerebellum, diencephalon, basal ganglia, the brainstem and the spinal cord.

Forebrain, Midbrain and Hindbrain

The forebrain consists of the telencephalon (cerebral cortex (the four lobes in Fig. 1.4), the basal ganglia (Fig. 1.6) and the limbic system (Fig. 1.5)) and the diencephalon (thalamus and hypothalamus, not shown). The hindbrain is composed of medulla oblongata, pons varolii and cerebellum, and is located between the spinal cord and the two hemispheres. The midbrain (mesencephalon) is located between hindbrain and forebrain (Fig. 1.4). Midbrain, pons varolii and medulla oblongata are summarised as brainstem.

Cerebral cortex

Cerebral cortex is divided into two hemispheres, which are connected via the corpus callosum. Four lobes can be distinguished: frontal, temporal, parietal and occipital lobe (Fig. 1.4). The functions of cerebral cortex are divided into motor, sensory and association areas. It is involved in attention, awareness, perception, language, memory, thought and consciousness.

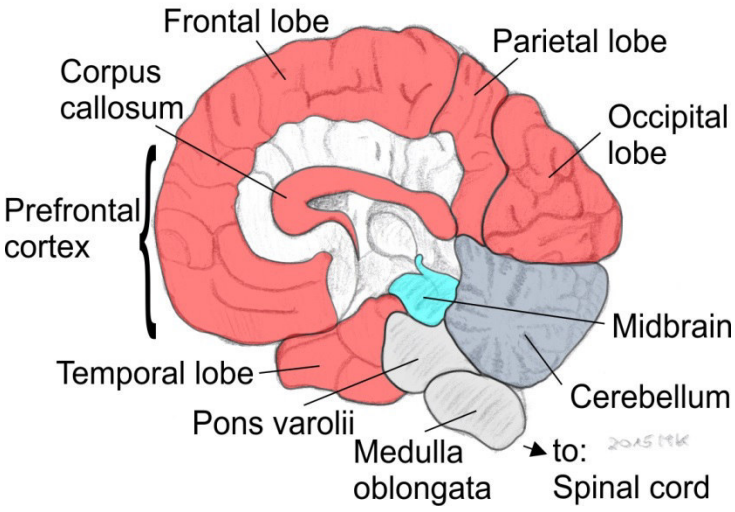

Fig. 1.4: Forebrain, midbrain and hindbrain. The four lobes (cerebral cortex) as well as the corpus callosum of forebrain are depicted in red, midbrain in turquoise and parts of hindbrain in grey. Image is based on Columbia University (15.07.2015).

The sensory areas receive the input from the sensory organs. Information about vision, audition and touch is transferred from thalamus to the so called primary sensory areas (not shown). The information from each sensory organ, such as ear, eye or hand, is send to the opposite hemisphere. This is also the case for the motor areas in the two hemispheres. The motor areas are responsible for activation of muscles and control of movement. All sensoric and motor areas are connected for control of motor action. Secondary motor areas are supposed to participate in planning and control of complex movements. Motivation areas (frontal cortex and limbic system) provide information about upcoming movement. These are transformed into plans for movement by the associative cortex. Association areas of cerebral cortex are the parts, which are not primary sensory areas or motor areas. They process information only, and forward them to basal ganglia, cerebellum and to the motor areas of cerebral cortex. They are also involved in processes of abstract thinking and language.

Limbic system

The limbic system (Fig. 1.5) consists of the cortical parts: gyrus cinguli, gyrus hippocampi (= hippocampus), gyrus parahippocampalis, parts of the olfactory system, as bulbus olfactorius, and of the subcortical parts: corpus amygdaloideum (= amygdala) and nucleus thalami anterior. The main parts are hippocampus and amygdala. Neuronal circuits are stabilised, when their connections, the synapses, are strengthened. This is controlled by the limbic system via projections of choline and noradrenaline. Information is memorised only when emotional interaction occurs

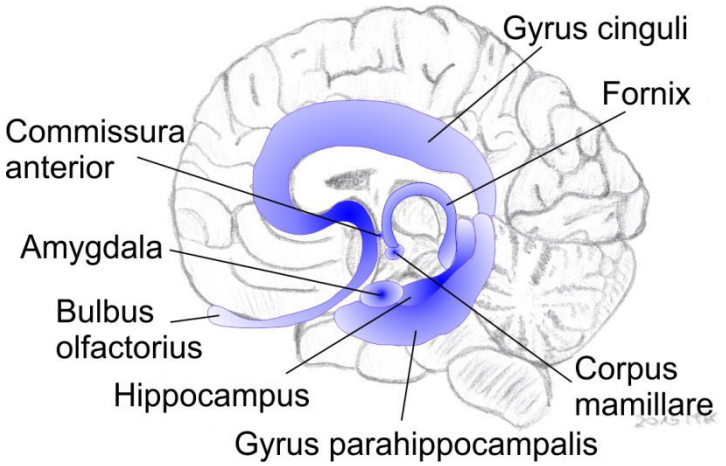

Fig. 1.5: Limbic system (as visible when brain is cut diagonally) is sketched in blue in front of the sagittal plane of projection. Image is based on Columbia University (15.07.2015) and Thews et al. (1999).

(so called affective memory) via connections of the amygdala to the association areas of the cerebral cortex. The connections of amygdala to the ventral striatum influence the motor control, while connections to hypothalamus and to the brainstem influence the autonomic nervous system and the endocrinal reactions. Cognition of new information and adaption of behaviour to new situations is achieved by connections from amygdala to the frontal cortex. Connections to hippocampus are important for development of memory. The main function of hippocampus is the consolidation of information from short-term memory to long-term. In animals, the limbic system is associated with instinct.

Basal ganglia

The basal ganglia (Fig. 1.6) consist of corpus striatum (nucleus caudatus + putamen), globus pallidus, nucleus subthalamicus and substantia nigra. These parts are involved in motivation-dependent planning of motor-driven action, conception of movement program, control of movement and memory of motor activity. The striatum is the largest part of the basal ganglia. It receives incoming signals from wide areas of the cerebral cortex, from substantia nigra pars compacta (SNc) and the thalamus (nucleus centromedianus, not shown). The outgoing areas of basal ganglia are substantia nigra pars reticulata (SNr) and globus pallidus (pars interna). Both send signals to the nucleus ventrolateralis of the thalamus, and from there, signals are transmitted to the cortex areas involved in motor activitites. Additionally SNr has an inhibitory effect on the colliculi superiors, which controls the eye movement. Internal pathways for signalling in the basal ganglia are the direct connection of striatum with globus pallidus (pars interna) and SNr, and the indirect pathway from striatum via globus pallidus (pars externa) to the nucleus subthalamicus, which is connected with globus pallidus (pars interna) and SNr. Another internal pathway starts at striatum via SNc back to the input areas. In the basal ganglia the neurotransmitters are the inhibiting γ–aminobutyric acid (GABA) and the excitatory glutamate. Axons from SNc to striatum release dopamine (DA), which stimulates the direct internal pathway and inhibits the indirect pathway. The basal ganglia are involved in the procedural long-term memory. (Thews et al. 1999)

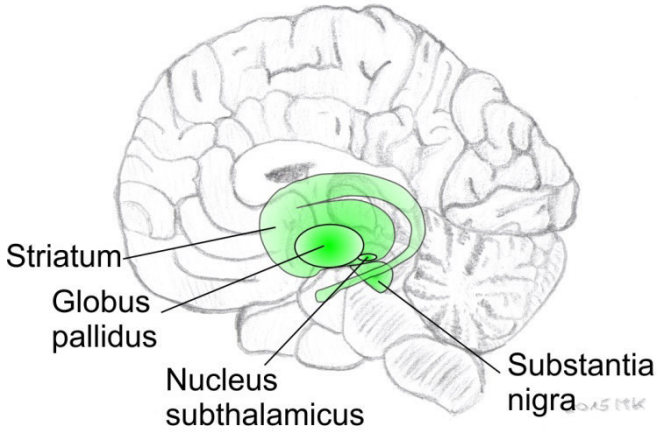

Fig. 1.6: Basal ganglia are sketched in green in front of the plane of projection. Image is combined, based on Columbia University (15.07.2015) and Buratovich (15.07.2015).

Cerebellum

Cerebellum (Fig. 1.4) consists of archicerebellum (balance and spatial orientation), palaeocerebellum (fine motor skills and limb movements) and neocerebellum (involved in planning movement, evaluation of sensory input for action and some cognitive funtions). Those three can be subdivided into smaller areas. The neocerebellum (cerebrocerebellum) receives input from the limbic system and from motor, sensory and posterior parietal cortex. The spinocerebellum (palaeocerebellum) receives input from motor and sensory cortex, spinal marrow and from visual and acoustic senses for comparison of the planned movement to its

performance. Deviations are corrected by outgoing signalling. The cerebellum is connected to the midbrain, pons varolii and medulla oblongata. The cerebellum is involved in planning, execution and practice of motor action. It adjusts movement to new situations.

Rat brain areas

The allocation of the brain regions in rat brain differs from the allocation in human brain. In Fig. 1.7 cerebellum (dark grey), cerebral cortex (red) and hippocampus, together with olfactory bulb, as part of the limbic system (blue) are sketched into a three dimensional rat brain skematic (drawn by hand, M. K., based upon Cheung and Cardinal (2005)).

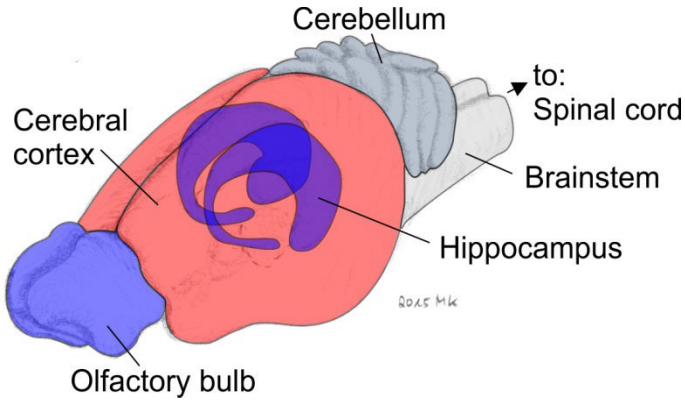

Fig. 1.7: Rat brain areas. Cerebral cortex (red), cerebellum and brainstem as regions of hindbrain (grey), hippocampus and olfactory bulb as parts of the limbic system (blue) are marked, based on: Cheung and Cardinal (2005)

1.4.2 Neurodegenerative diseases and role of mitochondria

Characteristic for neurodegenerative diseases is the loss of neurons in specific brain areas such as hippocampus (Alzheimer's disease), substantia nigra (Parkinson's disease), striatum (Huntington's disease) or in the structures of primary or secondary motor neurons (amyotrophic lateral sclerosis) (Plum et al. 2014).

Abnormal mitochondrial function is often found in neurodegenerative diseases like Alzheimer's, Parkinson's, Huntington's, as well as amyotrophic lateral sclerosis. The probability for incidence increases with age (E and Swerdlow 2012). E and Swerdlow (2012) suggest that dysfunctions of mitochondria, caused by defect proteins or mtDNA, increase ROS production and oxidative stress leading to neurodegeneration by neuronal necrosis. Likewise altered energy metabolism due to mitochondrial dysfunction decreases ATP production, impairs Ca^{2+} homeostasis and leads finally to neurodegeneration caused by apoptosis Fig. 1.8.

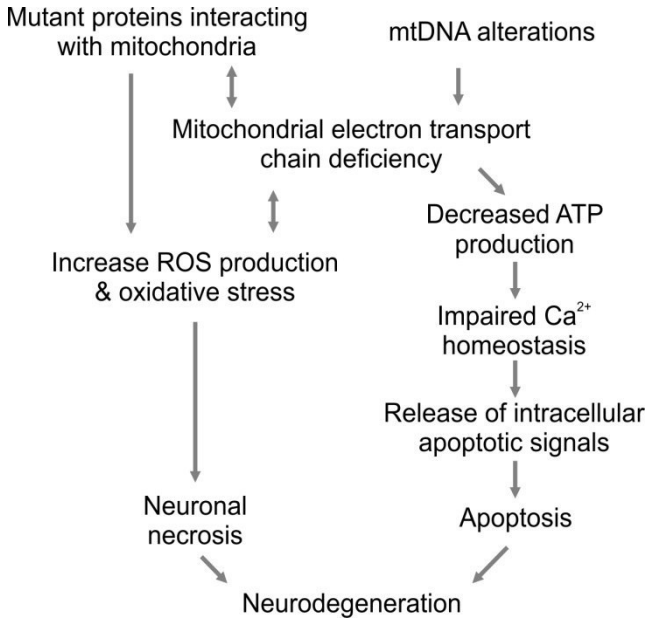

Fig. 1.8: Connections between mitochondrial dysfunction and neurodegeneration suggested by E and Swerdlow (2012) (modified)

Morbus Parkinson

The trigger of Parkinson's disease (PD) is not known in about 70-80% of the cases (idiopathic or primary parkinsonism) (Thews et al. 1999). Approximately 10-15 % of the cases are acquired by inheritance and the remaining cases are caused by side effects of other diseases, pharmaceuticals or contaminated addictive drugs (secondary parkinsonism).
The underlying cause of PD is the degeneration of dopaminergic neurons of substantia nigra (SN), which project to striatum (STR, Fig. 1.6). Physical symptoms of the disease occur not until about 80 % of the dopaminergic neurons are lost. Typical disorders are motor symptoms, such as tremor, slowdown up to lack of movement, rigour of limbs and body, as well as disorders of the autonomic nervous system or psychic imbalances (Thews et al. 1999).
Additionally to the degeneration of dopaminergic neurons, the aggregation of α-synuclein (appearance of Lewy bodies) is a pathological characteristic of idiopathic PD (Spillantini et al. 1997). α-Synuclein seems to impair mitochondrial function (E and Swerdlow 2012). It is known, that PD is accompanied by a mitochondrial dysfunction observed as a decline of mitochondrial CI activity in SN (E and Swerdlow 2012), resulting in an increased level of ROS, decreased production of ATP, increased intracellular Ca^{2+} concentration, excitotoxicity and degeneration of dopaminergic neurons in SN (E and Swerdlow 2012). Basso et al. (2004) observed an increased amount of CIII and CV in SN of patients with PD and suggested that this could be a compensatory mechanism for the decreased activity of CIII and CV.

Besides the compensatory processes of the respiratory chain also functional changes are observed for the remaining dopaminergic neurons, such as increased firing rate and increased synthesis of tyrosine hydroxylase (Song and Haber 2000), the enzyme which catalyses the conversion of L-tyrosine into L-3,4-dihydroxyphenylalanine, a precursor for the neuro-transmitter dopamine (DA) (Voet et al. 2002). Higher DA turnover and sprouting of axon terminals was also observed (Song and Haber 2000). Since the compensatory processes probably consume more energy, an enhanced energy production should be observable. Dopaminergic neurons have low mitochondrial mass, which makes them vulnerable to energy shortage (Liang et al. 2007). Defects of the energy providing OxPhos system could be the reason for breakdown of the compensatory mechanisms.

The compensatory mechanisms mask the early motor symptoms of PD. The early diagnosis is difficult (Gaenslen and Berg 2010) and a halt of the progress of the disease or cure is not possible yet. Therefore, it is of great interest to study the changes of the assembly state and amount of OxPhos complexes and their activities during degeneration of dopaminergic neurons in SN and STR for a better understanding of the molecular mechanisms involved in Parkinson's disease.

1.5 Calorie restriction

The reduction of food intake without malnutrition compared to *ad libitum* intake is defined as calorie restriction (CR). As reported by McCay et al. (1935), rodents have a prolonged life span when their food is limited. Also for other animals such as worms, fish, rodents and monkeys an increased life span under calorie restriction was found (Fontana et al. 2010). A reduction of 30-60 % in calorie intake initiated in early life of rodents caused a 30-60 % increase in maximum life span compared to animals fed *ad libitum*, while CR started in adulthood (age of 12 months) maximised the life span by about 10-20 % (Omodei and Fontana 2011).

CR delays the onset of age-associated diseases such as cardiovascular disease, several types of cancer, diabetes and ischemic injury as well as it should protect against neurodegenerative diseases. It is even proposed to induce neurogenesis in hippocampus and increase of plasticity effect besides other positive effects (Ribeiro et al. 2012). To explain all these effects, it is assumed, that the production of ROS by OxPhos is decreased, which occurs when CR without malnutrition is applied (Bevilacqua et al. 2005). During the 1950s, Harman (1956) found that free radicals attack cells as well as tissue and postulated that they cause ageing and degenerative diseases. Sohal et al. (2002) and Speakman (2005) assumed that ROS are continuously formed by the respiratory chain, but are scavenged by mitochondrial antioxidant enzymes. Speakman et al. (2004) and Speakman (2005) proposed that a dynamic and controlled uncoupling of respiration leads to a minimum of ROS production. OxPhos seems to be even more effective in the later years of life, as Silvestri et al. (2011) state “oxidative phosphorylation is more efficient in aged than in young [rat] skeletal muscle, since in old rats there is an increased respiratory control ratio”. In contrast to that Cocco et al. (2005) found that ageing decreases OxPhos in rat brain mitochondria (RBM). They also highlight that RBM “[…] have not been extensively studied. […]”

The question arises, whether the positive effects on healthy ageing and prolonged lifespan for rodents and other short-lived animals are translatable to ageing in humans. Non-human primates, specified rhesus monkeys, show similar age-related changes as humans, such as redistribution of body fat, greying and thinning of hair, loss of vigour, loss of muscle tone and loss of skin tone. They develop age-related diseases such as diabetes, neoplasia, sarcopenia, bone loss and impaired immune function as observed in humans (Colman et al. 2014). Their media lifespan for living in captivity is about 27 years (Mattison et al. 2012). Therefore the results of studies of non-human primates provide a link to the effects on humans. In the studies on 76 adult rhesus monkeys at the Wisconsin National Primat Research Center (WNPRC) by Colman et al. (2014) it was found that 30 % calorie restriction reduces age-related and all-cause mortality. The *ad libitum* fed control animals had a 2.9 times higher risk of death from an age-related cause and a 1.8 times higher risk for death form any cause, compared to the animals kept under CR. Another CR study on 120 rhesus monkeys was performed at the National Institute on Ageing (NIA) by Mattison et al. (2012). They analysed the metabolic health and the risk of death of young-onset and old-onset CR on the animals. They did not observe effects on lifespan of CR animals compared to controls, age-related deaths and all-cause mortality seemed to be the same. But they found that old-onset CR has a positive influence on metabolic health, they found triglycerides, cholesterol and fasting glucose levels reduced. However, a comparison between the studies of WNPRC and NIA

indicated different conditions of diet composition and amount of intake, as concluded from body weight and life time of animals. The missing difference in lifespan could be explained amongst others by the fact that even the control animals of NIA had been fed under conditions of mild restriction (Colman et al. 2014).

It is difficult to implement CR in clinical trials for humans. But epidemiological studies enable to analyse CR similar influences. For example the inhabitants of Okinawa (Japan) were known to consume about 15 % less than mainland Japanese and about 40 % less than the average daily intake of inhabitants of the United States. In people above 65 years from Okinawa the death rate from coronary heart disease and cancer was lower than for the mainland Japanese and United States residents. And the rate of centenarians with about 50 per 100,000 inhabitants is the highest in the world (Omodei and Fontana 2011). A volunteer group of people have founded the Calorie Restriction Society, practising self-imposed CR by reducing the calorie intake to about 30 % less than the control group. They eat a diet rich in nutrient dense foods while containing all essential nutrients. Protective effects on overweight/obesity, type 2 diabetes, inflammation and left ventricular diastolic dysfuntion are reported. Lower blood concentrations of cholesterol, low-density lipoprotein cholesterol, triglycerides, fasting glucose and fasting insulin were found as well as lower blood pressure and lower levels of inflammatory markers (Omodei and Fontana 2011). Omodei et al. (2015) analysed anorexic patients, as an extreme form of CR, to characterise the immune-metabolic profile, and found reduced amounts of immune cell populations, reduced glycolysis and OxPhos rates as well as higher anti-oxidant and anti-inflammatory levels. However, OxPhos capacity of mitochondria was on the same level as compared to healthy controls. They concluded that cells seem to be protected from biochemical stress.

In human cohorts several diets were analysed on their influence on cognitive function. Diets with additional antioxidants such as vitamin B6, B12, C, E or folic acid, flavonoids, with omega-3 fatty acids or Mediterranean diet were analysed, but they did not give enough evidence for a relationship between nutrition and cognitive function (Ferri et al. 2014).

The influences of CR on the ageing brain and the age-associated neurodegeneration have rarely been analysed yet. Therefore, it is of great interest to study the effects of CR during ageing on the mitochondrial proteome of brain tissue, for a better understanding of the mechanism, how CR triggers a longer and healthier life.

1.6 Motivation

The desire to understand the processes which occur during ageing and the causes of ageing-associated diseases is huge in our ageing society. It becomes more and more important to find possibilities to delay or even avoid the onset of ageing-associated diseases or at least to influence the health positively during ageing. Therefore, it is indispensable to find solutions for early diagnosis of the onset of ageing-associated diseases such as dementia and neurodegeration, especially because of irreversible degradation of neuronal cells. During ageing and development of ageing-associated diseases alterations of mitochondria, their genome, proteome, lipidome, metabolism and functions were observed (Groebe et al. 2007, Murphy 2009, Gilmer et al. 2010). The changed role of mitochondria in energy metabolism and in production of reactive oxygen species (ROS) amongst others has been widely discussed but still the causes for the observed changes in mitochondria during ageing and ageing-associated diseases are not understood, not to mention the attempts to influence the changes in a positive way. Mitochondria from late passage (senescent phenotype) human umbilical vein endothelial cells (HUVECs, 2.6.4) will be analysed in this thesis to understand the changes caused by nicotinamide adenine dinucleotide phosphate (NADPH) oxidase 4 (Nox4) (4.3), which generates ROS (Koziel et al. 2013). ROS are supposed to affect mitochondrial oxidative phosphorylation (OxPhos) complexes besides mtDNA or lipids but they are also involved in cell signalling or immune defence amongst other functions (Hancock et al. 2001). Cell culture provides a good model system for experimental analyses but cannot reflect a whole organ system in which different tissues are in interaction with each other as found in mammals. Animal models were established for analyses of ageing and ageing-associated diseases. Experiments were carried out to find general mechanisms and explanations for the causes of ageing and ageing-associated diseases in order to identify targets for delaying or avoiding onset of diseases, which might be transferred to humans in future. A lot of studies on rodents were performed using mitochondria of skeletal (Bevilacqua et al. 2005, Lombardi et al. 2009, Siegel et al. 2013) or heart muscle (Lee et al. 1999, Gómez et al. 2009, Tatarkova et al. 2011, Dai et al. 2014) or liver (Grinna 1977, Vorbeck et al. 1982, Dani et al. 2010) to analyse the effects of ageing or calorie restriction (CR). But the analyses of the OxPhos complexes from mitochondria of muscle or liver cannot be compared to the analyses of brain mitochondria. Even differences between interfibrillary and subsarcolemmal mitochondria of heart tissue exist (Thilmany 2013). Silvestri et al. (2011) stated "[…], it has emerged that the mitochondrial proteome differs greatly among tissues, depending on their functional requirements. […]". Frenzel (2011) describes in her studies of ageing differences between the rat brain mitochondria from the tissues cerebral cortex, striatum and hippocampus. Also Haripriya et al. (2004) analysed these three brain areas. However, often mitochondria from whole brain (Filburn et al. 1996, Tian et al. 1998, Olgun et al. 2002, Groebe et al. 2007) or from cerebral cortex (Cocco et al. 2005, Gilmer et al. 2010, Cerqueira et al. 2012) were analysed. Therefore, it is of great interest to study the ageing brain and the impact of ageing on the different brain areas. In this thesis the mitochondria of cerebellum, hippocampus and cerebrum from young and old Fischer rats (2.6.1) are studied for analyses of ageing and the effects of calorie restriction (4.1). Substantia nigra and striatum from Wistar rats (2.6.2) are analysed in an animal model of early Parkinson's disease (4.4). Cerebellum is involved in planning, execution and practice of motoric action. In new situations, the movement is adjusted there. The cerebrum contained the brain areas cerebral cortex, limbic

system excluding hippocampus, and the basal ganglia. Cerebral cortex contains the sensory, motor and association areas and is involved in planning and control of complex movements, attention, awareness, perception, language, memory, thought and consciousness. The limbic system is important for stabilisation of neuronal circuits. The transfer of information from short-term to long-term memory is mainly performed by hippocampus. Substantia nigra and striatum belong to the basal ganglia, which are involved in motivation-dependent conception of movement program and are thereby involved in the procedural long-term memory (Thews et al. 1999). Substantia nigra consists of dopaminergic neuron cell bodies projecting to striatum. Both areas are degenerated in consequence of Parkinson's disease. Remarkable is, that about 80 % of the dopaminergic neurons are lost before first physical symptoms of the disease arise (Thews et al. 1999). Consequently, all these brain areas have specific important tasks to manage and each of them is indispensable for proper function of the interplay between brain and body. The supply with energy is extremely important for biological neural networks, therefore many mitochondria are located there and their proper function is essential (Schwarz 2013) as mitochondrial dysfunctions seem to trigger ageing-associated neuro-degenerations (E and Swerdlow 2012). A trigger for a longer lifespan, a healthier life and to influence metabolism in a positive way is calorie restriction as shown for several animal models (Fontana et al. 2010, Ribeiro et al. 2012). CR is supposed to decrease the amount of produced ROS and therefore to prevent damage of the OxPhos complexes (Bevilacqua et al. 2005), but even 80 years after discovery of the lifespan prolonging effects, the molecular mechanism is still unresolved. The effects of CR on the central nervous system have been rarely analysed yet. Therefore, it is important to study the effects of CR on the mitochondrial proteome of brain tissue, in order to gain a better understanding of the alterations at the protein level. In this thesis the influences of calorie restriction on the proteome of mitochondria from cerebellum, hippocampus and cerebrum of rats are studied (4.1).

2 Materials

2.1 Chemicals

substance	abbrev.	manufacturer	p/o no.
1,4-Dithiotreitol p.a.	DTT	Carl Roth	6908.2
1,6-diphenyl-1,3,5-hexatriene	DPH	Sigma-Aldrich	D208000
3,3'-Diaminobenzidine	DAB	Sigma-Aldrich	D5637
4-Iodophenyl boronic acid		Sigma-Aldrich	471933
5-Bromo-4-chloro-3-indoylphosphate, disodiumsalt	BCIP	Carl Roth	A155.2
Acetic acid 100 %, p.a.	AcOH	Carl Roth	3738.5
Acetonitrile, HPLC gradient grade	ACN	AppliChem	A3189
Acetonitrile,Rotisolv® HPLC ultra gradient grade	ACN	Carl Roth	T195.2
Adenosine-5'-triphosphate	ATP	Sigma-Aldrich	A3377
Ammonium bicarbonate	ABC	Fluka	09832
Ammoniumperoxodisulphate	APS	Fluka	09915
Ammoniumphosphate monobasic, ultra		Fluka (BioChemika)	09709
Bis(2-hydroxyethyl)-imino-tris-(hydroxymethyl)-methane	Bis-Tris	Fluka	14880
Bovine serum albumine, fraction V	BSA	Carl Roth	8076.2
Bromophenol blue		Fluka	18030
CertiPUR® buffer solution pH(20°C)=4.00		Merck Millipore	109435
CertiPUR® buffer solution pH(20°C)=7.00		Merck Millipore	109439
CertiPUR® buffer solution pH(20°C)=9.00		Merck Millipore	109461
Cytochrome c, bovine heart		Sigma-Aldrich	C2037
Cytochrome c, equine heart		Calbiochem	250600
D-(-)-Mannitol		Carl Roth	4175
D-(+)-Sucrose		Carl Roth	4621.2
Digitonin		Acros	407560050 (Charge A0280740)
Dimethylsulfoxide	DMSO	Carl Roth	A994.2
Disodium hydrogen phosphate, p.a.	Na_2HPO_4	Fluka	71642
Ethanol, denatured	EtOH	supply store, Chemistry department, TU Darmstadt	
Ethylendiamine tetraacetate, tetrasodiumsalt, dihydrate	EDTA	Sigma-Aldrich	E-6511
Formaldehyde solution, 37 % in H_2O		Sigma-Aldrich	252549
Glycerol		Carl Roth	3783.2
Glycine p.a.		Carl Roth	3908.2
High molecular weight calibration kit for native electrophoresis	HMW	GE Healthcare	17-0445-01

substance	abbrev.	manufacturer	p/o no.
Hydrochloric acid, 30 % Suprapur®	HCl	Merck	1.00318
Hydrochloric acid, fuming 37 % p.a.	HCl	Carl Roth	4625.1
Hydrogenperoxyde, 30 %	H_2O_2	Merck	107209
Imidazole		Fluka	56750
Isopropanol, denatured		supply store, Chemistry department, TU Darmstadt	
Lead (II) nitrate		Fluka	1533.4
Low molecular weight calibration kit for SDS electrophoresis	LMW	GE Healthcare	17-0446-01
Luminol		Fluka	09253
MagicMark™ XP Western Protein Standard	MM	Invitrogen	LC5602
Magnesium nitrate hexahydrate		Sigma-Aldrich	63087
Magnesium sulphate		Carl Roth	P027.2
Magnesium chloride hexahydrate p.a.	$MgCl_2$	Carl Roth	A537.1
Methanol, denatured	MeOH	supply store, Chemistry department, TU Darmstadt	
MOPS		Carl Roth	6979.4
N,N,N′,N′-Tetramethylethylenediamine	TEMED	Sigma-Aldrich	T9281
N,N′-Dimethylformamide	DMF	Merck	2937
N-[Tris(hydroxymethyl)-methyl]-glycine, ≥99 % (titration)	Tricine	Sigma-Aldrich	T0377
N-2-Hydroxy piperazine-*N′*-2-ethanesulfonic acid	HEPES	Carl Roth	9105.4
Nitrotetrazolium Blue chloride	NBT	Carl Roth	4421.4
Peptide Mass Standards Kit for Calibration of AB Sciex MALDI TOF		AB Sciex	P2-3143-00
Potassium acetate		Fluka	60034
Potassium chloride	KCl	Carl Roth	6781.3
Potassium dihydrogen phosphate	KH_2PO_4	Carl Roth	3904
Potassium hexacyanoferrate (III)		Fluka	60300
Potassium hydroxide	KOH	Fluka	60370
Protease inhibitor cocktail for mammalian cell tissue use	PIC	Sigma-Aldrich	P8340
Refraction-2D™ Labeling Kit 4G or 8G	G-Dyes	^{NH}*Dye*AGNOSTICS	PR08 or PR08G
Roti®-Block, 10x concentrate		Carl Roth	A151.2
Roti®-Blot 2A, 10x concentrate		Carl Roth	P037.1
Roti®-Blot 2K, 10x concentrate		Carl Roth	P038.1
Roti®-Blue, 5x concentrate		Carl Roth	A152.1
Roti®-Free		Carl Roth	0083.1
Roti®-Nanoquant, 5x concentrate		Carl Roth	K880.1

substance	abbrev.	manufacturer	p/o no.
Rotiphorese® Gel 40 Acrylamide / Bisacrylamide 29:1	Gel AB	Carl Roth	A515.1
Rotiphorese® Gel A 30 % Acrylamide solution	Gel A	Carl Roth	3037.1
Rotiphorese® Gel B 2 % Bisacrylamide solution	Gel B	Carl Roth	3039.1
Serva Blue G (Coomassie Brilliant Blue G-250)	CBBG	Serva	35050
Silver nitrate p.a.	$AgNO_3$	Carl Roth	7908.2
Sodium carbonate, anhydrous, p.a.	Na_2CO_3	Carl Roth	A135.2
Sodium chloride p.a.	NaCl	Carl Roth	A3957.1
Sodium dihydrogen phosphate dihydrate	NaH_2PO_4 x 2 H_2O	Carl Roth	T879.1
Sodium dodecylsulphate, ultra pure	SDS	Carl Roth	2326.1
Sodium hydroxide p.a.	NaOH	Carl Roth	6771.1
Sodium phosphate dodecahydrate	Na_3PO_4 x 12 H_2O	Fluka	71642
Sodium succinate dibasic hexahydrate		Sigma-Aldrich	S2378
Sodium thiosulphate anhydrous	$Na_2S_2O_3$	Fluka	72049
Sodium thiosulphate pentahydrate p.a.	$Na_2S_2O_3$ x 5 H_2O	Merck	6516
SYPRO®Ruby protein gel stain	SyRu	Invitrogen	S21900
Trifluoroacetic acid	TFA	Fluka	91701
Tris(hydroxymethyl)-aminomethane, ≥99,9 %, p.a.	Tris	Carl Roth	4855.2
Trypsin Resuspension Dilution Buffer		Promega	V5111
Trypsin, lyophilised powder, proteomics grade		Sigma-Aldrich	T6567
Trypsin, lyophilised powder, sequencing grade		Promega	V5111
Tween® 20		Carl Roth	9127.1
α-Cyano-4-hydroxycinnamic acid	HCCA	Sigma-Aldrich	C-2020
β-Mercaptoethanol, 99 %, p.a.	MeSH	Carl Roth	4227.1
β-Nicotinamide adenine dinucleotide, reduced disodium salt hydrate	NADH	Sigma-Aldrich	N-6005
ε-Aminocaproic acid		AppliChem	A7011

2.2 Antibodies

Primary antibodies

target protein	host species	manufacturer	p/o no.
α MTCO1 (CIV)	mouse	abcam®	ab14705
α NDUFS1 (CI)	rabbit	Proteintech	12444-1-AP
α OxPhos V subunit alpha (CV)	mouse	Invitrogen	459240
α SDHA (CII)	mouse	abcam®	ab14715
α UQCRC2 (CIII)	mouse	abcam®	ab14745

Secondary antibodies

conjugate	target protein	host species	manufacturer	p/o no.
IgG-HRP	α mouse	donkey	Santa Cruz	sc-2318
IgG-HRP	α rabbit	donkey	Santa Cruz	sc-2317

2.3 Consumables

consumable	manufacturer	p/o no.
0.2 mL Thin-walled Tubes with Flat Caps	Thermo Scientific	AB-0620
alumina foil	Aldi Süd	
Biopsy Punch diameter 2 mm, sterile	Miltex	33-31
cannula with Luer-Lock connection, 1.00 mm x 200 mm	neoLab	2-3113
cannula with Luer-Lock connection, 1.50 mm x 100 mm	neoLab	2-3121
Disposable Bags	Carl Roth	E706.1
Disposable cuvettes, 1.5 mL semi-micro, PMMA	Brand	7591 15
Disposable pasteur pipettes, graduated, LDPE	Carl Roth	EA62.1
filter wellplate MultiScreen Solvinert, hydrophilic, PTFE, 0.45 µm	Millipore	MSRLN0410
G-Dye low retention tips (0.1-10 µL)	^{NH}*Dye*AGNOSTICS	PR57
G-Dye low retention tubes, 500 µL	^{NH}*Dye*AGNOSTICS	
Hand towel green, cellulose	Tork Universal	290135
Kapton® tape	^{NH}*Dye*AGNOSTICS	PR51
Kimtech Precision wipes	Kimberly-Clark Professional	05511
Multi®-safety microcentrifuge tubes, 0.5 ml	Carl Roth	7060.1
membrane filters (regenerated cellulose) 0.2 µm, diameter 50 mm	GE Healthcare, Whatman	10410314
membrane filters (regenerated cellulose) 0.45 µm, diameter 50 mm	Schleicher&Schuell	10410214
Parafilm M Laboratory film	Bemis Flexible Packaging	
Pasteur pipettes with long, thin tip, not graduated, LDPE	Carl Roth	EA58.1

consumable	manufacturer	p/o no.
PE foil	Aldi Süd	
pipette tips	Biozym	729025
pipette tips 10 µL	Biozym	720015
pipette tips MµltiFlex® tips 1-200 µl	Carl Roth	Y419.1
pipette tips Omnitip™ Fastrack 10 µL	ULPlast	81510
pipette tips Standard MAKRO 1-5 ml	Carl Roth	5846.1
pipette tips ultratips 1000 µL	Greiner BIO-ONE	740290
pipette tips ultratips 20-200 µL	Greiner BIO-ONE	739290
PP microplate, 96 well, Vshape	Greiner BIO-ONE	651201
PP-tube, 1.5 mL	Glasgerätebau Ochs	10-00122
PP-tube, 15 mL	Greiner BIO-ONE	188271
PP-tube, sterile, skirt, 50 mL	Greiner BIO-ONE	210261
Prespotted AnchorChipTarget PAC II 384 HCCA	Eppendorf for Bruker	255682
PS-microplate, 96 well, flat bottom	Greiner BIO-ONE	655101
reagent basin 60 mL	Thermo Scientific	9510027
Roti®-NC, nitrocellulose membrane	Carl Roth	HP40.1
Rotilabo® -blotting paper, 1.5 mm	Carl Roth	CL75.1
Rotiprotect®-latex gloves Type 2 powder free	Carl Roth	L949.1
Rotiprotect®-nitrile gloves eco	Carl Roth	TC12.1
Safe-Lock Tubes 2.0 mL	Eppendorf	0030 120.094
Sekuroka®-protective sleeves	Carl Roth	KP24.1
Sequiblot™ PVDF membrane	BioRad	162-0182
Surgical Disposable Scalpels	B Braun	5518083
tubing Tygon® LFL, ID: 2.79 mm wall: 0.84 mm	Saint-Gobain Performance plastics	070602-18
tubing Tygon® R3607, ID: 1.85 mm wall: 0.86 mm	Saint-Gobain Performance plastics	070534-20
$ZipTip_{C18}$	Millipore	ZTC18M960
$ZipTip_{C4}$	Millipore	ZTC04S096

2.4 Devices

application	device	manufacturer
balance	research R 200D	Sartorius
balance	universal U 4100S	Sartorius
centrifugation	5804R	Eppendorf
centrifugation	5810R	Eppendorf
centrifugation	Biofuge pico	Heraeus
centrifugation	rotor #3325B for Biofuge pico	Heraeus
centrifugation	rotor A-2-DWP for Eppendorf 5804R	Eppendorf
centrifugation	rotor A-4-62 for Eppendorf 5810R	Eppendorf
centrifugation	rotor F-34-6-38 for Eppendorf 5804R	Eppendorf
centrifugation	rotor F-45-30-11 for Eppendorf 5804R	Eppendorf
DIGE	Typhoon 9400 Variable Mode Imager	GE Healthcare
gel electrophoresis	Air-Cooled Vertical Electrophoresis Unit SE 400	Hoefer
gel electrophoresis	Chroma Dual Cooled Vertical Unit SE 600	Hoefer
gel electrophoresis	Dual gel caster SE 245	Hoefer
gel electrophoresis	Dual gel caster SE 6015	Hoefer
gel electrophoresis	Electrophoresis power supply EPS 1001	Amersham Pharmacia Biotech
gel electrophoresis	Electrophoresis power supply EPS 301	Amersham Biosciences
gel electrophoresis	Electrophoresis power supply EPS 600	Pharmacia
gel electrophoresis	Electrophoresis power supply EPS 601	Amersham Pharmacia Biotech
gel electrophoresis	gradient maker 2x 34 mL and 2x 19 mL	Workshop Chemistry department, TU Darmstadt
gel electrophoresis	Laminating machine	SilverCrest
gel electrophoresis	lifting platform DIN 12897	Bochem
gel electrophoresis	light transilluminator G-2004	GEPE
gel electrophoresis	low fluorescent glass plates for SE 600, 80-6442-14, 18 cm x 16 cm	GE Healthcare
gel electrophoresis	peristaltic pump Minipuls® 3	Gilson
gel electrophoresis	shaker 3016	GFL
gel electrophoresis	Small Format Vertical Electrophoresis System SE 250, SE 260	Hoefer
imaging system	Bio-Imaging-System ViewPix 900	Biostep/Epson
imaging system	fluorescent imaging system Typhoon 9400	GE Healthcare Life Sciences
imaging system	luminescent image analyser LAS-3000	Fujifilm
mass spectrometry	MALDI TOF/TOF Ultraflex I	Bruker
mass spectrometry	steel target, sample plate, SS, V700666 REV.C	PerSeptive Biosystems
mass spectrometry	UniEquip, thermoshaker	Laborgerätebau- und -vertriebs GmbH
mass spectrometry	Voyager DE™-Pro, BioSpectrometry™ Workstation	Applied Biosystems
mitochondria isolation	homogeniser, glass/teflon, tight-fit, 2 mL	Braun

application	device	manufacturer
mitochondria isolation	laboratory stirrer Eurostar digital	Ika
PC	Lenovo G560 Model 0679	Lenovo
pH adjustment	pH electrode BlueLine 14 pH	Schott
pH adjustment	pH electrode InLabMicro pH 0..14, 0..80°C	Mettler Toledo
pH adjustment	pH meter CG 842	Schott
photometry	cuvette 4 x 10 mm (emission x excitation) quartz SUPRASIL	Hellma Analytics
photometry	Fluostar/Polarstar Galaxy	BMG Labtechnologies
photometry	PTI M III fluorescence spectrometer	Photon Technology International
photometry	UV/Vis spectral photometer UV-2401 PC	Shimadzu
photometry	waterbath Lauda RCS, RC20	mgw
pipettes	8-channel pipettes Research, 10 µL 100 µL 300 µL	Eppendorf
pipettes	Pipetteman P2, P10, P20, P200	Gilson
pipettes	Research var. 1000 µL	Eppendorf
pipettes	SL-Pette 10-100 µL	SLG, Nichiryo
PMF	ultra sonic bath Sonorex TK 52 H	Bandelin
PMF	Unijet II, refridgerated, equipped with Univapo 150H	Uniequip
PMF	vacuum filtration system MultiScreen®HTS Vacuum Manifold	Millipore
print	HP Color Laserjet 4700dn	Hewlett Packard
print	HP Laserjet M1132 MFP	Hewlett Packard
solubilisation	waterbath 1004	GFL
stirring/mixing	electronic stirrer multipoint HP6	Variomag
stirring/mixing	magnetic stirrer Combimag Reo	Ika
stirring/mixing	magnetic stirrer Ikamag reo	Ika
stirring/mixing	vortex mixer Reax 3000	Heidolph
water	lab water purification system Simplicity equipped with Simpak® 2	Millipore
water	peristaltic liquiport	knf lab
water	Water still distinction D4000	Stuart
Western blot	Shaker HS 260 basic	Ika
Western blot	Trans-Blot® SD semi-dry electrophoretic transfer cell	BioRad

2.5 Software

software	originator
Adobe Reader XI Version 11.0.1	Adobe Systems
ChemDraw® Std Version 8.0.3	CambridgeSoft
Cisco AnyConnect Secure Mobility-Client Version 3.1.05160	Cisco Systems
Compass 1.3	Bruker
Corel DRAW® Home&Student X6	Corel Corporation
Corel PHOTOPAINT® Home&Student X6	Corel Corporation
Delta2D 4.3	Decodon
Endnote X7	Adept Scientific
Fluostar Galaxy V4.21-0	bmg
Image Quant tools	GE Healthcare
Image Reader LAS-3000 2.1	Fuji
ImageJ 1.47	National Institute of Health, USA
LEO's dictionaries	www.leo.org, LEO GmbH, Germany
Mascot database	Matrix Science
MS Office 2010 Professional	Microsoft
Pdf24 Creator Version 5.2.0	geek Software GmbH
ProteinScape 3.1	Bruker
PTI-Software Felix 1.42	Photon Technology International
PubMed database	National Center for Biotechnology Information, U.S. National Library of Medicine, USA
Real Statistics Resource Pack, Release 3.5.1	Charles Zaiontz http://www.real-statistics.com/
Typhoon Scanner Control	GE Healthcare
UniProt databases	European Bioinformatics Institute, Swiss Institute of Bioinformatics, Protein Information Resource
UVProbe 1.11	Shimadzu
Voyager Data Explorer™ Software Version 4	Applied Biosystems
Voyager Instrument Control Panel Version 5.1	Applied Biosystems
Voyager Sequence Control Panel Version 5.1	Applied Biosystems

2.6 Biological Samples

2.6.1 Rat brain samples for analysis of ageing and calorie restriction

The analysis of the effects of ageing and calorie restriction on rat brain samples was performed with the brain regions cerebellum (Fig. 1.4), cerebrum and hippocampus of male Fischer rats *(Rattus norvegicus)* (F344/DuCrlCrlj, from Charles River Laboratories Japan) which were provided by the research group of Prof. Dr. Sataro Goto, Juntendo University, Imbamura, Inbagun, Chiba 270-1695, Japan. The cerebrum consisted of the brain regions cerebral cortex (Fig. 1.4), basal ganglia (Fig. 1.6) and the limbic system (Fig. 1.5), from which the hippocampus was separated. Growth of animals and preparation was performed in Japan. Four animals were kept per cage. Samples were frozen in liquid nitrogen and transferred on dry ice to our lab, Technische Universität Darmstadt (TUD), Germany. They were stored at -80°C until isolation of mitochondria. Isolation of cerebrum mitochondria was performed by Dr. Diksha Dani in 2009, isolation of cerebellum and hippocampus mitochondria was performed by me in 2012 and in 2013, respectively. Isolated mitochondria were shock frozen in liquid nitrogen and stored at -80°C.

The three different brain regions, as mentioned above, originated from the same animals. The age of the animals were 6.5 months (young) and 27 months (old). They were nourished on free access to food every day *(ad libitum)* or on calorie restriction, the latter means feeding *ad libitum* on Mondays, Wednesdays and Fridays (alternate day feeding). The amount of food they consumed was about 60 % as an average of the *ad libitum* fed levels. Calorie restricted animals were fed *ad libitum* every day from birth until the age of 6 weeks to ensure a normal growth before the calorie restriction started. Dr. Sandra C. Thilmany calculated the level of calorie restriction from the ratio of the body weight of calorie restricted animals and the body weight of *ad libitum* nourished animals. She found a level of 40 % for young animals and 37 % for old animals (Thilmany 2013). Four groups of animals can be distinguished: young *ad libitum* fed rats (YAL), old *ad libitum* fed rats (OAL), young calorie restricted animals (YCR) and old calorie restricted animals (OCR). The brain regions originated from the same animals which Dr. Thilmany analysed in her dissertation (Thilmany 2013) together with her diploma student Michaela Söhn (2010). As described in Dr. Thilmany's thesis for heart and brain tissue, the individual animals of each group did not show abnormalities. Therefore, for each brain region separately, the individual animal samples of one group were pooled for my studies. For details see Table 2.1.

Table 2.1: Rat brain samples for analysis of ageing and calorie restriction
denotation, age and tissue weight

rat	age [months]	date of death	body weight [g]*1	tissue weight [g] (cerebrum)*2	pooled tissue weight [g] (cerebellum / hippocampus)
6.5-1 (YAL1)	6.5	16.12.2008	350	0.81	
6.5-2 (YAL2)	6.5	16.12.2008	351	1.02	
6.5-3 (YAL3)	6.5	16.12.2008	356	1.04	1.41 / 1.06
6.5-4 (YAL4)	6.5	16.12.2008	381	1.07	
6.5-5 (YAL5)	6.5	16.12.2008	360	0.99	
6.5-1 CR (YCR1)	6.5	16.12.2008	217	0.61	
6.5-2 CR (YCR2)	6.5	16.12.2008	196	1.03	
6.5-3 CR (YCR3)	6.5	16.12.2008	241	0.94	1.30 / 0.76
6.5-4 CR (YCR4)	6.5	16.12.2008	208	0.98	
6.5-5 CR (YCR5)	6.5	16.12.2008	211	0.92	
27M-1 (OAL1)	27	27.02.2009	451	0.44*3	
27M-2 (OAL2)	27	27.02.2009	314	0.36*3	
27M-3 (OAL3)	27	27.02.2009	417	0.50*3	1.70 / 1.27
27M-4 (OAL4)	27	27.02.2009	389	0.54*3	
27M-5 (OAL5)	27	27.02.2009	416	0.47*3	
27M-6 (OAL6)	27	27.02.2009	425	0.39*3	
27M-1 CR (OCR1)	27	27.02.2009	211	0.50*3	
27M-2 CR (OCR2)	27	27.02.2009	239	0.51*3	
27M-3 CR (OCR3)	27	27.02.2009	268	0.39*3	1.61 / 0.77
27M-4 CR (OCR4)	27	27.02.2009	260	0.43*3	
27M-5 CR (OCR5)	27	27.02.2009	265	0.47*3	
27M-6 CR (OCR6)	27	27.02.2009	273	0.30*3	

*1 data from Söhn (2010), *2 data from Thilmany (2013)
*3 marked samples: only halves of the cerebrum sections had been used for isolation of mitochondria by Dr. D. Dani, 2009

2.6.2 Rat brain samples for studies on Parkinson's disease

For studies of the neurodegenerative disease Parkinson's, animal studies were performed by Dr. Katarzyna Kuter, at Department of Neuropsychopharmacology, Institute of Pharmacology, Polish Academy of Sciences (IF-PAN), Smętna 12, 31-343 Kraków, Poland.

Male Wistar Han rats (Charles River, Germany) had free access to water and food and were kept in a twelve hour light/darkness cycle. All rats weighted between 250 and 300 g and were approximately 3 months old at the beginning of the experiment. The experiments were carried out in compliance with the Animal Experiments Bill of January 21, 2005; (published in Journal of Laws no. 33/2005 item 289, Poland), and according to the NIH Guide for the Care and Use of Laboratory Animals. They also received approval from the Local Ethical Committee. All efforts were made to minimize the number of animals and their suffering.

Preparation of animal model by injection of selective anti-dopaminergic toxin

Animals were stereotactically operated under deep ketamine/xylasine anaesthesia. 6-hydroxydopamine (6-OHDA) (3 µg / 3 µL 0.2 % ascorbic acid, Sigma-Aldrich, Germany), was injected into the medial forebrain bundle (MFB) to destroy dopaminergic cells by generation of reactive oxygen species (ROS) (further details in Zigmond (1997)). MFB consists of the neuronal fibers, passing from dopaminergic neuronal cell bodies of *substantia nigra pars compacta* (SNc) to *striatum* (STR), where their terminal endings are localized. Injection of 6-OHDA induces selective degeneration of dopaminergic neurons in SNc and disturbs the dopaminergic transmission in STR, which causes motor disability similar to Parkinson's disease based changes (Kolasiewicz et al. 2012). 30 minutes before toxin injection, the animals received desipramine (Sigma-Aldrich, Germany) to protect noradrenergic neurons. After the injection, animals woke up from anaesthesia and behavioural studies at different time-points were performed by Kuter et al. (submitted: September 2015).

Tissue preparation

4 days or 4 weeks after the injection, the animals were decapitated, and the tissues substantia nigra (SN) and striatum (STR) of both hemispheres were immediately dissected on an ice cold plate (4°C) and frozen on dry ice. The tissues were stored at -80°C, transported by Dr. Kuter on dry ice to TUD and stored again at -80°C until isolation of the mitochondria for proteome studies.

Isolation of rat brain mitochondria (RBM) (see section 3.1) and proteome studies of SN were carried out by Dr. Kuter and myself at TUD. Subsequent analyses of STR were carried out by Dr. Kuter under my mentorship at TUD.

Three groups of animals were analysed: a) sham operated rats (SH), as a control group, which had been injected solely with 0.2 % ascorbic acid, killed 4 weeks after injection, b) rats killed four days after injection of 6-OHDA in 0.2 % ascorbic acid (4DL) and c) rats killed four weeks after injection of 6-OHDA in 0.2 % ascorbic acid (4WL).

2.6.3 Bovine heart mitochondria

During a student's practical course in summer 2008 Dr. Monika Frenzel isolated mitochondria from a freshly prepared bovine heart obtained from a local slaughterhouse. The mitochondria were shockfrozen in liquid nitrogen and stored at -80°C. Age, sex and race of the animal are unknown. Bovine heart mitochondria are well-analysed and serve as a standard for molecular weight of oxidative phosphorylation (OxPhos) complexes and supercomplexes in our laboratory. Furthermore, they were used for peptide mass fingerprint analysis in my studies.

2.6.4 Cell culture samples for analysis of NADPH oxidase 4

Five types of NADPH oxidases (Nox1-5) are known yet. These enzymes contain six subunits and are membrane bound. Nox4 are located at the endoplasmatic reticulum, focal adhesions, in mitochondria and the nucleus. They produce superoxide radical anions by transfer of electrons to molecular oxygen and therefore provide ROS.

Analyses of NADPH oxidase 4 (Nox4) induced mitochondrial dysfunctions during ageing were carried out, using human umbilical vein endothelial cells (HUVEC). Early-passage cells (below passage 12) were compared to late-passage cells (at or after passage 20), which showed senescent phenotype. HUVECs were isolated and treated by Dr. Rafal Koziel as described in the joint publication (Koziel et al. 2013). Nox4 was knocked out (Nox4 KD) in HUVEC cells by lentiviral small hairpin ribonucleic acid (shRNA) vectors. Control cells were infected with non Nox4 specific shRNA vectors (control). Mitochondria were freshly isolated and shock frozen in liquid nitrogen by Dr. Koziel at Institute for Biomedical Aging Research (IBA), Innsbruck University, Rennweg 10, 6020 Innsbruck, Austria. They were transported on dry ice to TUD, where proteome studies were carried out by Dr. Koziel and me after introduction in the methods by myself.

3 Methods

3.1 Isolation of mitochondria from rat brain tissue

The isolation of organelles, especially mitochondria, is based on Reifschneider (2006). Tissue samples were homogenised before crude mitochondrial fraction was isolated by a differential centrifugation protocol, compare Söhn (2010). In contrast to M. Söhn's protocol, SCAVEGR, an antioxidant cocktail which contains albumin, was omitted because it would have artificially increased the protein amount (Thilmany 2013).

The frozen tissue was weighed on an ice-cooled watchglas. Then it was cut into small pieces with an ice-cooled scalpel and transferred to an ice-cooled tight-fit homogeniser. 4 mL of homogenisation buffer (Table 3.1, with PIC) per 1 g of tissue were added. Homogenisation was performed with seven strokes at 750 rpm with a tight-fit micropistill homogeniser (laboratory stirrer Eurostar digital, Ika, equipped with homogeniser, glass/teflon, tight-fit, 2 mL, Braun). The homogenate was centrifuged (Eppendorf 5804R, rotor: F34-6-38, 4°C, 7 min, 1,400 *g*) and the supernatant, which contained the mitochondria, collected and stored on ice. The pellet was resuspended with homogenisation buffer as a washing step and centrifuged again (4°C, 7 min, 1,400 *g*). The washing was performed twice. The merged supernatants were centrifuged (4°C, 7 min, 1,400 *g*) and the resulting supernatant was centrifuged (4°C, 8 min, 12500 *g*) for pelleting the mitochondria. The mitochondrial pellet was resuspended in storage buffer (see Table 3.1, with PIC), resulting in a slightly white cloudy liquid and stored shock frozen ($N_{2\,(l)}$) in aliquots at -80°C.

Table 3.1: Buffers for mitochondria isolation

Homogenisation buffer		Storage buffer	
210.0 mM	Mannitol	210.0 mM	Mannitol
70.0 mM	Sucrose	70.0 mM	Sucrose
1.0 mM	Na_4 EDTA*2 H_2O	5.0 mM	HEPES / NaOH
5.0 mM	HEPES / NaOH		
in Milli-Q-H_2O, pH 7.4, sterile-filtered, stored at -20°C		in Milli-Q-H_2O, pH 7.4, sterile-filtered, stored at -20°C	

0.5 % (v/v) Protease inhibitor cocktail (PIC) is added to all buffers directly before use.

3.2 Protein quantification – Bradford protein assay

According to the Bradford protein assay (Marshall and Williams 2004) Coomassie Brilliant Blue G-250 (CBBG, compare Fig. 3.1) adsorbs to the amino acid side chains of proteins in a specific amount via charge based and hydrophobic π–π-stacking interactions (Lottspeich and Engels 2012). Due to this adsorption, the colour of CBBG changes proportionally from λ=450 nm to λ=590 nm. This can be measured by UV/Vis-photometry. Additives like phosphoric acid or methanol support the process by denaturing membranes. In the present study, the premix Roti®-Nanoquant, 5x concentrate from Carl Roth, containing CBBG, was used.

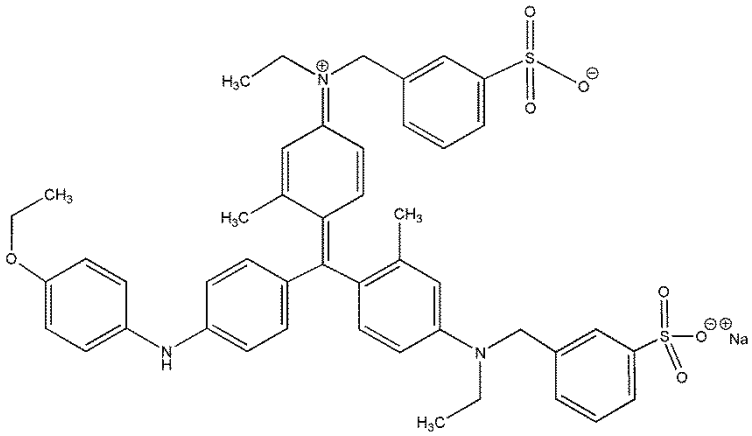

Fig. 3.1: Structure of Coomassie Brilliant Blue G-250, modified, Sigma-Aldrich (2014b)

3.2.1 In cuvettes

Using Bradford protein assay the protein amount of isolated mitochondria was determined. For absorbance measurements, the UV/Vis spectral photometer UV-2401 PC from Shimadzu was used. 0.4 mg/mL bovine serum albumine (BSA) in Milli-Q-H_2O served as a stock solution of the standard test series. 800 µL of 1x Roti®-Nanoquant (Roti®-Nanoquant, 5x concentrate diluted 1:5 with Milli-Q-H_2O) were added to each dilution of the standard and each dilution of the sample test series to a total volume of 1 mL. The final concentrations of the standard test series were 0, 1, 2, 4, 8, 12, 15, 20 and 25 µg/mL. The final dilutions of the sample test series were 1:2000, 1:1000, 1:2000/3, 1:400 and 1:800/3. Milli-Q-H_2O and 1x Roti®-Nanoquant (Thilmany 2013) served as a negative control.

Each series was repeated once. Incubation time was 10 minutes.

All samples were transferred into disposable poly(methyl methacrylate) (PMMA) cuvettes for measurement. Milli-Q-H_2O served as blank for the baseline. The absorbance ratio of the standard series (λ=590 nm / λ=450 nm) was plotted versus the concentration of the BSA standard series. The linear equation from the fit was used to calculate the concentration of the different sample dilutions. The latter were combined by calculating the mean.

3.2.2 In 96-wellplate

For samples with small available total protein amount, consequently the substantia nigra and striatum samples, the Bradford protein assay in cuvettes mentioned above (3.2.1) was modified by using 96 well plates. Final concentrations of the BSA standard and the dilutions of the samples were triplicated. Final volume per well was 250 µL, combined of 50 µL sample dilution and 200 µL 1x Roti®-Nanoquant. After 10 minutes incubation time the wavelength ratio 590 nm / 485 nm was measured in a 96 well plate reader (Fluostar/Polarstar Galaxy from BMG Labtechnologies, settings: absorption mode, test type: plate mode, reading

direction: horizontal, gain 019 and 004, no. of flashes: 42) (Frenzel 2006). Mathematical evaluation was performed as described in 3.2.1.

3.2.3 Control of protein quantification by sodium dodecyl sulphate polyacrylamide gel electrophoresis

For control of the described protein quantification (Bradford protein assay) 5 µL of isolated mitochondria were mixed 1:1 (v/v) with sodium dodecyl sulphate (SDS) loading buffer (compare Table 3.13). 10 µg calculated protein amount, based on the results of the antecedent Bradford test, of each sample-SDS loading buffer mix were loaded onto a 10 cm by 8 cm by 1.5 mm ten or fifteen well SDS polyacrylamide gel. 2 µL low molecular weight calibration kit for SDS electrophoresis (LMW, from GE Healthcare Amersham (2006b), contents see Table 3.2) served as standard. Details of SDS polyacrylamide gel electrophoresis (SDS PAGE) are described in 3.6. The gel was stained with Roti®-Blue (3.7.2) and the image scanned (compare 3.7.3). Evaluation was visually (by eye). Intensities of protein bands and protein lanes of the different samples were compared to each other. This method was already established by Thilmany (2013) but there quantified with an analysis software.

Table 3.2: Low molecular weight calibration kit (GE Healthcare Amersham 2006b)

Marker proteins of Low molecular weight calibration kit	
molecular weight (Mr)	protein
97,000	Phosphorylase b, rabbit muscle
66,000	Albumin, bovine serum
45,000	Ovalbumin, chicken egg white
30,000	Carbonic anhydrase, bovine erythrocyte
20,100	Trypsin inhibitor, soybean,
14,400	α-Lactalbumin, bovine milk

3.3 Solubilisation of mitochondrial proteins by detergent

Mitochondrial proteins were isolated of their membranes by solubilisation with the mild detergent digitonin (Fig. 3.2). The optimal detergent to protein ratio for RBM with 8 g digitonin per 1 g protein (d/p: 8g/g) was already determined by Frenzel et al. (2010). Krause (2004) established d/p: 3g/g for bovine heart mitochondria in his thesis. A differential centrifugation protocol was used as described below.

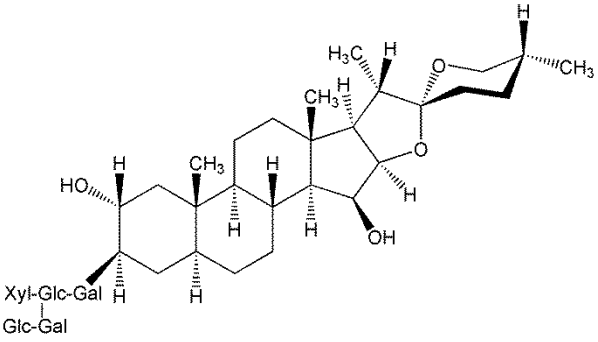

Fig. 3.2: Structure of the mild detergent digitonin, (Roth et al. 1988)

3.3.1 Solubilisation of tissue samples (bovine heart and rat brain)

First, the frozen sample was thawed and 300 µL of 1x solubilisation buffer (2x solubilisation buffer diluted with Milli-Q-water, Table 3.3) were added. A centrifugation step (4°C, 8 min, 20800 *g)* followed. The supernatant was removed and the pellet resuspended in the calculated amount of freshly prepared buffermix (Table 3.3, sample calculation in Fig. 3.3). The required volume of the 10 % (w/v) digitonin stock solution was added to result in a final volume of 1 % (v/v) and a mass ratio of d/p: 8g/g for rat brain samples. For bovine heart mitochondria samples 3 d/p: 3g/g were used. The mixture was homogenised using a vortex mixer and incubated on ice for 30 min Every 10 min the mixture was homogenised again. The incubation was terminated with a centrifugation step (4°C, 10 min, 20800 *g*). The supernatant containing the solubilised proteins (1.25 µg/µL protein concentration) was transferred into an ice-cooled reaction tube.

Table 3.3: Buffers for solubilisation of tissue samples

2x Solubilisation buffer		buffermix		empty well solution	
60.0 mM	HEPES	2x solubilisation buffer	500 µL	180 µL	buffermix
300.0 mM	Potassium acetate	PIC (0.5 % (v/v))	5 µL	20 µL	10 % Digitonin
20 %	Glycerol	Milli-Q-H_2O	395 µL		
in Milli-Q-H_2O,		10 % Digitonin	100 µL		
pH 7.4 (KOH), sterile filtered, stored at -20°C		total	1000 µL		

Empty well solution was prepared for filling empty wells in blue native (BN) gels to avoid perturbation of the neighboring lanes.

Sample calculation of digitonin amount for 260 µg protein and a final concentration of 1 % (v/v) digitonin and d/p: 8g/g:

1 g/g 1 µL/100µg protein 10 % (w/v) digitonin stock solution
↓·2.6
1 g/g 2.6 µL/260µg protein 10 % (w/v) digitonin stock solution
↓·8
8 g/g 20.8 µL/260µg protein 10 % (w/v) digitonin stock solution
↓·10
8 g/g 208 µL/260µg protein 1 % (v/v) digitonin solution

187.2 µL buffermix + 20.8 µL 10 % (w/v) digitonin stock solution
→ 1.25 µg/µL protein concentration

Fig. 3.3: Sample calculation of 1 % digitonin and buffermix amount for solubilisation of rat brain mitochondria

3.3.2 Solubilisation of tissue samples for application of differential gel electrophoresis

Solubilisation of mitochondrial proteins was performed according to solubilisation protocol in 3.3.1. A final digitonin concentration of 2 % (v/v) was used to increase final protein concentration to 2.5 µg/µL for subsequent differential gel electrophoresis (DIGE) labelling protocol (see 3.7.5). Sample calculation is provided in Fig. 3.4.

Sample calculation of digitonin amount for 260 µg protein and a final concentration of 2 % (v/v) digitonin and d/p: 8g/g:

usage of 2 % (v/v) final digitonin concentration:
83.2 µL buffermix + 20.8 µL 10 % (w/v) digitonin stock solution
= 104 µL total volume → 2.5 µg/µL protein concentration

Fig. 3.4: Sample calculation of 2% digitonin and buffermix amount, for solubilisation of rat brain mitochondria

3.4 Imidazole blue native polyacrylamide electrophoresis

Blue native gradient imidazole gels (BN gels) from total acrylamide concentration (% T) = 3 % to 13 % respectively 4 % to 13 % (compare 3.4.1) were used for separating proteins from tissue and cell culture samples. Total cross-linker concentration (% C) was 3 %. CBBG (Fig. 3.1), as a component of the cathode buffer (Table 3.7), provides negative charge for the gel run by non-denaturing charge based and hydrophobic π–π-stacking interaction with the native proteins (Krause and Seelert 2008), resulting in a separation of the native proteins according to their hydrodynamic radius and native mass.

3.4.1 Preparation of imidazole BN gels

Imidazole BN gel solutions were separately mixed together according to Table 3.5. The following steps were performed at +4°C. In case of 18 cm by 16 cm sized gels the complete amount of separating gel solutions was transferred into the tanks of the 2x 34 mL gradient maker and in case of 10.0 cm by 10.5 cm sized gels only 5 mL of each separating gel solution was transferred into the tanks of the 2x 19 mL gradient maker for casting the gradient separating gel. For casting 18 cm by 16 cm sized gels dual gel caster SE 6015 and for 10.0 cm by 10.5 cm sized gels dual gel caster SE 245 from Hoefer were used. All gels had a thickness of 1.5 mm. The gradient gels were casted from bottom to top using a cannula with Luer-Lock connection from neoLab. Excess Milli-Q-H_2O was initially in the tubing system, which covered the gradient gel at the end of casting. The set-up is shown in Fig. 3.5. The gel was moved for polymerisation of the separating gel from +4°C to room temperature (RT). After polymerisation, the excess water was removed and the stacking gel was casted above the separating gel including a 15 well comb for 18 cm by 16 cm gels or a 10 well comb for 10.0 cm by 10.5 cm sized gels at RT. Polymerised gels were stored at +4°C at least 12 hours (h) to complete polymerisation until load of samples, followed by gel run.

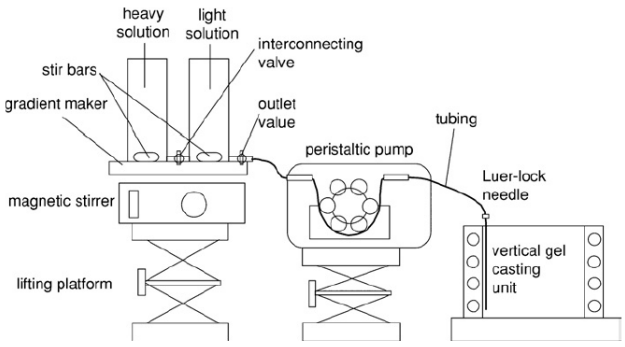

Fig. 3.5: Set-up for casting gradient gels, modified, Krause and Seelert (2008)

Table 3.4: Imidazole BN gel buffers

Imidazole BN gel buffers	
1.5 M	ε-aminocaproic acid
75.0 mM	imidazole
(optional + 60 % (w/v)	glycerol)

pH 7.0 (HCl), sterile filtered, stored at +4°C

Table 3.5: Imidazole BN gel composition

Imidazole BN gel		size 18 cm x 16 cm			size 10 cm x 10.5 cm		
		separating gels		stacking gel	separating gels		stacking gel
% T, % C	[%]	13.0, 3.0	4.0, 3.0	3.5, 3.0	13.0, 3.0	3.0, 3.0	3.0, 3.0
Rotiphorese® Gel A	[mL]	6.230	1.92	0.849	0.357	0.719	0.7275
Rotiphorese® Gel B	[mL]	2.890	0.889	0.394	/	0.3336	0.3375
Rotiphorese® Gel 40 (Gel AB)	[mL]	/	/	/	2.140	/	/
Imidazole BN gel buffer (Table 3.4)	[mL]	/	4.940	2.500	/	2.470	2.500
Imidazole BN gel buffer incl. 60 % (w/v) glycerol (Table 3.4)	[mL]	4.940	/	/	2.470	/	/
Milli-Q-H_2O	[mL]	0.715	7.000	3.692	2.400	3.850	3.828
TEMED	[µL]	4.10	6.80	5.95	2.05	3.40	10.00
10 % (w/v) APS	[µL]	41.00	68.00	59.50	20.50	34.00	100.00
total volume	[mL]	14.820	14.820	7.500	7.390	7.410	7.500

3.4.2 Imidazole BN gel run

Mitochondria from tissue or cell culture samples were solubilised according to 3.3 and loaded into the wells of the imidazole BN gel. As protein standard for BN gels 4 µL (18 cm by 16 cm sized gels) or 2 µL (10.0 cm by 10.5 cm sized gels) of the high molecular weight calibration kit for native electrophoresis (Table 3.6, GE Healthcare Amersham (2006a)) were loaded. 70 µg (18 cm by 16 cm sized gels) respectively 40 µg (10.0 cm by 10.5 cm sized gels) BHM were solubilised (d/p: 3g/g) and loaded as an additional protein standard.

Table 3.6: High molecular weight calibration kit (GE Healthcare Amersham 2006a)

Marker proteins of High molecular weight calibration kit	
molecular weight (Mr)	protein
669,000	Thyroglobulin, porcine thyroid
440,000	Ferritin, equine spleen
232,000	Catalase, bovine liver
140,000	Lactate dehydrogenase, bovine heart
66,000	Albumin, bovine serum

Table 3.7: Buffers for imidazole BN gel run

Cathode buffer (B) for imidazole BN PAGE	Cathode buffer (B:10) for imidazole BN PAGE	Anode buffer for imidazole BN PAGE
7.5 mM imidazole 50.0 mM Tricine 0.02 % (w/v) ServaBlue G	7.5 mM imidazole 50.0 mM Tricine 0.002 % (v/v) ServaBlueG	25.0 mM imidazole
pH 7.0 adjusts itself, filtered, stored at RT	pH adjusts itself, diluted from B with cathode buffer without ServaBlue G, stored at +4°C	pH 7.0 (HCl), stored at +4°C

18 cm by 16 cm sized gels:

Depending on the expected volume of the gels, Hoefer Air-Cooled Vertical Electrophoresis Unit SE 400 or Chroma Dual Cooled Vertical Unit SE 600 were used to run the loaded 18 cm

by 16 cm sized gels. At the beginning, anode buffer and cathode buffer B for imidazole BN gels (Table 3.7) were used. The run was started with 15 mA per gel and 100 V, until the dye front has left the stacking gel. Then 500V were applied till dye front has reached the midway of the separating gel. The cathode buffer B was then exchanged into cathode buffer B:10 and the gel was run till the dye front started to leave the separating gel.

10.0 cm by 10.5 cm sized gels:

The Small Format Vertical Electrophoresis System SE 250 and SE 260 were used to run 10.0 cm by 10.5 cm sized gels. From the start, anode buffer and cathode buffer B:10 for imidazole BN gel system, as described in Table 3.7, were used. The settings for the run were 15 mA per gel and 100 V until the dye front has left the stacking gel. Then the voltage was increased to 250 V and stopped when the dye front started to leave the separating gel.

Immediately after gel run the gels were used for further experiments.

3.5 Two-dimensional BN/SDS PAGE

Two-dimensional (2D) gel electrophoresis is achieved by BN polyacrylamide gel electrophoresis (PAGE) in the first dimension and subsequent SDS PAGE in the second dimension. Proteins hence are separated according to their native mass and hydrodynamic size in the first dimension. For the second dimension, SDS and β-mercaptoethanol (MeSH) denatures the proteins into negatively charged peptide chains, which are separated depending on their chain length (Reisinger and Eichacker 2007). In my studies Tris-Tricine SDS PAGE is applied for the second dimension as described in Schägger and von Jagow (1987).

Two different sizes of 2D-BN/SDS gels were used: 18 cm by 16 cm sized and 10.0 cm by 10.5 cm sized gels. 18 cm by 16 cm sized gels require BN gel lanes from an 18 cm by 16 cm sized BN gel and 10.0 cm by 10.5 cm sized 2D-BN/SDS gels require 10.0 cm by 10.5 cm sized BN gel lanes (3.4). The thickness was 1.5 mm for BN gels and 2D-BN/SDS gels.

3.5.1 Denaturation of proteins in BN gel lanes

BN gel lanes were cut immediately after gel run, sealed in disposable plastic bags and stored at +4°C for maximum 36 hours. Lanes were incubated twice for 30 minutes in 1 % (v/v) MeSH / 1 % (w/v) SDS (in Milli-Q-H_2O) and washed three times with Milli-Q-H_2O before placing close to upper edge between glassplates of Hoefer gel casting system.

3.5.2 Casting of 2D-BN/SDS gels

Hoefer dual gel caster were used for casting the 2D-BN/SDS gel at RT. SDS separating gel and the two stacking gels (composition in Table 3.9) were casted around the denatured BN gel lane, compare sketch in Fig. 3.6. A single tooth of a comb was used to form one well for the molecular weight size marker. After polymerisation of the gel, the run was started immediately.

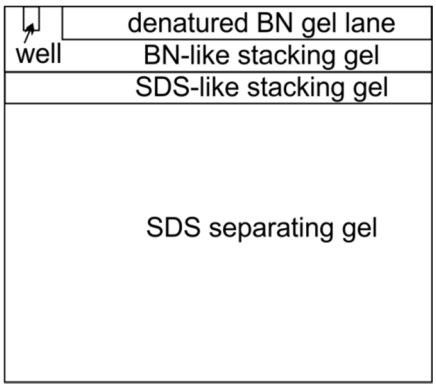

Fig. 3.6: Scheme of 2D-BN/SDS gel

Table 3.8: 2D-SDS gel buffers

2D-SDS gel buffer	
3.0 M	Tris
0.15 % (w/v)	SDS
(optional + 30 % (w/v)	glycerol)
pH 8.5 (HCl), stored at RT	

Table 3.9: 2D-BN/SDS gel composition

2D-BN/SDS gel		size 18 cm x 16 cm			size 10 cm x 10.5 cm		
gel		separating	SDS-like stacking	BN-like stacking	separating	SDS-like stacking	BN-like stacking
% T, % C	[%]	13.0, 3.0	5.0, 3.0	5.0, 3.0	13.0, 3.0	5.0, 3.0	5.0, 3.0
Rotiphorese® Gel A	[mL]	1.300	0.810	0.810	0.650	0.405	0.405
Rotiphorese® Gel B	[mL]	/	0.375	0.375	/	0.188	0.188
Rotiphorese® Gel 40 (Gel AB)	[mL]	8.800	/	/	4.400	/	/
2D-SDS gel buffer (Table 3.8)	[mL]	/	1.650	/	/	0.825	/
2D-SDS gel buffer incl. 30 % glycerol (Table 3.8)	[mL]	10.000	/	/	5.000	/	/
BN gel buffer (without glycerol) (Table 3.4)	[mL]	/	/	1.650	/	/	0.825
Milli-Q-H_2O	[mL]	9.750	2.140	2.065	4.875	1.070	1.033
20 % (w/v) SDS	[µL]	/	/	50.00	/	/	25.00
TEMED	[µL]	15.00	2.50	3.50	7.50	1.25	1.75
10 % (w/v) APS	[µL]	150.00	25.00	35.00	75.00	12.50	17.50
total volume	[mL]	30.015	5.000	4.989	15.010	2.500	2.495

3.5.3 2D-BN/SDS gel run

3 µL of LMW (Table 3.2) were loaded as a standard into the well before gel run started. The gel run was performed with electrophoresis buffers (see Table 3.10) using Hoefer electrophoresis units applying 50 V and 80 mA per gel until the dye front reached the separating gel. Voltage was then increased up to 95 V and left for 10-14 h. When dye front was still visible, voltage was increased up to 175 V till dye front had left the gel and run was finished.

In case of DIGE labelled protein samples (compare 3.7.5) special fluorescent free glass plates (GE Healthcare) were used and the gels were covered with alumina foil to avoid light exposure.

The finished 2D-BN/SDS gel was directly used for its further application.

Table 3.10: Buffers for 2D-BN/SDS PAGE run

Anode buffer for 2D-BN/SDS PAGE	Cathode buffer for 2D-BN/SDSPAGE
100.0 mM Tris	100.0 mM Tris
	100.0 mM Tricine
pH 8.9 (HCl),	0.05 % (w/v) SDS
stored at +4°C	pH 8.25 adjusts itself,
	stored at +4°C

3.6 SDS PAGE

The detergent SDS (Fig. 3.7) denatures proteins by destroying non-covalent bonds and covering the native charge by a negative charge proportional to the mass of the number of amino acids. It surrounds the peptides like stretched clouds. Subsequently, protein complexes lose their quaternary structure and are disassembled into their subunits, which are separated in SDS PAGE depending on their mass. In this thesis SDS PAGE is performed based on the system of U. K. Laemmli (Laemmli 1970), which is also explained in detail in Lottspeich and Engels (2012).

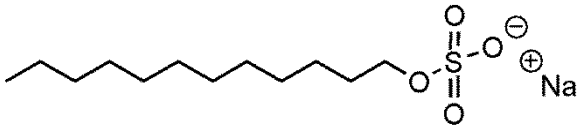

Fig. 3.7: Structure of SDS, modified (Sigma-Aldrich 2014c)

3.6.1 Casting of SDS gels

SDS gels were casted according to recipe quoted in Table 3.12 using a dual gel caster SE 245 from Hoefer. For 0.75 mm thick gels the gel solutions had to be degassed before adding SDS, *N,N,N′,N′*-tetramethylethylenediamine (TEMED) and ammoniumperoxodisulphate (APS). After casting the separating gel, the surface was covered with denatured isopropanol to avoid air contact. After polymerisation of the separating gel, the isopropanol was removed and the stacking gel casted. Usually, 10 well combs were used while casting the stacking gel.

SDS gels could be stored at +4°C for several days wrapped in wet cellulose towels and polyethylene (PE) foil.

Table 3.11: SDS gel buffers

SDS separating gel buffer	SDS stacking gel buffer
1.5 M Tris	1.0 M Tris
pH 8.8 (HCl), stored at RT	pH 6.8 (HCl), stored at RT

Table 3.12: SDS gel composition

SDS gel		size: 10 cm x 8 cm	
amount of gels and thickness		2x 0.75 mm or 1x 1.5 mm separating gel	2x 0.75 mm or 1x 1.5 mm stacking gel
% T, % C	[%]	13.0, 4.0	5.0, 3.3
Rotiphorese® Gel A	[mL]	4.160	/
Rotiphorese® Gel B	[mL]	2.600	/
Rotiphorese® Gel 40 (Gel AB)	[mL]	/	0.625
SDS separating gel buffer (Table 3.11)	[mL]	2.500	/
SDS stacking gel buffer (Table 3.11)	[mL]	/	0.625
Dist.-H_2O	[mL]	0.600	3.670
important information:		degas solution when casting 0.75 mm thick gels	
20 % (w/v) SDS	[µL]	50.0	25.0
TEMED	[µL]	7.5	5.0
10 % (w/v) APS	[µL]	75.0	50.0
total volume	[mL]	9.993	5.000

3.6.2 SDS gel run

Before SDS gel run the samples were mixed 1:1 (v/v) with SDS loading buffer (Table 3.13) and loaded into the wells of the 10 cm by 8 cm sized SDS gel (Table 3.12). As a marker 1.5 µL of LMW (Table 3.2) were loaded. If needed 40 µg (b. sol. d/p: 3g/g) of BHM were loaded as an additional marker. For the run, the gels were fixed in the Small Format Vertical Electrophoresis System SE 250 or SE 260, which was connected to water cooling. Glycine electrophoresis buffer (Table 3.13) was used for the run. 50 mA per gel and 100 V were applied until the dye front left the stacking gel. Then the voltage was increased to 200 V and turned off when the dye front has left the separating gel.

Finished gels were treated immediately after run according to their purpose.

Table 3.13: SDS loading buffer and Glycine SDS electrophoresis buffer

SDS loading buffer		Glycine SDS electrophoresis buffer	
15 % (w/v)	Sucrose	0.4 M	Glycine
2.5 % (w/v)	SDS	50.0 mM	Tris
0.25 % (w/v)	Na_2CO_3	0.1 % (w/v)	SDS
0.04 % (w/v)	Bromophenol blue		
25.0 mM	DTT		
stored at -20°C		pH 8.5 adjusts itself, stored at RT	

3.7 Methods for visualisation and quantitation of proteins after 2D BN/SDS PAGE

In this thesis different methods for visualisation and quantitation of the proteins after PAGE were used. Silver staining according to Blum et al. (1987) is extremely sensitive but is not useful for protein quantification (Table 3.14), however very effective for visualisation of the protein spots in 2D-BN/SDS gels, which is important for cutting protein spots before peptide mass fingerprint (PMF, see 3.9). For quantification of protein spots in 2D-BN/SDS gels (compare 3.11.1) highly sensitive (Table 3.14) fluorescent staining with SYPRO® Ruby (Bio-Rad 2000) or fluorescent labelling with G-Dyes, Refraction-2D™ (^{NH}*Dye*AGNOSTICS 2012-2013) was applied. After quantitation the 2D-BN/SDS gels were additionally stained with silver for visualisation of the protein spots. Furthermore Roti® Blue (Carl Roth 2011) as a colloidal CBBG staining method with a similar dynamic range and an only slightly lower sensitivity (Table 3.14) was used for visual control of protein quantification (3.2.3) and for staining of first dimensional gels (3.4).

Table 3.14: Different visualisation methods and their properties

Method	Silver	Roti®-Blue	SYPRO® Ruby	Refraction-2D™
Protocol, Manufacturer	Blum et al., Electrophoresis, 5, 1987, 93-99.	Carl Roth Roti® Blue A152.1	BIO RAD SYPRO® Ruby protein gel stain 170-3138	^{NH}*Dye*AGNOSTICS G-Dyes PR08, PR08G
Sensitivity / spot	0.5 ng	< 30 ng	1-10 ng	< 0.03 ng
Quantitative	no	yes	yes	yes
Linear dynamic range	no	10^3	10^3	10^{4-5}
MS compatibility	yes	yes	yes	yes
Reference	Blum et al. (1987)	Carl Roth (2011)	Bio-Rad (2000)	^{NH}*Dye*AGNOSTICS (2012-2013)

3.7.1 Silver stain

Silver staining is divided into several steps as depicted in Table 3.15. The fixing steps cause lower background staining. Thiosulphate containing sensitizer increases the affinity of silver to the proteins by silver sulphide formation and leads to a faster and more sensitive reduction of silver later on. During silver impregnation step, the proteins form complexes with silver ions. The latter are reduced by formaldehyde in alkaline solution in the development step (staining solution in Table 3.15). Thiosulphate forms soluble silver complexes, preventing high background staining. Last steps are stop and storage, preventing overdevelopment. Washing steps between the incubation steps remove excess chemicals from previous steps. (For details see Blum et al. (1987) and Rabilloud et al. (1994)).

Table 3.15: Solutions for silver staining

solution	quantity	component
Fixing I	50 % (v/v)	MeOH
	12 % (v/v)	AcOH
Fixing II	50 % (v/v)	EtOH
Sensitizer	0,81 mM	$Na_2S_2O_3$ x 5 H_2O
Silver	11,77 mM	$AgNO_3$
	0,028 % (v/v)	Formaldehyde
Stain	0,57 M	Na_2CO_3
	0,20 mM	$Na_2S_2O_3$ x 5 H_2O
	0,019 % (v/v)	Formaldehyde
Stop	10 % (v/v)	AcOH
Storage	1 % (v/v)	AcOH

All solutions for silver staining were made with distilled water. Silver staining of 2D-BN/SDS gels (3.5) was performed by shaking the gels in different solutions (Table 3.15) in the following order:

- minimum 60 min Fixing I solution
- minimum 60 min Fixing II solution
- 1 min Sensitizer solution
- 1 min dist. H_2O
- 20 min Silver solution
- 1 min dist. H_2O
- staining solution, until the protein spots on the gel start to become dark brown (not black)
- 1 min dist. H_2O
- 10 min Stop solution
- minimum 30 min storage solution

After shaking the gel in storage solution, the gel image was scanned according to 3.7.3.

3.7.2 Colloidal Coomassie Brilliant Blue G-250 stain

As already described in 3.2, CBBG binds to proteins and peptides through charge based and hydrophobic π–π-stacking interaction. Unspecific background staining was removed by destain solution.

Colloidal CBBG staining of polyacrylamide gels was performed by application of Roti®-Blue according to the provided manual from Carl Roth (2011). Roti®-Blue was diluted as specified with 20 % (v/v) denatured methanol (MeOH) and 60 % (v/v) Milli-Q-H_2O. Gels were soaked in diluted Roti®-Blue solution until lanes and background were saturated with blue colour. Then the gels were put into Roti®-Blue destain solution (25 % MeOH, denatured, in Milli-Q-H_2O) until the background of the gel was free of CBBG. Subsequently the gel was shaken in water to remove MeOH before scanning the image (3.7.3).

SDS gels have to be put in Roti®-Blue destain solution at least for 30 min before staining with Roti®-Blue as described above.

3.7.3 Scanned gel images

Silver or CBBG stained gels were scanned with the Bio-Imaging-System ViewPix 900 (Biostep/Epson) after staining. The settings were 600 dpi and 24 bit colour depth for coloured images and 600 dpi and 16 bit grey scale for grey scale images. File format was tiff, no compression.

Gels were sealed in foil and stored at +4°C after scan.

3.7.4 SyproRuby stain

The fluorescent stain SYPRO® Ruby binds non-covalently to basic amino acids and the polypeptide backbone (Molecular Probes Invitrogen detection technologies 2007). It is an organic complex containing ruthenium (Berggren et al. 2000). Excitation maxima are found at ~280 nm and ~450 nm. Emission maximum is at ~610 nm (Bio-Rad 2000).

2D-BN/SDS gels (3.5) were stained with fluorescent dye for subsequent quantification of the protein spots with evaluation software (Delta2D, Decodon, compare 3.11.1). Therefore, immediately after gel run, 2D-BN/SDS gels were bathed in SyproRuby fixing solution (10 % (v/v) denatured MeOH, 7 % (v/v) acetic acid (AcOH)) at least for one hour (Bio-Rad 2000). Afterwards, the gels were stained with SYPRO® Ruby protein gel stain (Invitrogen) for 3 hours followed by 10 min shaking in SyproRuby fixing solution. Subsequently, the gel was washed for 10 min in Milli-Q-H_2O.

Images were taken with a CCD camera system (luminescent image analyser LAS-3000, Fujifilm) and the accessory software Image Reader LAS-3000 2.1. The settings were: blue light, 605 nm filter, iris F=0.85, tray position 4, exposure type: increment, interval time: 10 sec. The software alarmed, when the images are oversaturated. The image, before oversaturation appeared, was saved as ".inf" and ".img" files for later quantification (compare 3.11.1) and as ".tif" file for visualisation.

After the images were taken, the gels were stained with silver (3.7.1) or wrapped in foil for storage at +4°C.

3.7.5 DIGE labelling technique

In contrary to all staining techniques mentioned before, the DIGE labelling technique has to be applied to proteins before loading and run of the polyacrylamide gel. Samples must have a pH between 8.0 to 8.5 for labelling (^{NH}*Dye*AGNOSTICS 2012). Minimal labelling of the protein sample's lysine residues with *N*-hydroxysuccinimide ester activated fluorescent dyes is applied. GE Healthcare (2005) describes that on average 1-2 % of the lysine residues of a protein are labelled. It can be found in the product guide of ^{NH}*Dye*AGNOSTICS (2012), that about 3 % of all proteins are covalently labelled with exactly one molecule of fluorescent dye. The mass of one molecule fluorescent dye is about 450 Da (GE Healthcare 2005). Usually three fluorescent dyes, emitting at different wavelengths, are used for labelling the samples which shall be compared (Table 3.16).

Table 3.16: Excitation and emission wavelengths for the different G-Dyes ([NH]*Dye*AGNOSTICS 2011)

G-Dye	excitation max	emission max
G-Dye100	498 nm	524 nm
G-Dye200	554 nm	575 nm
G-Dye300	648 nm	663 nm

This enables to load three different samples onto one gel for the gel run. G-Dye100 usually is used for labelling the internal standard (IS), which consists of all different samples, pooled at the same protein amounts. The labelled IS is loaded on each gel for normalisation to get rid of gel to gel variation. G-Dye200 and G-Dye300 are applied to the samples which shall be compared. Special is the so called "dye-swap". Each sample is at least used two times, each time labelled with a different dye (G Dye200 or G Dye300), to level out different labelling efficiencies (Karp et al. 2004). After gel run, the gels were scanned with a fluorescent imaging system (Typhoon 9400, see below).

Sample preparation

Samples were solubilised with d/p: 8g/g and final digitonin concentration of 2 % (v/v) according to 3.3.2. To prepare the samples for the fluorescent dye covalent labelling step (minimal lysine labelling), they were transferred into low retention tubes. Low retention tips were used from this point. Next, the pH was adjusted with 1.0 M potassium hydroxide (KOH) to 8.0 - 8.5 (final KOH concentration: 17.56 mM), then vortex mixed and short spun.

The necessary volume of 1 M KOH was tested in a larger reaction batch (approx. 140 µL) as follows. A defined volume of 1x solubilisation buffer, pH 7.4, was provided and using a 2 µL pipette (Pipetteman G2, Gilson) a defined volume of 1.0 M KOH was added until pH meter (CG 842, Schott, equipped with pH electrode InLabMicro, Mettler Toledo), calibrated with CertiPUR® buffer solutions pH 7.00 and pH 9.00, Merck Millipore) showed a pH of 8.5. Quadruplication verified this.

Labelling and gel run conditions

Labelling was performed according to protocol for Refraction-2D™ Labeling Kit (4G or 8G) from [NH]*Dye*AGNOSTICS with 50 µg (b. sol.) protein per 1G unit and without additional sample buffer. The samples were covered with alumina foil to avoid direct light exposure.

To the pH adjusted sample 1 µL of G-Dye working solution was added, the solution was vortex mixed and spun down. This was followed by incubation on ice for 30 min and then the reaction stopped by adding 1 µL stop solution (lysine solution in excess), mixed and short centrifugation. After 10 min incubation on ice, the samples were ready for the gel run. Gel run was performed for the first dimension as described in 3.4 and for the second dimension as outlined in 3.5 using special fluorescent free glass plates. Contact to direct light was avoided by covering the samples or the electrophoresis units with alumina foil. Gels were stored at +4°C until transport to research group of Prof. Dr. K.-D. Entian, where the fluorescent imaging system (Typhoon 9400, GE Healthcare Life Sciences) was located.

Settings Typhoon scanner and image recording

Stripes of Kapton® tape were placed as described on page p8-11 in GE Healthcare (2006) below the spacers of the gel sandwich, providing a defined space between glass plate of the gel and the surface of the scanner, which was filled with distilled water for matching refractive index. Then a Multiple Sample Scan was performed for four gels at the same time, running the software Typhoon Scanner Control. Settings: acquisition mode: fluorescence, pixel size: 100 microns, focal plane +3 mm (because of scan between glass plates of the sandwich), channel 1: filter 520BP40, blue laser 488 nm, channel 2: filter 580BP30, green laser 532 nm and channel 3: filter 670BP30, red laser 633 nm. 600 V were applied per channel.

Evaluation software

After the scan, the Typhoon Scanner Control software provided ".ds" and ".gel" files which were saved and uploaded to the evaluation software Delta2D from Decodon for 2D-gel spot quantification (see 3.11.1). To create overlaid coloured images (".tif" format) from the ".gel" files, the software tools ImageQuantTools and ImageJ have been used.

3.8 In-gel activity tests

BN PAGE was performed according to 3.4 for qualitative or quantitative in-gel activity tests of the mitochondrial OxPhos complexes I (CI: NADH: ubiquinone oxidoreductase), IV (CIV: cytochrome c oxidase) and the reverse reaction (hydrolysis of ATP) of complex V (CV: ATP synthase). Directly after gel run, the gels were washed in Milli-Q-H_2O and placed into the appropriate activity test solution. The accumulation of precipitate during in-gel activity tests can be followed by taking time dependent images. Grey scale images can be evaluated quantitatively by the software Delta2D (3.11.2). Coloured images reflect the formation of the precipitate qualitatively. Images were scanned according to 3.7.3. For CV in-gel activity test images, a black glass plate was used as background.

For CI in-gel activity test, nitrotetrazolium blue chloride (NBT) was reduced by NADH dehydrogenase and forms an insoluble blue/purple precipitate of NBT diformazan (Grandier-Vazeille and Guérin 1996) (Fig. 3.8).

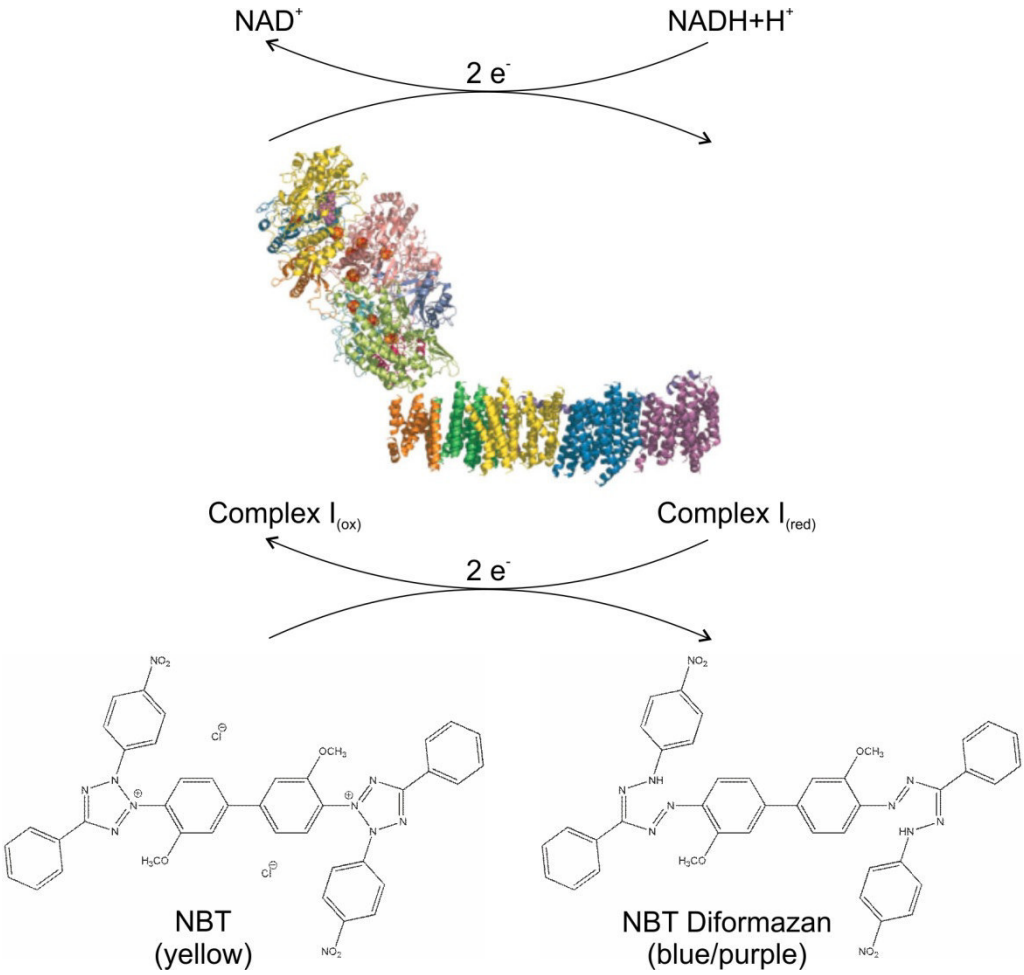

Fig. 3.8: Reactions of CI in-gel activity test, NADH dehydrogenase oxidises $NADH+H^+$ to NAD^+ and reduces yellow NBT to NBT diformazan, yielding an insoluble blue/purple precipitate. Modified: Image from the RCSB PDB (www.rcsb.org) of PDB ID 3M9S (Efremov et al. 2010), modified: structures of NBT and NBT diformazan (Sigma-Aldrich 2008), whole image modified from Heidrich (2011).

In CIV activity test, cytochrome c was oxidised by CIV. Cytochrome c is reduced by 3,3'-diaminobenzidine (DAB), which was oxidised and polymerised in parallel. A brownish precipitate was formed. The exact mechanism of this reaction is not known yet (Fig. 3.9) (Sabar et al. 2005).

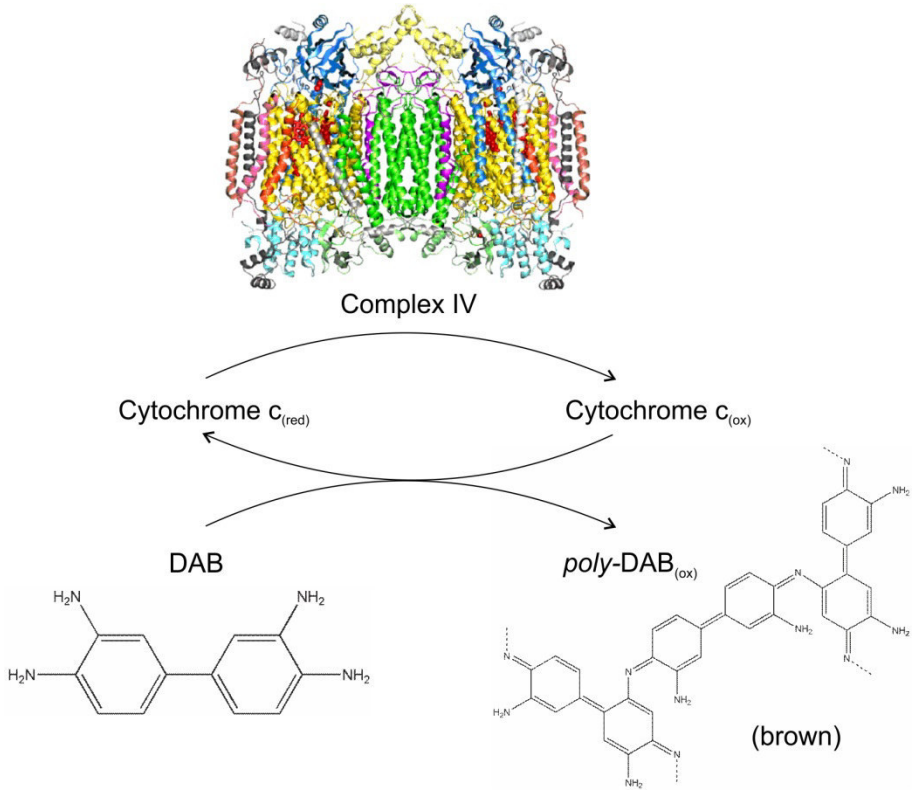

Fig. 3.9: Reactions of CIV in-gel activity test, CIV oxidises cytochrome c, which is reduced by DAB. The latter forms a brownish precipitate of polymerised and oxidised DAB. Modified: Image from the RCSB PDB (www.rcsb.org) of PDB ID 2OCC (Tsukihara et al. 1996), whole image modified from Heidrich (2011).

The hydrolysis of ATP is the reverse reaction to the energy providing function of ATP synthase (ATP synthesis) in the respiratory chain. This can be followed in-gel by the formation of white precipitate of lead phosphate evolved from the reaction of lead (II) nitrate with phosphate residues, the latter derived from the hydrolysis of ATP by CV (Fig. 3.10)(Wittig et al. 2007).

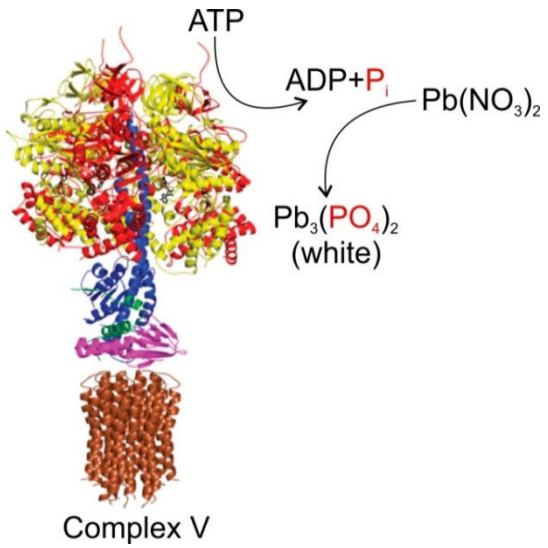

Fig. 3.10: CV in-gel activity test: reactions for hydrolysis of ATP by ATP synthase. CV hydrolises ATP to ADP+P_i. The nitrate of $Pb(NO_3)_2$ is substituted by PO_4^{3-}, forming white ($Pb_3(PO_4)_2$), which precipitates.Modified: Image from the RCSB PDB (www.rcsb.org) of PDB ID 2XND (Watt et al. 2010), whole image modified from Heidrich (2011).

3.8.1 Complex I and complex IV in-gel activity test

Immediately after BN gel run (3.4) the fresh gel was shaken for 15 min in Milli-Q-H_2O. For quantitative in-gel activity test, an image was scanned immediately (3.7.3) to serve as time point "zero". The gel was afterwards put into the activity test solution (Table 3.17) and shaken for 120 min (CI test) or 150 min (CIV test), respectively. tiff images in grey scale were taken as described in 3.7.3 at intervals listed in Table 3.18. For visualisation only, coloured images were recorded at several time-points. After the last image was taken, the gel was placed into activity test stop solution (Table 3.17) for 30 min before sealing in disposable plastic bags and storage at +4°C. The scanned images were evaluated according to 3.11.2.

Table 3.17: CI and CIV in-gel activity test solutions and activity test stop solution

Activity test solution CI			Activity test solution CIV			Activity test stop solution	
100.0 mM	Tris	} pH 7.4	50.0 mM	$Na_3PO_4x12H_2O$	} pH 7.2	50 % (v/v)	MeOH
768.0 mM	Glycine		25.0 µM	Cytochrome C		10 % (v/v)	AcOH
0.49 mM	NBT		1.58 mM	DAB			
0.1 mM	NADH						
stored at -20°C			stored at -20°C			stored at RT	

Table 3.18: Scanned time intervals for quantitative in-gel activity test

time points of image scan	
time [min]	time interval [min]
0	/
5-60	5
70-90	10
105-120	15
135-150*	15*

*(only CIV test)

3.8.2 Complex V in-gel activity test

The CV in-gel activity test was performed similar to the activity tests of complexes I and IV (3.8.1). The contents of the CV in-gel activity test solution and the stop solution are compiled in Table 3.19. The test was performed only qualitatively for identification of homooligomers. Coloured images of the gel lanes were taken (3.7.3). A black glass plate served as background for gaining better contrast to the white precipitate on the bands, exhibiting hydrolysis activity.

Table 3.19: CV in-gel activity test solution and stop solution

Activity test solution CV			CV activity test stop solution	
35.0 mM	Tris	} pH 7.8 (HNO_3)	50 % (v/v)	MeOH
270.0 mM	Glycine			
14.0 mM	$Mg(NO_3)_2x6H_2O$			
0.2% (w/v)	$Pb(NO_3)_2$			
8.0 mM	ATP			
stored at -20°C			stored at RT	

3.9 Peptide mass fingerprinting, MALDI-TOF-MS identification of protein spots

With the bioanalytical method "peptide mass fingerprinting" (PMF), protein spots of 2D gels can be identified. In order to do so, spots are cut out of the silver stained 2D-BN/SDS gel (3.5 and 3.7.1), destained and prepared for a digest with the protease trypsin. This enzyme cuts proteins selectively into defined peptides at the carboxyl side of each lysine and arginine, if the following residue is not a proline (Voet et al. 2002). The resulting peptides are eluated from the gel spots and loaded onto a target for the matrix assisted laser desorption / ionisation (MALDI) time of flight (TOF) mass spectrometry analysis. The peptides are cocrystallised with the electron transferring matrix α-Cyano-4-hydroxycinnamic acid (HCCA) at the steel target. The target is then loaded into the MALDI-TOF mass spectrometer (MALDI-TOF-MS) evacuated chamber and the analysis started. The laser of the MS excites the matrix molecules and energy and protons are transferred to the cocrystallised peptides, which are ionized and evaporated. An electric field accelerates the charged peptides before entering the evacuated TOF chamber. The ions fly with a defined velocity, depending on their mass to charge ratio (m/z) through the TOF chamber. Their needed time to pass the chamber is measured with a detector. The software calculates the specific m/z for each hitting ion and plots the intensity against the m/z in a spectrum (Lottspeich and Engels 2012). Each ionized peptide shows a specific peak, which can be identified with the help of references in databases like Mascot (Matrix Science). The peptides found in the spectra can be assigned to the proteins, which have been in the protein spot of the 2D gel. For external calibration of the system, Peptide Mass Standards Kit for Calibration (AB Sciex) is also loaded onto the target and measured (Table 3.20). Self-digested trypsin peaks serve as internal standard (Table 3.21).

18 cm by 16 cm sized 2D-BN/SDS gels were prepared according to section 3.5. 150 µg protein sample were solubilised and loaded into one well on the 1st dimension gel. After 2nd dimension gel run, the gels were stained with silver as described in section 3.7.1. The gels were wrapped in plastic bags and stored at +4°C.

Milli-Q-H_2O was used for solubilisation, for all silver stain solutions and during the complete peptide mass fingerprint procedure (see below), and apart from that, distilled water was used.

To avoid keratin contamination in all steps latex gloves and sleeve guards were worn.

3.9.1 Peptide mass fingerprinting, applied by AG Dencher, TUD

Excision of the protein containing gel spots

The 2D gel was placed onto a glass plate on a light table inside a laminar airflow cabinet. Each protein spot of interest was cut into small pieces (about 1-4 mm^3) using a scalpel and transferred into a well of a filter wellplate (MultiScreen Solvinert, Millipore) using a V-bottom 96-well polypropylene (PP) microplate (Greiner BIO-ONE) as bottom.

Destaining the protein spots

To each well of the filter wellplate, 30.0 mM potassium hexacyanoferrate (III) solution and 100.0 mM sodium thiosulphate solution (1:1) were added. The gel pieces were incubated until the brownish colour of the silver stain disappeared. Then the supernatant solution was sucked through the filter plate with a special vacuum filtration system (MultiScreen®HTS, Vacuum Manifold, Millipore) connected to a vacuum pump (Unijet II, refridgerated, equipped with Univapo 150H). The now yellow coloured gel pieces were washed with Milli-Q-H_2O once and incubated one time in Milli-Q-H_2O for 15 min, followed by multiple short washing steps with Milli-Q-H_2O until the gel pieces were free from colour.

Tryptic digest of the proteins

Before start of tryptic digest, the destained gel pieces were incubated for 20 min in 50.0 mM ammonium bicarbonate solution. The solution was removed and two incubation steps with 25.0 mM ammonium bicarbonate in 50 % (v/v) acetonitrile solution for 20 min followed. After removal of the solution, the gel pieces were incubated for 5 min in acetonitrile and dried by application of vacuum (3 in Hg vac) to the filter plate with the MultiScreen®HTS.

Trypsin solution was prepared by dissolving the lyophilised trypsin powder from Sigma in 1.0 mM hydrochloric acid (HCl, ultrapure, in Milli-Q-H_2O) resulting in a final concentration of 20 µg/mL. This trypsin solution was stored in aliquots at -20°C. The hydrochloric acid trypsin solution was diluted with 25 mM ammonium bicarbonate solution to a final concentration of 2.22 µg/mL trypsin, shortly before adding to the dried protein containing gel pieces. The gel pieces were incubated in this 2.22 µg/mL trypsin solution at +4°C for 20 min and then at +37°C for 8 hours in a thermoshaker UniEquip (Laborgerätebau- und -vertriebs GmbH).

A new V-bottom 96-well PP microplate was put beneath the filter wellplate. To extract the peptides, 1 % (v/v) trifluoroacetic acid (TFA) in 50 % (v/v) acetonitrile (ACN) was added and sonication was applied for 20 min at RT. Then the peptide solution was sucked into the V-bottom plate beneath the filter plate. (In later trials this step was replaced by using the Speed-Vak to centrifuge the solution from the filter plate into the V-bottom plate.) Afterwards, the V-bottom plate was centrifuged in the heated and evacuated Speed-Vak, until the solution evaporated completely. The peptides were resolubilised in 1 % (v/v) TFA (in Milli-Q-H_2O) by application of ultrasound.

Desalting of the peptides by using ZipTips

Resolubilised peptides were desalted by using $ZipTip_{C18}$ from Millipore. $ZipTip_{C18}$ were preconditioned by washing twice with 100 % (v/v) ACN, twice with 1 % (v/v) TFA in 50 % (v/v) ACN and twice with 0.5 % (v/v) TFA (in Milli-Q-H_2O). Peptides were bound by aspirating and dispensing of the trypsin peptide solution through the $ZipTip_{C18}$. Salts were extracted by a threefold washing step with 0.5 % (v/v) TFA (in Milli-Q-H_2O).

Extraction of peptides and loading of the target

Peptides were eluted from the $ZipTip_{C18}$ with 0.1 % (v/v) TFA in 50 % (v/v) ACN and directly placed onto the MALDI steel target (PerSeptive Biosystems). A ratio of 1:5 (v/v) matrix solution / peptide solution was added for cocrystallisation. α-Cyano-4-hydroxycinnamic acid (HCCA, 5mg/mL in 0.1 % (v/v) TFA in 50 % (v/v) ACN) was used as matrix.

For external calibration, a mixture of Calibration mixture 1 and Calibration mixture 2 (each 1:50 (v/v) in 50 % (v/v) ACN with 0.1 % (v/v) TFA) from Peptide Mass Standards Kit for Calibration of AB Sciex MALDI TOF MS (Table 3.20) was also cocrystallised with HCCA on the target.

The loaded target was dried at RT.

Table 3.20: Peptide Mass Standards Kit for Calibration of AB Sciex MALDI TOF MS

Calibration mixture 1			Calibration mixture 2		
protein	charge	monoisotopic mass [Da]	protein	charge	monoisotopic mass [Da]
des-Arg^1-Bradykinin	+1	904.4681	Angiotensin I	+1	1,296.6853
Angiotensin I	+1	1,296.6853	ACTH (1–17 clip)	+1	2,093.0867
Glu1-Fibrinopeptide B	+1	1,570.6774	ACTH (18–39 clip)	+1	2,465.1989
Neurotensin	+1	1,672.9175	ACTH (7–38 clip)	+1	3,657.9294
			Insulin (bovine)	+1	5,730.6087
				+2	2,865.8083

Internal calibration was achieved using the trypsin peaks (Table 3.21).

Table 3.21: Typical peptides and masses form self-digested trypsin, often found peptides are marked in blue (modified Schrattenholz (2001))

Peaks of trypsin self-digest		
Aminoacids	M_I	sequence
3-6	514.32	IQVR
57-64	841.50	VATVSLPR
47-56	1044.56	LSSPATLNSR
65-82	1767.79	SCAAAGTECLISGWGNTK
7-26	2210.10	LGEHNIDVLGNEQFINAAK
27-46	2282.17	IITHPNFNGNTLDNDIMLIK
27-56	3308.72	IITHPNFNGNTLDNDIMLIKLSSPATLNSR

MALDI-TOF MS Measurements

Measurements of m/z of the peptides were performed using a MALDI-TOF MS Voyager DE™-Pro, BioSpectrometry™ Workstation. The following settings were applied (Table 3.22).

Table 3.22: Settings for Voyager MALDI-TOF MS measurement

Settings for MALDI-TOF MS measurement	
instrument mode:	reflector, positive
shots / spectrum:	150
mass range / Da:	500 to 5000
low mass gate / Da:	500
calibration, matrix:	HCCA
laser intensity:	2100

Evaluation with Software / Settings

Spectra were edited with the Software Voyager Data Explorer™. Mass calibration, baseline correction and noise reduction were performed. A peak list of the monoisotopic masses was created and transferred into Mascot database search engine (Matrix Science). The settings for the search of the peptides are listed in Table 3.23.

Table 3.23: Settings for peptide identification in Mascot database

Settings for peptide identification		
Database:	SwissProt	
Enzyme:	trypsin	allow up to 1 missed cleavages
Taxonomy:	Rattus	rat brain samples
	Mammalia (mammals)	bovine heart
Fixed modifications:	none selected	
Variable modifications	Oxidation (M)	
Peptide tolerance:	± 150 ppm	
Significance threshold:	$p < 0.05$	
Mass values:	MH^+	monoisotopic

The results were copied into Excel datasheet and formatted for visualisation.

3.9.2 Peptide mass fingerprinting, applied by Proteome Analysis Unit, DDZ

Excision and destaining of the protein spots was performed at TUD. The destained spots were then transferred to the collaborating research laboratory at Deutsches Diabetes Zentrum Düsseldorf (DDZ), where tryptic digest and analysis of the peptides by MALDI-TOF/TOF-MS was carried out.

Excision of the protein containing gel spots

The gel was transferred to a glass plate on a light table inside a laminar airflow cabinet. The protein spots of interest were cut out with a skin punch (Ø 2.0 mm), which was moistened with water, and placed into a free well of a special 96-hole-wellplate (with well containing a hole at the bottom of Ø 0.8 mm). From time to time the gel and the cut gel spots were wetted with water, keeping them from drying out.

Destaining the protein spots

The wellplate with the protein spots was centrifuged with an Eppendorf 5804R, equipped with a wellplate rotor A-2-DWP at room temperature for 2 minutes at 1000 rpm to remove supernatant water. To each well 30 mM potassium hexacyanoferrate (III) solution and 100 mM sodium thiosulphate solution were added. The spots were incubated until the gel pieces were free from silver (no brownish colour). Supernatant liquid was removed by centrifugation (settings as above). The yellow gel pieces were washed with water twice. Incubation time for the first washing was one to two minutes, for the second wash 15 minutes. The one minute washing was repeated until the gel spots were colourless.

After the last centrifugation step some water was added to each well. The hole-wellplate was covered with a cover plate and a new standard 96 wellplate was placed below it. Both plates were sealed with Parafilm® for storage at +4°C until transportation (at RT) to the collaborating laboratory at DDZ, Düsseldorf, where the subsequent steps were performed.

Tryptic digest of the proteins

To prepare the tryptic digest, the gel spots were washed three times alternately with 25 mM ammonium bicarbonate solution and 25 mM ammonium bicarbonate solution containing 50 % acetonitrile. Incubation time was 10 minutes for each wash. After each washing step the supernatant liquid was removed by a 2 minute centrifugation step at 1000 rpm with an Eppendorf 5810R equipped with a wellplate rotor A-4-62 at room temperature.

After the last removal of supernatant, acetonitrile was added to each well and incubated for 10 minutes with closed cover plate. After incubation, the liquid was carefully removed with a micropipette from the dried gel pieces. The wellplate was allowed to stand without lid for 15 minutes at RT in order to let the remaining solvent evaporate.

Lyophilised trypsin (Promega) was dissolved in enclosed “Trypsin Resuspension Dilution Buffer” (1 µg/µL), incubated 15 minutes at 30°C. This solution was diluted with 25 mM ammonium bicarbonate solution containing 2 % acetonitrile resulting in a final trypsin concentration of 5 ng/µL and stored on ice bath. With that solution the protein gel spots were covered and the wellplate was capped and incubated at 4°C for 30 minutes, then left over night (at least 4 hours) at 37°C for the tryptic digest.

Extraction of peptides and loading of the target

1 % trifluoroacetic acid (TFA) solution was added to each well and incubated for 30 minutes at RT. The sample solution was loaded onto an HCCA Prespotted AnchorChip (PAC) II Target (Eppendorf) using “HCCA Affinity Preparation” technique as described by the manufacturer Bruker Daltonik (2012). After 3 min incubation of the sample solution on the target, the washing solution, consisting of 10.0 mM ammoniumphosphate monobasic in 0.1 % (v/v) TFA, was added to the sample spot. After short incubation, the whole spot was removed with a pipette.

MALDI-TOF/TOF MS measurements and evaluation with Software / Settings

Measurements of m/z of the peptides were carried out using a MALDI-TOF/TOF MS Ultraflex I from Bruker. Settings are listed in Table 3.24.

Table 3.24: Settings for MALDI-TOF/TOF MS measurement

Settings for MALDI-TOF/TOF MS measurement	
instrument mode:	reflector, positive
shots / spectrum:	sum up 600 in 100 shot steps (fuzzy logic)
mass range / Da:	680-4000, peak selection for evaluation (900 to 2300)
low mass gate / Da:	680
calibration, matrix:	PAC II, HCCA
laser frequency:	50 Hz
laser intensity:	automatically adapted by fuzzy logic control module

The PAC II target was equipped with an external calibration standard by the manufacturer Bruker Daltonik (2012) (Table 3.25). Trypsin peaks served as internal standard. Acquired spectra were calibrated and saved automatically with the software Compass 1.3 (Bruker).

Table 3.25: Masses of external calibration standard, provided on PAC II target.

PAC II Peptide Calibration Standard	
protein	monoisotopic mass [Da]
Calibrant 1	757.39916
Calibrant 2	1,046.54180
Calibrant 3	1,296.68480
Calibrant 4	1,672.91700
Calibrant 5	1,758.93261
Calibrant 6	2,016.98860
Calibrant 7	2,406.28880
Calibrant 8	2,981.58570
Calibrant 9	3,574.87650

Peaklists, formatted in ".xml", were transferred to the software ProteinScape 3.1 (Bruker), which converted the spectra into peaklists of monoisotopic masses and automatically started search in Mascot database. Search parameters are listed in Table 3.26. Evaluated data was transferred into Excel sheets and processed for visualisation.

Table 3.26: Settings for peptide identification with Bruker MALDI-TOF/TOF MS Ultraflex I

Settings for peptide identification		
Database:	SwissProt	
Enzyme:	trypsin, allow up to 1 missed cleavages	
Taxonomy:	Rattus	rat brain samples
	Mammalia (mammals)	bovine heart
Fixed modifications:	none selected	
Variable modifications:	Oxidation (M) Carbamidomethyl (C)	
Peptide tolerance:	± 100 ppm	
Significance threshold:	$p < 0.05$	
Mass values:	MH^+	monoisotopic

3.10 Western blot analysis of OxPhos complexes

The method for Western blot (WB) analysis of proteins on 2D-BN/SDS gels was established in our laboratory by Dipl. Biochem. Victoria Decker together with her bachelor student Stefanie Eckes and her internship student Elisabeth Krämer.

M. Sc. Olga Ankudin performed the WB analysis of the RBM on her own as contract work. I provided her with isolated RBM from cerebellum (OAL) for solubilisation (with d/p: 8g/g, 3.3.1), followed by 2D-BN/SDS PAGE with 10.0 cm by 10.5 cm sized 2D-BN/SDS gels (3.5). As protein standards, MagicMark™ XP Western Protein Standard (MM, 3 µL) was loaded additionally to LMW (2 µL, Table 3.2) into the well of 2D-BN/SDS gels. After PAGE, M. Sc. Ankudin performed WB as follows:

Nitrocellulose membrane and Rotilabo®-blotting paper (two pieces) were cut according to the size of the 2D-BN/SDS gel (the blotting paper: +3 mm extra in horizontal and vertical dimensions). Membrane and papers were wetted in Towbin buffer (Table 3.27) and gel as well as membrane were sandwiched and placed between anode and cathode of the Trans-Blot® SD semi-dry electrophoretic transfer cell (BioRad) for protein transfer at 20 V, 400 mA, for one hour. After finished protein transfer, incubation of the membrane with primary (Table 3.28) and secondary (Table 3.29) antibody solutions and washing steps were performed on a shaker as in Table 3.30.

Table 3.27: Towbin buffer and PBST buffer for WB analysis

Towbin buffer			Phosphate buffered saline Tween (PBST)	
25.0 mM	Tris	} pH 7.4	140 mM	NaCl
192.0 mM	Glycine		10 mM	Na_2HPO_4
20 % (v/v)	MeOH		2.7 mM	KCl
			2.0 mM	KH_2PO_4
stored at RT			0.1 % (w/v)	Tween® 20
			pH 7.4 (HCl), stored at RT	

Table 3.28: Primary antibodies for WB analysis of OxPhos complexes

target protein	target name as in UniProt database	host species	concentration [µg/mL]
α NDUFS1 (CI)	NDUS1	rabbit	1.0
α SDHA (CII)	DHSA	mouse	0.1
α UQCRC2 (CIII)	QCR2	mouse	1.0
α MTCO1 (CIV)	COX1	mouse	0.5
α OxPhos V subunit alpha (CV)	ATPA	mouse	1.0

Table 3.29: Secondary antibodies for WB analysis

conjugate	target protein	host species	concentration [µg/mL]
IgG-HRP	α rabbit	donkey	0.4
IgG-HRP	α mouse	donkey	0.4

Table 3.30: Incubation steps of nitrocellulose membrane for WB analysis of OxPhos complexes

n times	time [min]	incubation solution	condition
1	30	1:10 diluted Roti®-Block (10x concentrate)	RT
1	over night	primary antibody solution (Table 3.28)	+4°C
3	5	PBST (Table 3.27)	RT
1	120	secondary antibody solution (Table 3.29)	RT
3	5	PBST (Table 3.27)	RT

Enhanced chemiluminescence (ECL, Table 3.31) reaction (Haan and Behrmann 2007) of immune globuline G horseradish peroxidase (IgG-HRP) conjugated secondary antibody enabled the protein detection. Images were taken with the CCD camera system (luminescent image analyser LAS-3000, Fujifilm) and the accessory software Image Reader LAS-3000 2.1. The settings were: light none, filter blank, iris F=0.85, tray position 1, exposure type: increment, interval time: 10 sec. The software alarmed, when the images were oversaturated. The image, before oversaturation appeared, was saved as ".tif" file.

Table 3.31: ECL reagent for protein detection for WB analysis

reagent for enhanced chemiluminescence of HRP		
100 mM	Tris	}pH 8.8 (HCl)
1.25 mM	Luminol in DMSO	
2.0 mM	4-iodophenylboronic acid	
30 % (v/v)	Hydrogenperoxide	

The membrane of CI WB analysis was stripped once for subsequent analysis of CII. Stripping of the membrane was performed as in Table 3.32, followed by washing and incubation steps as listed in Table 3.30.

Table 3.32: Steps of membrane stripping for WB analysis

n times	time [min]	incubation solution	condition
2	10	mild stripping buffer (Table 3.33)	RT
2	10	1xPBS (same as PBST without Tween® 20)	RT
2	5	PBST (Table 3.27)	RT
1	30	1:10 diluted Roti®-Block (10x concentrate)	RT

Table 3.33: Mild stripping buffer for stripping of WB membrane

mild stripping buffer		
200 mM	Glycine	} pH 2.2 (HCl)
0.1 % (w/v)	SDS	
1.0 % (v/v)	Tween® 20	

3.11 Quantitative analysis of protein bands/spots on gels

For quantitation of gel images, it is important to note that the printed images in this publication differ optically from the evaluated original grey scale images, as obtained from scanning system "Bio-Imaging-System ViewPix 900" (3.7.3) or CCD camera "LAS-3000" (3.7.4) or fluorescent imaging system "Typhoon 9400" (3.7.5). The differences originate from losses of resolution due to saving, use of coloured images for visualisation instead of grey scale images and lower print quality. Even the "fused image" obtained from the software "Delta2D" (3.11.1 and 3.11.2) does not reflect the original staining intensities, it is just a tool for visualisation on screen.

3.11.1 Quantitative evaluation of 2D-BN/SDS gels

SyproRuby, CBBG and silver stained gels

Samples were solubilised as described in 3.3.1. 18 cm by 16 cm sized 2D-BN/SDS gels were prepared according to 3.5 and stained with SyproRuby (3.7.4), CBBG (3.7.2) or silver (3.7.1). Images of SyproRuby stained gels were gained from CCD camera system, LAS-3000 (3.7.4), CBBG and silver stained gel images from Bio-Imaging-System ViewPix 900 (3.7.3).

DIGE gels

After solubilisation (3.3.2), proteins were labelled (3.7.5), and according to 3.5 18 cm by 16 cm sized 2D-BN/SDS gels were prepared. After gel run, images were scanned by me at the research group of Prof. Dr. K.-D. Entian, who provided the fluorescent imaging system (Typhoon 9400), for details see 3.7.5.

Evaluation of 2D-BN/SDS gels with Delta2D

The protein spots were quantified with the software Delta2D 4.3 from Decodon. Gel images from one project, such as all 2D-gels from one rat brain region, were imported into the software as described by the software provider in the guidelines "Getting Started" by Decodon (2011a) and "Getting Started DIGE" by Decodon (2011b). Gel images were grouped and warped. During warping, a connection via mathematical vectors between identical protein spots of different gels is generated. A fusion image of all gels, based on the warping, was created by forming an overlay. In this fusion image, a set of gel spots was marked and each spot labelled with a number. This set of labelled spots was transferred to all single gel images. The software calculates the grey values within the area of a marked protein spot. Protein spots are illustrated as 3D spots. As example for the evaluation, one spot of a silver stained gel (subunit COX1) is depicted in Fig. 3.11A. The same spot, but from previous SyproRuby staining of that gel, is visible as 3D spot, as illustrated by the software Delta2D in Fig. 3.11B. The image

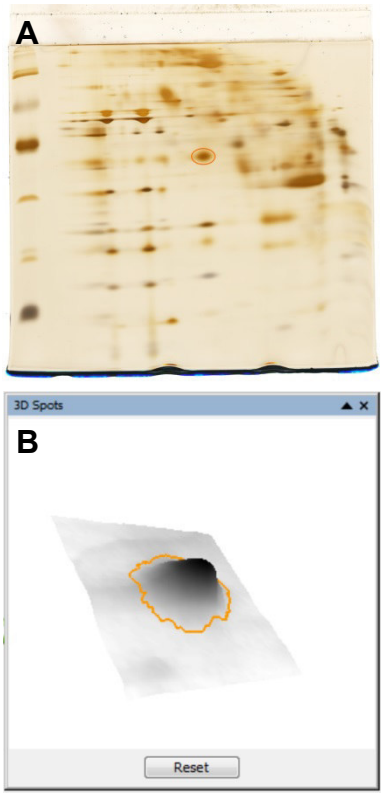

Fig. 3.11: Example for illustration of protein spots in Delta2D.
A: Image of silver stained 2D-BN/SDS gel.
B: 3D spot illustration in Rollups 3D Spots tool, Delta2D.
A & B: One spot (COX1) is marked in orange as example for the 3D illustration in Delta2D.

shows the Rollups tool 3D Spots. The quantification of the spot is achieved by calculating the absolute grey value pixel volume V of all grey value pixels from the spot. A total absolute grey value volume is calculated in the background of the software, for the whole set of marked spots of one gel. It is used for normalisation of staining differences between gels by calculating the ratio from the absolute grey value pixel volume V of one spot to the total absolute grey value pixel volume V of all spots. This evaluation results for each spot in the value "V %", the relative grey value pixel volume. These relative grey units are directly proportional to the protein amount of the spot. Delta2D software transfers all data for each spot into an Excel sheet, for example V % and the label. Further evaluation was carried out as follows:

Evaluation of 2D-BN/SDS gels with Excel

Spot values (in V %) were combined into meaningful entities (4.2.5) e.g. ATP synthase's subunits alpha, beta, gamma, FoB1/b and Fo/O/d, representing ATP synthase monomer. The sum was calculated for each technical repeat, therefore for each 2D-BN/SDS gel. The mean and the standard error of means were calculated for all technical repeats. Statistics were performed as described in 3.11.3.

3.11.2 Quantitative evaluation of in-gel activity tests and CBBG stained BN gels

Samples were solubilised as described in 3.3.1 and separated with BN PAGE (3.4). The prepared BN gel was placed into activity test solution for respective OxPhos complexes as mentioned in 3.8 or into diluted Roti®-Blue solution as described in 3.7.2 and tiff images were recorded (3.7.3).

Evaluation of in-gel activity tests and CBBG stained BN gels with Delta2D

As described for protein spots in the guidelines of Decodon (2011a), the grey scale images of one in-gel activity test at different time points or the grey scale images of the CBBG stained BN gels were uploaded into the software Delta2D. The gel images were warped together and fused. On the fusion image, bands were detected and labelled. All detected bands and labels were transferred onto the single gel images.

As explained above for protein spots in 2D-gels (3.11.1), Delta2D calculates for each marked band likewise the absolute grey value pixel volume V. These grey units are proportional to the protein amount of the spots. For every marked band on each image, label and V were transferred into an Excel sheet for further evaluation.

Evaluation of CBBG stained BN gels with Excel

The mean and the standard error of the V values of the technical repeats were calculated for each detected band. Mean and standard error were outlined in a bar plot. Statistical evaluation was performed as described in 3.11.3.

Evaluation of in-gel activity test gels with Excel

In-gel activity tests were evaluated similar to Thilmany (2013). The growth of precipitate had to be correlated to the specific activity (a_{spec}) of the OxPhos (super-)complexes in the considered band.

The V value at time point t_0 represents the background staining of the band due to CBBG bound to the proteins from previous gel run. At this time point, precipitate from the activity test solution has not yet formed, which means that the CBBG staining originates only from the staining of the protein amount in the band. Therefore it serves also as a relative measure of protein amount.

To calculate the growth of precipitate of one band, the V value at t_0 is subtracted from the V values of the same band from all other time points t_x. The development of precipitate is proportional to the protein amount, so it needs to be divided by the protein amount of the band at t_0 to result in the specific activity per protein amount in the band:

$$a_{spec} = \frac{t_x - t_0}{t_0}$$

An additional factor (f_1) has to be considered for the specific activity of supercomplexes. In supercomplexes, the precipitate is formed only by a part of the supercomplex, namely the active subunit of the individual complex. f_1 is calculated by the quotient of the masses of the complexes and supercomplexes according to Schägger and Pfeiffer (2000) (Table 4.7). As an example for CI activity test, f_1 for the supercomplex $I_1III_2IV_2$ is calculated as follows:

$$f_1 = \frac{1000\ kDa}{1000\ kDa + 500\ kDa + 2 \cdot 200\ kDa} = \frac{1000\ kDa}{1900\ kDa},$$

but for CIV activity test: $f_1 = \frac{2 \cdot 200\ kDa}{1000\ kDa + 500\ kDa + 2 \cdot 200\ kDa} = \frac{400\ kDa}{1900\ kDa}$.

Therefore f_1 is included into the equation for calculation of the specific activity:

$$a_{spec} = \frac{t_x - t_0}{t_0 \cdot f_1}$$

Supercomplexes can contain more than one copy of CIV. Thus for CIV activity test, it is essential to divide by another factor (f_2), representing the number of copies of individual CIV to compare with the individual complex:

$$a_{spec} = \frac{t_x - t_0}{t_0 \cdot f_1 \cdot f_2}$$

The obtained V values were plotted against time and the regression line was sketched. The slope represents the specific activity in grey units per minute for each selected band.

The band of ATP synthase monomer was used as control for unspecific precipitate development. The slope of its specific activity must not increase with time for activity test of CI and CIV.

The mathematical procedure was performed for each technical repeat. Mean and standard error of the technical repeats were calculated and outlined in a bar plot. Statistics were applied according to 3.11.3.

3.11.3 Statistics

Significant changes were determined using the Excel 2010 add-in "Real Statistics Resource Pack", Release 3.5.1 by Charles Zaiontz (http://www.real-statistics.com/). The unpaired, two tailed t test for unequal variances (also called "Welch t test", GraphPad Software Inc. (1995-2014) or "Smith/Welch/Satterthwaite (SWS) test", Moser and Stevens (1992)) was performed, since it is simple to apply, it is appropriateness for small sample sizes, due to the fact that no previous test routine is needed and because of its robustness. According to de Winter (2013) small sample sizes are feasible in t tests when the effect size is large. The t test for unequal variances is recommended by Moser and Stevens (1992) for equal sample sizes. They state that the SWS test and the t test "[…] all have the same sizes and powers whenever the sample sizes are equal. Therefore, a preliminary variance test is superfluous, as it simply adds an extra analysis step. Thus, in the equal sample size case, either the t test or the SWS test is appropriate." The GraphPad Statistics Guide (GraphPad Software Inc. 1995-2014) describes for the standard unpaired t test and the unequal variance t test: "When the two groups have the same sample size, the standard error is identical for the two t tests." Another reason for choosing the t test for unequal variances is its robustness against small violations of assumptions (particularly normal distribution) as Weiß (2013) states: "[…] *t*-Tests [sind] robust: Wie mit Monte-Carlo Studien nachgewiesen wurde, sind geringfügige Verletzungen der Prämissen (insbesondere der Normalverteilung) tolerierbar."

The null hypothesis H_0 is based on the assumption that there are no changes between both samples ($\mu_1^2 = \mu_2^2$). The null hypothesis is rejected, when $p < \alpha$ (0.05) (statistically significant (stat. sig.), marked with "*"), or if $p < \alpha$ (0.01) (statistically highly significant (stat. high. sig.), marked with "**") in the bar plots. The latter stand for the mean of the technical repeats and the error bars show the standard error of means.

Changes were marked in text with (not stat. sig.), when error bars of the compared samples in bar plots do not overlap along the lines of Cumming et al. (2007).

3.12 Measurement of mitochondrial membrane “fluidity”

M. Sc. Stefanie Kern carried out all anisotropy measurements and evaluations during and after her master thesis. For details of the measurement and evaluations see Kern (2013). As samples I provided her with isolated mitochondria of the rat brain parts cerebellum, cerebrum and hippocampus as described in 2.6.1.

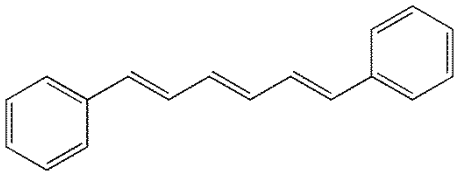

Fig. 3.12: Structure of 1,6-diphenyl-1,3,5-hexatriene (DPH), (Sigma-Aldrich 2014a)

For the analysis of the membrane “fluidity” of mitochondria, the fluorescence probe, 1,6-diphenyl-1,3,5-hexatriene (DPH, Fig. 3.12), was intercalated into the hydrophobic domain of membranes of mitochondria. For this purpose, a stock of 2.0 mM DPH (Sigma-Aldrich) in tetrahydrofuran (THF) was diluted with phosphate buffered saline (PBS, Table 3.34) and stirred in the dark at 42°C for evaporation of THF. The final concentration of DPH in PBS was 10.0 µM. Intercalation was possible by incubation of the mitochondria with the fluorescence probe DPH in PBS for one hour in the dark (composition as in Table 3.34, anisotropy labelling mixture).

Table 3.34: Solutions for fluorescence anisotropy measurement

Phosphate buffered saline (PBS)		Anisotropy labelling mixture	
140 mM	NaCl	86.0 nM ≡ 0.02 ng/µL	DPH
8.1 mM	Na_2HPO_4	0.01 µg/µL	mitochondria
2.7 mM	KCl	in	PBS
1.5 mM	KH_2PO_4	1.25 mL	total volume
pH 7.4 (HCl), stored at RT			

The steady-state fluorescence polarisation was measured, resulting in general information on the physical state of the lipid phase of mitochondrial membranes (Shinitzky and Barenholz 1978). Assuming that the anisotropy r of DPH is proportional to the order parameter and the viscosity of the surrounding membrane (Heyn 1979), and viscosity is inversely proportional to the “fluidity” of the membrane (Eckmann et al. 2014), changes of anisotropy can be oversimplified interpreted as changes of membrane “fluidity”.

A PTI M III fluorescence spectrometer (Photon Technology International) in T-configuration was used by S. Kern for the measurements. For temperature control, a waterbath (Lauda RCS, RC20 from mgw) at 37°C was connected to the sample holder. The measurement was repeated ten-times in a 4 x 10 mm (emission x excitation) quartz cuvette (SUPRASIL, Hellma Analytics). The analysis was performed with the software Felix (Photon Technology International) in the acquisition mode “timebased” with the following settings:

Table 3.35: Settings for anisotropy measurement (Kern 2013)

Settings for PTI M III fluorescence spectrometer		
Excitation:	376 nm (DPH)	
Emission 1:	455 nm (DPH)	
Emission 2:	OD 1;	KV 418
Points/sec:	1	
Duration:	10 sec.	
Repeats:	0	
Shutter:	Automatic	
Slit width:	slit 1, 2	12 nm
	slit 3	2 nm
	slit 4, 5	6 nm
Voltage range:	detector A	1050 V - 1150 V
	detector B	650-700 V

Excitation was performed with vertically polarised (V) monochromatic light and the emission intensity I was measured horizontally (H) and vertically (V). The anisotropy r can then be calculated with the equation $r = \frac{I_{VV} - G \cdot I_{VH}}{I_{VV} + 2G \cdot I_{VH}}$ with the G-factor of the instrument $G = \frac{I_{HV}}{I_{HH}}$.

I_{HH}: polarizer horizontal, analyser horizontal; I_{HV}: polarizer horizontal, analyser vertical; I_{VH}: polarizer vertical, analyser horizontal; I_{VV}: polarizer vertical, analyser vertical

Before each measurement of the anisotropy r, the G-factor of the instrument was determined (Kern 2013). Evaluation was performed with Microsoft Office 2007 (Excel) by Stefanie Kern as described (Kern 2013).

4 Results and discussion

4.1 Comparison of methods for protein quantitation in 2D-BN/SDS gels

For quantitation of protein amount after separation with 2D-BN/SDS PAGE, different methods were applied as explained in 3.7 and compared. Together with my practical course student B. Sc. Stefanie Kern, I prepared and stained the gels. Quantitation was performed by me. A few results were previously shown at my posters at Molecular Life Sciences 2013, Int. Symposium of the GBM in Frankfurt am Main, Germany, at GBS Jahrestagung 2013 in Darmstadt, Germany and at GDCH Wissenschaftsforum Chemie 2013, in Darmstadt, Germany.

For each staining method (CBBG, SyproRuby and silver), 100 µg BHM protein were solubilised with a d/p ratio of 3 respectively 6g/g (3.3.1). After solubilisation the mitochondrial proteins were separated by 2D-BN/SDS PAGE (3.5) on 18 cm by 16 cm sized gels. After PAGE, the gels were stained with CBBG (3.7.2), SyproRuby (3.7.4) or silver (3.7.1) and grey-scale images were recorded (see 3.7.3 for scanned images of CBBG and silver stained images and 3.7.4 for images from CCD camera of gels stained with fluorescent dye SyproRuby).

For DIGE experiment, 75 µg of BHM protein were solubilised with a ratio of d/p: 3 respectively 6g/g. Thereof 50 µg (b. sol.) were labelled with G-200 and 50 µg (b. sol.) with G-300, while 25 µg (b. sol.) of each sample were combined and labelled with G-100 as internal standard (IS) (3.7.5). Thereafter separation by 2D-BN/SDS PAGE followed, and grey scale images had been taken (3.7.5 for DIGE images from fluorescent imaging system).

Please keep in mind, that printed gel images, as presented below, differ from quantitatively analysed original grey scale images (as explained in 3.11).

In Fig. 4.1A the images of the CBBG and in Fig. 4.1B the images of the silver stained gels are depicted. Fig. 4.1A1 and Fig. 4.1B1 show the images of the gels from solubilisation with d/p: 3g/g BHM, and Fig. 4.1A2 and Fig. 4.1B2 with d/p: 6g/g.

By eye, differences are visible for ATP synthase subunit alpha and beta for the dimer (marked with orange rectangle). Both spots appear to be more intense in CBBG stained gel image after sol. with d/p: 6g/g BHM than for d/p: 3g/g and vice versa for the SyproRuby stained gel images. Different background staining of the two CBBG stained gel images is visible, but in case of quantitation the software Delta2D provides a tool for background substraction (3.11). Quantitation in spite of different migration pattern of the protein spots is possible by warping the gels (3.11).

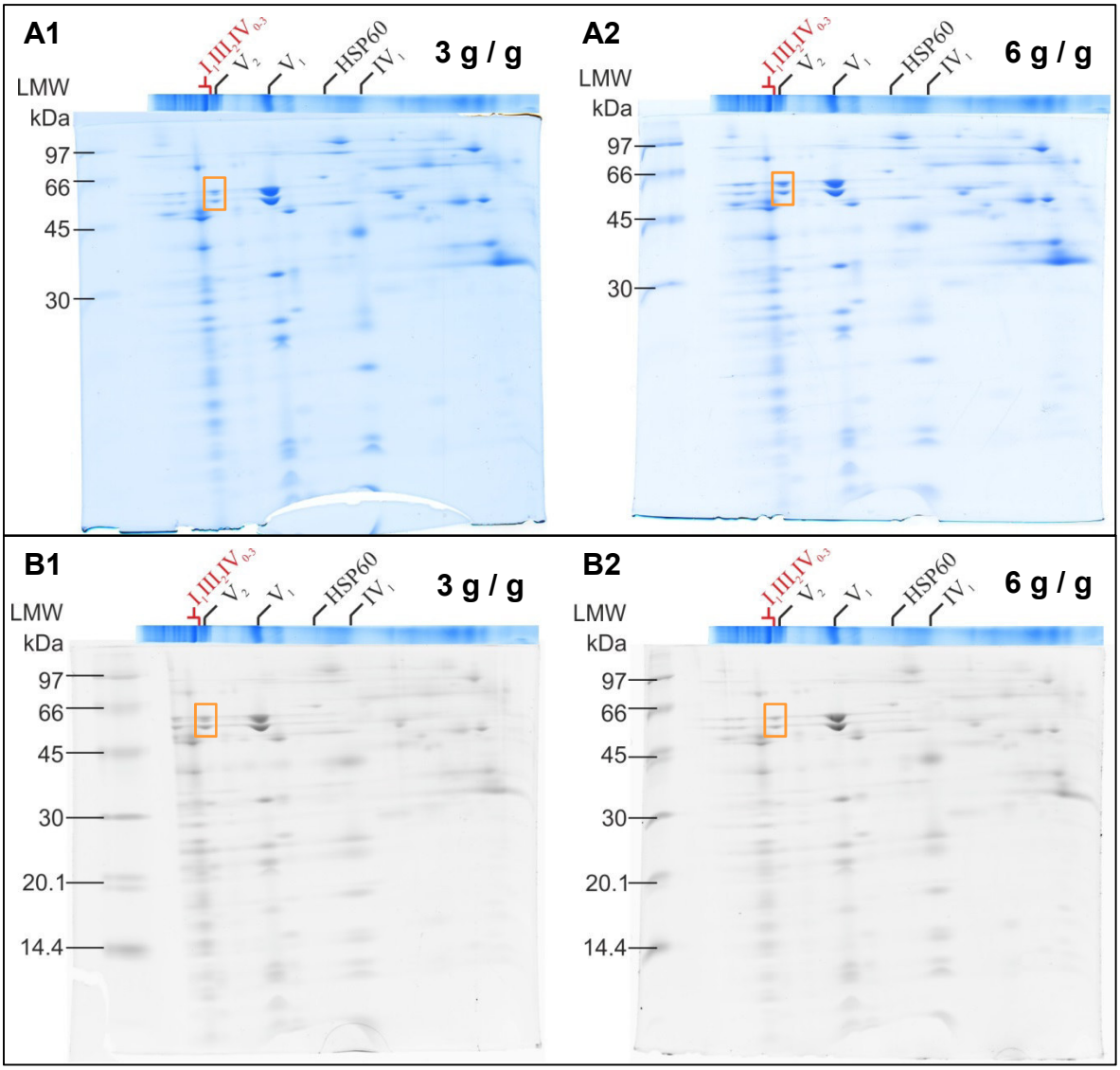

Fig. 4.1: Images of CBBG and SyproRuby stained 2D-BN/SDS gels. For each gel 100 µg (b. sol. d/p: 3 respectively 6g/g) BHM were separated by 2D-BN/SDS PAGE (18 cm by 16 cm sized gels) and stained with CBBG or SyproRuby for comparison. **A1:** BHM, d/p: 3g/g, CBBG stained **A2:** BHM, d/p: 6g/g, CBBG stained **B1:** BHM, d/p: 3g/g, SyproRuby stained **B2:** BHM, d/p: 6g/g, SyproRuby stained
The image of the CBBG stained BN gel lane was arranged horizontally above the 2D-BN/SDS gel images for assignment of bands. LMW was marked. Subunits alpha and beta of ATP synthase dimer were marked with orange rectangle.

In Fig. 4.2A the images of the DIGE gels are depicted and in Fig. 4.2B the images of the silver stained gels. In Fig. 4.2A1 the gel image of BHM, sol. with d/p: 3g/g and labelled with G-200 is depicted, while in Fig. 4.2A2 the gel image of BHM, sol. with d/p: 6g/g and labelled with G-300 is shown. In Fig. 4.2A3 the internal standard (IS), labelled with G-100, is depicted. In Fig. 4.2A4 the overlay of all three images is shown. As already observed for SyproRuby stained gels (Fig. 4.1), both spots of subunits alpha and beta of ATP synthase dimer (marked with orange rectangle) seem to be more intense in the gel image after sol. with d/p: 3g/g BHM than for d/p: 6g/g. Increased intensity is proportional to the protein amount in protein spots. Therefore the protein amount of subunits alpha and beta of CV dimer sol. with d/p: 6 g/g is smaller than sol. with d/p: 3g/g. This can be explained by a higher amount of digitonin, leading to stronger dissociation of the dimers into monomers.

When the images of the DIGE gels are compared with images of all other stained gels, it is observable that subunit COX1 of CIV (purple rectangle in Fig. 4.2) is missing.

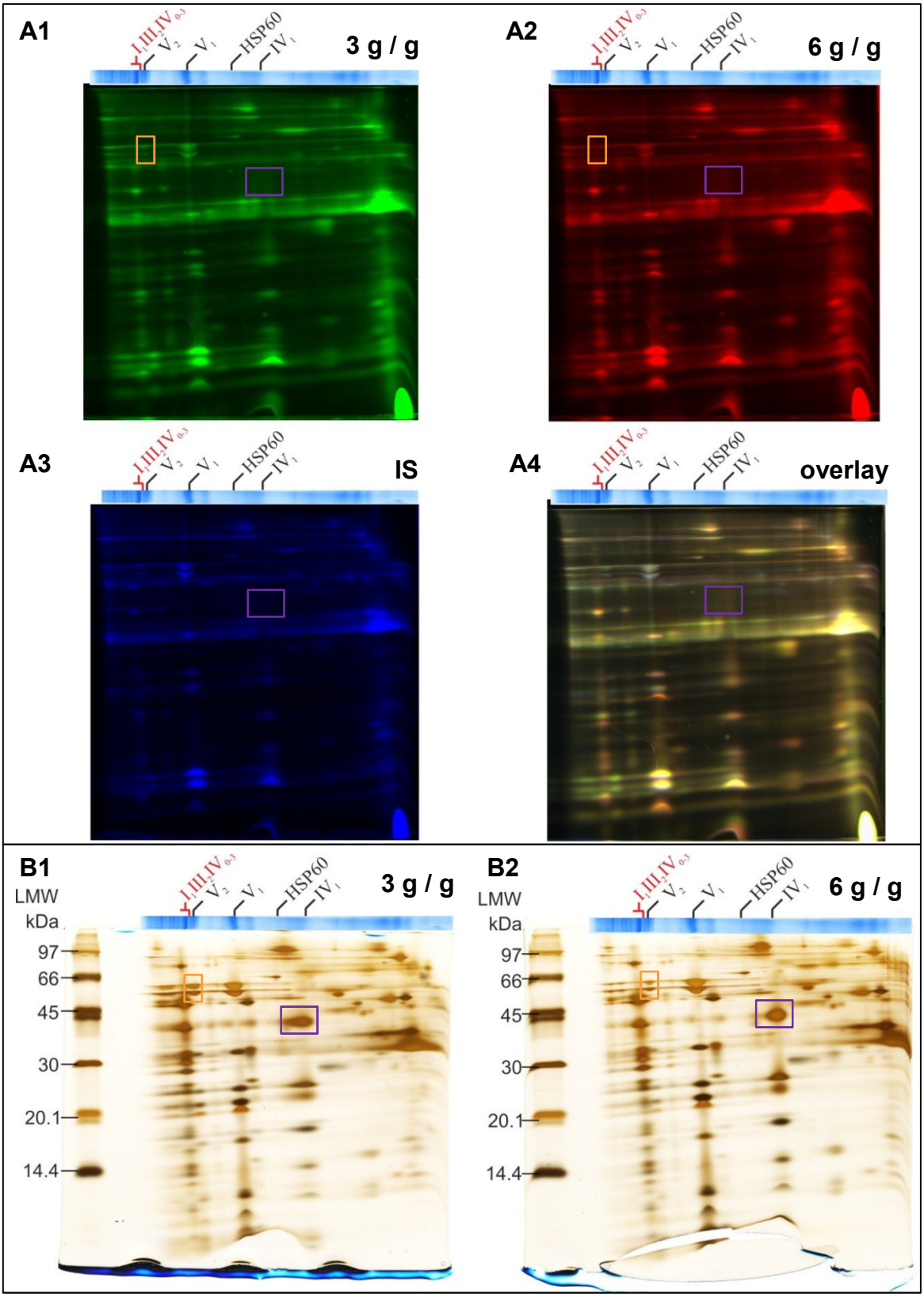

Fig. 4.2: Images of DIGE 2D-BN/SDS gels and silver stained 2D-BN/SDS gels (all 18 cm by 16 cm in size). A1-A4: DIGE gel images of the same 2D-BN/SDS gel, **A1 & A2:** 50 µg BHM each were solubilised with a d/p ratio of 3 respectively 6g/g, labelled with **G-Dye 200** or **G-Dye 300** and separated together with internal standard (IS) by 2D-BN/SDS PAGE. **A3:** Two times 25 µg BHM were solubilised with d/p: 3 and 6g/g, mixed and labelled. **G-Dye 100** served as **IS**. **A4:** Image of the overlay of images A1-A3. **B1-B2:** For each gel 100 µg BHM were solubilised and separated by 2D/BN-SDS PAGE and stained with silver. LMW was marked. **B1:** BHM, d/p: 3g/g **B2:** BHM, d/p: 6g/g BHM. The image of the CBBG stained BN gel lane was arranged horizontally above the 2D-BN/SDS gel images for assignment of bands. CV dimer, subunits alpha and beta were marked with **orange** rectangle. Subunit COX1 of CIV was marked with **purple** rectangle.

In Fig. 4.2B1 the silver stained image after sol. with d/p: 3g/g is depicted and in Fig. 4.2B2 after sol. with d/p: 6g/g. As observed for SyproRuby stained and DIGE labelled gels, both protein spots of subunits alpha and beta for ATP synthase dimer (orange rectangle) appear to be more intense in the gel image after sol. with d/p: 3g/g than for d/p: 6g/g.

In Fig. 4.3 the fused image from Delta2D of all ten analysed grey scale images for the different staining and labelling techniques is depicted. Ten proteins spots, used for quantitation, are marked in orange (Fig. 4.3) and listed in Table 4.1. Spots of CI, CIII, CIV and CV as well as the heat shock protein CH60 were selected for quantitation. The spots were identified by PMF or Western blot (see 4.2.3). The results are presented in Fig. 4.4 and Fig. 4.5.

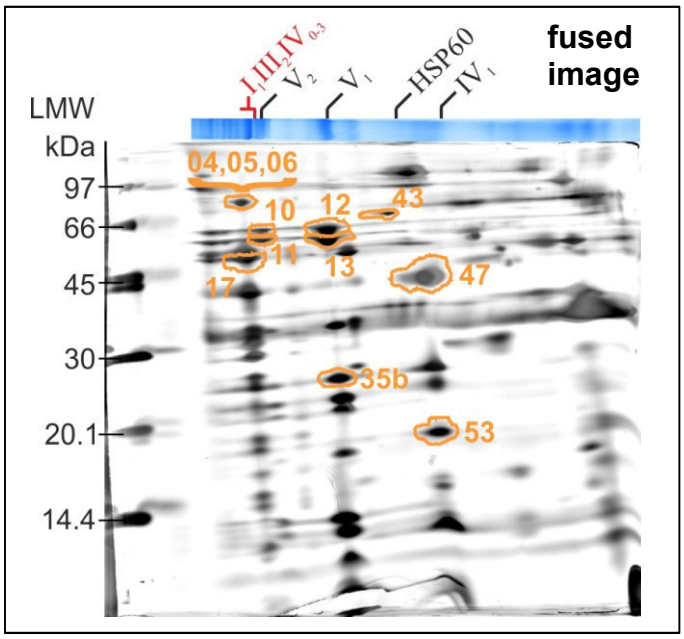

Fig. 4.3: Fused image for analysis of different staining methods. Images of CBBG, SyproRuby, silver stained and DIGE 2D-BN/SDS gels were fused for quantitation with software Delta2D. Ten spots were picked for comparison (orange). The image of the CBBG stained BN gel lane was arranged horizontally above the fused image for assignment of bands. LMW was marked.

Table 4.1: Selected protein spots for quantitative comparison of staining and labelling methods

spot no.	complex	subunit
10	CV(dimer)	alpha
11	CV(dimer)	beta
12	CV(monomer)	alpha
13	CV(monomer)	beta
35b	CV(monomer)	b
04, 05, 06	CI	NDUFS1
17	CIII	QCR2
47	CIV	COX1
53	CIV	COX4_1
43	heat shock protein	CH60

In Fig. 4.4 the intensities (in rel. grey units) for the ten analysed protein spots (Table 4.1) are depicted for each staining (CBBG, SyproRuby, silver) and labelling (DIGE) method. The intensities are directly related to the protein amount of the spot (3.11). The results for sol. with d/p: 3g/g BHM are depicted in Fig. 4.4A and for sol. with d/p: 6g/g BHM in Fig. 4.4B. It is observable that in both cases the intensities, respective protein amounts, of the DIGE spots are mostly smaller than the intensities of the other staining methods. This is also independent of the analysed OxPhos complexes.

When the various staining methods are compared, CBBG and SyproRuby staining follow mainly the same trends, while silver staining differs (as well as from trend of DIGE), for example for spot no. 12, 04, 05, 06 the intensity is lower than CBBG and SyproRuby while for 13, 35b, and 47 it is higher than for both.

When the trend of DIGE labelling is compared to the trends of the staining methods, it seems to follow the trends but the intensities are all over smaller, with the exception of spot no. 47 (COX1), whose intensity is much smaller than the intensities of all staining methods.

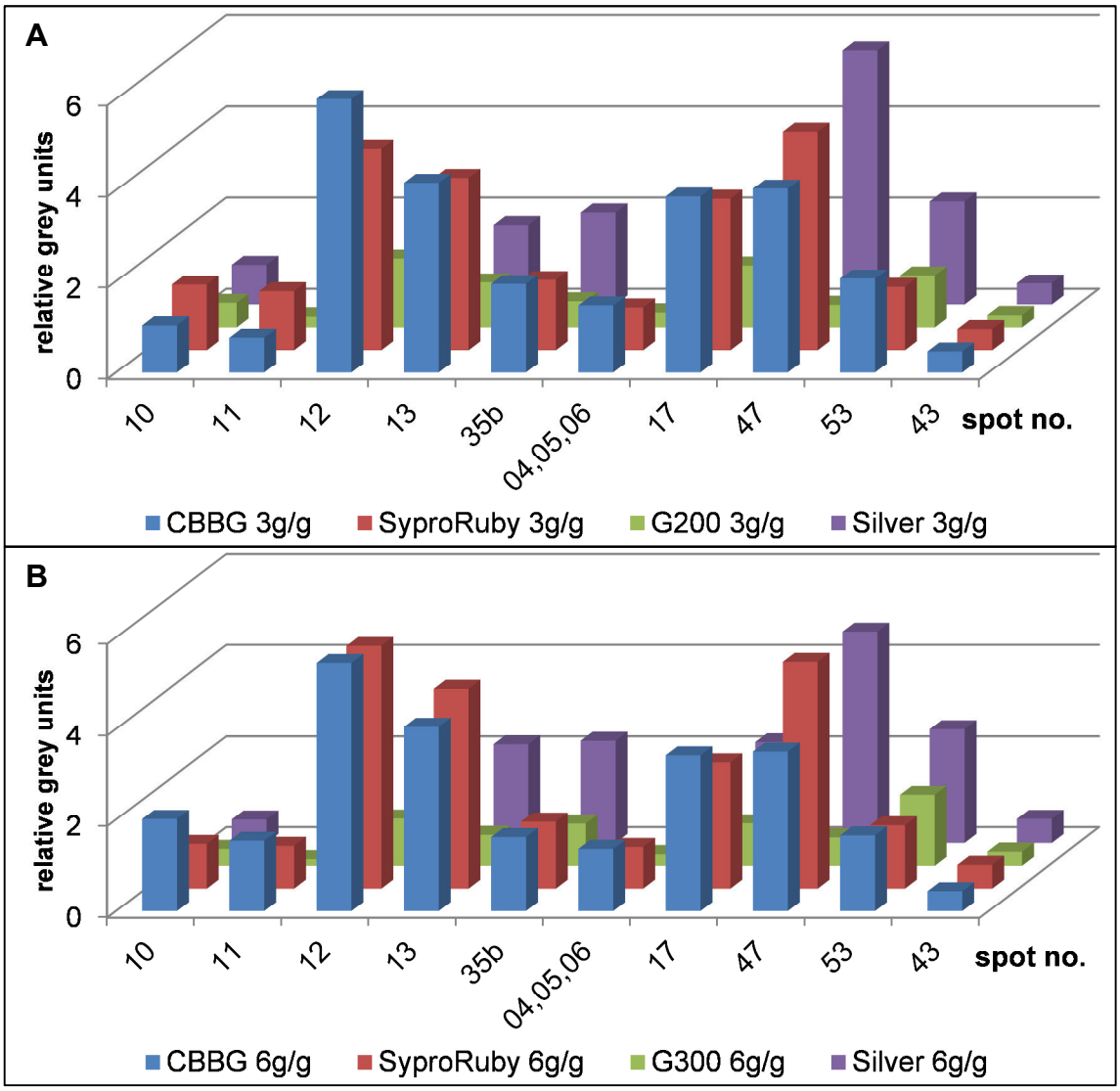

Fig. 4.4: Quantitation of ten BHM protein spots, solubilised with d/p: 3g/g or 6g/g, for different stained or labelled 2D-BN/SDS gels. Bars show intensities in rel. grey units for spots from CBBG and SyproRuby stained, DIGE (G-200 and G-300) labelled and silver stained 2D-BN/SDS gels. **A:** Results for solubilisation with 3 g dig. / g **B:** Results for solubilisation with 6 g dig. / g

Usually, quantitation is used for comparison of two different samples like treated and untreated sample or young and old sample. This should be simulated by calculating the ratios of the results from sol. with d/p: 3g/g BHM and d/p: 6g/g BHM for each spot. The results are depicted in Fig. 4.5. Provided that solubilisation and PAGE do not influence the results, the staining and labelling methods would be perfectly matchable, when the bars in Fig. 4.5 have exact the same height. This is not the case. But most of the bars are in the same range. It is noticable that for CV dimer, alpha and beta (spot no. 10 and 11) in CBBG stained gel show a much smaller ratio (about one third) than all the other visualisation methods. CBBG, SyproRuby and silver stainings seem to follow the similar trends, although CBBG shows slightly higher ratios than the other staining techniques for all spots except 10, 11 and 47. For spot 47 (CIV, COX1) silver staining shows a higher ratio. The DIGE labelling technique shows a higher ratio for CV monomer alpha and beta (spot no. 12 and 13) as well as for CI NDUFS1 (spots 04, 05, 06) and CIII QCR2 (spot no. 17) than the other staining methods. In spot no. 35b, 47, 53 and 43 the ratio for DIGE is smaller than the ratios of the other methods.

Subunits alpha and beta in monomer and dimer of CV should be present in the same amount. Therefore their comparison in Fig. 4.5 should provide another indication for the appropriateness of the staining method. The bars depicting the ratios of spot no. 10 and 11 as well as spot no. 12 and 13 should be of the same height. CBBG and SyproRuby show only slight differences in these ratios, while DIGE shows a higher difference for the ratios of spot no. 10 and 11. Silver does not show the same ratios at all. The differences between alpha and beta are large.

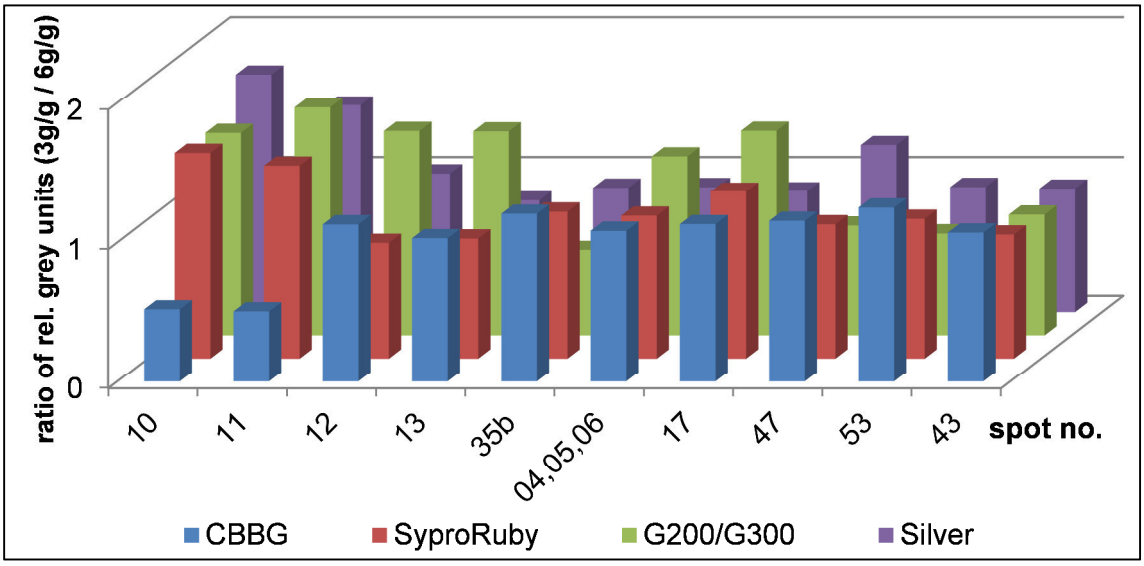

Fig. 4.5: Change detection of different solubilisation ratios for ten BHM spots for comparison of different gel staining methods. Bars show ratios (rel. grey units) of sol. with d/p: 3g/g and d/p: 6g/g for spots from CBBG and SyproRuby stained, DIGE (G-200/G-300) labelled and silver stained 2D-BN/SDS gels.

As expected, silver staining is not suitable for quantitative evaluation of protein spots. Rabilloud et al. (1994) describe in detail the mechanism of silver staining and explain, that reduction of silver ions to metallic silver is an autocatalytic process, which means, that at a spot were more silver ions are in complex with protein, the reduction is faster than at another spot with less complexed silver ions. But when too much silver ions are complexed, e.g. in the middle of a large protein spot, the reduction is faster at the borders of the spot, due to

diffusion processes, and results in a spot with light colour in the center and dark borders. The development of the silver staining is therefore irregular and not quantitative. This is observable by the deviant purple bars in Fig. 4.4 and Fig. 4.5.

It was expected that CBBG and SyproRuby staining seem to provide the most comparable results. According to Smejkal et al. (2004) both stainings seem to bind in similar way to proteins. They suppose that both bind "[…] primarily through the electrostatic interaction of protonated amines with sulfonates." From the manufacturer it is known that SyproRuby binds non-covalently to basic amino acids and the polypeptide backbone and Lottspeich and Engels (2012) provide the information that CBBG binds through charge based and hydrophobic π–π-stacking interaction to proteins. The similarity is quite good observable in Fig. 4.4A and B, however a difference becomes visible when the ratios are calculated and depicted as in Fig. 4.5 (especially for spots 10 and 11). Might be, that the different sensitivities of the stainings become important here (Table 3.14).

Finally, DIGE labelling technique gives different results. The trends are the same as for SyproRuby and CBBG staining, but with much lower all-over intensities (Fig. 4.4A and B). However, when the trends of the ratios are compared (Fig. 4.5), a quite different pattern becomes obvious. There are several reasons, which could explain this finding:

One reason could be, that a labelling step has to be performed before gel run takes place. This could have led to loss of protein amount due to additional pipetting steps or due to changed hydrophobicity of the labelled protein in the test tube, although special low retention tubes and tips were used.

Even though rather unlikely, another reason could be, that the threshold of the sensitivity had been exceeded, because only half of the amount of solubilised proteins (50 µg) were labelled with one dye and loaded on the DIGE gel for comparison with the stained gels, for which 100 µg of solubilised proteins were loaded.

Another fact is, that in acrylamide gels, the different labelling dyes show slightly unequal quantum yields for small protein spots, which effect is diminished by the application of a so called "dye-swap" (compare 3.7.5) (Karp et al. 2004). Here, the dye-swap was not applied, which could have led to errors, as reflected in Fig. 4.5.

In general, it is difficult to decide, which method is the best to visualise and quantify the protein spots in 2D gels. Each stain or label has its own characteristics for protein binding and visualisation. Certainly, a method which is reproducible and provides a linear range as well as enough large sensitivity, as SyproRuby staining or DIGE labelling, is the right way to go. It depends on the experimental setup and the analysed samples, especially on the available amount of analysable protein. However, it is important to stay with the same method for conclusions about compared analyses.

Of course, another fact for the decision is the price for the experiment. For example, when two samples should be compared to each other (three technical repeats each), how much would be the price (only for visualisation of proteins)? Assumed, the samples would be comparable in treatment with the RBM samples used in this thesis:

For SyproRuby staining six 18 cm by 16 cm sized gels would have to be prepared and stained with 750 mL of SYPRO®Ruby Protein Gel Stain (now: life technologies). 100 µg (b. sol.) of protein would be needed for each gel, in total 300 µg per sample.

For the DIGE minimal labelling technique only three 18 cm by 16 cm sized gels would have to be prepared, but the samples would have to be labelled before. Onto each gel 75 µg (b. sol.) of each protein sample would be loaded (25 µg for internal standard (IS) + 50 µg labelled with one dye), in total 225 µg of each sample for all three gels.

The list prices (homepages from 28.07.2015) for 1 L SYPRO®Ruby Protein Gel Stain (S-12000, life technologies) are 369 €, compared to 680 € for one Refraction-2D™ Labeling Kit 4G (^{NH}*Dye*AGNOSTICS). This means, calculated to the needed amount for the experiment, that SyproRuby staining would cost 276.75 € compared to 510.00 € for the DIGE labelling.

SyproRuby staining would save 233.25 €, but 75 µg of each sample would be needed extra.

The experiments for analyses of effects of ageing and calorie restriction were performed by staining with SYPRO®Ruby Protein Gel Stain, on the one hand because of the more favourable price for staining and on the other hand for the reason, that enough protein quantity was available from the analysed tissues.

The experiments for analysis of the Parkinson's model were performed with DIGE dyes, because of the only small amount of protein from the very tiny tissues substantia nigra and striatum.

4.2 Proteome changes caused by age and calorie restriction

4.2.1 Isolation of mitochondrial proteins and quantification by Bradford protein assay

Mitochondria from the rat brain areas cerebellum and hippocampus (2.6.1) were isolated according to 3.1. Weight of pooled tissue and volume of isolated mitochondrial suspension of the different animal groups (YAL: young *ad libitum*, YCR: young calorie restricted, OAL: old *ad libitum*, OCR: old calorie restricted) are listed in Table 4.2.

Table 4.2: Weight of pooled tissue and volume of isolated mitochondrial suspension from cerebellum and hippocampus for ageing and calorie restriction analysis

rats	age [months]	tissue	pooled tissue weight [g]	volume of isolated mitochondrial suspension [µL]
YAL1-5	6.5	cerebellum	1.41	2200
		hippocampus	1.06	2535
YCR1-5	6.5	cerebellum	1.30	2100
		hippocampus	0.76	2125
OAL1-6	27	cerebellum	1.70	2185
		hippocampus	1.27	2625
OCR1-6	27	cerebellum	1.61	2200
		hippocampus	0.77	2045

YAL: young *ad libitum*, YCR: young calorie restricted, OAL: old *ad libitum*, OCR: old calorie restricted

The protein quantification was performed in cuvettes with the Bradford protein assay (3.2.1). The rat brain samples of cerebellum and hippocampus were analysed as pool. Results are given in Table 4.3.

Table 4.3: Determined protein concentration of mitochondrial suspension and total protein content of hippocampus and cerebellum mitochondria

rats	age [months]	tissue	protein concentration [mg/mL]	total protein content of isolated mitochondria [mg]
YAL1-5	6.5	cerebellum	2.49	5.47
		hippocampus	5.60	14.20
YCR1-5	6.5	cerebellum	3.44	7.22
		hippocampus	5.43	11.54
OAL1-6	27	cerebellum	2.20	4.81
		hippocampus	6.08	15.89
OCR1-6	27	cerebellum	3.05	6.72
		hippocampus	6.71	13.72

Cerebrum mitochondria of each individual animal were isolated by Dr. Diksha Dani in 2009. Data are listed in Table 2.1. Dr. Dani determined the protein amount for the cerebrum samples, but the total mitochondrial protein content of cerebrum was not documented by her. However, problems with the protein quantitation occurred, for which reason Söhn (2010) calculated a correction factor, determined by SDS PAGE. To re-approve these results, the mitochondrial proteins of cerebrum of each individual animal were quantified by Bradford protein assay separately and the determined protein amounts are listed in Table 4.4.

Table 4.4: Determined protein concentration of mitochondrial suspension from cerebrum

rat	age [months]	protein concentration [mg/mL]
6.5-1 (YAL1)	6.5	3.02
6.5-2 (YAL2)	6.5	4.70
6.5-3 (YAL3)	6.5	3.27
6.5-4 (YAL4)	6.5	2.31
6.5-5 (YAL5)	6.5	2.46
6.5-1 CR (YCR1)	6.5	2.15
6.5-2 CR (YCR2)	6.5	3.74
6.5-3 CR (YCR3)	6.5	4.66
6.5-4 CR (YCR4)	6.5	3.88
6.5-5 CR (YCR5)	6.5	4.54
27M-1 (OAL1)	27	2.20
27M-2 (OAL2)	27	1.80
27M-3 (OAL3)	27	1.90
27M-4 (OAL4)	27	2.85
27M-5 (OAL5)	27	2.86
27M-6 (OAL6)	27	2.29
27M-1 CR (OCR1)	27	2.32
27M-2 CR (OCR2)	27	2.21
27M-3 CR (OCR3)	27	2.33
27M-4 CR (OCR4)	27	2.64
27M-5 CR (OCR5)	27	2.47
27M-6 CR (OCR6)	27	1.20

Deviations to the determined protein amounts of Söhn (2010) were in average at -33.0 % for single values (maxima at +11.8 % and -62.1 %). Therefore, the new protein quantitation was controlled by SDS PAGE, in addition to the quantitation of the cerebellum and hippocampus samples (see this chapter, below).

For comparison of the cerebrum samples with pooled hippocampus and pooled cerebellum samples, the identical amount in µg of each individual cerebrum mitochondria sample for each animal group (YAL; YCR; OAL, OCR) was pooled. From the individual protein concentration (Table 4.4) the mean was calculated as "pooled" protein concentration for cerebrum mitochondria (Table 4.5).

Table 4.5: Calculated protein concentration of pooled mitochondrial suspension from cerebrum

rats	age [months]	tissue	protein concentration [mg/mL]
YAL1-5	6.5	cerebrum	3.15
YCR1-5	6.5	cerebrum	3.79
OAL1-6	27	cerebrum	2.32
OCR1-6	27	cerebrum	2.19

Control of protein quantification by SDS PAGE

The results of the protein quantification with Bradford assay were controlled as described in 3.2.3. Therefor 10 µg mitochondrial protein (as determined by Bradford assay) of each RBM sample were incubated in SDS containing SDS-loading buffer and separated by SDS PAGE. The SDS gels were stained with CBBG and examined by eye.

In Fig. 4.6 images of CBBG stained SDS gels with RBM of the regions cerebellum (left gel) and hippocampus (right gel) are depicted. Cerebellum and hippocampus samples were loaded as pooled samples of each group (YAL, YCR, OAL and OCR).

Visual examination of the lanes shows similar staining intensities between the lanes of the different groups (YAL, YCR, OAL and OCR) for each respective brain region (cerebellum and hippocampus, Fig. 4.6). For the respective brain area, the staining intensities of the lanes of the four animal groups are similar.

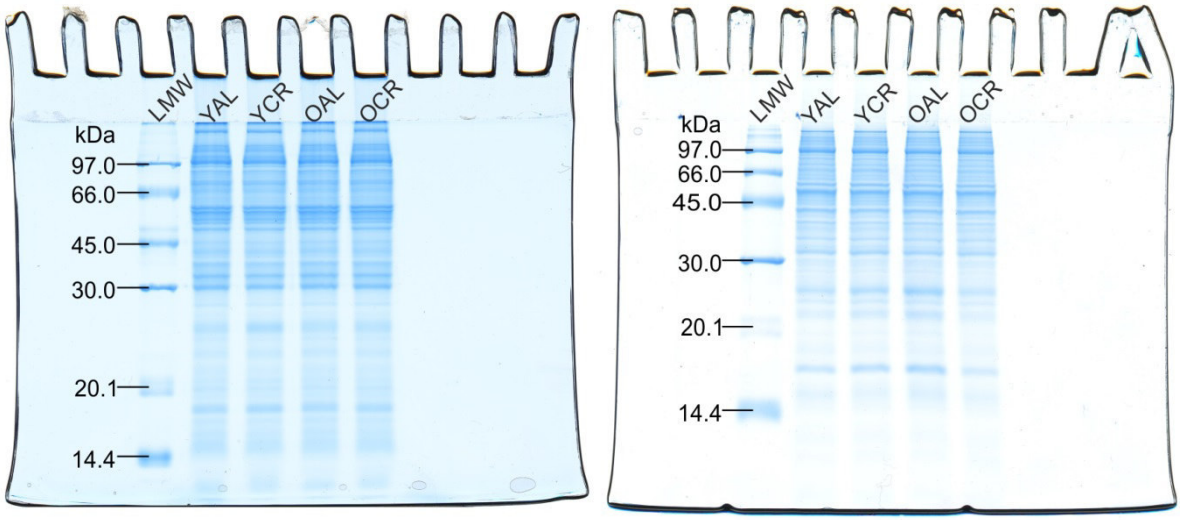

Fig. 4.6: Control of protein quantification for cerebellum and hippocampus by CBBG stained SDS gels. 10 µg (before solubilisation with SDS included in SDS loading buffer) pooled mitochondrial proteins of each group (YAL, YCR, OAL OCR) were loaded into the wells of the SDS gel. 2 µL of LMW were also loaded. **Left gel image:** cerebellum mitochondria, **right gel image:** hippocampus mitochondria. For the respective brain area, staining intensities are similar for lanes and bands.

The mitochondria from the rat brain region cerebrum were isolated from individual animal samples of the groups YAL, YCR, OAL and OCR. 10 µg of each individual sample were incubated in SDS loading buffer and loaded on SDS gels, for control of protein quantification. The images of the CBBG stained gels are shown in Fig. 4.7.

When visually compared to each other, the lanes of each individual mitochondria sample of cerebrum have similar CBBG staining intensities. Also the bands of the different samples show similar staining intensities.

Because of the similar staining intensities, an application of a correction factor as described by Söhn (2010) was not applied.

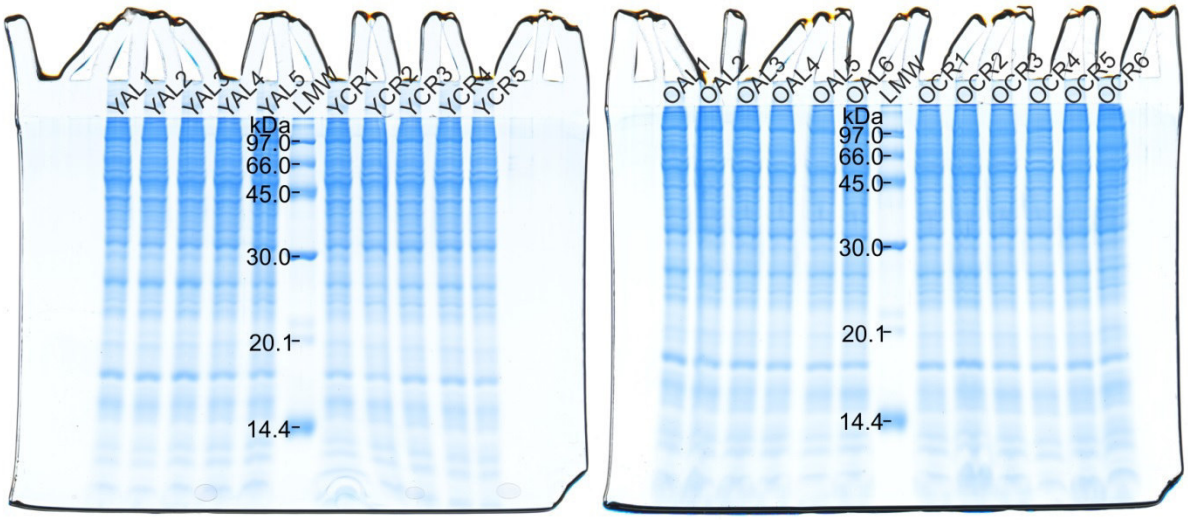

Fig. 4.7: Control of protein quantification for cerebrum by CBBG stained SDS gels. 10 µg (before solubilisation with SDS included in SDS loading buffer) mitochondrial proteins of each individual animal from the different groups (YAL, YCR, OAL OCR) were loaded into the wells of the SDS gel. 2 µL of LMW were also loaded. **Left gel image:** YAL and YCR, **Right gel image:** OAL and OCR. Similar staining intensities of bands and lanes are visible.

4.2.2 Effects of ageing and calorie restriction on body and tissue weight and amount of isolated mitochondrial proteins

In Table 4.6 the average body and tissue weight as well as the average protein content of the isolated mitochondria from the respective tissues are listed for cerebellum and hippocampus. It is observable that in average 0.4 % (w/w) mitochondrial proteins of the average tissue weight were isolated from cerebellum and 1.5 % (w/w) from hippocampus. Cerebrum mitochondria of each individual animal were isolated by Dr. Diksha Dani in 2009. Data are shown in Table 2.1. The average tissue weight before isolation of mitochondria was mathematically doubled in case of OAL and OCR samples for comparison in Table 4.6 and Fig. 4.8, because Dr. D. Dani used only cerebrum halves. The total mitochondrial protein content of cerebrum was not documented by Dr. D. Dani.

Table 4.6: Average body and tissue weight and average protein content of isolated mitochondria from cerebellum and hippocampus

animal group	age [months]	Ø body weight [g]	tissue	Ø tissue weight [g]	Ø total protein content of isolated mitochondria [mg]
YAL	6.5	360	cerebellum	0.28	1.09
			hippocampus	0.21	2.84
			cerebrum	0.99	/
YCR	6.5	215	cerebellum	0.26	1.45
			hippocampus	0.15	2.31
			cerebrum	0.90	/
OAL	27	402	cerebellum	0.28	0.80
			hippocampus	0.21	2.65
			cerebrum	0.90	/
OCR	27	253	cerebellum	0.27	1.12
			hippocampus	0.13	2.29
			cerebrum	0.87	/

In Fig. 4.8 the average body weight per animal of the analysed rats is depicted as well as the average tissue weight for cerebellum, hippocampus and cerebrum and the average total protein content for cerebellum and hippocampus. Ageing leads to increased average body weight of the animals under *ad libitum* nutrition (YAL vs. OAL, +12 %) and under calorie restriction (YCR vs. OCR, +18 %). It is observable that the average body weight decreases under short-term (YAL vs. YCR, -40 %) and long-term (OAL vs. OCR, -37 %) calorie restriction. This is similar to the findings of Matsuo et al. (1993) for Fischer rats at age of 6-9 months (young) and 28-30 months (old): YAL vs. OAL +9.4 %, YCR vs. OCR +13.3 %, YAL vs. YCR -36 % and OAL vs. OCR -33.1 %. Young animals under calorie restriction start with a lower body weight than *ad libitum* ones, but both animal groups gain approximately the same percentage of additional body weight with age.

Average tissue weight of cerebellum, hippocampus and cerebrum is decreased by ageing under *ad libitum* nutrition (YAL vs. OAL, +0 %, -1 %, -9 %). This was also observed by Coffey et al. (1992) for healthy adult humans. They found by magnetic resonance imaging that ageing is associated with diminishment of the volumes of cerebral hemispheres (0.23% per year), the frontal lobes (0.55% per year), the temporal lobes (0.28% per year), and the amygdala-hippocampal complex (0.30% per year).

Ageing under calorie restriction influences the average tissue weight of cerebellum, hippocampus and cerebrum in a different way (YCR vs. OCR, +4%, -15 %, -3 %). The decrease of hippocampus tissue is larger in animals under calorie restriction, while cerebrum is less reduced and cerebellum is even increased.

It is observable that the average tissue weight decreases under short-term (YAL vs. YCR, -8 %, -29 %, -9 %) and long-term (OAL vs. OCR, -5 %, -39 %, -3 %) calorie restriction. This seems to be related to the diminished body weight of the animals. It is noticeable that the reduction of the weight of hippocampus is much stronger than the reduction of the weight of cerebellum and cerebrum.

The reducing effect of calorie restriction on tissue weight is stronger for hippocampus of aged calorie restricted animals and is intensified by the effect of ageing as well. However long-term calorie restriction seems to compensate the reducing effect of ageing in cerebellum and cerebrum. However, also inaccurate dissection of the tissues might have contributed to the different tissue weights but the good expertise of the Goto laboratory minimizes this factor.

Average total protein content of mitochondria from cerebellum and hippocampus decreases with age under *ad libitum* nutrition (YAL vs. OAL, -27 %, -7 %) just as under calorie restriction (YCR vs. OCR, -23%, -1 %), while short-term calorie restriction (ST) (YAL vs. YCR) and long-term calorie restriction (LT) (OAL vs. OCR) increases the average total protein content of mitochondria from cerebellum (ST: +32 %, LT: +40 %) and decreases it for hippocampus (ST: -19 %, LT: -14 %). This means, that ageing has the same effects on both, *ad libitum* nourished animals and calorie restricted animals for both tissues, while in young animals under calorie restriction the amount of mitochondrial proteins in cerebellum is increased compared to those *ad libitum* nourished and stays at similar level until age of 27 months. The finding of increased mitochondrial protein amount for cerebellum is in line with the conclusion of Cerqueira et al. (2012), that a large increase of mitochondrial mass occurs under calorie restriction in their experiments on mice brain. For hippocampus, the mitochondrial proteins are decreased in young animals under calorie restriction and stay at

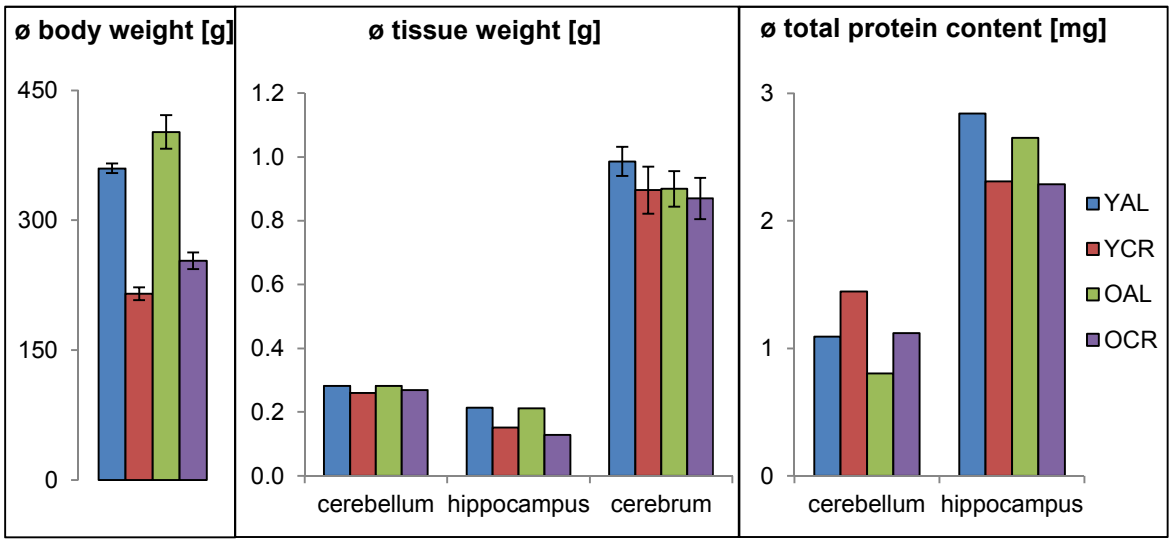

Fig. 4.8: Average body and tissue weight and average protein content. The average of the body weight from the individual animals, the average tissue weight of cerebellum, hippocampus and cerebrum and the average total mitochondrial protein content for cerebellum and hippocampus were calculated and depicted. Error bars are standard error of means from n=5 animals for YAL and YCR and n=6 for OAL and OCR. In case of cerebellum and hippocampus no standard error is given, because of pooled handling.

similar level until age of 27 months.

In Fig. 4.9 the ratio of the average tissue weight to the average body weight is depicted for cerebellum, hippocampus and cerebrum in % (w/w) (Table 4.6).

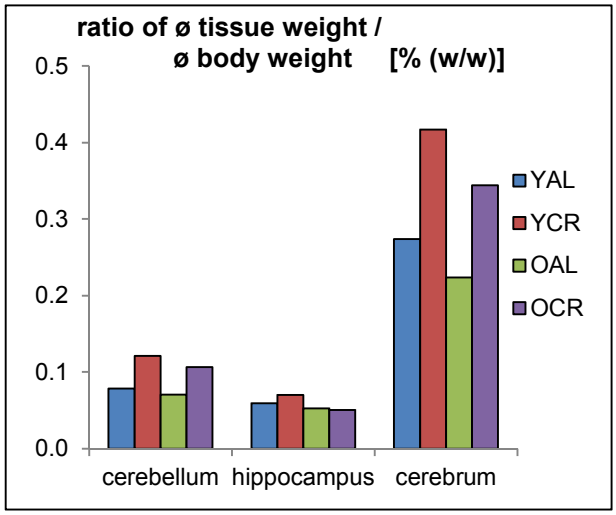

Fig. 4.9: Ratio of average tissue weight divided by average body weight in % (w/w). For cerebellum, hippocampus and cerebrum the ratios were calculated and depicted for the pooled animal groups YAL, YCR, OAL and OCR.

Ageing decreases the ratio for cerebellum and cerebrum in the same way for animals kept under *ad libitum* feeding (YAL vs. OAL, -10 %, -11 %, -18 %) and under calorie restriction (YCR vs. OCR, -12 %, -28 %, -18 %), while under calorie restriction the ratio is even more decreased for hippocampus.

Short-term calorie restriction (YAL vs. YCR) increases the ratio in all three tissues (+54 %, +19 %, +52 %) as well as long-term calorie restriction (OAL vs. OCR) for cerebellum and cerebrum (+51 %, +54 %), while for hippocampus the ratio slightly decreased (-4 %). In summary, the ratio of average tissue weight to average body weight decreases with age independently from nutrition and in all three tissues. Short-term and long-term calorie restriction show similar (increasing) effects on the ratios for all three tissues, what means, that already in young animals the changes occurred and are kept until age of 27 months.

In fact, the tissue had been frozen before analysis and this could have an influence on the tissue weight and quality of mitochondria (Frenzel 2011). Loss of tissue weight, maybe caused by loss of water, could have influenced the ratio of the average tissue weight to the average body weight to smaller values for all tissues. But the storage time and the procedure of freezing and thawing were the same for all tissues and therefore should have influenced all tissue samples in the same manner. Therefore the results can still be compared relatively to each other.

4.2.3 Identification of proteins in BN gels and 2D-BN/SDS gels

Mitochondrial proteins were solubilised (3.3) and separated by BN-PAGE (3.4), using 18 cm by 16 cm sized gels. Afterwards, the BN gel lanes were stained with CBBG (3.7.2) and by in-gel activity test solutions (3.8), for identification of the bands containing respiratory chain complex I, IV and V (CI, CIV and CV). The scanned images (3.7.3) of the lanes were compared in parallel, and the complexes of oxidative phosphorylation (OxPhos) were assigned to the bands in the BN gels as described by Schägger and Pfeiffer (2000), Schäfer et al. (2006), Wittig (2008), with the experience of the Dencher laboratory (Reifschneider 2006, Frenzel 2011, Thilmany 2013) and with the results of the PMF and WB analysis (see below). Schägger and Pfeiffer (2000) published the approximate masses for OxPhos complexes from bovine heart with ~130 kDa for complex II_1, ~200 kDa for complex IV_1, ~500 kDa for complex III_2, ~750 kDa for complex V_1 and ~1000 kDa for complex I_1. According to these values, the masses of the homo- and heterooligomers were calculated and listed in Table 4.7.

Table 4.7: Calculated approximate masses of OxPhos complexes

complex / supercomplex	mass [kDa]	complex / supercomplex	abbrev.	mass [kDa]
II_1	130	I_1IV_2		1400
IV_1	200	V_2		1500
IV_2	400	I_1III_2	a	1500
III_2	500	$I_1III_2IV_1$	b	1700
V_1	750	$I_1III_2IV_2$	c	1900
III_2IV_1	700	$I_1III_2IV_3$	d	2100
I_1	1000			

The mass standard HMW (Table 3.6) served as indication for the assignment, too. However it has to be considered, that the running behaviour of water soluble proteins, which served as standard, is different from membrane proteins.

For the identification of protein spots in 2D-BN/SDS gels, the solubilised proteins were separated by 2D-BN/SDS PAGE (3.5). The gel was stained with silver (3.7.1) before identification of the protein spots by PMF (3.9). Identified proteins are listed in following tables, sorted according to the assignment to the OxPhos complexes or different metabolic pathways, as TCA cycle, glycolysis or proteins of cellular stress management. The given colours for these groups are the same for all analysed samples. The tables contain information about the “spot no.”, as illustrated in the gel image, the “MS type”, “accession” and “protein” name, as listed in UniProt databases, molecular weight “MW” in kDa, the “Mascot Score”, identified no. of “peptides” and the protein sequence coverage “SC” in %. The “MS type” is divided into three types according to the applied method: “MS DDZ” stands for MS analysis at Deutsches Diabetes Zentrum, Düsseldorf (DDZ) and “MS/MS DDZ” for MS/MS analysis at DDZ. For both types, the method described in 3.9.2 was used. “MS TUD” reflects measurements at the TUD, where the method 3.9.1 was applied. The column “accession” contains information about the found protein subunit, abbreviated as in UniProt database and additional information about the applied taxonomy database. If spots were identified several times, they are listed for each measurement. This is indicated by more than one listed Mascot score in the table.

In general, spots of the same subunit, but from different complex assemblies, can be found in horizontal positions on the 2D gel, whereas different subunits of the same complex can be detected in vertical positions.

WB analyses of the OxPhos complexes were used as verification of the MS results.

The combination of images of BN gel lanes and 2D-BN/SDS gels gives a reliable basis for identification and assignment of bands and spots for further analysis, e.g. for quantitation.

Bovine heart mitochondria

BHM is an often used standard, therefore, the bands in BN gels and spots in 2D-BN/SDS gels were analysed and assigned first. Furthermore, the protein pattern of BHM and RBM should be compared with the aim to assign the unknown bands and spots of RBM with the help of the known bands and spots of the standard BHM.

For qualitative analysis of BN gel bands, 70 µg before solubilisation with a digitonin to protein ratio of 3 g/g (b. sol. d/p: 3g/g) of BHM were separated with BN PAGE and stained with CBBG or placed into in-gel activity test solutions for visualisation of bands containing CI, CIV and CV (hydrolysis activity of ATP synthase). Additionally a lane with HMW was loaded for CBBG staining. For the 2D-BN/SDS PAGE, 100 µg (b. sol. d/p: 3g/g) of BHM were solubilised before gel run. Afterwards the gel was stained with silver, followed by PMF.

The composed image, of stained BN gel lanes and the 2D gel image, is illustrated in Fig. 4.10. HMW (orange) is marked on the CBBG gel lane and LMW (black) on the silver stained 2D gel. Bands for the OxPhos complexes are marked from lower to higher mass range as follows: II_1, IV_1, IV_2, III_2, V_1, III_2IV_1, I_1, I_1IV_2, V_2 and supercomplexes a = I_1III_2, b = $I_1III_2IV_1$, c = $I_1III_2IV_2$ and d = $I_1III_2IV_3$. The approximate masses of the OxPhos complexes are given in Table 4.7. It is important to note, that these masses do not reflect the exact masses of the complexes according to their amino acid composition.

The protein spots are marked with diverse colours, dependent on the classification of the proteins. The legend of Fig. 4.10 presents the assignment. Subunits of **CI** are marked in **yellow**, subunits of **CII** in **pink**, subunits of **CIII** in **green**, subunits of **CIV** in **orange** and subunits of **ATP synthase (CV)** in **blue**. Proteins which could be assigned to the **TCA cycle** were coloured in **purple**, proteins of cellular **stress management** were depicted in **dark green**. **Other** proteins, which were identified, are marked in **grey**. Protein spots marked in **black** were identified by Western blot (WB) analysis by Decker (presumably 2016) or by referring to PMF of RBM (see below). This colour code is also used in the tables below, which list the identified protein spots.

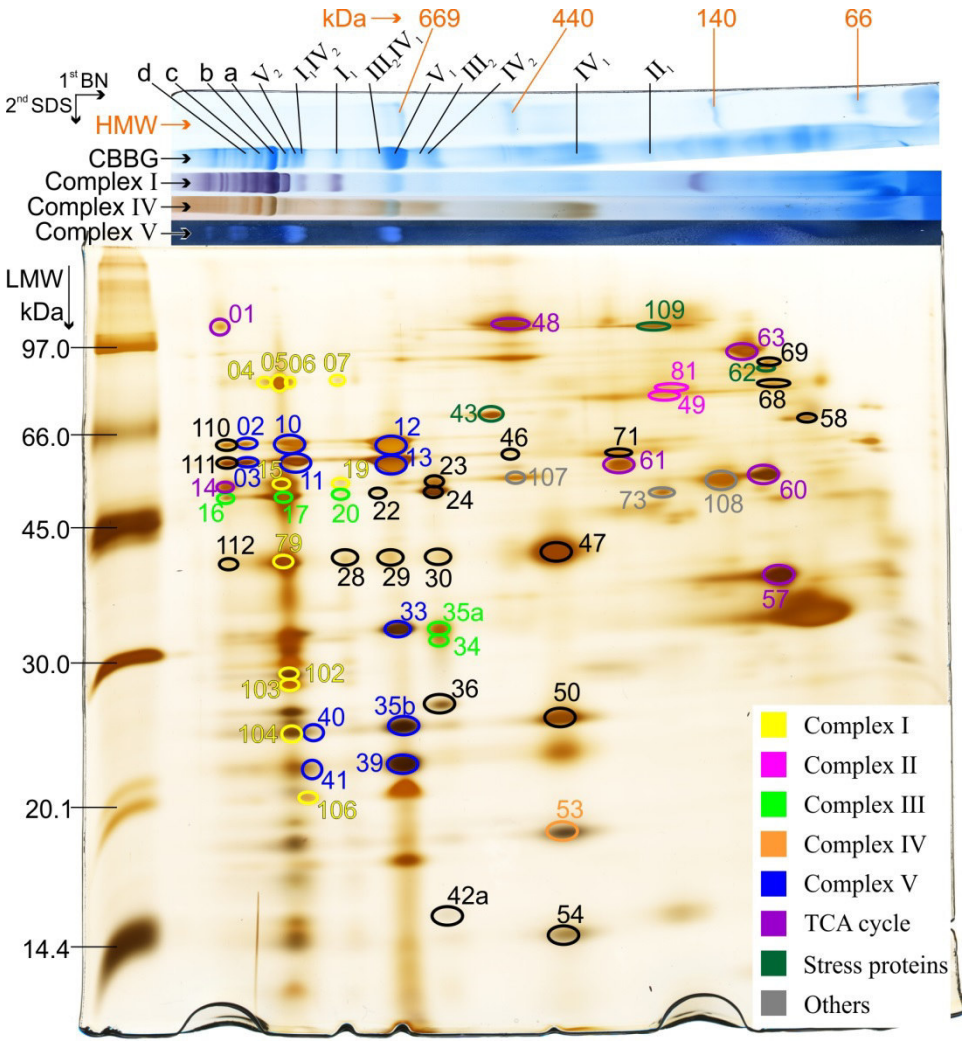

Fig. 4.10: BHM: 2D-gel for PMF analysis, 100 µg proteins of BHM (b. sol. d/p: 3g/g) were separated with 2D-BN/SDS PAGE and analysed according to 3.9. The images of the CBBG stained BN gel lane and the in-gel activity test lanes (CI, CIV and CV) (70 µg BHM each, b. sol. d/p: 3g/g) were arranged horizontal above the image of the silver stained second dimensional SDS gel for assignment of bands. Masses of LMW and HMW were marked. Identified spots were marked in colour as depicted in the legend. Spots, marked in black, were identified by WB analysis of BHM (Decker presumably 2016) or by similarity of identified protein spots of RBM (see below). a = I_1III_2, b = $I_1III_2IV_1$, c = $I_1III_2IV_2$, d = $I_1III_2IV_3$

The settings for the search in Mascot database are listed in Table 3.23 and Table 3.26. The taxonomy “Mammalia (mammals)” was chosen as search parameter in Mascot database for the analysis of BHM (3.9). Therefore the column “accession” reflects in which taxonomy database the protein was found. In most cases, “BOVIN” or “HUMAN” could be assigned. Especially in the case of MS/MS analysis, the coverage of the database for “BOVIN” is not yet sufficient, hence the search revealed successful results for “HUMAN”, as a genetically related mammal, whose database counts currently a larger number of entries. Additionally, the abbreviation for the identified subunit according to UniProt database is listed in the column “accession”. For significant MS results, the “Mascot Score” for “Mammalia” has to be greater than 61 ($p<0.05$). MS/MS results are significant, when verifying the MS result.

For CI, eleven protein spots of six different subunits could be identified, as listed in Table 4.8. Most of them seem to be located along a vertical line, originating from supercomplex $I_1III_2IV_1$. Mammalian CI consists of 45 different subunits. Seven are encoded by the mitochondrial genome (ND1, ND2, ND3, ND4, ND5, ND6 and ND4L) (Papa et al. 2012), but were not identified in this analysis of BHM.

Table 4.8: BHM: identified subunits of CI

spot no.	MS type	acces-sion	protein	MW [kDa]	Mascot Score	pep-tides	SC [%]
04	MS DDZ	NDUS1_BOVIN	NADH-ubiquinone oxidoreductase 75 kDa subunit, mitochondrial OS=Bos taurus GN=NDUFS1 PE=1 SV=1	79.4	142.0	19	38.5
	MS/MS DDZ	NDUS1_HUMAN	NADH-ubiquinone oxidoreductase 75 kDa subunit, mitochondrial OS=Homo sapiens GN=NDUFS1 PE=1 SV=3	79.4	45.5	1	2.2
05	MS DDZ	NDUS1_BOVIN	NADH-ubiquinone oxidoreductase 75 kDa subunit, mitochondrial OS=Bos taurus GN=NDUFS1 PE=1 SV=1	79.4	109.0	22	32.0
	MS/MS DDZ	NDUS1_HUMAN	NADH-ubiquinone oxidoreductase 75 kDa subunit, mitochondrial OS=Homo sapiens GN=NDUFS1 PE=1 SV=3	79.4	38.4	1	2.6
06	MS DDZ	NDUS1_BOVIN	NADH-ubiquinone oxidoreductase 75 kDa subunit, mitochondrial OS=Bos taurus GN=NDUFS1 PE=1 SV=1	79.4	82.0	16	19.4
	MS/MS DDZ	NDUS1_HUMAN	NADH-ubiquinone oxidoreductase 75 kDa subunit, mitochondrial OS=Homo sapiens GN=NDUFS1 PE=1 SV=3	79.4	52.1	1	1.7
07	MS TUD	NDUS1_BOVIN	NADH-ubiquinone oxidoreductase 75 kDa subunit, mitochondrial OS=Bos taurus GN=NDUFS1 PE=1 SV=1	79.4	131.0	18	30.0
15	MS DDZ	NDUS2_BOVIN	NADH dehydrogenase [ubiquinone] iron-sulfur protein 2, mitochondrial OS=Bos taurus GN=NDUFS2 PE=1 SV=2	52.5	79.4	17	36.7
19	MS DDZ	NDUS2_BOVIN	NADH dehydrogenase [ubiquinone] iron-sulfur protein 2, mitochondrial OS=Bos taurus GN=NDUFS2 PE=1 SV=2	52.5	75.5	16	29.6
	MS DDZ	NDUS2_HUMAN	NADH dehydrogenase [ubiquinone] iron-sulfur protein 2, mitochondrial OS=Homo sapiens GN=NDUFS2 PE=1 SV=2	52.5	65.8	16	26.3
79	MS DDZ	NDUA9_BOVIN	NADH dehydrogenase [ubiquinone] 1 alpha subcomplex subunit 9, mitochondrial OS=Bos taurus GN=NDUFA9 PE=1 SV=1	42.8	100.0	13	45.8
102	MS DDZ	NDUS3_BOVIN	NADH dehydrogenase [ubiquinone] iron-sulfur protein 3, mitochondrial OS=Bos taurus GN=NDUFS3 PE=1 SV=1	30.3	116.0	14	48.1
103	MS DDZ	NDUS3_MESAU	NADH dehydrogenase [ubiquinone] iron-sulfur protein 3, mitochondrial (Fragments) OS=Mesocricetus auratus GN=NDUFS3 PE=1 SV=1	11.1	72.9	7	66.0
104	MS/MS DDZ	NDUV2_HUMAN	NADH dehydrogenase [ubiquinone] flavoprotein 2, mitochondrial OS=Homo sapiens GN=NDUFV2 PE=1 SV=2	27.4	62.0	1	5.2
106	MS/MS DDZ	NDUB8_HUMAN	NADH dehydrogenase [ubiquinone] 1 beta subcomplex subunit 8, mitochondrial OS= Homo sapiens GN=NDUFB8 PE=1 SV=1	21.8	44.2	1	5.9

Two nearby spots of CII were identified, but only from one subunit (Table 4.9). In mammals, CII consists of four subunits, all nuclear encoded (Papa et al. 2012).

Table 4.9: BHM: identified subunits of CII

spot no.	MS type	acces-sion	protein	MW [kDa]	Mascot Score	pep-tides	SC [%]
49	MS DDZ	DHSA_ BOVIN	Succinate dehydrogenase [ubiquinone] flavoprotein subunit, mitochondrial OS=Bos taurus GN=SDHA PE=1 SV=3	72.9	71.4	13	23.3
81	MS/MS DDZ	DHSA_ HUMAN	Succinate dehydrogenase [ubiquinone] flavoprotein subunit, mitochondrial OS=Homo sapiens GN=SDHA PE=1 SV=2	72.6	59.4	1	2.1

Six spots of three different subunits from CIII were found (Table 4.10). In total the mammalian CIII is composed of eleven subunits. Only one subunit is encoded by mitochondrial genome (CYB) (Papa et al. 2012). Identified spot no. 35a belongs to CYB. Three of the identified subunits are located in a horizontal line, representing one subunit (QCR2). Spot no. 103 was identified as CY1 from CIII in MS/MS spectra, while the corresponding MS analysis identified it as NDUS3 of CI. Spot no. 103 lies on a vertical line below the supercomplex $I_1III_2IV_1$. This could indicate an association of the subunits.

Table 4.10: BHM: identified subunits of CIII

spot no.	MS type	acces-sion	protein	MW [kDa]	Mascot Score	pep-tides	SC [%]
16	MS DDZ	QCR2_ BOVIN	Cytochrome b-c1 complex subunit 2, mitochondrial OS=Bos taurus GN=UQCRC2 PE=1 SV=2	48.1	91.2	12	36.2
17	MS DDZ	QCR2_ BOVIN			102.0	11	35.1
	MS DDZ	QCR2_ BOVIN			60.0	12	33.0
20	MS DDZ	QCR2_ BOVIN			63.9	8	19.9
35a	MS/MS DDZ	CYB_ HUMAN	Cytochrome b OS=Homo sapiens GN=MT-CYB PE=1 SV=2	42.7	46.6	1	2.4
34	MS/MS DDZ	CY1_ HUMAN	Cytochrome c1, heme protein, mitochondrial OS=Homo sapiens GN=CYC1 PE=1 SV=3	35.4	68.8	1	3.7
103	MS/MS DDZ	CY1_ HUMAN			55.9	1	3.7

Only one subunit of CIV could be identified by PMF for BHM (Table 4.11). CIV in mammals has 13 subunits, three of them are encoded by mitochondrial DNA (Cox1, Cox2, Cox3) (Papa et al. 2012), but these were not identified for BHM. Four of the subunits could be assigned with the help of WBs and the analysis of RBM by PMF (see this chapter below).

Table 4.11: BHM: identified subunits of CIV

spot no.	MS type	acces-sion	protein	MW [kDa]	Mascot Score	pep-tides	SC [%]
53	MS DDZ	COX41_ BOVIN	Cytochrome c oxidase subunit 4 isoform 1, mitochondrial OS=Bos taurus GN=COX4I1 PE=1 SV=1	19.6	148.0	13	57.4

For ATP synthase (CV), eleven spots of six subunits were detected (Table 4.12). In mammals it consists of 16 different subunits, two of them are encoded by the mitochondrial genes (ATPase6, A6L) (Papa et al. 2012), but both were not identified in this analysis of BHM. ATP synthase subunit alpha and beta were identified in three spots each in a horizontal line, for monomer, dimer and next higher multimer, perhaps trimer or tetramer. Other subunits were found below the monomer and dimer in a vertical line, shifted to lower masses.

Table 4.12: BHM: identified subunits of CV

spot no.	MS type	acces-sion	protein	MW [kDa]	Mascot Score	pep-tides	SC [%]
02	MS DDZ	ATPA_ BOVIN	ATP synthase subunit alpha, mitochondrial OS=Bos taurus GN=ATP5A1 PE=1 SV=1	59.7	162.0	16	36.7
03	MS/MS DDZ	ATPB_ HUMAN	ATP synthase subunit beta, mitochondrial OS=Homo sapiens GN=ATP5B PE=1 SV=3	56.5	99.4	2	5.5
10	MS DDZ	ATPA_ BOVIN	ATP synthase subunit alpha, mitochondrial OS=Bos taurus GN=ATP5A1 PE=1 SV=1	59.7	267.0	30	51.0
	MS/MS DDZ	ATPA_ HUMAN	ATP synthase subunit alpha, mitochondrial OS=Homo sapiens GN=ATP5A1 PE=1 SV=1	59.7	41.4	1	2.9
11	MS DDZ	ATPB_ BOVIN	ATP synthase subunit beta, mitochondrial OS=Bos taurus GN=ATP5B PE=1 SV=2	56.2	70.7	12	26.1
12	MS DDZ	ATPA_ BOVIN	ATP synthase subunit alpha, mitochondrial OS=Bos taurus GN=ATP5A1 PE=1 SV=1	59.7	183.0	25	47.7
	MS/MS DDZ	ATPA_ HUMAN	ATP synthase subunit alpha, mitochondrial OS=Homo sapiens GN=ATP5A1 PE=1 SV=1	59.7	40.8	1	2.7
	MS DDZ	ATPA_ BOVIN	ATP synthase subunit alpha, mitochondrial OS=Bos taurus GN=ATP5A1 PE=1 SV=1	59.7	156.0	20	35.0
13	MS/MS DDZ	ATPB_ HUMAN	ATP synthase subunit beta, mitochondrial OS=Homo sapiens GN=ATP5B PE=1 SV=3	56.5	160.0	2	5.5
33	MS DDZ	ATPG_ BOVIN	ATP synthase subunit gamma, mitochondrial OS=Bos taurus GN=ATP5C1 PE=1 SV=3	33.1	139.0	18	42.6
	MS/MS DDZ	ATPG_ HUMAN	ATP synthase subunit gamma, mitochondrial OS=Homo sapiens GN=ATP5C1 PE=1 SV=1	33.0	47.6	1	5.0
35b	MS DDZ	AT5F1_ BOVIN	ATP synthase subunit b, mitochondrial OS=Bos taurus GN=ATP5F1 PE=1 SV=2	28.8	185.0	29	59.4
	MS/MS DDZ	AT5F1_ HUMAN	ATP synthase subunit b, mitochondrial OS=Homo sapiens GN=ATP5F1 PE=1 SV=2	28.9	69.3	1	3.1
39	MS TUD	ATP5O_ BOVIN	ATP synthase subunit O, mitochondrial OS=Bos taurus GN=ATP5O PE=1 SV=2	23.3	89.0	12	53.0
40	MS DDZ	AT5F1_ BOVIN	ATP synthase subunit b, mitochondrial OS=Bos taurus GN=ATP5F1 PE=1 SV=2	28.8	123.0	17	50.0
	MS/MS DDZ	AT5F1_ HUMAN	ATP synthase subunit b, mitochondrial OS=Homo sapiens GN=ATP5F1 PE=1 SV=2	28.9	67.0	1	3.1
41	MS DDZ	ATP5H_ BOVIN	ATP synthase subunit d, mitochondrial OS=Bos taurus GN=ATP5H PE=1 SV=2	18.7	62.8	7	38.5

In addition to the proteins of oxidative phosphorylation, proteins belonging to other metabolic pathways were identified, too.

Seven subunits or proteins belonging to the TCA cycle were identified: 2-oxoglutarate dehydrogenase (ODO1), dihydrolipoyllysine-residue succinyl-transferase (ODO2), NAD(P) transhydrogenase (NNTM), malate dehydrogenase (MDHM), citrate synthase (CISY), fumarate hydratase (FUMH) and aconitate hydratase (ACON). They are marked in purple in Fig. 4.10 and listed in Table 4.13.

Table 4.13: BHM: identified proteins of TCA cycle

spot no.	MS type	acces-sion	protein	MW [kDa]	Mascot Score	pep-tides	SC [%]
01	MS DDZ	ODO1_BOVIN	2-oxoglutarate dehydrogenase, mitochondrial OS=Bos taurus GN=OGDH PE=2 SV=1	115.7	200.0	33	30.8
14	MS DDZ	ODO2_BOVIN	Dihydrolipoyllysine-residue succinyl-transferase component of 2-oxoglutarate dehydrogenase complex, mitochondrial OS=Bos taurus GN=DLST PE=1 SV=2	48.9	92.9	19	34.5
	MS/MS DDZ	ODO2_HUMAN	Dihydrolipoyllysine-residue succinyl-transferase component of 2-oxoglutarate dehydrogenase complex, mitochondrial OS=Homo sapiens GN=DLST PE=1 SV=4	48.7	67.5	1	3.8
48	MS DDZ	NNTM_BOVIN	NAD(P) transhydrogenase, mitochondrial OS=Bos taurus GN=NNT PE=1 SV=3	113.8	158.0	28	24.7
	MS/MS DDZ	NNTM_HUMAN	NAD(P) transhydrogenase, mitochondrial OS=Homo sapiens GN=NNT PE=1 SV=3	113.8	45.2	1	1.2
57	MS DDZ	MDHM_BOVIN	Malate dehydrogenase, mitochondrial OS=Bos taurus GN=MDH2 PE=1 SV=1	35.6	85.1	10	39.6
	MS/MS DDZ	MDHM_HUMAN	Malate dehydrogenase, mitochondrial OS=Homo sapiens GN=MDH2 PE=1 SV=3	35.5	42.8	1	3.3
60	MS/MS DDZ	CISY_HUMAN	Citrate synthase, mitochondrial OS=Homo sapiens GN=CS PE=1 SV=2	51.7	109.7	2	3.9
61	MS DDZ	FUMH_PIG	Fumarate hydratase, mitochondrial OS=Sus scrofa GN=FH PE=1 SV=1	50.0	108.0	13	30.7
	MS DDZ	FUMH_MACFA	Fumarate hydratase, mitochondrial OS=Macaca fascicularis GN=FH PE=2 SV=1	54.7	96.0	12	29.8
	MS/MS DDZ	FUMH_HUMAN	Fumarate hydratase, mitochondrial OS=Homo sapiens GN=FH PE=1 SV=3	54.6	72.8	1	3.5
63	MS DDZ	ACON_BOVIN	Aconitate hydratase, mitochondrial OS=Bos taurus GN=ACO2 PE=1 SV=4	85.3	161.0	23	33.7
	MS DDZ	ACON_BOVIN			161.0	23	33.7

Three proteins of cellular stress management were identified (Table 4.14): 60 kDa heat shock protein (CH60), 78 kDa glucose-regulated protein (GRP78) and endoplasmin (ENPL).

Table 4.14: BHM: identified proteins of stress management

spot no.	MS type	acces-sion	protein	MW [kDa]	Mascot Score	pep-tides	SC [%]
43	MS DDZ	CH60_HUMAN	60 kDa heat shock protein, mitochondrial OS=Homo sapiens GN=HSPD1 PE=1 SV=2	61.0	75.8	16	27.7
62	MS DDZ	GRP78_HUMAN	78 kDa glucose-regulated protein OS=Homo sapiens GN=HSPA5 PE=1 SV=2	72.3	89.8	15	32.1
	MS/MS DDZ	GRP78_HUMAN		72.3	60.2	1	2.6
109	MS DDZ	ENPL_BOVIN	Endoplasmin OS=Bos taurus GN=HSP90B1 PE=2 SV=1	92.4	144.0	27	34.1
	MS/MS DDZ	ENPL_HUMAN	Endoplasmin OS=Homo sapiens GN=HSP90B1 PE=1 SV=1	92.4	53.6	1	1.7

A few other proteins were also identified as listed in Table 4.15. Medium-chain specific acyl-CoA dehydrogenase (ACADM) and trifunctional enzyme subunit beta (ECHB) are involved in mitochondrial fatty-acid beta oxidation (Uniprot databases). Mitochondrial $NADP^+$-dependent isocitrate dehydrogenase (IDHP) catalyses the decarboxylation of isocitrate into 2-oxoglutarate, while reducing $NADP^+$ to NADPH. NADPH is needed for regeneration of reduced glutathione in the mitochondria. Glutathione functions as antioxidant and therefore as a scavenger of ROS (Jo et al. 2001).

Table 4.15: BHM: varying identified proteins

spot no.	MS type	acces-sion	protein	MW [kDa]	Mascot Score	pep-tides	SC [%]
73	MS DDZ	ACADM_BOVIN	Medium-chain specific acyl-CoA dehydrogenase, mitochondrial OS=Bos taurus GN=ACADM PE=2 SV=1	46.5	217.0	17	43.2
107	MS DDZ	ECHB_BOVIN	Trifunctional enzyme subunit beta, mitochondrial OS=Bos taurus GN=HADHB PE=2 SV=1	51.3	113.0	17	32.4
	MS/MS DDZ	ECHB_HUMAN	Trifunctional enzyme subunit beta, mitochondrial OS=Homo sapiens GN=HADHB PE=1 SV=3	51.3	41.6	1	4.2
108	MS DDZ	IDHP_BOVIN	Isocitrate dehydrogenase [NADP], mitochondrial OS=Bos taurus GN=IDH2 PE=1 SV=2	50.7	148.0	20	40.9

From WB analysis as part of the dissertation of Decker (presumably 2016), BHM protein spot numbers 04, 05, 06 and 07 can be assigned to subunit NDUS1 from CI in line with the findings from PMF (Table 4.8). Also, the subunit DHSA of CII was identified by PMF for spots 49 and 81 (Table 4.9), which are in agreement with Decker's findings. The spot numbers 16, 17, 20, 22 and 24, could be assigned to subunit QCR2 from CIII according to Decker's WB analysis. For the spots 16, 17 and 20, this could be verified by PMF (Table 4.10). CIV subunit COX1 was not identified by PMF. However, the spot numbers 28, 29, 30, 47, 79 and 112 could be assigned to COX1 in Decker's WB analysis, as also indicated by the respective staining differences. Spot no. 79 was identified as subunit NDUA9 (from CI) by PMF (Table 4.8). For the latter, a mass of 42.8 kDa is given in UniProt database, versus 57.0 kDa for subunit COX1. Probably, the spots overlap, because spot no. 79 could be a mixture of subunits of CI and CIV, due to its origin from the supercomplex $I_1III_2IV_1$, if the vertical line is followed up to the appropriate BN gel band. For ATP synthase, the subunits alpha (spots 02, 10, 12, Table 4.12) and beta (spots 03, 11, 13, Table 4.12) were identified by PMF. This is in line with Decker's WB analysis, where the alpha subunit can be assigned to spots 02, 10, 12 and 110, and the beta subunit to spots 03, 11, 13 and 111.

Additional to the OxPhos complexes, the heat shock protein CH60 was identified in spot no. 43 by PMF (Table 4.14), which can also be found in the WB for CH60 by Decker.

Other spots, marked in black, were assigned by comparison with the results of PMF for RBM. These include spot numbers 46, 50, 54, 57, 58, 68, 69, and 71 (see below). Spots 36 and 42a were assigned by relating the results from PMF of RBM by Reifschneider et al. (2006) to the current results of RBM (see below).

Not all of the identified proteins are assumed mitochondrial (membrane) proteins. This is in line with the isolation of crude mitochondrial fraction from tissue (3.1).

Assignment of protein bands from Rat brain mitochondria in BN gels

RBM were analysed by BN PAGE and 2D-BN/SDS PAGE, using 18 cm by 16 cm sized gels. Assignment of bands in BN gels and spots in 2D gels is a pre-requisite for all further analyses, e.g. quantitation. The already assigned bands and spots of BHM, as a related mammal, served as standard for comparison (see above).

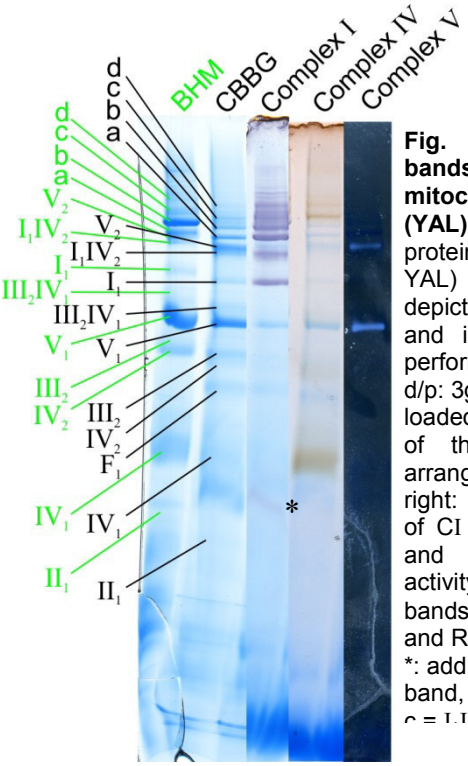

Fig. 4.11: Assignment of bands in BN gel for rat mitochondria of cerebellum (YAL), 100 µg (b. sol. d/p: 8g/g) proteins of RBM (cerebellum, YAL) were separated on each depicted lane. CBBG staining and in-gel activity tests were performed. 70 µg (b. sol. d/p: 3g/g) proteins of BHM were loaded as standard. The images of the stained lanes were arranged side by side (left to right: CBBG, in-gel activity test of CI (120 min), CIV (150 min) and CV (72 h, = hydrolysis activity of CV). Assignment of bands is given for BHM (green) and RBM (black).
*: additional unspecific stained band, a = I_1III_2, b = $I_1III_2IV_1$, c = $I_1III_2IV_2$, d = $I_1III_2IV_2$

For assignment of bands in BN gels, 100 µg (b. sol. d/p: 8g/g, 3.3.1) proteins of RBM (cerebellum, hippocampus and cerebrum) were separated by BN PAGE (3.4). After gel run, the lanes were stained with CBBG (3.7.2) or by performing in-gel activity tests of CI, CIV and CV (3.8). The latter was only applied to cerebellum mitochondria for qualitative identification of homooligomers of ATP synthase. Images were taken (3.7.3) and analysed visually.

Fig. 4.11 shows a combination of images of differently stained BN gel lanes for cerebellum mitochondria (YAL). The image of the CBBG stained gel lanes includes an additional lane with 70 µg (b. sol. d/p: 3g/g) proteins of BHM as a reference (marked in green). The other lanes show the typical blue / purple precipitate (NBT diformazan) for CI in-gel activity, the brownish precipitate (*poly*-DAB) for CIV in-gel activity and the white precipitate ($Pb_3(PO_4)_2$) for CV in-gel activity, the latter reflects the hydrolysis activity of ATP synthase. The assignment of the bands is shown in black for RBM and in green for BHM.

The lane from CV activity test depicts two distinct white bands (with blue background staining from CBBG, originated from the cathode buffer) of ATP synthase after 72 hours of staining. Due to the fact that the BN gels were gradient gels with 4 % T on top and 13 % T on the bottom, the masses of proteins should decrease from top to bottom. The band with lower mass can be assigned to the ATP synthase monomer V_1 and the one shifted to higher masses should be the dimer V_2. Both bands are also observable as distinct blueish bands in the other stained gel lanes, if followed in horizontal direction. It is apparent, that V_1 from RBM migrated approximately the same distance as V_1 from BHM, while V_2 of BHM is shifted to slightly higher mass than V_2 from RBM. A difference in intensities is visible since the band of V_1 is more intense than the one of V_2.

When hydrolysis active bands are compared with the CI in-gel activity test staining (Fig. 4.11), both bands, V_1 and V_2, can be allocated as distinct blueish bands amongst the blue / purple CI containing bands. Between V_1 and V_2, two blue / purple bands, containing active CI, could be assigned. The lower band should be complex I_1 (approx. 1000 kDa). This band is

not present in CIV in-gel activity test lane, while the upper one should be a combination of CI and IV, because it is apparent in both lanes, albeit just a slight brownish smear in CIV in-gel activity lane, which might be caused by low in-gel activity. Probably it can be assigned as supercomplex I_1IV_2, due to its mass of 1400 kDa, which is below 1500 kDa of V_2. Above the band of V_2 in CI in-gel activity test lane, there are four intense blue / purple bands allocated to the supercomplexes a = I_1III_2, b = $I_1III_2IV_1$, c = $I_1III_2IV_2$ and d = $I_1III_2IV_3$. The most intense supercomplex band in CBBG and CI in-gel activity test for RBM is the one of I_1III_2, while for BHM it is $I_1III_2IV_1$.

As expected, in CIV in-gel activity test the band of I_1III_2 exhibits just blueish staining. But unexpected was, that also the band of supercomplex $I_1III_2IV_1$ seems to lack CIV in-gel activity, because no brownish stain is observable. Referring to the quantitative analysis of CIV in-gel activity test (4.2.6), $I_1III_2IV_1$ exhibits at least slight activity, not visible by eye. Supercomplexes $I_1III_2IV_2$ and $I_1III_2IV_3$ appear as distinct bands in CIV in-gel activity test, but the one of $I_1III_2IV_2$ is the most intense distinct brownish band of that gel lane.

Additional bands with higher masses appear above the assigned supercomplex $I_1III_2IV_3$ for CI and CIV in-gel activity test. They are more distinct in CI in-gel activity test and more smeared in CIV in-gel activity test. Those could not be assigned to specific stoichiometries of complexes. Hence they were disregarded for further analysis.

Just above the blueish band of complex V_1 in CIV in-gel activity test, an additional weak brownish, smeared band is observable. It does not show CI activity. It is supposed to be III_2IV_1, according to its apparent mass (700 kDa).

Below the band of complex V_1 in CIV in-gel activity test, two more smeared brownish bands are apparent. The one with higher mass is less intense than the one with lower mass. Both cannot be found in CI in-gel activity test. By reason of their location in the gradient gel, they were assigned to the dimer IV_2 and monomer IV_1, respectively

In CI in-gel activity test, an additional band is stained in blue / purple (marked with *). It is located below the corresponding IV_1 band of CIV in-gel activity test. Due to the facts, that it appears usually after a longer incubation time than the other bands, that it exhibits only weak intensity and could not be allocated to a specific complex, this band is also disregarded for further analysis.

All of these assignments are transferred to the CBBG stained BN gel lane (Fig. 4.11). Three additional bands are marked there: II_1, F_1 and III_2. Those were assigned with the help of identified protein spots by PMF and WB analysis from 2D-BN/SDS gels (see below).

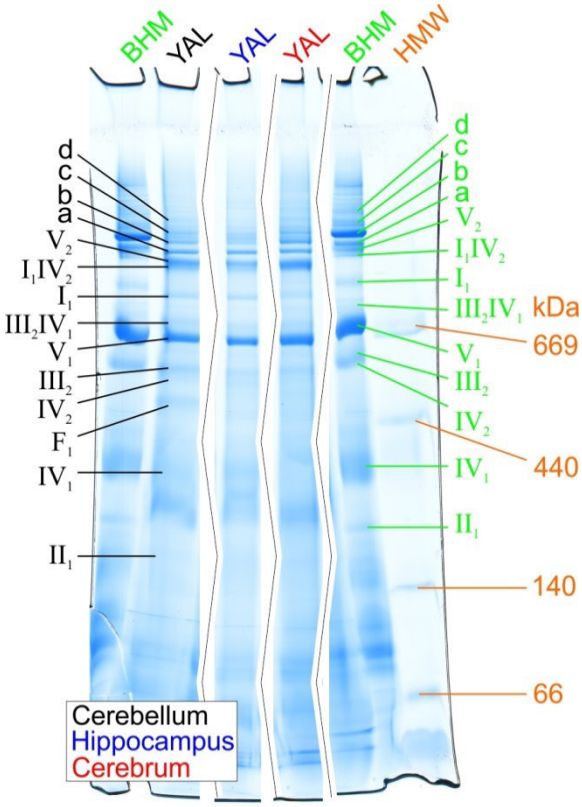

Fig. 4.12: Comparison of band positions in CBBG stained BN gel for RBM from the three different brain areas cerebellum, hippocampus and cerebrum (all YAL). 100 µg (b. sol. d/p: 8g/g) proteins of RBM were loaded on each lane. 70 µg (b. sol. d/p: 3g/g) proteins of the standard BHM as well as 4 µL of HMW were loaded into additional lanes. Gel run was followed by CBBG staining. Bands are assigned for cerebellum YAL (black), BHM (green) and HMW (orange). RBM samples are colour coded as follows: cerebellum in black, hippocampus in blue, cerebrum in red. Vertical zig-zag lines mark the intersections made in the original images which are attached in "7 Supplements" (BN1-3, Fig. 7.1, Fig. 7.2). a = I_1III_2, b = $I_1III_2IV_1$, c = $I_1III_2IV_2$, d = $I_1III_2IV_3$

Fig. 4.12 depicts a combined image of CBBG stained BN gel lanes. The intersections of the images are indicated by vertical zig-zag lines. 100 µg (b. sol. d/p: 8g/g) of mitochondrial proteins from YAL groups of the three brain areas cerebellum (black), hippocampus (blue) and cerebrum (red) were loaded per lane. 70 g (b. sol. d/p: 3g/g) proteins of BHM (green) were loaded for comparison. HMW served as mass standard (orange). The OxPhos complexes were assigned to BHM and RBM as explained above for Fig. 4.11. The original images of the CBBG stained BN gels (BN1-3) are illustrated in "7 Supplements", Fig. 7.1 and Fig. 7.2.

In Fig. 4.12 it is visible, that the marked (super)complexes of the different tissues (cerebellum, hippocampus and cerebrum) show the same electrophoretic migration pattern on BN gels. Only the intensities of the different gel lanes differ slightly, which is caused by different background staining. The same migration behaviour is also found for the other sample groups (YCR, OAL, OCR) of all three tissues, e.g. when loaded on the same BN gel (observable at BN1-3 in "7 Supplements", Fig. 7.1 and Fig. 7.2).

The migration behaviour of the (super)complexes of RBM in BN gel differs compared to BHM, as visible in Fig. 4.12 and all other BN gel images. BHM complexes of higher mass than IV_1 seem to migrate slower through the BN gel than the corresponding complexes of the RBM samples, therefore the equivalent bands are located slightly higher in the gel. This effect can be explained on the one hand, that protein complexes of RBM differ in molecular weight and on the other hand that different ratios of digitonin to protein amount during solubilisation were applied (d/p: 3g/g for BHM and d/p: 8g/g for RBM) resulting in different degree of delipidation. Probably, the micelles with the solubilised protein complexes contain different amounts of remaining lipids and digitonin, for solubilised RBM and BHM.

Fig. 4.13 depicts images of BN gel lanes, which were stained with CI in-gel activity test solution. 70 µg (b. sol. d/p: 3g/g) proteins of BHM were loaded on one lane, additional to lanes with 100 µg (b. sol. d/p: 8g/g) proteins of RBM for each brain area. Images of lanes depicted in Fig. 4.13 are separated RBM proteins from cerebellum, hippocampus and cerebrum, each from respective YAL groups. The original images show all groups for each brain area (see "7 Supplements", Fig. 7.10). For BHM and cerebrum, the bands are assigned to OxPhos complexes as in Fig. 4.11. It is obvious, that the migration behaviour for all shown RBM samples is similar. Only in the area above supercomplex $I_1III_2IV_3$, the pattern of the bands differs slightly. But the complex composition of these bands is unknown, therefore they were not assigned. The differences in the migration pattern of the proteins from BHM compared to RBM, as already observed and explained for CBBG stained BN gels (Fig. 4.12), is also visible in Fig. 4.13.

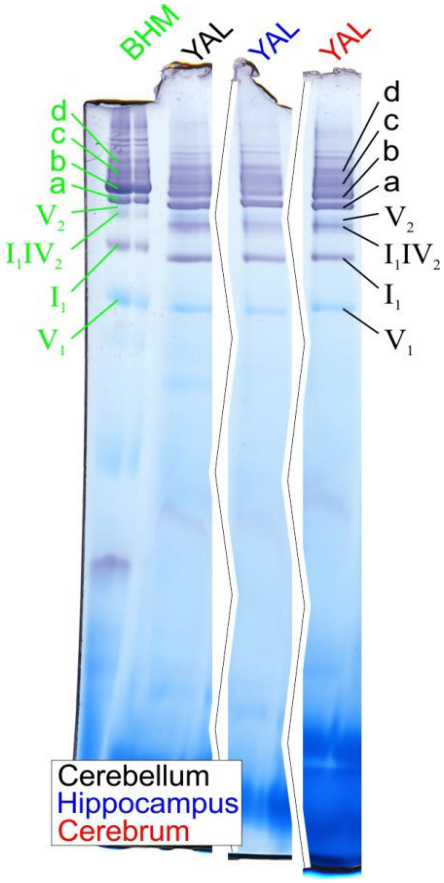

Fig. 4.13: CI in-gel activity test, band positions for RBM of different brain areas (cerebellum, hippocampus, cerebrum, all YAL), 100 µg (b. sol. d/p: 8g/g) proteins of RBM were loaded on each lane. 70 µg (b. sol. d/p: 3g/g) of the standard BHM were loaded into an additional lane. After gel run, CI in-gel activity test was performed. Bands are assigned for cerebrum YAL (black) and BHM (green). RBM samples are colour coded as follows: cerebellum in black, hippocampus in blue, cerebrum in red. The vertical zig-zag lines mark the intersections, made in the original images, which are present at "7 Supplements", Fig. 7.10.
a = I_1III_2, b = $I_1III_2IV_1$, c = $I_1III_2IV_2$, d = $I_1III_2IV_3$

Fig. 4.14 illustrates a composed picture of images of BN gel lanes, incubated in CIV in-gel activity test solution. The lanes include mitochondrial proteins of the three different rat brain areas of the respective YAL groups and BHM. The lane with proteins of cerebellum is marked in black, of hippocampus in blue, of cerebrum in red and of BHM in green.

The original gel images (attached in "7 Supplements", Fig. 7.12) contain lanes of all animal groups (YAL, YCR, OAL, OCR) of each brain area. In Fig. 4.14 the OxPhos complexes are assigned to the protein bands of BHM and cerebrum as explained above (Fig.

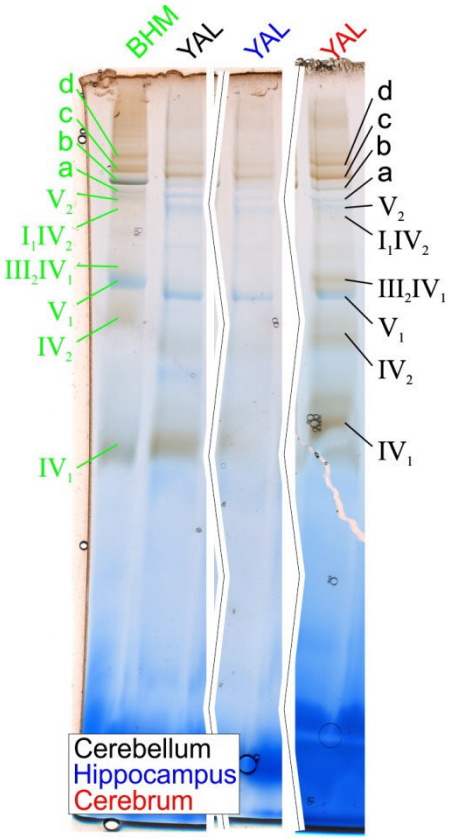

Fig. 4.14: CIV in-gel activity test, band positions for RBM of different brain areas (cerebellum, hippocampus, cerebrum, all YAL), 100 µg (b. sol. d/p: 8g/g) proteins of RBM were loaded on each lane. 70 µg (b. sol. d/p: 3g/g) of the protein standard BHM were loaded into an additional lane. After gel run, CIV in-gel activity test was performed. Bands are assigned for cerebrum YAL (black) and BHM (green). RBM samples are colour coded as follows: cerebellum in black, hippocampus in blue, cerebrum in red. The zig-zag lines mark the intersections, made in the original images, which are attached in "7 Supplements", Fig. 7.12.
a = I_1III_2, b = $I_1III_2IV_1$, c = $I_1III_2IV_2$, d = $I_1III_2IV_3$

4.11). The running behaviour of the (super)complexes is similar for all three lanes of RBM. This is also observable for the other animal groups (YCR, OAL, OCR, not shown here), when the entire image as in "7 Supplements", Fig. 7.12 is considered. The staining intensities differ for each lane of Fig. 4.14. The brownish precipitate is the weakest for mitochondrial proteins of hippocampus, followed by cerebellum and the lane of cerebrum shows the most intense staining. The explanation for this observation is, that different gels and solutions were used for each CIV in-gel activity test of respective brain area.

As well as observed and explained for CBBG stained gels (Fig. 4.12), the difference in migration behaviour of the proteins from BHM compared to RBM is visible in Fig. 4.14.

Identification of protein spots from RBM in 2D-BN/SDS gels

For identification of protein spots of RBM (cerebellum, hippocampus and cerebrum), 200 µg proteins (b. sol. d/p: 8g/g, 3.3.1) of each brain area were separated by 2D-BN/SDS PAGE (3.5). Gels were stained with silver (3.7.1) and PMF (3.9) was performed.

The images of the gels are depicted in Fig. 4.15 (cerebellum), Fig. 4.16 (hippocampus) and Fig. 4.17 (cerebrum). A CBBG stained BN gel lane with the assigned OxPhos complexes as in Fig. 4.11 and Fig. 4.12 was placed horizontally above the silver stained second dimensional SDS gel. The protein spots are marked with diverse colours, dependent on the classification of the proteins. The legends of Fig. 4.15, Fig. 4.16 and Fig. 4.17 illustrate the assignment. Subunits of **CI** are marked in **yellow**, subunits of **CII** in **pink**, subunits of **CIII** in **green**, subunits of **CIV** in **orange** and subunits of **ATP synthase (CV)** in **blue**. Proteins which were assigned to the **TCA cycle** are coloured in **purple**, proteins belonging to **glycolysis** in **brown,** those related to both**, TCA cycle and glycolysis**, in **brown and purple**. Proteins of cellular **stress management** are depicted in **dark green**. Spots / subunits of **Na^+/K^+ ATPase** are marked in **red**. **Other** identified proteins are marked in **grey**. Protein spots assigned in **black** were not identified by PMF of the respective brain area, but at least identified for one of the other brain areas, or by WB analysis of RBM (see below), or they were assigned by referring to PMF of BHM or WB analysis of BHM as described by Decker (presumably 2016). This colour code is also used in the tables below, which list the identified subunits of the proteins.

The assignment of complexes II_1, III_2 and F_1 portion in BN gel lanes was performed on the basis of the identification of protein spots by PMF. By comparison of Fig. 4.15, Fig. 4.16 and Fig. 4.17, spot numbers 49 and 81 can be assigned to CII (Table 4.17) and following in vertical direction to a slightly blueish band in the BN gel lane. Complex III_2 was marked in the BN gel lane on vertical direction through the spot numbers 23, 24, 35a, 36 and 42a. 23 and 24 were identified by PMF of RBM as subunits of CIII (Table 4.18), as well as spot no. 35a by PMF of BHM (Table 4.10) and spots 36 and 42a were assigned according to Reifschneider et al. (2006) (see below). The spots 44 and 46 were identified as subunits alpha and beta of ATP synthase (Table 4.20) and due to their position in the 2D gel should be part of the separated F_1 portion. F_1 was assigned in the BN gel lane by following the spots in vertical direction to a very weak blueish band in the BN gel.

47 protein spots were identified by PMF for cerebellum mitochondria and coloured in the image of the 2D-BN/SDS gel (Fig. 4.15).

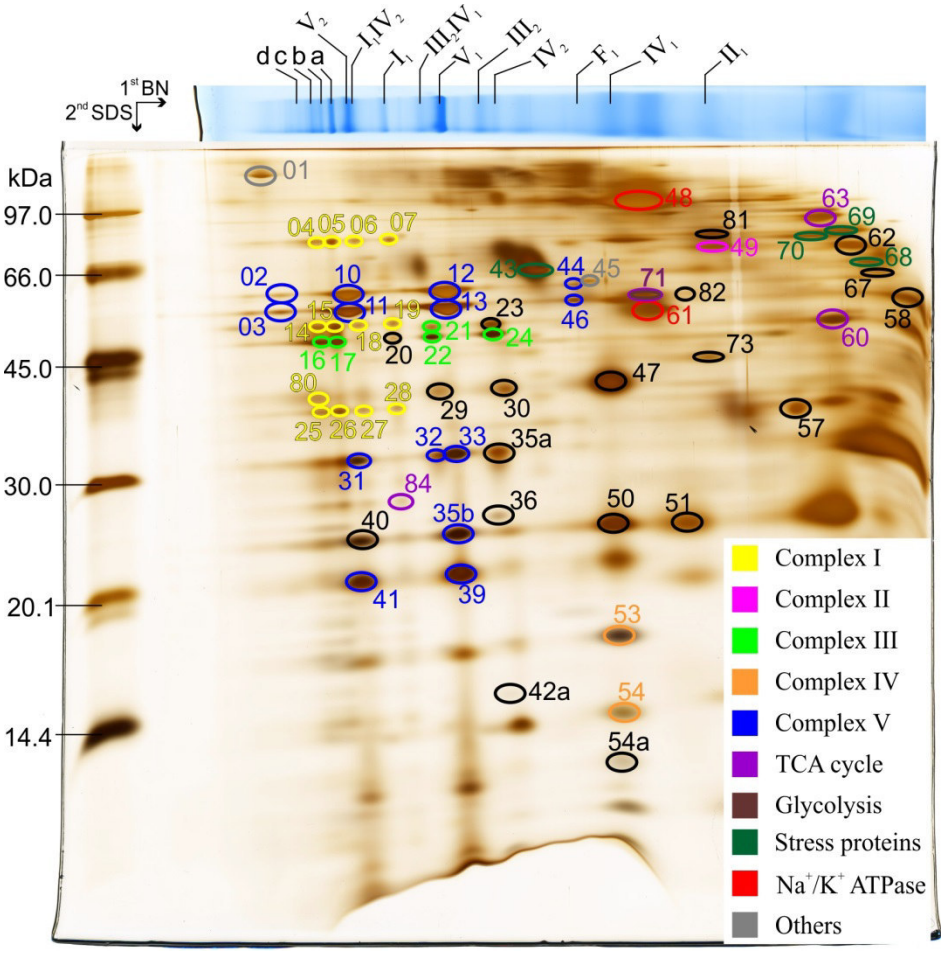

Fig. 4.15: Cerebellum RBM: 2D-gel for PMF analysis, 200 µg (b. sol. d/p: 8g/g) proteins of RBM from cerebellum were separated by 2D-BN/SDS PAGE and analysed according to 3.9. The image of the CBBG stained BN gel lane was arranged horizontally above the image of the silver stained second dimensional SDS gel, for assignment of bands. Masses of LMW were marked. Identified spots were marked in colour as depicted in the legend. Protein spots marked in black were not identified by PMF of this brain area, but identified for at least one of the other areas or assigned by comparison with the standard BHM or the publication of Reifschneider et al. (2006),
a = I_1III_2, b = $I_1III_2IV_1$, c = $I_1III_2IV_2$, d = $I_1III_2IV_3$

For hippocampus RBM 35 protein spots were identified by PMF and marked in colour in the 2D-BN/SDS gel image (Fig. 4.16).

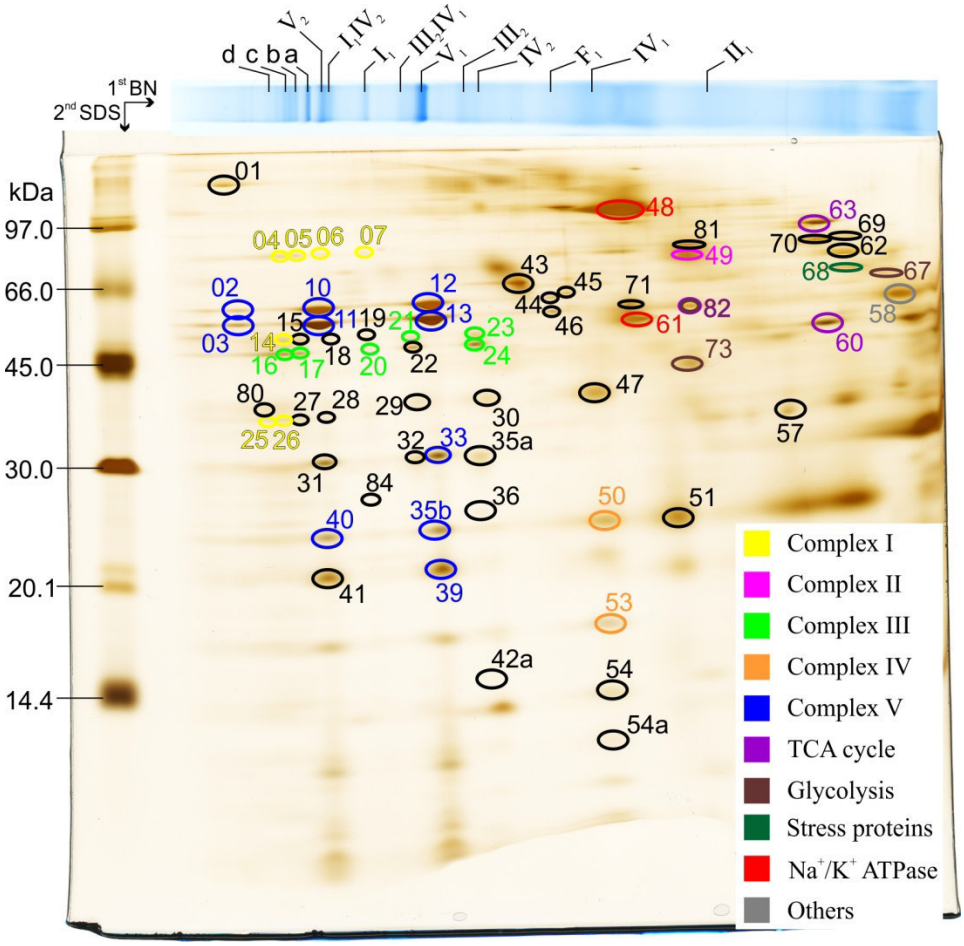

Fig. 4.16: Hippocampus RBM: 2D-gel for PMF analysis, 200 µg (b. sol. d/p: 8g/g) proteins of RBM from hippocampus were separated by 2D-BN/SDS PAGE and analysed according to 3.9. The image of the CBBG stained BN gel lane was arranged horizontally above the image of the silver stained second dimensional SDS gel, for assignment of bands. Masses of LMW were marked. Identified spots were marked in colour as depicted in the legend. Protein spots marked in black were not identified by PMF of this brain area, but identified for at least one of the other areas or assigned by comparison with the standard BHM or the publication of Reifschneider et al. (2006)
a = I_1III_2, b = $I_1III_2IV_1$, c = $I_1III_2IV_2$, d = $I_1III_2IV_3$

33 protein spots were identified by PMF for rat cerebrum mitochondria and marked in colour in Fig. 4.17.

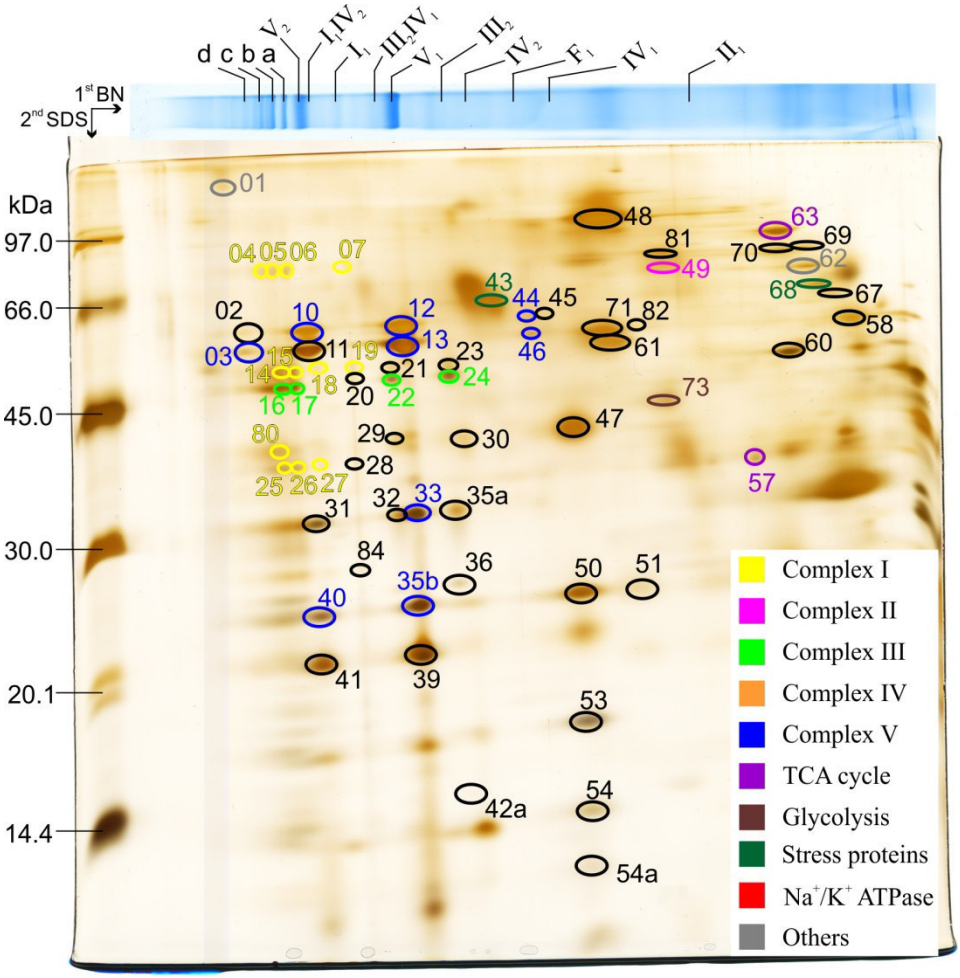

Fig. 4.17: Cerebrum RBM: 2D-gel for PMF analysis, 200 µg (b. sol. d/p: 8g/g) proteins of RBM from cerebrum were separated by 2D-BN/SDS PAGE and analysed according to 3.9. The image of the CBBG stained BN gel lane was arranged horizontally above the image of the silver stained second dimensional SDS gel, for assignment of bands. Masses of LMW were marked. Identified spots were marked in colour as depicted in the legend. Protein spots marked in black were not identified by PMF of this brain area, but identified for at least one of the other areas or assigned by comparison with the standard BHM or the publication of Reifschneider et al. (2006)
a = I_1III_2, b = $I_1III_2IV_1$, c = $I_1III_2IV_2$, d = $I_1III_2IV_3$

The settings for the search in Mascot database are listed in Table 3.23 and Table 3.26. The taxonomy "Rattus" was chosen as search parameter in Mascot database for the analysis of RBM (for details see 3.9). Therefore, the column "accession" reflects the taxonomy database in which the protein was found, namely "RAT", besides the information about the the identified protein subunit as listed in UniProt database. For significant MS results, the "Mascot Score" for "Rattus" has to be greater than 52 ($p<0.05$). MS/MS results are significant when verifying the MS result. The abbreviations used in column "tissue" are Cer = cerebellum, Hip = hippocampus and Cbrum = Cerebrum. They indicate from which brain area the identified protein spots originated.

Four subunits of CI were identified and assigned to 13 proteins spots, of which seven spots were identically identified for all brain areas and five identical for cerebellum and cerebrum (Table 4.16). These five spots gave no result for the analysed hippocampus samples. Only one protein spot was identified unique for cerebellum, while respective spots of hippocampus and cerebrum mitochondria gave no results.

Table 4.16: RBM: identified subunits of CI

spot no.	tissue	MS type	accession	protein	MW [kDa]	Mascot Score	pep-tides	SC [%]
04	Cer	MS DDZ	NDUS1_RAT	NADH-ubiquinone oxidoreductase 75 kDa subunit, mitochondrial OS=Rattus norvegicus GN=Ndufs1 PE=1 SV=1	79.4	216.0	29	33.4
	Cer	MS/MS DDZ	NDUS1_RAT			44.5	1	1.2
	Hip	MS DDZ	NDUS1_RAT			116.0	20	34.9
	Hip	MS/MS DDZ	NDUS1_RAT			41.6	1	2.2
	Cbrum	MS DDZ	NDUS1_RAT			62.7	15	22.8
05	Cer	MS DDZ	NDUS1_RAT			190.0	25	40.6
	Cer	MS DDZ	NDUS1_RAT			94.8	9	15.7
	Cer	MS TUD	NDUS1_RAT			75.0	13	26.0
	Hip	MS DDZ	NDUS1_RAT			155.0	25	44.7
	Hip	MS/MS DDZ	NDUS1_RAT			43.9	1	2.2
	Cbrum	MS DDZ	NDUS1_RAT			138.0	26	36.3
06	Cer	MS DDZ	NDUS1_RAT			159.0	15	21.3
	Hip	MS DDZ	NDUS1_RAT			163.0	24	36.2
	Hip	MS/MS DDZ	NDUS1_RAT			39.1	1	2.6
	Cbrum	MS DDZ	NDUS1_RAT			108.0	18	29.2
07	Cer	MS DDZ	NDUS1_RAT			152.0	14	20.8
	Cer	MS/MS DDZ	NDUS1_RAT			29.8	1	1.2
	Hip	MS DDZ	NDUS1_RAT			79.6	18	27.6
	Cbrum	MS DDZ	NDUS1_RAT			58.1	13	22.0
14	Cer	MS DDZ	NDUS2_RAT	NADH dehydrogenase [ubiquinone] iron-sulfur protein 2, mitochondrial OS=Rattus norvegicus GN=Ndufs2 PE=1 SV=1	52.5	116.0	22	48.4
	Cer	MS/MS DDZ	NDUS2_RAT			44.3	1	1.9
	Hip	MS DDZ	NDUS2_RAT			121.0	23	42.1
	Hip	MS/MS DDZ	NDUS2_RAT			45.7	1	1.9
	Cbrum	MS DDZ	NDUS2_RAT			110.0	19	33.5
15	Cer	MS DDZ	NDUS2_RAT			183.0	28	61.1
	Cer	MS DDZ	NDUS2_RAT			146.0	18	32.2
	Cbrum	MS DDZ	NDUS2_RAT			81.7	18	29.8
18	Cer	MS DDZ	NDUS2_RAT			76.7	10	19.9
	Cer	MS/MS DDZ	NDUS2_RAT			87.5	3	9.7
	Cbrum	MS DDZ	NDUS2_RAT			102.0	21	34.3
19	Cer	MS DDZ	NDUS2_RAT			59.8	9	19.9
	Cbrum	MS DDZ	NDUS2_RAT			59.7	12	20.5
25	Cer	MS DDZ	NDUA9_RAT	NADH dehydrogenase [ubiquinone] 1 alpha subcomplex subunit 9, mitochondrial OS=Rattus norvegicus GN=Ndufa9 PE=1 SV=2	42.5	82.6	9	18.6
	Hip	MS DDZ	NDUA9_RAT			82.9	13	33.7
	Hip	MS/MS DDZ	NDUA9_RAT			45.3	1	3.4
	Cbrum	MS DDZ	NDUA9_RAT			136	18	42.4
26	Cer	MS DDZ	NDUA9_RAT			126.0	13	27.3
	Cer	MS/MS DDZ	NDUA9_RAT			73.5	1	3.4
	Hip	MS DDZ	NDUA9_RAT			208.0	18	49.9
	Cbrum	MS DDZ	NDUA9_RAT			163.0	21	48.5
27	Cer	MS DDZ	NDUA9_RAT			130.0	18	40.8
	Cer	MS/MS DDZ	NDUA9_RAT			42.6	1	2.4
	Cbrum	MS DDZ	NDUA9_RAT			105.0	15	38.7
28	Cer	MS DDZ	NDUA9_RAT			126.0	17	46.4
	Cer	MS/MS DDZ	NDUA9_RAT			34.2	1	2.4
80	Cer	MS DDZ	NDUAA_RAT	NADH dehydrogenase [ubiquinone] 1 alpha subcomplex subunit 10, mitochondrial OS=Rattus norvegicus GN=Ndufa10 PE=1 SV=1	40.5	77.8	13	47.6
	Cbrum	MS DDZ	NDUAA_RAT			83.5	10	36.3

Only one subunit of CII could be identified. Mitochondrial succinate dehydrogenase [ubiquinone] flavoprotein subunit (DHSA) was found for spot no. 49 of all brain areas (Table 4.17).

Table 4.17: RBM: identified subunits of CII

spot no.	tissue	MS type	accession	protein	MW [kDa]	Mascot Score	pep-tides	SC [%]
49	Cer	MS DDZ	DHSA_RAT	Succinate dehydrogenase [ubiquinone] flavoprotein subunit, mitochondrial OS=Rattus norvegicus GN=Sdha PE=1 SV=1	71.6	181.0	23	31.7
	Cer	MS/MS DDZ	DHSA_RAT			31.2	1	1.8
	Hip	MS DDZ	DHSA_RAT			117.0	19	28.0
	Cbrum	MS DDZ	SDHA_RAT			125.0	19	26.8

Three subunits of CIII were identified in seven spots, of which three spots were identically identified for all brain parts and one for both, cerebellum and hippocampus, and another one for both, cerebellum and cerebrum, and two spots only for hippocampus (Table 4.18).

Table 4.18: RBM: identified subunits of CIII

spot no.	tissue	MS type	accession	protein	MW [kDa]	Mascot Score	pep-tides	SC [%]
16	Cer	MS DDZ	QCR2_RAT	Cytochrome b-c1 complex subunit 2, mitochondrial OS=Rattus norvegicus GN=Uqcrc2 PE=1 SV=2	48.4	270.0	25	46.5
	Cer	MS/MS DDZ	QCR2_RAT			197.9	4	10.2
	Hip	MS DDZ	QCR2_RAT			143.0	19	45.1
	Hip	MS/MS DDZ	QCR2_RAT			38.5	1	3.5
	Cbrum	MS DDZ	QCR2_RAT			144.0	13	35.8
	Cbrum	MS/MS DDZ	QCR2_RAT			95.8	1	3.1
17	Cer	MS DDZ	QCR2_RAT			167.0	19	48.0
	Cer	MS/MS DDZ	QCR2_RAT			55.2	1	3.1
	Hip	MS/MS DDZ	QCR2_RAT			135.1	3	9.1
	Cbrum	MS DDZ	QCR2_RAT			116.0	16	40.7
	Cbrum	MS/MS DDZ	QCR2_RAT			96.6	1	3.1
20	Hip	MS DDZ	QCR2_RAT			65.0	12	36.3
21	Cer	MS DDZ	QCR1_RAT	Cytochrome b-c1 complex subunit 1, mitochondrial OS=Rattus norvegicus GN=Uqcrc1 PE=1 SV=1	52.8	54.2	8	16.0
	Hip	MS DDZ	QCR1_RAT			62.8	10	27.9
22	Cer	MS DDZ	QCR2_RAT	Cytochrome b-c1 complex subunit 2, mitochondrial OS=Rattus norvegicus GN=Uqcrc2 PE=1 SV=2	48.4	198.0	17	42.5
	Cer	MS DDZ	QCR2_RAT			162.0	16	36.1
	Cbrum	MS DDZ	QCR2_RAT			68.3	11	33.0
23	Hip	MS DDZ	QCR1_RAT	Cytochrome b-c1 complex subunit 1, mitochondrial OS=Rattus norvegicus GN=Uqcrc1 PE=1 SV=1	52.8	119.0	15	24.2
24	Cer	MS DDZ	QCR2_RAT	Cytochrome b-c1 complex subunit 2, mitochondrial OS=Rattus norvegicus GN=Uqcrc2 PE=1 SV=2	48.4	189.0	16	36.9
	Cer	MS TUD	QCR2_RAT			70.0	7	20.0
	Hip	MS DDZ	QCR2_RAT			111.0	10	25.9
	Hip	MS/MS DDZ	QCR2_RAT			53.4	1	3.1
	Cbrum	MS DDZ	QCR2_RAT			118.0	17	41.6
	Cbrum	MS/MS DDZ	QCR2_RAT			75.8	1	3.1

Three subunits of CIV were found in three protein spots. Only one of these spots was identified for two brain areas, cerebellum and hippocampus, while the other two were only identified for one brain area each. One of the identified subunits, COX2, is encoded by mtDNA (Table 4.19).

Table 4.19: RBM: identified subunits of CIV

spot no.	tissue	MS type	accession	protein	MW [kDa]	Mascot Score	pep-tides	SC [%]
50	Hip	MS/MS DDZ	COX2_RAT	Cytochrome c oxidase subunit 2 OS=Rattus norvegicus GN=Mtco2 PE=2 SV=2	25.9	24.2	1	7.5
53	Cer	MS DDZ	COX41_RAT	Cytochrome c oxidase subunit 4 isoform 1, mitochondrial OS=Rattus norvegicus GN=Cox4i1 PE=1 SV=1	19.5	96.3	12	58.6
	Cer	MS DDZ	COX41_RAT			73.7	6	38.5
	Hip	MS DDZ	COX41_RAT			142.0	14	66.3
	Hip	MS/MS DDZ	COX41_RAT			31.0	1	6.5
54	Cer	MS/MS DDZ	COX5A_RAT	Cytochrome c oxidase subunit 5A, mitochondrial OS=Rattus norvegicus GN=Cox5a PE=1 SV=1	16.1	27.2	1	11.6

Six subunits from CV were identified in 15 spots (Table 4.20). Six of these protein spots were identified for all three brain areas, while three of them were identified for cerebellum and hippocampus, two for cerebellum and cerebrum, one for hippocampus and cerebrum, and the remaining spots only for one brain area. In spot no. 39, the subunits O (ATPO) and d (ATP5H) were identified. Their protein spots seem to overlap, as both subunits are, besides subunits b and F6, part of the peripheral stalk of ATP synthase (Papa et al. 2012).

Table 4.20: RBM: identified subunits of CV

spot no.	tissue	MS type	accession	protein	MW [kDa]	Mascot Score	pep-tides	SC [%]
02	Cer	MS DDZ	ATPA_RAT	ATP synthase subunit alpha, mitochondrial OS=Rattus norvegicus GN=Atp5a1 PE=1 SV=2	59.7	269.0	24	39.1
	Cer	MS/MS DDZ	ATPA_RAT			132.6	3	6.1
	Hip	MS/MS DDZ	ATPA_RAT			89.2	2	4.2
03	Cer	MS DDZ	ATPB_RAT	ATP synthase subunit beta, mitochondrial OS=Rattus norvegicus GN=Atp5b PE=1 SV=2	56.3	116.0	23	40.3
	Cer	MS/MS DDZ	ATPB_RAT			202.9	3	8.5
	Hip	MS DDZ	ATPB_RAT			74.9	15	37.2
	Hip	MS/MS DDZ	ATPB_RAT			56.4	1	3.6
	Cbrum	MS DDZ	ATPB_RAT			69.3	10	19.8
10	Cer	MS DDZ	ATPA_RAT	ATP synthase subunit alpha, mitochondrial OS=Rattus norvegicus GN=Atp5a1 PE=1 SV=2	59.7	119.0	17	31.5
	Cer	MS/MS DDZ	ATPA_RAT			34.3	1	2.4
	Cer	MS DDZ	ATPA_RAT			130.0	22	45.6
	Cer	MS DDZ	ATPA_RAT			61.2	12	25.9
	Hip	MS DDZ	ATPA_RAT			196.0	31	51.9
	Hip	MS/MS DDZ	ATPA_RAT			41.1	1	2.7
	Cbrum	MS DDZ	ATPA_RAT			162.0	17	35.6
11	Cer	MS DDZ	ATPB_RAT	ATP synthase subunit beta, mitochondrial OS=Rattus norvegicus GN=Atp5b PE=1 SV=2	56.3	235.0	28	62.2
	Cer	MS/MS DDZ	ATPB_RAT			350.3	4	12.3
	Hip	MS/MS DDZ	ATPB_RAT			39.6	1	2.6

Table 4.21: RBM: identified subunits of CV (continued)

spot no.	tissue	MS type	accession	protein	MW [kDa]	Mascot Score	pep-tides	SC [%]
12	Cer	MS DDZ	ATPA_RAT	ATP synthase subunit alpha, mitochondrial OS=Rattus norvegicus GN=Atp5a1 PE=1 SV=2	59.7	132.0	18	31.6
	Cer	MS/MS DDZ	ATPA_RAT			33.8	1	2.4
	Cer	MS DDZ	ATPA_RAT			107.0	17	33.3
	Cer	MS DDZ	ATPA_RAT			94.0	16	29.8
	Hip	MS DDZ	ATPA_RAT			211.0	28	51.0
	Hip	MS/MS DDZ	ATPA_RAT			43.5	1	3.8
	Cbrum	MS DDZ	ATPA_RAT			91.4	10	19.7
13	Cer	MS DDZ	ATPB_RAT	ATP synthase subunit beta, mitochondrial OS=Rattus norvegicus GN=Atp5b PE=1 SV=2	56.3	252.0	34	62.2
	Cer	MS/MS DDZ	ATPB_RAT			403.3	5	12.9
	Hip	MS DDZ	ATPB_RAT			197.0	27	50.5
	Hip	MS/MS DDZ	ATPB_RAT			59.3	1	2.8
	Cbrum	MS DDZ	ATPB_RAT			86.3	10	22.9
31	Cer	MS DDZ	ATPG_RAT	ATP synthase subunit gamma, mitochondrial OS=Rattus norvegicus GN=Atp5c1 PE=1 SV=2	30.2	136	13	42.9
32	Cer	MS/MS DDZ	ATPG_RAT			40.4	1	3.7
33	Cer	MS DDZ	ATPG_RAT			170.0	18	48.4
	Cer	MS DDZ	ATPG_RAT			86.4	11	36.6
	Hip	MS DDZ	ATPG_RAT			71.7	8	22.7
	Hip	MS/MS DDZ	ATPG_RAT			39.6	1	5.5
	Cbrum	MS DDZ	ATPG_RAT			66.5	9	31.5
	Cbrum	MS/MS DDZ	ATPG_RAT			72.0	1	4.4
35b	Cer	MS DDZ	AT5F1_RAT	ATP synthase subunit b, mitochondrial OS=Rattus norvegicus GN=Atp5f1 PE=1 SV=1	28.9	106.0	16	35.5
	Cer	MS/MS DDZ	AT5F1_RAT			39.5	1	3.1
	Cer	MS DDZ	AT5F1_RAT			61.2	5	19.1
	Hip	MS DDZ	AT5F1_RAT			86.1	13	36.3
	Hip	MS/MS DDZ	AT5F1_RAT			69.4	1	3.1
	Cbrum	MS DDZ	AT5F1_RAT			82.6	13	27.3
39	Cer	MS DDZ	ATP5H_RAT	ATP synthase subunit d, mitochondrial OS=Rattus norvegicus GN=Atp5h PE=1 SV=3	18.8	80.9	8	47.8
	Cer	MS DDZ	ATPO_RAT	ATP synthase subunit O, mitochondrial OS=Rattus norvegicus GN=Atp5o PE=1 SV=1	23.4	69.1	10	52.6
	Cer	MS DDZ	ATPO_RAT			55.5	5	29.1
	Hip	MS DDZ	ATPO_RAT			68.9	12	48.4
	Hip	MS DDZ	ATP5H_RAT	ATP synthase subunit d, mitochondrial OS=Rattus norvegicus GN=Atp5h PE=1 SV=3	18.8	58.7	8	55.3
	Hip	MS/MS DDZ	ATPO_RAT	ATP synthase subunit O, mitochondrial OS=Rattus norvegicus GN=Atp5o PE=1 SV=1	23.4	34.3	1	6.6
40	Hip	MS DDZ	AT5F1_RAT	ATP synthase subunit b, mitochondrial OS=Rattus norvegicus GN=Atp5f1 PE=1 SV=1	28.9	62.3	7	27.7
	Hip	MS/MS DDZ	AT5F1_RAT			73.2	1	3.1
	Cbrum	MS DDZ	AT5F1_RAT			105.0	21	41.8
41	Cer	MS DDZ	ATPO_RAT	ATP synthase subunit O, mitochondrial OS=Rattus norvegicus GN=Atp5o PE=1 SV=1	23.4	57.3	5	29.1
44	Cer	MS DDZ	ATPA_RAT	ATP synthase subunit alpha, mitochondrial OS=Rattus norvegicus GN=Atp5a1 PE=1 SV=2	59.7	185.0	19	26.9
	Cer	MS/MS DDZ	ATPA_RAT			65.9	2	5.2
	Cbrum	MS DDZ	ATPA_RAT			157.0	23	47.2
46	Cer	MS DDZ	ATPB_RAT	ATP synthase subunit beta, mitochondrial OS=Rattus norvegicus GN=Atp5b PE=1 SV=2	56.3	89.5	13	27.2
	Cer	MS/MS DDZ	ATPB_RAT			143.4	3	9.1
	Cbrum	MS DDZ	ATPB_RAT			64.5	13	23.4
	Cbrum	MS/MS DDZ	ATPB_RAT			71.6	1	2.6

Four proteins of the TCA cycle were identified and listed in Table 4.22. Mitochondrial aconitase (ACON) was found for all brain areas, while citrate synthase (CISY) was identified in cerebellum and hippocampus, and malate dehydrogenase (MDHM) and 2-oxoglutarate dehydrogenase (ODO1) only for one brain area.
The chemical reactions of the TCA cycle take place in the mitochondrial matrix and can be divided into eight steps, where acetyl residues are oxidised into carbon dioxide, while energy-rich compounds as reduced nicotinamide adenine dinucleotide (NADH), hydroquinone form of flavin adenine dinucleotide ($FADH_2$) and guanosine-5'-triphosphate (GTP) are formed. Each of the eight steps is catalysed by an enzyme, four of whom were identified.
CISY catalyses the first step of the TCA cycle, in which the acetyl residue of acetyl coenzyme A (CoA) is transferred to oxaloacetate together with water to form citric acid. ACON catalyses the second step, where citrate is isomerised into iso-citrate via the intermediate *cis*-aconitate. The fourth enzyme of the TCA cycle is the oxoglutarate dehydrogenase complex (or α-ketoglutarate dehydrogenase complex), which is assembled of three subunits: oxoglutarate dehydrogenase (ODO1), dihydrolipoyl succinyltransferase and dihydrolipoyl dehydrogenase (DLDH, Table 4.23). The oxoglutarate dehydrogenase complex catalyses the oxidative decarboxylation of α-ketoglutarate into succinyl-CoA, while NAD^+ is reduced to $NADH+H^+$. MDHM catalyses the last step of the TCA cycle and completes the circuit. Hereby malate is oxidised into oxaloacetate and NAD+ is reduced to $NADH+H^+$. (Voet et al. 2002)

Table 4.22: RBM: identified proteins of TCA cycle

spot no.	tissue	MS type	accession	protein	MW [kDa]	Mascot Score	pep-tides	SC [%]
57	Cbrum	MS DDZ	MDHM_RAT	Malate dehydrogenase, mito-chondrial OS=Rattus norve-gicus GN=Mdh2 PE=1 SV=2	35.7	63.5	10	36.4
60	Cer	MS DDZ	CISY_RAT	Citrate synthase, mitochondrial OS=Rattus norvegicus GN=Cs PE=1 SV=1	51.8	61.0	10	22.7
	Cer	MS/MS DDZ	CISY_RAT			76.5	1	2.4
	Hip	MS DDZ	CISY_RAT			104.0	20	30.9
	Hip	MS/MS DDZ	CISY_RAT			61.4	1	2.1
63	Cer	MS DDZ	ACON_RAT	Aconitate hydratase, mitochondrial OS=Rattus norvegicus GN=Aco2 PE=1 SV=2	85.4	136.0	19	25.5
	Cer	MS/MS DDZ	ACON_RAT			49.3	1	2.1
	Hip	MS DDZ	ACON_RAT			135.0	24	35.8
	Hip	MS/MS DDZ	ACON_RAT			50.8	1	2.1
	Cbrum	MS DDZ	ACON_RAT			117.0	20	34.2
84	Cer	MS DDZ	ODO1_RAT	2-oxoglutarate dehydrogenase, mitochondrial OS=Rattus norvegicus GN=Ogdh PE=1 SV=1	116.2	55.2	9	11.2

The protein spots 71 (cerebellum) and 82 (hippocampus) could be assigned to dihydrolipoyl dehydrogenase (DLDH), a common component (E3) of three alpha-ketoacid dehydrogenase complexes, which oxidise pyruvate (pyruvate dehydrogenase complex), α-ketoglutarate (α-ketoglutarate dehydrogenase complex) and the branched-chain α-ketoacids (branched-chain amino acid-dehydrogenase complex) (Carothers et al. 1989). Thereby it is involved in glycolysis and the TCA cycle and therefore was marked in brown and purple (Table 4.23).

Table 4.23: RBM: identified proteins, occurring in TCA cycle and glycolysis

spot no.	tissue	MS type	accession	protein	MW [kDa]	Mascot Score	pep-tides	SC [%]
71	Cer	MS DDZ	DLDH_RAT	Dihydrolipoyl dehydrogenase, mitochondrial OS=Rattus norvegicus GN=Dld PE=1 SV=1	54.0	86.6	11	27.3
	Cer	MS DDZ	DLDH_RAT			73.4	9	24.6
	Cer	MS DDZ	DLDH_RAT			61.5	12	21.8
82	Hip	MS DDZ	DLDH_RAT			67.9	12	36.0
	Hip	MS/MS DDZ	DLDH_RAT			41.1	1	3.7

Two proteins involved in the metabolic pathway “glycolysis”, which takes place in the cytosol, were identified and listed in Table 4.24. ALDOA/C are found in brain and catalyse the fragmentation of fructose-1,6-bisphosphate into dihydroxyacetone phosphate and glyceraldehyde 3-phosphate in glycolysis. KPYM transfers a phosphate residue from phosphoenolpyruvate to ADP, resulting in ATP and pyruvate. The latter is transported by carriers into the mitochondrial matrix, where it is converted into acetyl-CoA by the pyruvate dehydrogenase complex (Table 4.23).(Voet et al. 2002)

Table 4.24: RBM: identified proteins of glycolysis

spot no.	tissue	MS type	accession	protein	MW [kDa]	Mascot Score	pep-tides	SC [%]
67	Hip	MS DDZ	KPYM_RAT	Pyruvate kinase isozymes M1/M2 OS=Rattus norvegicus GN=Pkm PE=1 SV=3	57.8	60.5	12	29.6
73	Hip	MS DDZ	ALDOA_RAT	Fructose-bisphosphate aldolase A OS=Rattus norvegicus GN=Aldoa PE=1 SV=2	39.3	88.8	11	29.7
	Hip	MS/MS DDZ	ALDOA_RAT			36.9	1	3.3
	Hip	MS DDZ	ALDOC_RAT	Fructose-bisphosphate aldolase C OS=Rattus norvegicus GN=Aldoc PE=1 SV=3	39.3	84.3	11	28.4
	Cbrum	MS DDZ	ALDOC_RAT			107.0	16	43.0
	Cbrum	MS DDZ	ALDOA_RAT	Fructose-bisphosphate aldolase A OS=Rattus norvegicus GN=Aldoa PE=1 SV=2	39.3	99.2	13	35.7

Four proteins involved in stress management of the cell were identified and listed in Table 4.25. In protein spot no. 43, the heat shock protein CH60 seems to overlap with the excitatory amino acid transporter (EAA1), both were identified there, but EAA1 with a lower score than CH60. EAA1 is a sodium-dependent glutamate/aspartate transporter, located at the synaptic cleft and found in cerebellum and cerebrum (Storck et al. 1992). The 78 kDa glucose-regulated protein (GRP78) is a heat shock protein, which is associated with the endoplasmatic reticulum (ER). The protein disulfide-isomerase A4 (PDIA4) rearranges disulfide bonds in proteins and is likewise associated with the ER (both UniProt databases). Protein disulfide-isomerases A1 and A3 as well as GRP78 are associated with mitochondria-associated ER membranes (MAM) (Schon and Area-Gomez 2013). Therefore it is supposable that A4 is associated with MAMs too.

Table 4.25: RBM: identified proteins of stress management

spot no.	tissue	MS type	accession	protein	MW [kDa]	Mascot Score	pep-tides	SC [%]
43	Cer	MS DDZ	CH60_RAT	60 kDa heat shock protein, mitochondrial OS=Rattus norvegicus GN=Hspd1 PE=1 SV=1	60.9	109.0	14	26.7
	Cer	MS DDZ	EAA1_RAT	Excitatory amino acid transporter 1 OS=Rattus norvegicus GN=Slc1a3 PE=1 SV=2	59.7	105.0	15	18.2
	Cer	MS/MS DDZ	EAA1_RAT			77.2	2	6.4
	Cer	MS/MS DDZ	EAA1_RAT			100.4	2	6.4
	Cbrum	MS DDZ	CH60_RAT	60 kDa heat shock protein, mitochondrial OS=Rattus norvegicus GN=Hspd1 PE=1 SV=1	60.9	77.6	16	32.6
	Cbrum	MS/MS DDZ	CH60_RAT			124.1	2	7.5
	Cbrum	MS DDZ	EAA1_RAT	Excitatory amino acid transporter 1 OS=Rattus norvegicus GN=Slc1a3 PE=1 SV=2	59.7	56.6	12	20.4
68	Cer	MS DDZ	CH60_RAT	60 kDa heat shock protein, mitochondrial OS=Rattus norvegicus GN=Hspd1 PE=1 SV=1	60.9	69.9	15	33.7
	Hip	MS DDZ	CH60_RAT			74.8	14	28.8
	Hip	MS/MS DDZ	CH60_RAT			88.6	1	4.4
	Cbrum	MS DDZ	CH60_RAT			110.0	20	39.8
69	Cer	MS DDZ	PDIA4_RAT	Protein disulfide-isomerase A4 OS=Rattus norvegicus GN=Pdia4 PE=1 SV=2	72.7	110.0	19	26.1
70	Cer	MS DDZ	GRP78_RAT	78 kDa glucose-regulated protein OS=Rattus norvegicus GN=Hspa5 PE=1 SV=1	72.3	217.0	29	51.4
	Cer	MS/MS DDZ	GRP78_RAT			54.1	1	2.6

For cerebellum and hippocampus, two (alpha and beta) of three subunits from Na^+/K^+-ATPase (UniProt databases) were identified and listed in Table 4.26. Na^+/K^+-ATPase transports actively three sodium ions out of the cell and imports simultaneously two potassium ions into the cell by splitting ATP into ADP and phosphate for this energy consuming step. Na^+/K^+-ATPase is necessary to maintain the resting potential of the nerve cells and consumes up to 70 % of the produced ATP (Voet et al. 2002).

Table 4.26: RBM: identified protein spots of Na^+/K^+ ATPase

spot no.	tissue	MS type	accession	protein	MW [kDa]	Mascot Score	pep-tides	SC [%]
48	Cer	MS DDZ	AT1A3_RAT	Sodium/potassium-transporting ATPase subunit alpha-3 OS=Rattus norvegicus GN=Atp1a3 PE=1 SV=2	111.6	83.6	26	30.3
	Cer	MS/MS DDZ	AT1A3_RAT			80.5	1	1.8
	Hip	MS/MS DDZ	AT1A3_RAT			61.1	1	1.8
61	Cer	MS DDZ	AT1B1_RAT	Sodium/potassium-transporting ATPase subunit beta-1 OS=Rattus norvegicus GN=Atp1b1 PE=1 SV=1	35.2	82.2	12	28.6
	Cer	MS/MS DDZ	AT1B1_RAT			73.1	2	7.2
	Hip	MS/MS DDZ	AT1B1_RAT			44.5	1	3.6

Four other proteins were identified and listed in Table 4.27. Mitochondrial glutamate dehydrogenase (DHE3) catalyses the transformation of glutamate into α-ketoglutarate, as a precursor stage for the TCA cycle, as well as urea cycle, and is supposed to control the glutamate concentration on nerve terminals (Michaelis et al. 2011). Clathrin is involved in membrane trafficking by endocytosis. It stabilises by formation of clathrin coated vesicles at Golgi apparatus as well as at synapses (Voet et al. 2002). For spot no. 58 from hippocampus mitochondria, different subunits of tubulin were found and listed in order of the Mascot score. Tubulin is the major part of microtubules, which are part of the cytoskeleton of the cell. They are involved in transport of organelles as mitochondria (Koolman et al. 2003). Syntaxin-

binding protein 1 (STXB1) is associated with the regulation of synaptic vesicle docking and fusion (UniProt databases).

Table 4.27: RBM: additionally identified proteins

spot no.	tissue	MS type	accession	protein	MW [kDa]	Mascot Score	pep-tides	SC [%]
01	Cer	MS DDZZ	CLH1_RAT	Clathrin heavy chain 1 OS=Rattus norvegicus GN=Cltc PE=1 SV=3	191.5	154.0	24	13.9
	Cer	MS/MS DDZ	CLH1_RAT			79.9	2	1.8
	Cbrum	MS DDZ	CLH1_RAT			68.6	20	15.1
45	Cer	MS DDZ	DHE3_RAT	Glutamate dehydrogenase 1, mitochondrial OS=Rattus norvegicus GN=Glud1 PE=1 SV=2	61.4	142.0	16	28.9
	Cer	MS/MS DDZ	DHE3_RAT			172.4	2	6.6
58	Hip	MS DDZ	TBB2A_RAT	Tubulin beta-2A chain OS=Rattus norvegicus GN=Tubb2a PE=1 SV=1	49.9	136.0	20	46.1
	Hip	MS DDZ	TBB2B_RAT	Tubulin beta-2B chain OS=Rattus norvegicus GN=Tubb2b PE=1 SV=1	49.9	123.0	20	46.1
	Hip	MS DDZ	TBB4B_RAT	Tubulin beta-4B chain OS=Rattus norvegicus GN=Tubb4b PE=1 SV=1	49.8	113.0	19	39.8
	Hip	MS DDZ	TBB5_RAT	Tubulin beta-5 chain OS=Rattus norvegicus GN=Tubb5 PE=1 SV=1	49.6	101.0	19	40.5
	Hip	MS DDZ	TBB3_RAT	Tubulin beta-3 chain OS=Rattus norvegicus GN=Tubb3 PE=1 SV=1	50.4	95.2	18	33.1
	Hip	MS DDZ	TBA1A_RAT	Tubulin alpha-1A chain OS=Rattus norvegicus GN=Tuba1a PE=1 SV=1	50.1	79.5	15	41.7
	Hip	MS DDZ	TBA3_RAT	Tubulin alpha-3 chain OS=Rattus norvegicus GN=Tuba3a PE=2 SV=1	49.9	70.9	15	41.6
	Hip	MS DDZ	TBA1B_RAT	Tubulin alpha-1B chain OS=Rattus norvegicus GN=Tuba1b PE=1 SV=1	50.1	69.9	14	38.8
	Hip	MS DDZ	TBA1C_RAT	Tubulin alpha-1C chain OS=Rattus norvegicus GN=Tuba1c PE=1 SV=1	49.9	69.4	16	47.9
	Hip	MS DDZ	TBA8_RAT	Tubulin alpha-8 chain OS=Rattus norvegicus GN=Tuba8 PE=2 SV=1	50.0	60.9	14	37.2
62	Cbrum	MS DDZ	STXB1_RAT	Syntaxin-binding protein 1 OS=Rattus norvegicus GN=Stxbp1 PE=1 SV=1	67.5	78.5	18	33.2
	Cbrum	MS/MS DDZ	STXB1_RAT			74.5	2	4.4

As already found for BHM, also for RBM not all of the identified proteins are currently proposed mitochondrial (membrane) proteins. This is in line with the isolation of crude mitochondrial fraction from tissue (3.1). But most of the identified proteins are associated with energy metabolism, involved in stress management or are part of the processes at synapses.

Of more than 80 known subunits of OxPhos complexes 16 subunits were identified for RBM and 17 for BHM in this thesis.

For the in Fig. 4.18A assigned OxPhos complexes or the different metabolic pathways or other assigned proteins in Fig. 4.18B, the total number of identified protein spots of RBM was

depicted as well as the number of spots identically identified in different rat brain areas. For this it was differentiated whether the spots were identified for all brain areas (cerebellum, hippocampus, cerebrum) or two of them or only for one area.

For OxPhos complexes (Fig. 4.18A), most of the spots were identically identified in two or more brain areas. 17 of 39 were found in all three areas and 13 in two areas. Eight spots were found in just one brain area, while respective spots of the other areas gave no result. The identification of only one spot of CV (no. 39) resulted in two different subunits (d and O), which belong both to the peripheral stalk of ATP synthase.

According to Fig. 4.18B, only a few spots originating from proteins of metabolic pathways or other proteins were found in more than one brain area. Of 18 identified spots in total, seven were identically identified in two or three brain areas. The identification of only one protein spot (no. 43, stress management of the cell) resulted in two possible proteins (CH60 or

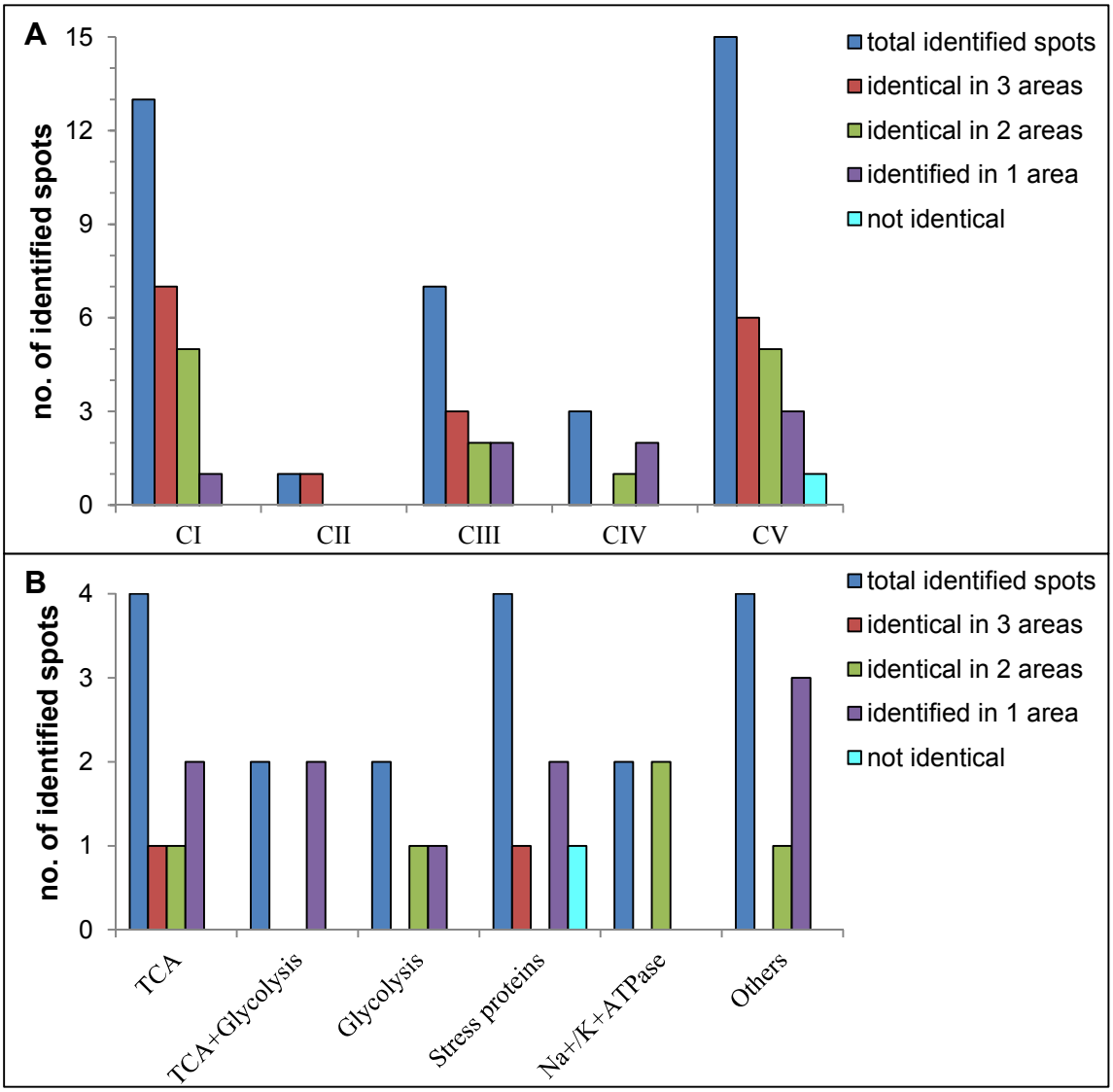

Fig. 4.18: Number of identically identified protein spots by PMF for the different rat brain areas. The total number of identified spots for the assigned OxPhos complex or for each assigned metabolic pathway was calculated. The number of spots was determined, which were identical in all rat brain areas (cerebellum, hippocampus and cerebrum), in two of them or just identified in one area. Also, the number for not identical spots was plotted. **A:** spots belonging to OxPhos complexes, **B:** spots from different metabolic pathways: TCA cycle, glycolysis or proteins of cellular stress management and others.
CI = complex I, CII = complex II, CIII = complex III, CIV = complex IV, CV = complex V

EAA1), but for both originating brain areas, most likely explained by an overlay of the protein spots in the 2D gel.

In total, 13 subunits of OxPhos complexes were identified identically for 26 protein spots compared to Reifschneider et al. (2006). Even, 13 additional protein spots in the 2D gel were assigned to the same subunits. Four extra subunits of OxPhos proteins were assigned for seven protein spots.

From non-OxPhos proteins, ten subunits or proteins were identified identically to Reifschneider et al. (2006) and six additional subunits were found. However, the area of lower mass proteins in the 2D-BN/SDS gel (upper right corner) is difficult to assign, because of many very small, often smeared, protein spots, which are difficult to distinguish. Therefore the assignment has to be handled with care for this area.

The identically identification of so many mitochondrial protein subunits all-over the 2D-BN/SDS gel gives further evidence for the comparability of the migration pattern of those described by Reifschneider et al. (2006) to those of the three analysed brain areas. Additional spots (36, 42a, 51 and 54a) could be assigned by relating the previous results from PMF of RBM by Reifschneider et al. (2006) to the current results of RBM for further analysis such as quantitation. For CIII three additional spots were assigned: spot no. 36 as “Rieske Fe-S protein precursor” (NCBInr 206681) and spot no. 42a as “similar to ubichinone-cytochrome c oxidoreductase, binding protein” (NCBInr 34866011), both from Reifschneider et al. (2006). Spot no. 35a was assigned as “cytochrome b” (CYB) by comparison with the results from PMF of BHM (Table 4.10). For CIV one additional subunit was assigned for spot 54a as “cytochrome c oxidase subunit Via (85AA)” (NCBInr 818021). An additional spot, no. 51, was assigned as “lipophilin” (proteolipid protein) (NCBInr 206224), (both Reifschneider et al. (2006)). Lipophilin is a membrane protein and involved in formation of the myelin sheath (UniProt databases).

Five subunits of OxPhos complexes of RBM were additionally identified by WB analyses (Fig. 4.19). For each applied antibody 40 µg (b. sol. d/p: 8g/g) RBM (cerebellum, OAL) were solubilised (3.3), separated by 2D-BN/SDS PAGE (3.5) and WB analysis (3.10). M. Sc. Olga Ankudin performed the analyses as contract work. Fig. 4.19A displays the image of a silver stained 10.0 cm by 10.5 cm sized performed 2D-BN/SDS gel after WB analysis. The image of the CBBG stained BN gel lane was attached horizontally above for assignment of bands respectively OxPhos complexes. The mass standard LMW was marked. The assigned protein spots are connected to the results of the WBs by coloured squares as in Fig. 4.19B-F. The subunits NDUS1 (CI, Fig. 4.19B), DHSA (CII, Fig. 4.19C), QCR2 (CIII, Fig. 4.19D), COX1 (CIV, Fig. 4.19E) and alpha (CV, Fig. 4.19F) could be assigned and are in line with the findings of the PMF analysis (see current chapter). By comparison of Fig. 4.19 to Fig. 4.15, Fig. 4.16 and Fig. 4.17, NDUS1 could be assigned to spot no. 04, 05, 06 and 07, DHSA to no. 49 and 81, QCR2 to no. 16, 17, 20, 22 and 24, COX1 to no. 29, 30 and 47 and alpha to no. 02, 10 and 12.

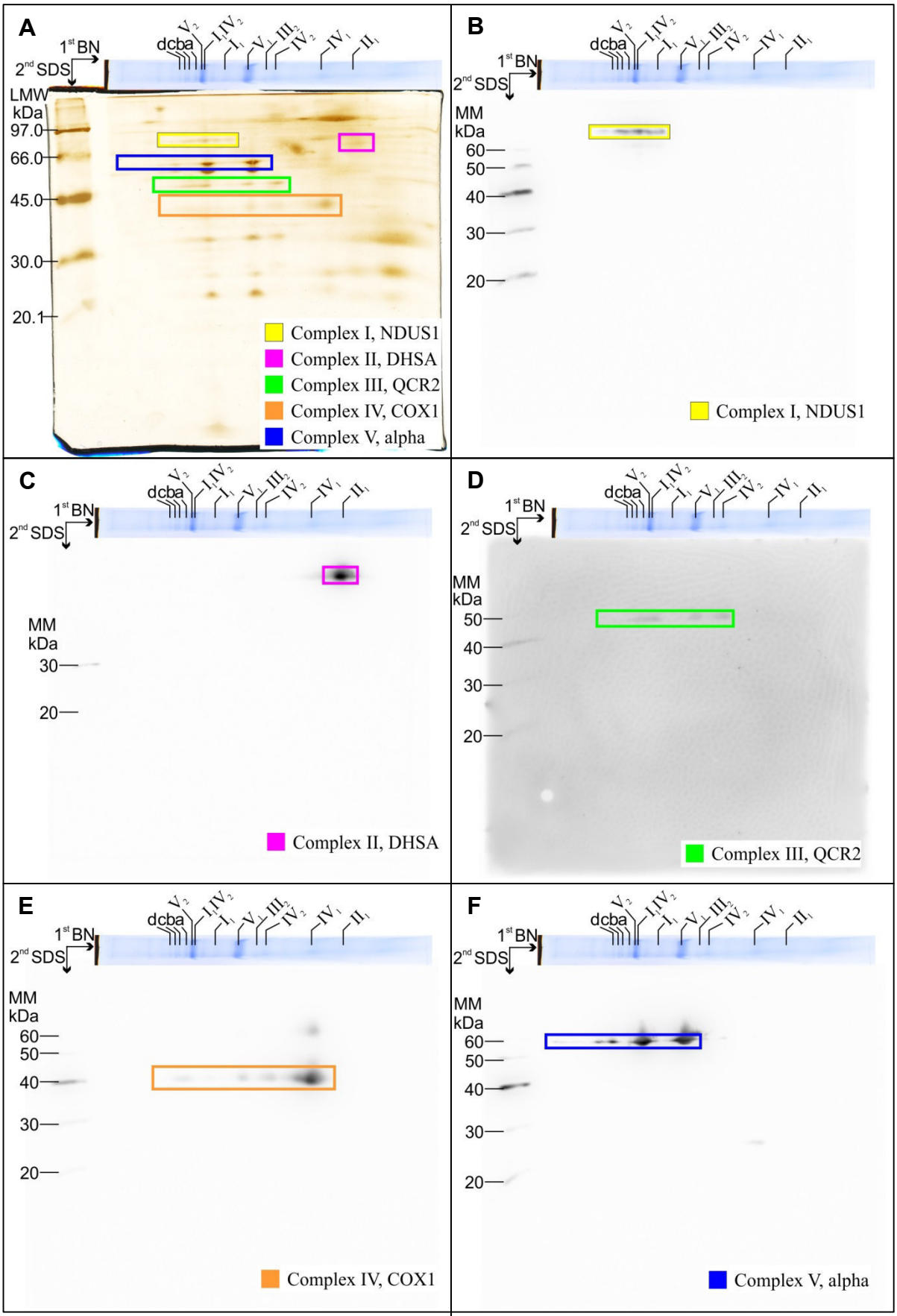

Fig. 4.19: WB analysis of OxPhos complexes from RBM. 40 µg (b. sol. d/p: 8g/g) RBM (cerebellum, OAL) were separated by 2D-BN/SDS PAGE (10.0 cm by 10.5 cm sized gel) followed by WB analysis. .**A:** silver stained 2D-BN/SDS gel (after WB), **B:** WB, anti CI (NDUS1), **C:** WB, anti CII (DHSA), **D:** WB, anti CIII (QCR2), **E:** WB, anti CIV (COX1), **F:** WB, anti CV (alpha). **A-F:** The image of the CBBG stained BN gel lane was arranged horizontally above the images of gel and WBs for assignment of bands. LMW and MM were marked.

Provided that proteins of BHM and RBM show the same electrophoretic migration behaviour in 2D-BN/SDS gels, the results of WB analysis for BHM described by Decker (presumably 2016) could be transferred to RBM samples, as well as the results from PMF (see above). When subunit COX1 from CIV of BHM is compared to RBM the protein spots 29, 30 and 47 of RBM can be assigned to COX1.

To compare the results of the protein spot identification of BHM to those of RBM, the number of identical protein spots for OxPhos complexes was analysed (Fig. 4.20).

The number of all protein spots, which were identified for BHM and RBM, was plotted as "total spots" for each OxPhos complex in Fig. 4.20. The red bars depict, how many spots were identified identically for BHM and RBM. The number of not identically identified spots was also calculated and plotted in Fig. 4.20 for each complex. Only for two spots of CV the results did not match. These were spot no. 39 and no. 41. The identification of spot no. 39 resulted in subunits O and d for RBM, both belonging to the peripheral stalk of ATP synthase, while the analysis of the same spot of BHM resulted only in subunit O. Spot no. 41 was identified as subunit O for RBM and subunit d for BHM. This reflects the close structural association of both subunits.

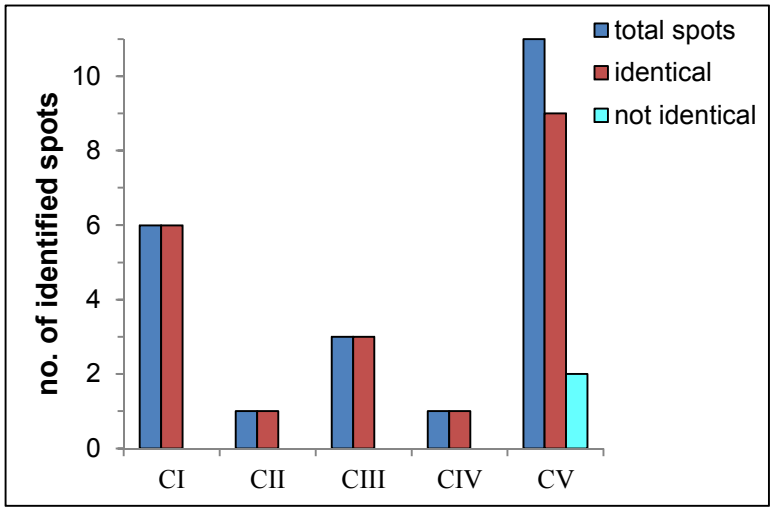

Fig. 4.20: Matching of identified protein spots from BHM to RBM for OxPhos complexes. The total number of corresponding identified protein spots of BHM and RBM was plotted for the OxPhos complexes. From these spots, the number of identical and non-identical spots was depicted.

To summarise, out of 22 identified protein spots in both samples (BHM and RBM) only two did not match, however originated from subunits of the same protein subunit. This provides evidence for the comparability of the protein migration pattern in 2D-BN/SDS gels of BHM to RBM.

4.2.4 Quantitation of protein amount in bands of CBBG stained BN gels

Two different techniques have been used for quantitation of the amount of mitochondrial proteins in gels for years now. On the one hand, quantitation of mitochondrial proteins was performed by densitometric analysis of gel bands from BN PAGE, amongst others by Schagger (1995), Sabar et al. (2005), Gómez et al. (2009), Lombardi et al. (2009), Frenzel (2011) and Silvestri et al. (2015). On the other hand, quantitation of mitochondrial proteins was applied by densitometric examination of protein spots, equivalent to the subunits of the proteins, originating from 2D-BN/SDS PAGE, amongst others applied by Schagger (1995), Andringa et al. (2010), Frenzel (2011)and Verma et al. (2015).

To compare those two techniques for quantitation of mitochondrial protein amount, bands of CBBG stained BN gels were analysed and compared (end of this chapter) to protein spot quantitation from 2D-BN/SDS gels (4.2.5). Please keep in mind that printed images differ from evaluated original grey scale images as described in 3.11.

For each brain region (cerebellum, hippocampus and cerebrum), pooled mitochondria of the animal groups YAL, YCR, OAL and OCR were solubilised with a ratio of 8 g digitonin per 1 g protein (d/p: 8g/g) (3.3.1). 100 µg before solubilisation (b. sol.) of mitochondrial protein were loaded per BN gel lane. 70 µg BHM (b. sol. d/p: 3g/g) and 3 µL HMW were loaded additionally to serve as standard. Three BN gels were performed as technical repeats as described in 3.4. After the run, they were stained with CBBG (3.7.2) and coloured and grey scale images were taken (3.7.3). The latter were quantitatively analysed (3.11.2). The bands of complexes I_1IV_2 and V_2 could not be evaluated, because of their overlap in BN gel. The bars in the diagrams represent the mean of the technical repeats (n=3), the error bars the standard error. The grey units are given for each band respectively complex. Statistically significant changes are marked with asterisks. Black asterisks show age-related changes and red ones mark changes caused by calorie restriction. Significance levels are 0.05 (*) and 0.01 (**).

The three entire gel images and the fused image for quantitation are shown in “7 Supplements”, Fig. 7.1 and Fig. 7.2, sections of the images in this chapter below. The OxPhos complexes and supercomplexes are marked in the images for BHM and for one rat brain sample, representatively for all rat brain samples. The allocation (Fig. 4.21, Fig. 4.23, Fig. 4.25) was carried out according to 4.2.3. The masses of HMW are labelled in orange.

Cerebellum

In Fig. 4.21 the left section of one of the BN gel images is shown. The entire image (BN3) is attached in "7 Supplements", Fig. 7.2. The separated mitochondrial proteins from cerebellum of the four groups (YAL, YCR, OAL, OCR) are visible. The standards BHM and HMW are also assigned. By eye, no pronounced differences in intensities between the four groups of cerebellum rat brain are visible. Only complex IV_1 seems to be more intense in old animals than in young ones. It is clearly visible that the standard BHM shows slightly different migration behaviour compared to the rat brain samples (see 4.2.3). Latter show identical migration behaviour. By eye, some of the bands cannot be exactly distinguished, but it is possible with the software Delta2D in the tool "Rollups 3D Spots" on the fused grey scale images. A figure of the fused image is attached in "7 Supplements", Fig. 7.2. Concerning HMW (Table 3.6), the band at 232 kDa of catalase is missing or just weakly smeared visible, as already observed by members of our working group e.g. Thilmany (2013). Another fact is, that the (water soluble) standard proteins of HMW run faster through the gel (to lower masses), than the marked (membrane) complexes (4.2.3).

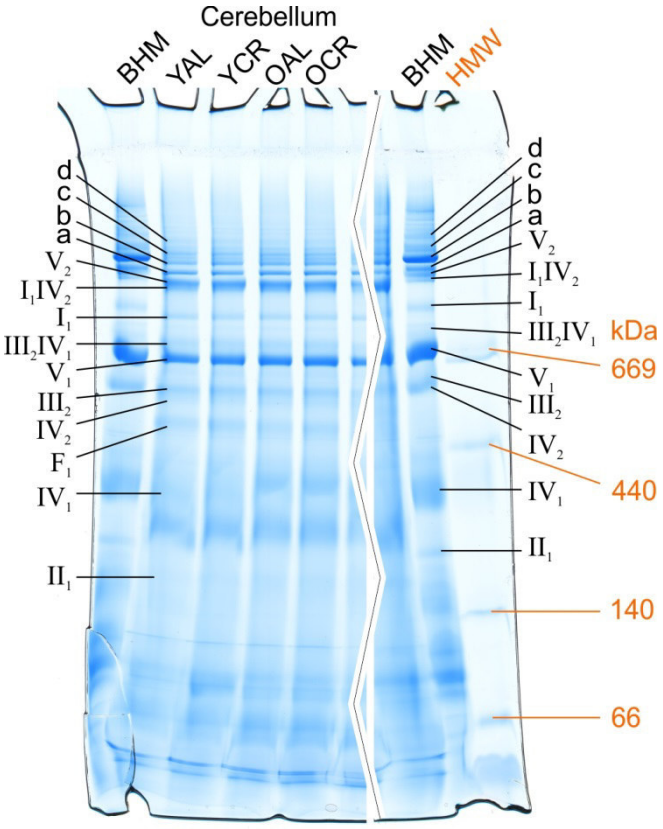

Fig. 4.21: BN gel for quantification of protein amount from RBM of cerebellum. From each cerebellum animal group (YAL, YCR, OAL, OCR) 100 µg mitochondrial proteins were solubilised with d/p: 8g/g and separated by BN PAGE, followed by CBBG staining. 70 µg (b. sol. d/p: 3g/g) BHM and HMW (marked in orange) served as standard, OxPhos complexes and supercomplexes are marked. a = I_1III_2, b = $I_1III_2IV_1$, c = $I_1III_2IV_2$, d = $I_1III_2IV_3$. The vertical zig-zag line indicates the intersection of the image.

For the cerebellum samples, the results of the quantitative evaluation (3.11.2 and 3.11.3) of the grey scale BN gel images are depicted in Fig. 4.22. In Fig. 4.22 it is observable for mitochondria of cerebellum that the protein amount decreases with age (black asterisks) of *ad libitum* fed animals (YAL vs. OAL) for complexes I_1 (-28.5 % stat. high sig.), III_2IV_1 (-15.7 % stat. sig.) and I_1III_2 (-19.5 %, stat. sig.) and for III_2 (-10.4 %), $I_1III_2IV_2$ (-19.8 %) and V_1 (-9.2 %, all not stat. sig.). For aged animals under calorie restriction (YCR vs. OCR), a decrease is observable for supercomplexes III_2IV_1 (-10.0 %) and $I_1III_2IV_3$ (-12.7 %, both not stat. sig.). In contrast to that, ageing in calorie restricted rats (YCR vs. OCR) increases the protein amount for complex IV_1 (+29.5 %, stat. high sig.) and II_1 (+18.9 %, not stat. sig.) and for $I_1III_2IV_1$ (+7.7 %, not stat. sig.) from *ad libitum* fed rats (YAL vs. OAL).

Short-term calorie restriction (YAL vs. YCR, red asterisks) decreases the protein amount of complex I_1 (-21.9 %, stat. sig.) and in complexes I_1III_2 (-11.1 %), $I_1III_2IV_2$ (-20.5 %) and V_1 (-12.2 %, all not stat. sig.). Long-term calorie restriction leads to decreased protein amount for

complex $I_1III_2IV_1$ (-9.7 %, stat. sig.), whereas the protein amount of complexes II_1 (+15.0 %), IV_1 (+12.6 %) and I_1III_2 (+12.5 %) increases (all stat. sig.).

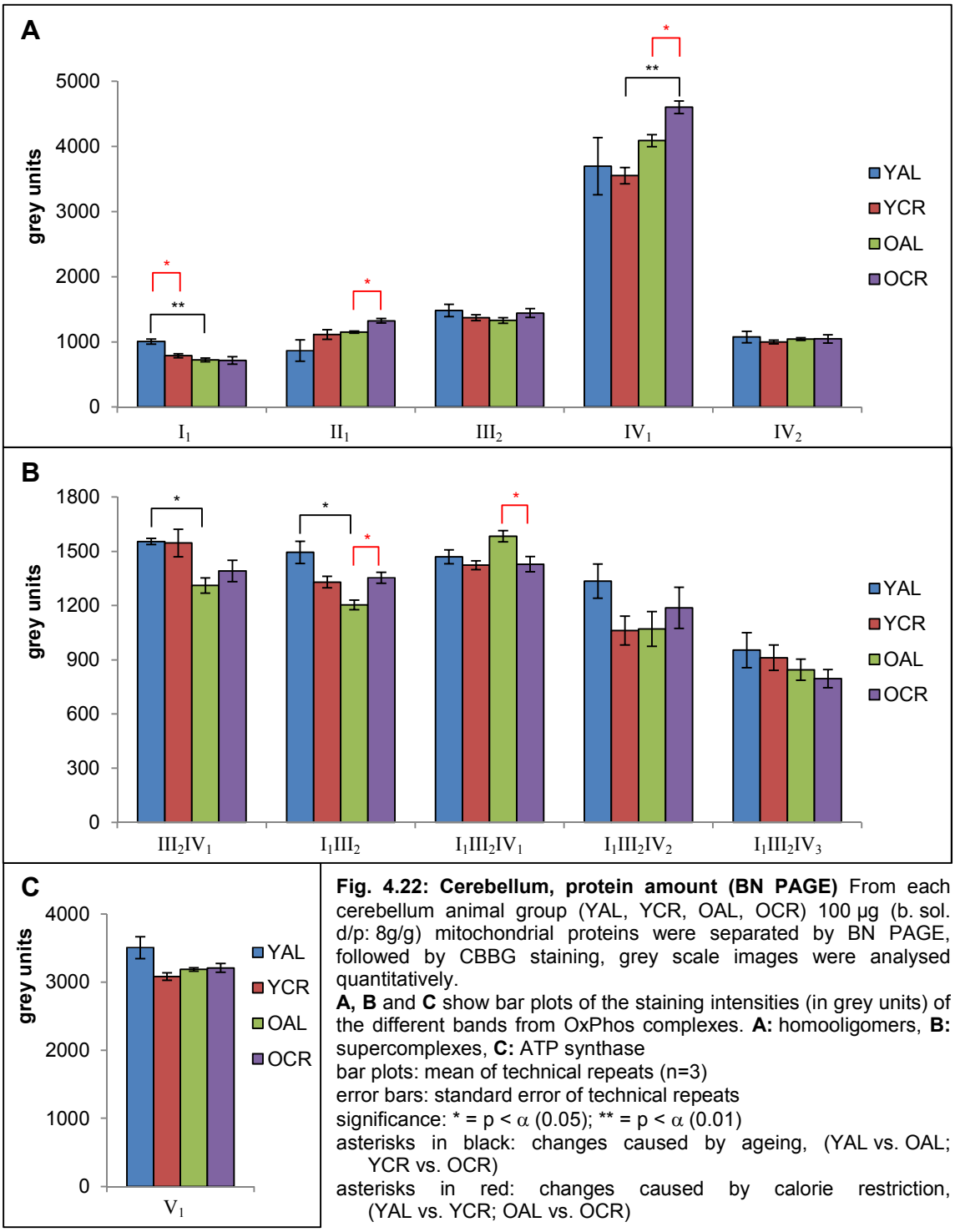

Fig. 4.22: Cerebellum, protein amount (BN PAGE) From each cerebellum animal group (YAL, YCR, OAL, OCR) 100 µg (b. sol. d/p: 8g/g) mitochondrial proteins were separated by BN PAGE, followed by CBBG staining, grey scale images were analysed quantitatively.
A, B and **C** show bar plots of the staining intensities (in grey units) of the different bands from OxPhos complexes. **A:** homooligomers, **B:** supercomplexes, **C:** ATP synthase
bar plots: mean of technical repeats (n=3)
error bars: standard error of technical repeats
significance: * = $p < \alpha$ (0.05); ** = $p < \alpha$ (0.01)
asterisks in black: changes caused by ageing, (YAL vs. OAL; YCR vs. OCR)
asterisks in red: changes caused by calorie restriction, (YAL vs. YCR; OAL vs. OCR)

Hippocampus

In Fig. 4.23 the middle section of a BN gel (BN3) image is shown. The entire image is attached in "7 Supplements", Fig. 7.2. The solubilised and separated mitochondrial protein samples of hippocampus are labelled in blue. The standards BHM and HMW (orange) are also marked. As already mentioned above for cerebellum samples, the standard BHM shows the same differences in migration behaviour compared to the RBM samples. By eye, there seems to be no difference between the intensities of the bands of the four animal groups of hippocampus RBM samples.

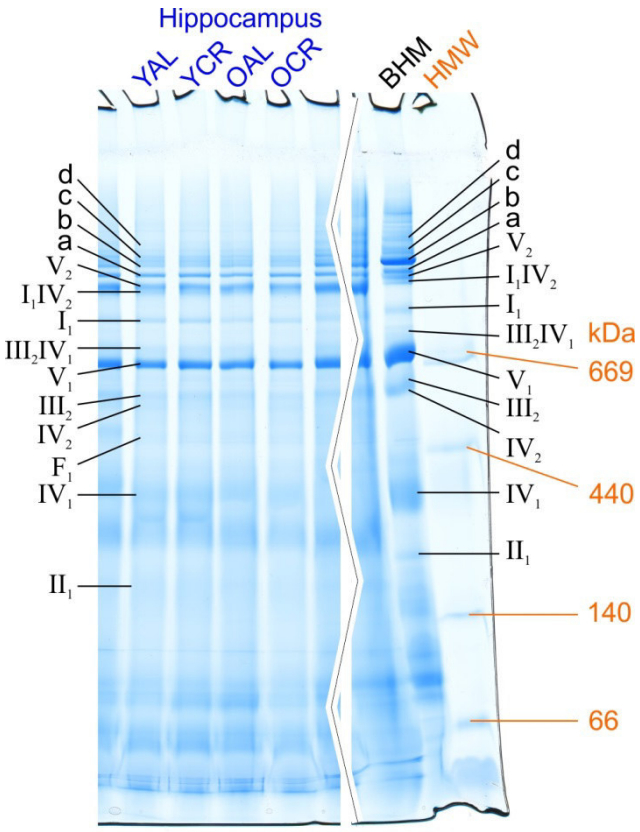

Fig. 4.23: Hippocampus, BN gel for quantification of protein amount, from each hippocampus animal group (YAL, YCR, OAL, OCR) 100 µg mitochondrial proteins (b. sol. d/p: 8g/g) were separated by BN PAGE, followed by CBBG staining. 70 µg (b. sol. d/p: 3g/g) BHM and HMW (marked in orange) served as standard, OxPhos complexes and supercomplexes are marked. a = I_1III_2, b = $I_1III_2IV_1$, c = $I_1III_2IV_2$, d = $I_1III_2IV_3$. The vertical zig-zag line indicates the intersection of the image.

In Fig. 4.24 quantitative results from the evaluation of the fused image (compare "7 Supplements", Fig. 7.2) with Delta2D are shown (for details see 3.11.2, 3.11.3).

As observable in Fig. 4.24 ageing (black asterisks) of *ad libitum* fed rats (YAL vs. OAL) increases the amount of mitochondrial protein from hippocampus for complexes II_1 (+27.8 %), $I_1III_2IV_3$ (+24.7 %) and ATP synthase monomer V_1 (+15.7 %, all stat. sig.) and IV_1 (+8.4 %), $I_1III_2IV_1$ (+16.2 %) and $I_1III_2IV_2$ (+22.4 %, all not stat. sig.).

Ageing under conditions of calorie restriction (YCR vs. OCR) decreases the mitochondrial protein amount in hippocampus for the complexes II_1 (-27.2 %), III_2 (-13.8 %), IV_1 (-27.5 %), and ATP synthase monomer V_1 (-13.7 %, all stat. sig.), and for I_1 (-20.3 %), IV_2 (-16.3 %) and the supercomplexes $I_1III_2IV_1$ (-6.2 %), $I_1III_2IV_2$ (-17.5 %) and $I_1III_2IV_3$ (-8.8 %, all not stat. sig.).

Short-term calorie restriction (YAL vs. YCR, red asterisks, Fig. 4.24) increases the protein amount for III_2 (+24.6 %), $I_1III_2IV_1$ (+5.2 %), $I_1III_2IV_3$ (+16.2 %) and ATP synthase monomer V_1 (19.9 %, all stat. sig.) and for I_1 (+17.4 %), II_1 (+13.0 %), IV_1 (+23.9 %), I_1III_2 (+13.1 %) and $I_1III_2IV_2$ (+16.5 %, all not stat. sig.).

Long-term calorie restriction (OAL vs. OCR, red asterisks) reduces the protein amount in hippocampus as indicated for II_1 (-35.6 %), IV_1 (-17.1 %), the supercomplexes $I_1III_2IV_1$ (-15.1 %), $I_1III_2IV_2$ (-21.5 %) and $I_1III_2IV_3$ (-15.0 %) and ATP synthase monomer V_1 (-10.5 %, all stat. sig.), and for IV_2 (-14.5 %) and III_2IV_1 (-7.7 %, both not stat. sig.). In

contrast to that, exclusively the amount of I_1III_2 is increased (+8.7 %, not stat. sig.) during long-term calorie restriction.

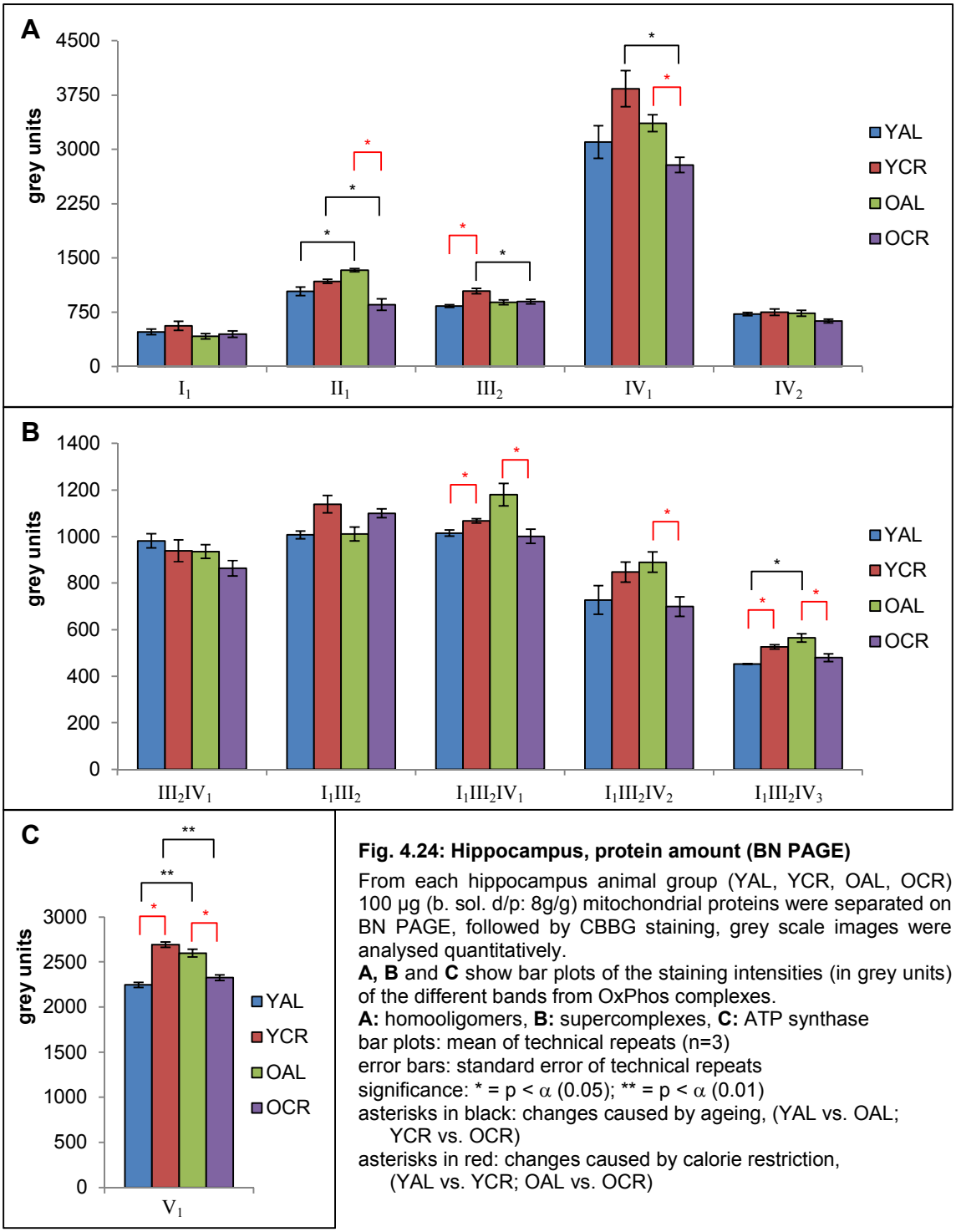

Fig. 4.24: Hippocampus, protein amount (BN PAGE)

From each hippocampus animal group (YAL, YCR, OAL, OCR) 100 µg (b. sol. d/p: 8g/g) mitochondrial proteins were separated on BN PAGE, followed by CBBG staining, grey scale images were analysed quantitatively.
A, B and **C** show bar plots of the staining intensities (in grey units) of the different bands from OxPhos complexes.
A: homooligomers, **B:** supercomplexes, **C:** ATP synthase
bar plots: mean of technical repeats (n=3)
error bars: standard error of technical repeats
significance: * = $p < \alpha$ (0.05); ** = $p < \alpha$ (0.01)
asterisks in black: changes caused by ageing, (YAL vs. OAL; YCR vs. OCR)
asterisks in red: changes caused by calorie restriction, (YAL vs. YCR; OAL vs. OCR)

Cerebrum

Cerebrum mitochondrial proteins were separated by BN PAGE. The right section of the image of the CBBG stained BN gel (BN3) is shown in Fig. 4.25. The entire image is attached at "7 Supplements", Fig. 7.2. The different animal groups are marked in red, the standards BHM and HMW (orange) are also labelled. As already described for cerebellum and hippocampus, the same shifts and running behaviour for BHM and HMW are visible. The running behaviour seems to be identical for the four different cerebrum animal groups. By eye, there are no visible changes in the intensity of the bands of the four different rat groups, only in the area above the supercomplex $I_1III_2IV_3$ (=d) of OCR, the unknown higher bands seem to be more intense.

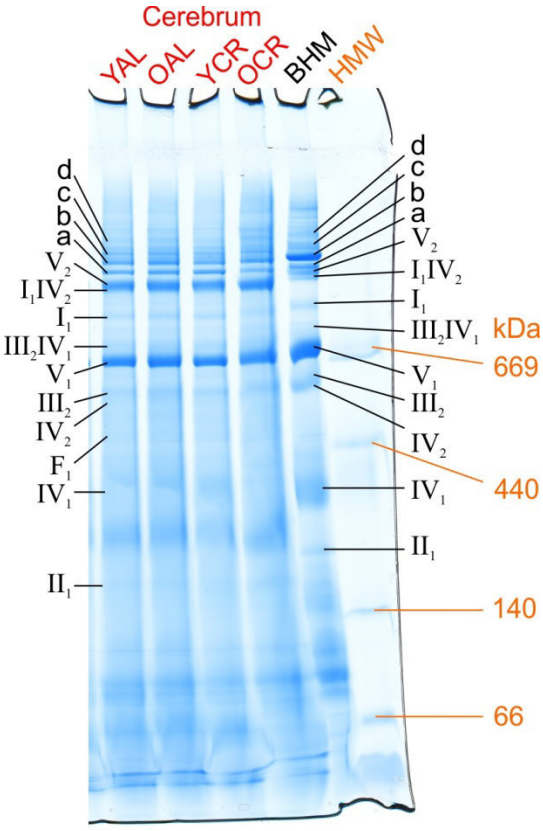

Fig. 4.25: Cerebrum, BN gel for quantification of protein amount, from each cerebrum animal group (YAL, YCR, OAL, OCR) 100 µg (b. sol. d/p: 8g/g) mitochondrial proteins were separated by BN PAGE, followed by CBBG staining. 70 µg (b. sol. d/p: 3g/g) BHM and HMW (marked in orange) served as standard, OxPhos complexes and supercomplexes are marked. a = I_1III_2, b = $I_1III_2IV_1$, c = $I_1III_2IV_2$, d = $I_1III_2IV_3$.

The results of the quantitative evaluation of the band intensities from the fused image (see "7 Supplements", Fig. 7.2) are depicted in Fig. 4.26.

In cerebrum of *ad libitum* fed animals (YAL vs. OAL) ageing (black asterisks) increases the protein amount of the complexes I_1 (+45.0 %), III_2 (+33.8 %), III_2IV_1 (+31.2 %), $I_1III_2IV_2$ (+27.6 %) and $I_1III_2IV_3$ (+25.1 %), ATP synthase monomer V_1 (+23.5 %, all stat. sig.) and for the complexes IV_2 (+28.3 %), I_1III_2 (+36.1 %) and $I_1III_2IV_1$ (+16.9 %, all not stat. sig.) according to Fig. 4.26.

For cerebrum of calorie restricted animals (YCR vs. OCR), the protein amount of I_1 (+34.8 %), III_2 (+79.2 %), IV_2 (+30.5 %), III_2IV_1 (+29.8 %), $I_1III_2IV_1$ (+31.9 %), $I_1III_2IV_2$ (+52.3 %), $I_1III_2IV_3$ (+77.1 %) and ATP synthase monomer V_1 (+41.6 %) increase (all stat. sig.) with age (black asterisks), even for complex II_1 (+21.1 %, not stat. sig.). In contrast to the observed increase in protein amount, only complex I_1III_2 decreases (-10.0 %, not stat. sig).

According to short-term calorie restriction (YAL vs. YCR), the cerebrum protein amount of complex II_1 (-23.7 %) is decreased (not stat. sig.), whereas for complex I_1III_2 (+33.4 %) an increased protein amount is observable (not stat. sig.).

Long-term calorie restriction (OAL vs. OCR, red asterisks) leads to an increase of cerebrum protein amount for complexes III_2 (+41.7 %), $I_1III_2IV_1$ (+9.9 %), $I_1III_2IV_2$ (+15.0 %), $I_1III_2IV_3$ (+27.1 %) and ATP synthase monomer V_1 (+21.6 %, all stat. sig.) and for I_1 (+10.0 %) and III_2IV_1 (+4.3 %, both not stat. sig.). Only complex I_1III_2 (-11.8 %) shows a decreased protein amount (stat. sig.).

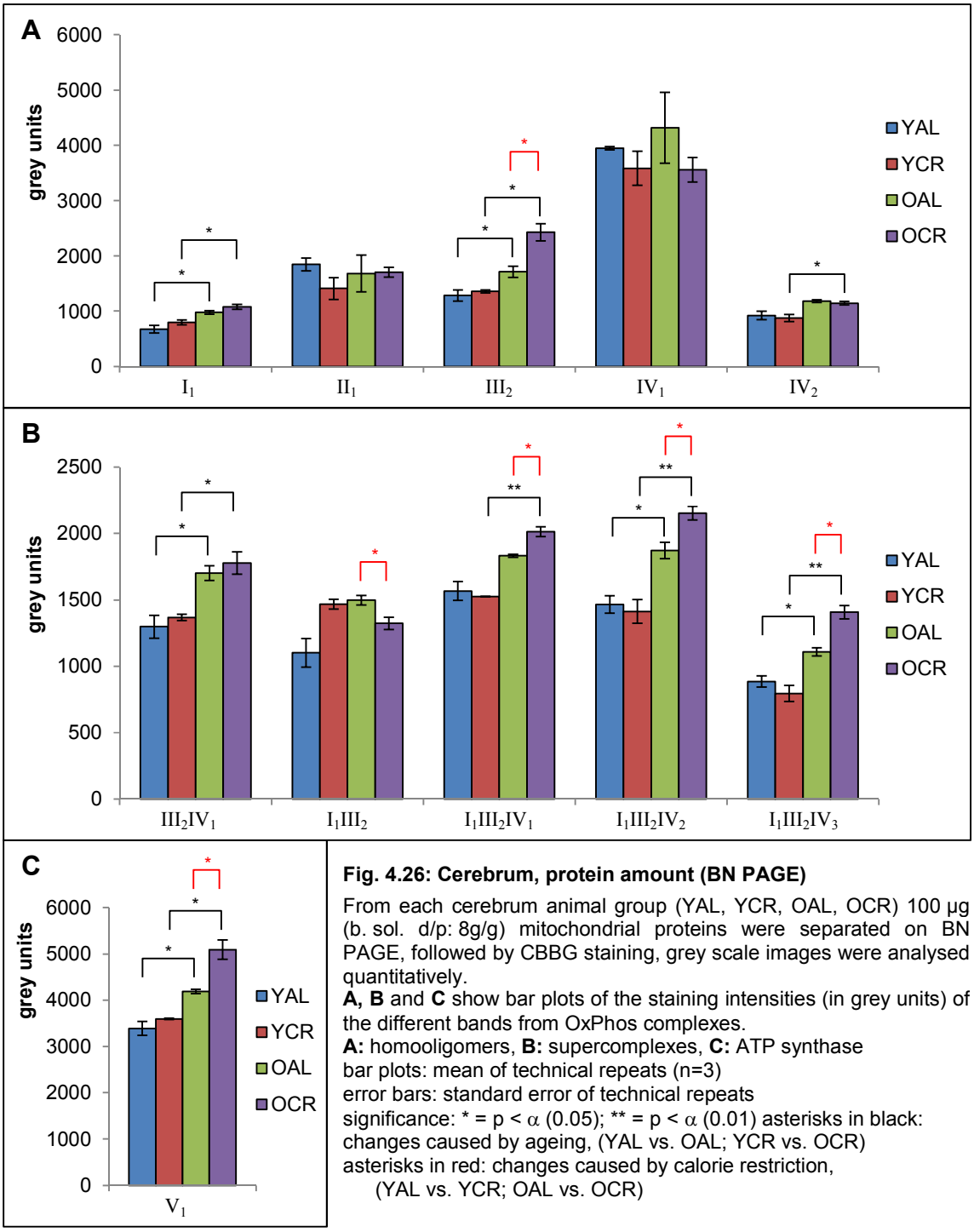

Fig. 4.26: Cerebrum, protein amount (BN PAGE)

From each cerebrum animal group (YAL, YCR, OAL, OCR) 100 µg (b. sol. d/p: 8g/g) mitochondrial proteins were separated on BN PAGE, followed by CBBG staining, grey scale images were analysed quantitatively.
A, B and **C** show bar plots of the staining intensities (in grey units) of the different bands from OxPhos complexes.
A: homooligomers, **B:** supercomplexes, **C:** ATP synthase
bar plots: mean of technical repeats (n=3)
error bars: standard error of technical repeats
significance: * = $p < \alpha$ (0.05); ** = $p < \alpha$ (0.01) asterisks in black: changes caused by ageing, (YAL vs. OAL; YCR vs. OCR)
asterisks in red: changes caused by calorie restriction, (YAL vs. YCR; OAL vs. OCR)

Summary

Table 4.28 gives an overview of the quantitative results of the BN gel analysis as described above in the separate chapters for the different brain parts. For each tissue sample, the results for changes in age for *ad libitum* fed animals (AL: YAL vs. OAL) and under calorie restriction (CR: YCR vs. OCR) are presented as well as the effects of short-term (ST: YAL vs. YCR) and long-term (LT: OAL vs. OCR) calorie restriction. The arrows represent the increasing (△) or decreasing (▽) protein amount for the compared animal groups as a summary of the findings. Both arrows are used in **grey** (**not stat. sig.**), **orange** (**stat. sig.**) and **red** (**stat. high sig.**). Black dashes (▬) were placed, where **no variation** could be examined. Main tendencies are described below. For more details, see the chapters about the different brain parts.

In cerebellum it is observable that the protein amount is decreasing during ageing of *ad libitum* fed rats (Table 4.28). Calorie restriction during ageing increases the protein amount of specific homooligomers and decreases the amount of some supercomplexes. Short-term calorie restriction reduces the protein amount in cerebellum, while for animals under the influence of long-term calorie restriction the protein amount is mainly increased.

In hippocampus the protein amount rises in *ad libitum* fed animals caused by ageing, whereas in calorie restricted animals the amount is decreased. Short-term calorie restriction causes increased protein amount in hippocampus but a decrease is observed for long-term calorie restriction.

The cerebrum protein amount rises with age, independently from *ad libitum* or calorie restricted nutrition. The same tendency is visible for long-term calorie restriction. Short-term calorie restriction effects only complexes II_1 (▽) and I_1III_2 (△).

In general, it is important to note, that changes occur in individual or homooligomeric complexes in the same way as in their oligomeric or supercomplex assemblies.

Table 4.28: Overview of the changes in protein amount as observed in BN PAGE analysis

figures	entity	Cerebellum				Hippocampus				Cerebrum			
		AL	CR	ST	LT	AL	CR	ST	LT	AL	CR	ST	LT
4.22A 4.24A 4.26A	I_1	▼	▬	▽	▬	▬	▽	△	▬	△	△	▬	△
	II_1	▬	△	▬	△	△	▽	△	▽	▬	△	▽	▬
	III_2	▽	▬	▬	▬	▬	▽	△	▬	△	△	▬	△
	IV_1	▬	△	▬	▲	△	▽	△	▽	▬	▬	▬	▬
	IV_2	▬	▬	▬	▬	▬	▽	▬	▽	△	△	▬	▬
4.22B 4.24B 4.26B	III_2IV_1	▽	▽	▬	▬	▬	▬	▬	▽	△	△	▬	△
	I_1III_2	▽	▬	▽	△	▬	▬	△	△	△	▽	△	▽
	$I_1III_2IV_1$	△	▬	▬	▽	△	▽	△	▽	△	△	▬	△
	$I_1III_2IV_2$	▽	▬	▽	▬	△	▽	△	▽	△	△	▬	△
	$I_1III_2IV_3$	▬	▽	▬	▬	△	▽	△	▽	△	△	▬	△
4.22C 4.24C 4.26C	V_1	▽	▬	▽	▬	△	▽	△	▽	△	△	▬	△

symbols: "△": increase, "▽": decrease, "▬": no change;
colours of symbols: red: stat. high sig., orange: stat. sig., grey: not stat. sig.
colours of shades: pink: opposed to 2D analysis, green: conform with 2D analysis, turquoise: not included in 2D analysis
abbrev.: AL: *ad libitum*, CR: calorie restriction, ST: short-term calorie restriction, LT: long-term calorie restriction

Comparison of quantitation of protein amount in BN gels and 2D-BN/SDS gels

The results of the quantitative BN PAGE analysis (4.2.4) were compared to the results of 2D-BN/SDS PAGE (4.2.5). When trends of changes in amount of protein from analysed BN gels **conformed** to analysis of 2D gels, they were shaded in **green** in Table 4.28. **Opposed results** were shaded in **pink**. Results, which were not shaded, did not contradict. There, the amount of protein remained unchanged for one of the analysis methods and the other showed a trend. Results shaded in **turquoise** were **not included in 2D analysis**, because the associated spots were not identified (4.2.3).

Out of 108 comparable protein complexes for BN gel analysis and 2D-BN/SDS gel analysis, the trends of changes due to ageing and calorie restriction conformed in 47 cases. In 45 cases, the results did not contradict. However, in 16 cases the results were opposed. The opposed results differed in average by $\Delta = 32.3$ %, with a minimum of $\Delta = 17.5$ % and a maximum of $\Delta = 68.2$ %. The quantified changes for ageing and calorie restriction are in the threshold of the average differences of the two methods. This would mean, that the quantified changes for both methods are not trustworthy. But there are some facts, which have to be considered, for decision which method is the appropriate for quantitation of proteins:

- SyproRuby staining is more sensitive to the spot amount (Table 3.14, 4.1) than CBBG staining (-BN, +2D)
- it is difficult to distinguish, whether a protein band from a BN gel contains only one protein or one protein complex or an undesired overlay of more than one (-BN, +2D)
- provided that the protein band of a BN gel contains only one protein, it would be the whole protein and not only several subunits, which would be quantified finally (+BN, -2D)
- the spots can be directly related to identified subunits of proteins in 2D gels, which would exclude the problem of overlaid proteins, provided that the quantitation of the subunit performs as like as the whole protein amount (-BN, +2D)
- a more detailed analysis is possible in 2D gels, for example the performance of one complex in individual form can be compared to the performance of this complex in its different supercomplex assemblies (-BN, +2D)
- the analysis of BN gels is less time consuming, than the analysis of 2D-BN/SDS gels (+BN, -2D)

The disadvantages for BN gel analysis (-BN, +2D) predominate the advantages (+BN, -2D), especially the facts, that SyproRuby staining is more sensitive and that protein bands in BN gels could overlay, argue strongly against the method of BN gel analysis for quantitation of protein amount in BN gel bands.

Therefore the results of 2D-BN/SDS PAGE are regarded as more trustworthy and used for evaluation of the changes by ageing and calorie restriction.

4.2.5 Quantitation of proteins spots by 2D-BN/SDS PAGE analysis

As already described in 4.2.4, two different gel based techniques for protein quantitation have been used for publications about mitochondrial proteome changes. On the one hand, quantitation by densitometric analysis of gel bands from BN PAGE (4.2.4) and on the other hand, by densitometric examination of protein spots, equivalent to the subunits of the proteins originating from 2D-BN/SDS PAGE (details see 4.2.3).

To compare those two techniques for quantitation of age and calorie restriction alterations in mitochondrial protein amount, bands of CBBG stained BN gels were analysed and compared (end of chapter 4.2.4) to protein spot quantitation from SYPRO® Ruby stained 2D-BN/SDS gels (see below). Please keep in mind that printed images differ from evaluated original grey scale images as described in 3.11.

120 µg (b. sol. d/p: 8g/g, 3.3.1) mitochondrial proteins were separated by BN PAGE as described in 3.4. The lanes were cut and handled as in 3.5 to obtain 2D-BN/SDS gels, which were stained with SYPRO® Ruby and, after taking grey scale images (3.7.4), with silver. The images of the silver stained gels are depicted in "7 Supplements", Fig. 7.3-Fig. 7.8. From each animal group (YAL, YCR, OAL, OCR) of cerebellum, hippocampus and cerebrum, 2D-BN/SDS PAGE was performed in triplicates (n=3), resulting in 36 2D gels. Analysis of the data was performed with Delta2D and Excel (3.11.1, 3.11.3). For each animal group (YAL, YCR, OAL, OCR) the mean and the standard error of the spot intensities (relative grey units) of the technical repeats (n=3) were calculated and are shown as bar plots. Significant changes were marked with asterisks: * = $p < \alpha$ (0.05), ** = $p < \alpha$ (0.01). Asterisks in black show changes caused by ageing, (YAL vs. OAL; YCR vs. OCR), asterisks in red changes by calorie restriction, (YAL vs. YCR; OAL vs. OCR). The fused images are attached in "7 Supplements", Fig. 7.9. Only identified spots (4.2.3) were used for quantitation of protein amount as marked in Fig. 4.27.

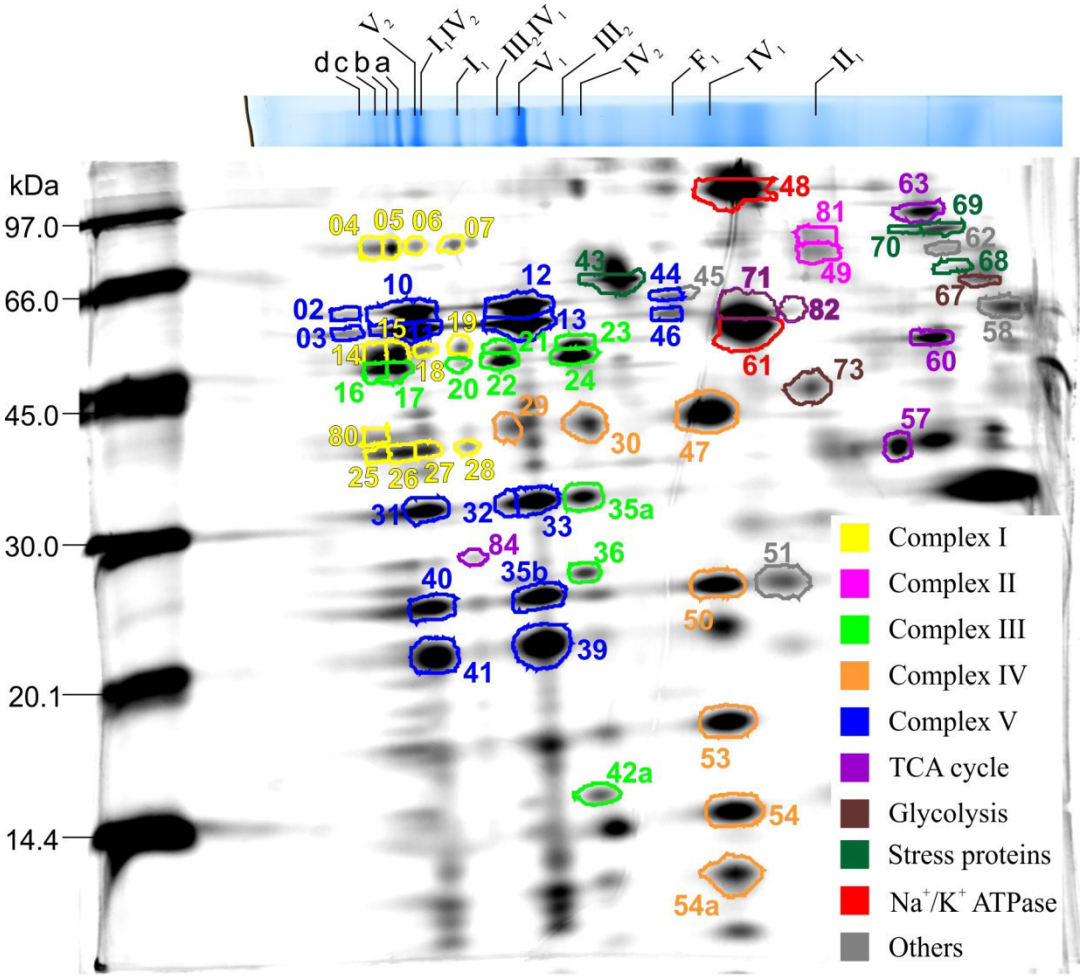

Fig. 4.27: Evaluated protein spots for quantitation (2D gels). Fused image (cerebellum) of 2D-BN/SDS gel images was taken as example. The image of the CBBG stained BN gel lane was arranged horizontally above the fused image, for assignment of bands (4.2.3). Spots are marked in different colours as specified in legend. Mass standard LMW is shown.

Spots were combined into entities, representing individual, homooligomeric and heterooligomeric OxPhos complexes and other mitochondrial proteins to compile bar plots, as described in Table 4.29.

Table 4.29: Combined spots for bar plots (quantitation of 2D gel spots)

figures	entity	examined subunits*[1]	spot no.
4.28A 4.36A 4.44A	I_1	NDUS1, NDUS2, NDUA9	7, 19, 28
	I_1IV_2		6, 18, 27
	I_1III_2		5, 15, 26
	$I_1III_2IV_1$		4, 14, 25
	total CI	all identified	4, 5, 6, 7, 14, 15, 18, 19, 25, 26, 27, 28, 80
4.28B 4.36B 4.44B	III_2	QCR2	24
	III_2IV_1		22
	III_4		20
	I_1III_2		17
	$I_1III_2IV_1$		16
	total CIII	all identified	16, 17, 20, 21, 22, 23, 24, 35a, 36*[2], 42a*[2]
4.28C 4.36C 4.44C	IV_1	COX1	47*[3]
	IV_2		30*[3]
	III_2IV_1		29*[3]
	total CIV	all identified	29*[3], 30*[3], 47*[3], 50, 53, 54, 54a*[2]
4.29 4.37 4.45	total III_2IV_1	all identified for III_2IV_1	21, 22, 29
	total I_1III_2	all identified for I_1III_2	5, 15, 17, 26
	total $I_1III_2IV_1$	all identified for $I_1III_2IV_1$	4, 14, 16, 25, 80
4.30 4.38 4.46	total CII	all identified	49, 81
4.31A 4.39A 4.47A	total CV	all identified	02, 03, 10, 11, 12, 13, 31, 32, 33, 35b, 39, 40, 41
	V_1	all identified for V_1	12, 13, 32, 33, 35b, 39
	V_2	all identified for V_2	10, 11, 31, 40, 41
	V_3	all identified for V_3	02, 03
4.31B 4.39B 4.47B	alpha	all α subunits	02, 10, 12, 44
	beta	all β subunits	03, 11, 13, 46
	alpha+beta	all α + all β subunits	02, 03, 10, 11, 12, 13, 44, 46
	F_o portion	all identified for F_o	35b, 40, 41, 39
	F_1 portion	α + β subunits for F_1	44, 46
4.32 4.40 4.48	mtDNA encoded subunits	CYB	35a
		COX2	50
4.33 4.41 4.49	Stress proteins	CH60	43, 68
		PDIA4	69
		GRP78	70
4.34A 4.42A 4.50A	TCA cycle	MDHM	57
		CISY	60
		ACON	63
		ODO1	84
4.34B 4.42B 4.50B	TCA cycle & Glycolysis	DLDH	71, 82
4.34C 4.42C 4.50C	Glycolysis	KPYM	67
		ALDOA/C	73
4.35 4.43 4.51	Na^+/K^+ ATPase	AT1A3, AT1B1	48, 61
	lipophilin	PLP1	51*[2]
	tubulin	TBB2A	58
	syntaxinBP	STXB1	62
	GLDH	DHE3	45

Assignment of spots: *[1]: by PMF, see 4.2.3 *[2]: by Reifschneider et al. (2006) *[3]: by WB analysis, see 4.2.3

Cerebellum

In Fig. 4.28A the sum of the spot intensities of the CI subunits NADH-ubiquinone oxidoreductase 75 kDa subunit (NDUS1), NADH dehydrogenase [ubiquinone] iron-sulfur protein 2 (NDUS2) and NADH dehydrogenase [ubiquinone] 1 alpha subcomplex subunit 9 (NDUA9) are plotted for the complexes I_1, I_1IV_2, I_1III_2 and $I_1III_2IV_1$ in comparison with the spot intensities for total CI. This enables to compare changes in amount of individual CI to supercomplex assemblies containing CI and to the sum of all identified spots containing CI (total CI). Detailed information about the spots (location and no.) are displayed in Fig. 4.27 and Table 4.29

For *ad libitum* nourished animals (YAL vs. OAL), there are no changes in amount of CI caused by ageing (black asterisks) in cerebellum (Fig. 4.28A). But the protein amount of CI is increased for old calorie restricted animals compared to young ones (YCR vs. OCR) for complexes I_1 (+41.0 %), I_1III_2 (+21.0 %) and total CI (+23.7 %, all stat. sig.) and for complex I_1IV_2 (+64.8 %, not stat. sig.).

Short-term calorie restriction (YAL vs. YCR, red asterisks) leads to a lower protein amount of CI for complexes I_1 (-29.5 %) and I_1III_2 (-21.7 %, both stat. sig.) and for total CI (-14.4 %, not stat. sig.). Long-term calorie restriction (OAL vs. OCR, red asterisks) increases the protein amount of CI in I_1IV_2 (+49.5 %, not stat. sig.).

Fig. 4.28B shows the spot intensities for the CIII subunit cytochrome b-c1 complex subunit 2 (QCR2) for the homooligomeric complexes III_2 and III_4, and for the supercomplexes III_2IV_1, I_1III_2 and $I_1III_2IV_1$ compared to the sum of the intensities of all identified spots of CIII (total CIII). This permits to compare the changes in CIII protein amount in individual complexes to supercomplexes versus the protein amount of total CIII.

Ageing decreases the protein amount of CIII of *ad libitum* fed animals (YAL vs. OAL) for complexes III_2 (-10.8 %), I_1III_2 (-10.9 %) and total CIII (-6.6 %, all not stat. sig.). In complex III_2IV_1 the protein amount of CIII increases (+10.1 %, not stat. sig.). Aged calorie restricted animals (YCR vs. OCR) show an increased protein amount for complexes III_2IV_1 (+21.7 %), I_1III_2 (+17.7 %) and for total CIII (+10.2 %, all not stat. sig.).

Short-term calorie restriction (YAL vs. YCR, red asterisks) reduces CIII protein amount for complexes III_2 (-17.6 %), I_1III_2 (-20.9 %) and total CIII (-15.3 %, all stat. sig.) and for complex III_2IV_1 (-7.3 %, stat. high. sig.). Long-term calorie restriction (OAL vs. OCR, red asterisks) does not influence the protein amount.

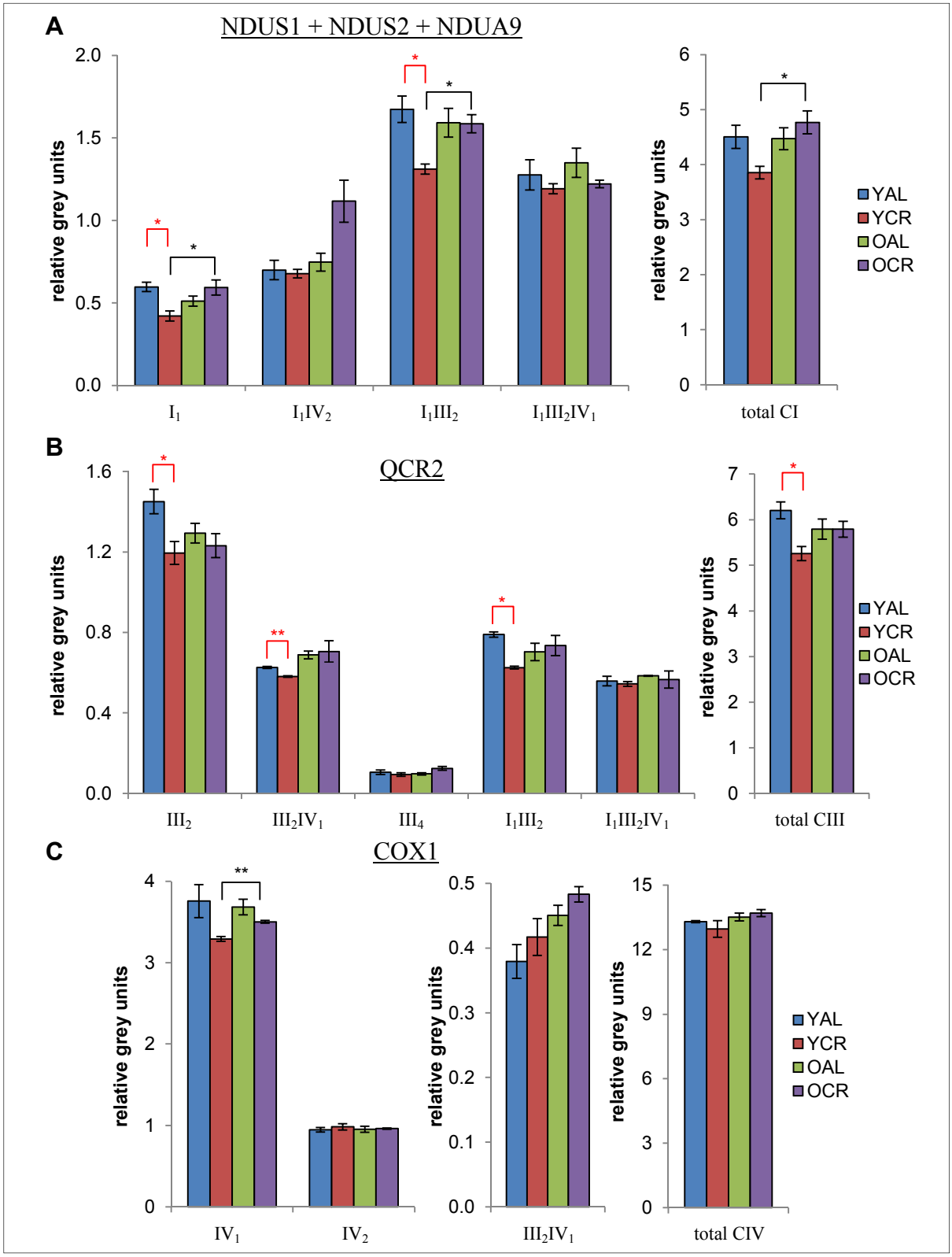

Fig. 4.28: Cerebellum: protein amount in 2D spots for CI, CIII and CIV. A: The sum of the intensities of subunits NDUS1, NDUS2 and NDUA9 for individual complex I_1 and supercomplexes are compared with the sum of the intensities of all identified subunits of CI (total CI); **B:** intensities of subunit QCR2 for complex III_2 and supercomplexes are compared with the sum of the intensities of all identified subunits of CIII (total CIII); **C:** intensities of subunit COX1 for homooligomeric complexes IV_1 and IV_2 and supercomplex III_2IV_1 are compared with the sum of the intensities of all identified subunits of total CIV.
bar plots: mean of technical repeats (n=3), error bars: standard error of technical repeats
significance: * = $p < \alpha$ (0.05); ** = $p < \alpha$ (0.01)
asterisks in black: changes caused by ageing, (YAL vs. OAL; YCR vs. OCR)
asterisks in red: changes caused by calorie restriction, (YAL vs. YCR; OAL vs. OCR)

The spot intensities of cytochrome c oxidase subunit 1 (COX1) were plotted for analysis of the different complexes in homooligomeric form (IV_1, IV_2) and the supercomplex III_2IV_1 for comparison to the spot intensity of total CIV in Fig. 4.28C.

Only for aged calorie restricted animals (YCR vs. OCR, black asterisk) the protein amount of CIV in cerebellum is for complex IV_1 increased (+6.4 %, stat. high. sig.).

For short-term (YAL vs. YCR, -12.4 %) and long-term (OAL vs. OCR, -4.9 %) calorie restriction, a declined protein amount (not stat. sig.) is observable for complex IV_1 for both compared animal groups.

The sum of the intensities in rel. grey units of all identified subunits for the supercomplexes III_2IV_1, I_1III_2 and $I_1III_2IV_1$ are plotted in Fig. 4.29. Age-related differences can be observed for the protein amount of complex III_2IV_1, which rises (+11.3 %, not stat. sig.) in old *ad libitum* nourished rats (YAL vs. OAL). Old calorie restricted animals exhibit increase of protein amount (stat. sig.) in complexes III_2IV_1 (+20.7 %) and I_1III_2 (+19.9 %) during ageing (black asterisks, YCR vs. OCR).

Decline of protein amount of supercomplexes I_1III_2 (-21.4 %, stat. high. sig.) and III_2IV_1 (-5.8 %, not stat. sig.) is observable for short-term calorie restriction (YAL vs. YCR, red asterisk). Long-term calorie restriction (OAL vs. OCR) decreases the protein amount of supercomplex $I_1III_2IV_1$ (-7.7 %, not stat. sig.).

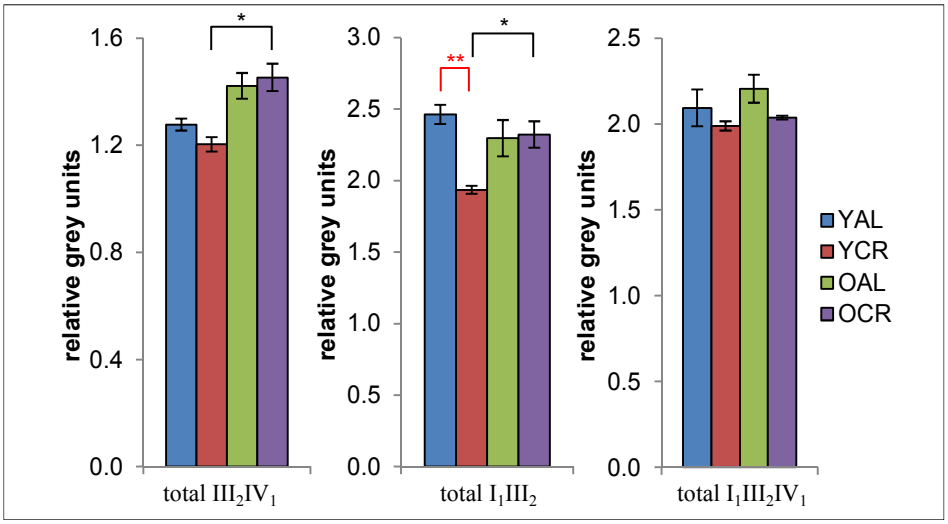

Fig. 4.29: Cerebellum: protein amount in 2D spots for supercomplexes containing CI, CIII and CIV. For each animal group, the sum of intensities (rel. grey units) of all identified subunits are plotted for the supercomplexes III_2IV_1, I_1III_2 and $I_1III_2IV_1$.
bar plots: mean of technical repeats (n=3), error bars: standard error of technical repeats
significance: * = $p < \alpha$ (0.05); ** = $p < \alpha$ (0.01)
asterisks in black: changes caused by ageing, (YAL vs. OAL; YCR vs. OCR)
asterisks in red: changes caused by calorie restriction, (YAL vs. YCR; OAL vs. OCR)

Fig. 4.30 depicts the sum of the spot intensities in relative grey units for all identified subunits of CII in cerebellum mitochondria. No significant changes of the protein amount for any of the animal groups (YAL, YCR, OAL, OCR) caused by ageing or calorie restriction are observable.

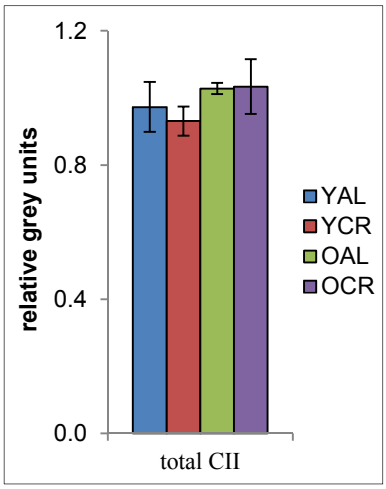

Fig. 4.30: Cerebellum: protein amount in 2D spots for CII. Sum of intensities in rel. grey units of total CII are presented for each animal group.
bar plots:
mean of technical repeats (n=3),
error bars:
standard error of technical repeats,
significance:
* = $p < \alpha$ (0.05); ** = $p < \alpha$ (0.01),
asterisks in black:
changes caused by ageing, (YAL vs. OAL; YCR vs. OCR)
asterisks in red:
changes caused by calorie restriction, (YAL vs. YCR; OAL vs. OCR)

In Fig. 4.31A intensities of all identified spots of ATP synthase (total CV) are compared with homooligomeric assemblies of ATP synthases, monomer V_1, dimer V_2 and next higher homooligomer V_3. The exact assembly of the next higher oligomer of ATP synthase is not clearly identified yet, it is assigned as trimer by Krause et al. (2005) or tetramer by Wittig and Schagger (2008). The large standard error for V_3 of OAL is based on one divergent value of the technical repeats.

Changes in ageing (black asterisks) are present only for calorie restricted animals (YCR vs. OCR) as increased protein amount for total CV (+15.9 %), V_2 (+23.6 %) and V_3 (+19.2 %, all stat. sig.), as well as for V_1 (+10.3 %, not stat. sig.).

Short-term calorie restriction (YAL vs. YCR, red asterisk) decreases the protein amount for total CV (-12.2 %) and V_1 (-9.9 %, not stat. sig.) and in V_2 (-20.3 %, stat. sig.). Long-term calorie restriction (OAL vs. OCR) does not show any effect.

Fig. 4.31B illustrates the spot intensities for ATP synthase's subunits α, β, the sum α+β, for F_o and F_1 portion. As expected, it is observable that α- and β-subunits show the similar distribution and intensities.

Only for animals nourished with calorie restriction (YCR vs. OCR) ageing (black asterisks) leads to increased protein amount for subunits α+β (+17.0 %) and F_1 portion (+29.4 %, both stat. sig.) and for individual subunit α (+17.8 %), individual subunit β (+16.3 %) and F_o portion (+16.5 %, all three not stat. sig.).

Short-term calorie restriction (YAL vs. YCR, red asterisks) declines the protein amount of individual subunit α (-14.4 %) and the F_o portion (-10.7 %, both stat. sig.) and for all the other illustrated ATP synthase subunits, individual β (-14.0 %), the sum α+β (-14.2 %) and F_1 portion (-17.5 %, all not stat. sig.). Long-term calorie restriction (OAL vs. OCR) increases the protein amount of F_1 portion (+17.9 %, not stat. sig.).

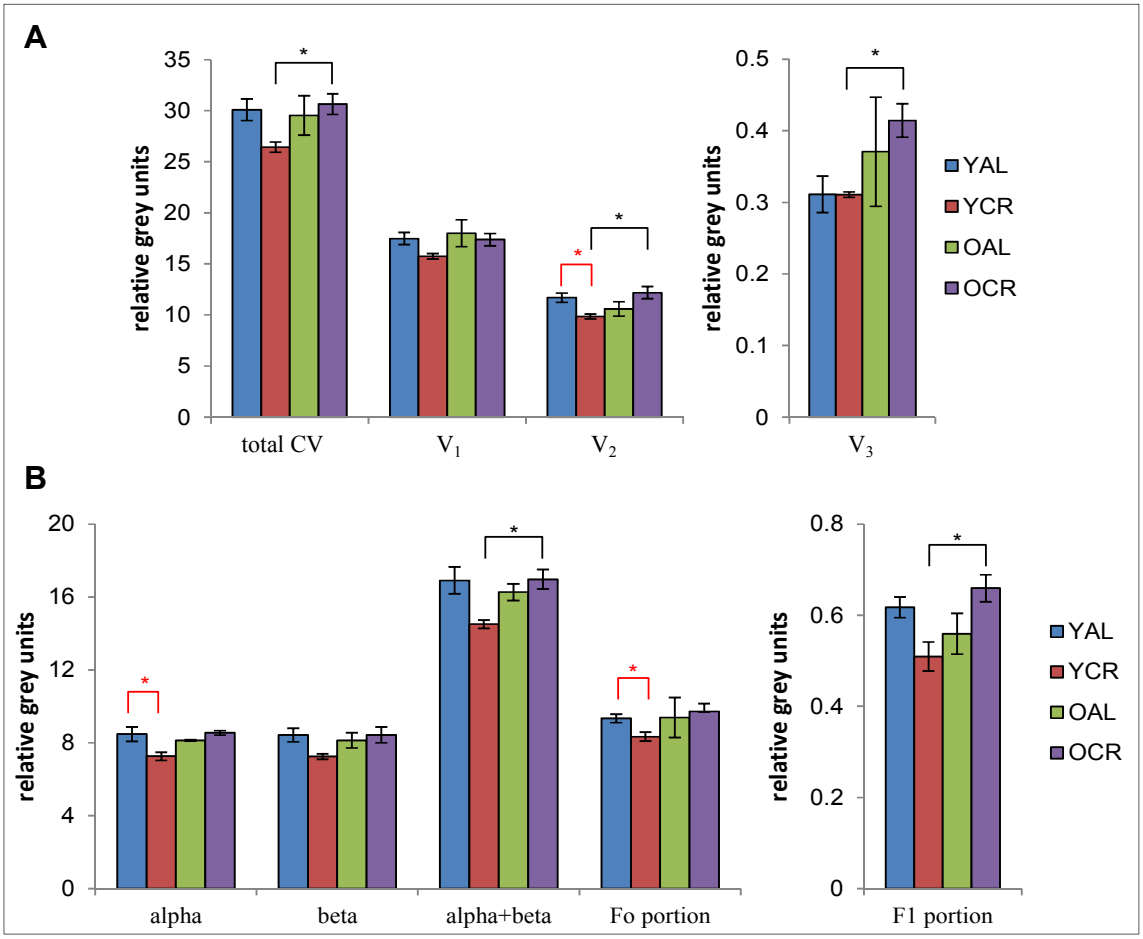

Fig. 4.31: Cerebellum: protein amount in 2D spots for CV, **A:** intensities of total ATP synthase (total CV) are compared with those of identified subunits of monomer (V_1), dimer (V_2) and homooligomer V_3; the large standard error of V_3 of OAL is due to one divergent value of the technical repeats. **B:** intensities (in rel. grey units) of ATP synthase's subunits α, β and α+β are plotted, as well as F_o and F_1 portion.
bar plots: mean of technical repeats (n=3), error bars: standard error of technical repeats
significance: * = $p < \alpha$ (0.05); ** = $p < \alpha$ (0.01)
asterisks in black: changes caused by ageing, (YAL vs. OAL; YCR vs. OCR)
asterisks in red: changes caused by calorie restriction, (YAL vs. YCR; OAL vs. OCR)

For analysis of the influences of ageing and calorie restriction on proteins encoded by the mtDNA, the spots for the identified subunits cytochrome b (CYB) of CIII and cytochrome c oxidase subunit 2 (COX2) of CIV were quantified. The result is shown in Fig. 4.32. Ageing (no black asterisks) seems to have no influences on the mtDNA encoded proteins in cerebellum, neither under *ad libitum* nutrition nor under calorie restriction. Short-term calorie restriction (YAL vs. YCR, red asterisk) decreases the CYB amount (-16.4 %, stat. sig.).

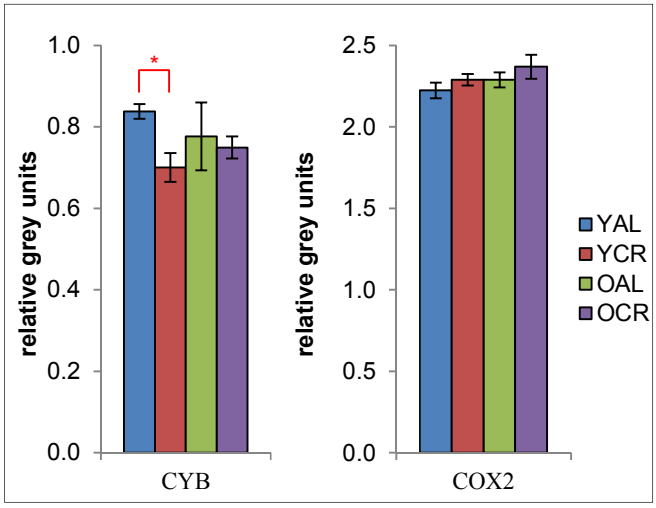

Fig. 4.32: Cerebellum: protein amount in 2D spots for mtDNA encoded OxPhos subunits CYB and COX2. Intensities in rel. grey units of CYB and COX2 are presented for each animal group.
bar plots:
mean of technical repeats (n=3),
error bars:
standard error of technical repeats,
significance:
* = $p < \alpha$ (0.05); ** = $p < \alpha$ (0.01),
asterisks in black:
changes caused by ageing,
(YAL vs. OAL; YCR vs. OCR)
asterisks in red:
changes caused by calorie restriction,
(YAL vs. YCR; OAL vs. OCR)

In Fig. 4.33, Fig. 4.34 and Fig. 4.35 the spot intensities (in rel. grey units) of 15 non-OxPhos proteins are depicted.

In Fig. 4.33 the changes in amount of the mitochondrial 60 kDa heat shock protein (CH60), the protein disulfide-isomerase A4 (PDIA4) and the 78 kDa glucose-regulated protein (GRP78) are displayed for the different animal groups. They are involved in stress management of the cell.

Ageing (black asterisks) decreases the protein amount only in calorie restricted animals (YCR vs. OCR) for CH60 (-13.6 %) and PDIA4 (-32.7 %, both stat. sig.) and also for GRP78 (-9.5 %, not stat. sig.). *Ad libitum* fed animals show no changes of these stress proteins.

Short-term calorie restriction (YAL vs. YCR, red asterisk) increases the protein amount of CH60 (+13.7 %, stat. sig.), PDIA4 (+12.4 %) and GRP78 (+42.6 %, not stat. sig.), while long-term calorie restriction (OAL vs. OCR) has no effects on these stress proteins.

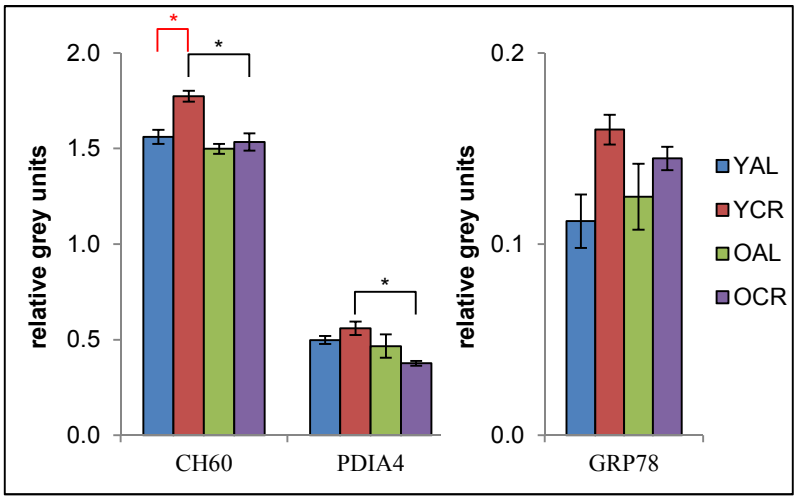

Fig. 4.33: Cerebellum: protein amount in 2D spots of proteins of cellular stress management. Intensities in rel. grey units of diverse stress proteins are presented for each animal group.
bar plots: mean of technical repeats (n=3), error bars: standard error of technical repeats
significance: * = $p < \alpha$ (0.05);
** = $p < \alpha$ (0.01)
asterisks in black: changes caused by ageing, (YAL vs. OAL; YCR vs. OCR)
asterisks in red: changes caused by calorie restriction, (YAL vs. YCR; OAL vs. OCR)

In Fig. 4.34 spot intensities (in rel. grey units) of proteins from TCA cycle (Fig. 4.34A), one protein involved in TCA cycle and glycolysis, mitochondrial dihydrolipoyl dehydrogenase (DLDH) (Fig. 4.34B), and proteins involved in glycolysis (Fig. 4.34C) are depicted. In Fig. 4.34A changes of the mitochondrial proteins from TCA cycle, malate dehydrogenase (MDHM), citrate synthase (CISY), aconitate hydratase (ACON) and 2-oxoglutarate dehydro-

genase (ODO1) are displayed. MDHM does not change under any condition. Ageing decreases (not stat. sig.) the protein amount of CISY (-16.0 %) and ACON (-8.1 %) only in calorie restricted animals (YCR vs. OCR).

Short-term calorie restriction (YAL vs. YCR) increases the protein amount of CISY (+12.4 %) and ACON (+19.6 %, both not stat. sig.), while for ODO1 the amount is decreased (-25.9 %, not stat. sig.). Long-term calorie restriction (OAL vs. OCR) does not change any amount of these proteins involved in TCA cycle.

In Fig. 4.34B changes of DLDH are shown. Ageing of animals under calorie restriction (YCR vs. OCR) reduces the protein amount (-9.7 %, not stat. sig.), while *ad libitum* fed animals show no changes. Short-term (YAL vs. YCR, -7.4 %) as well as long-term (OAL vs. OCR, -14.5 %) calorie restriction decreases the protein amount of DLDH (both not stat. sig.).

In Fig. 4.34C changes of the proteins pyruvate kinase isozymes M1/M2 (KPYM) and fructose-bisphosphate aldolase A/C (ALDOA/C) are depicted. Both proteins involved in glycolysis do not change by ageing or calorie restriction.

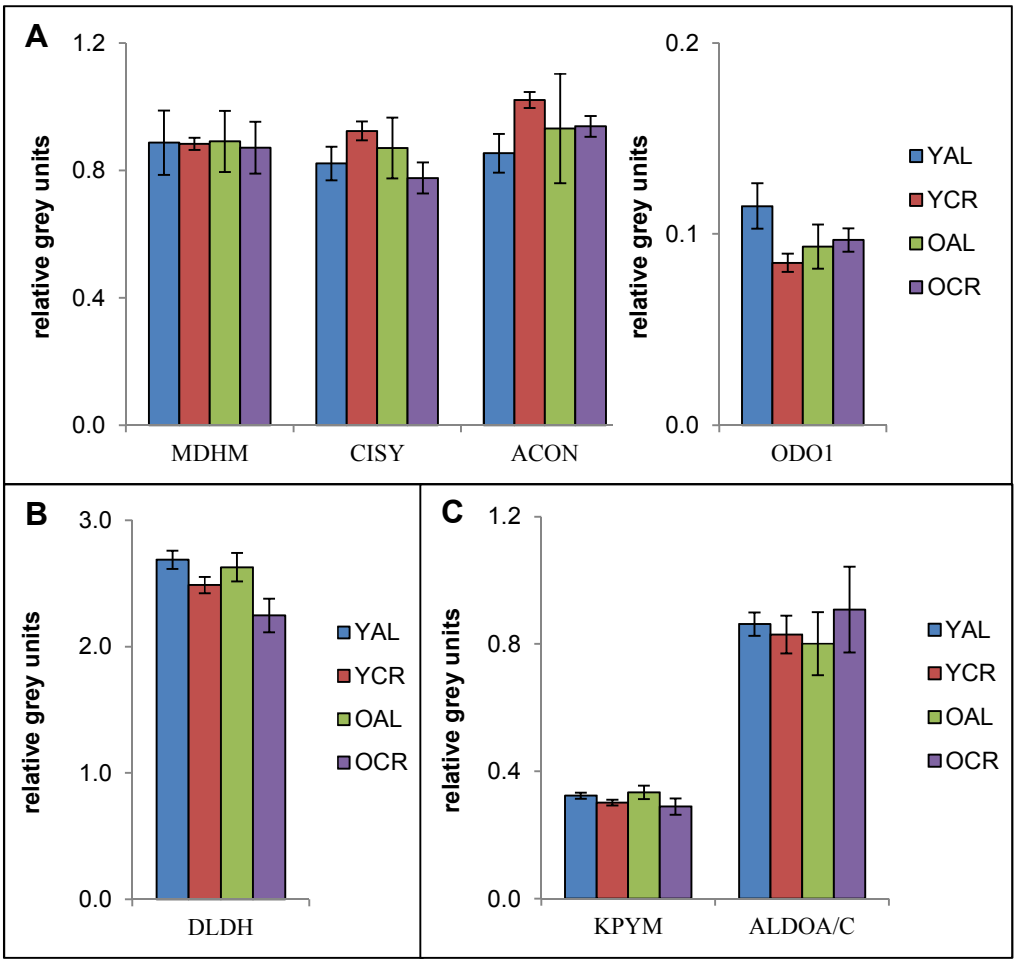

Fig. 4.34: Cerebellum:protein amount in 2D spots of proteins involved in TCA cycle and glycolysis. A: Intensities (in rel. grey units) of proteins from TCA cycle are presented for each animal group. **B:** Intensity (in rel. grey units) of DLDH protein, which is involved in TCA cycle and glycolysis, is depicted for each animal group. **C:** Intensities (in rel. grey units) of proteins involved in glycolysis are depicted for each animal group.
bar plots: mean of technical repeats (n=3), error bars: standard error of technical repeats
significance: * = $p < \alpha$ (0.05); ** = $p < \alpha$ (0.01)
asterisks in black: changes caused by ageing, (YAL vs. OAL; YCR vs. OCR)
asterisks in red: changes caused by calorie restriction, (YAL vs. YCR; OAL vs. OCR)

In Fig. 4.35 the spot intensities (rel. grey units) of lipophilin (PLP1), tubulin (TBB2A), syntaxin binding protein (STXB1), glutamate dehydrogenase (GLDH) and Na^+/K^+ ATPase are plotted. Ageing (black asterisks) increases (not stat. sig.) the protein amount for *ad libitum* nourished animals (YAL vs. OAL) of PLP1 (+23.5 %), TBB2A (+35.1 %) and GLDH (+31.3 %). But for calorie restricted animals (YCR vs. OCR) ageing leads to a decreased protein amount for PLP1 (-27.9 %, stat. sig.), TBB2A (-13.4 %, not stat. sig.), for STXB1 (-53.6 %, stat. high. sig.) and for Na^+/K^+ ATPase (-1.6 %, not stat. sig.). Only for GLDH an increase (+54.1 %, not stat. sig.) is visible, but with a large error bar for YCR.

Short-term calorie restriction (YAL vs. YCR, red asterisk) increases the protein amount for PLP1 (+95.0 %, stat. high. sig.), TBB2A (+36.8 %) and STXB1 (+31.5 %, both not stat. sig.), while for Na^+/K^+ ATPase the amount is diminished (-6.3 %, not stat. sig.). Long-term calorie restriction (OAL vs. OCR) leads to lower protein amount of STXB1 (-31.2 %), GLDH (-15.3 %) and Na^+/K^+ ATPase (-8.2 %, all not stat. sig.).

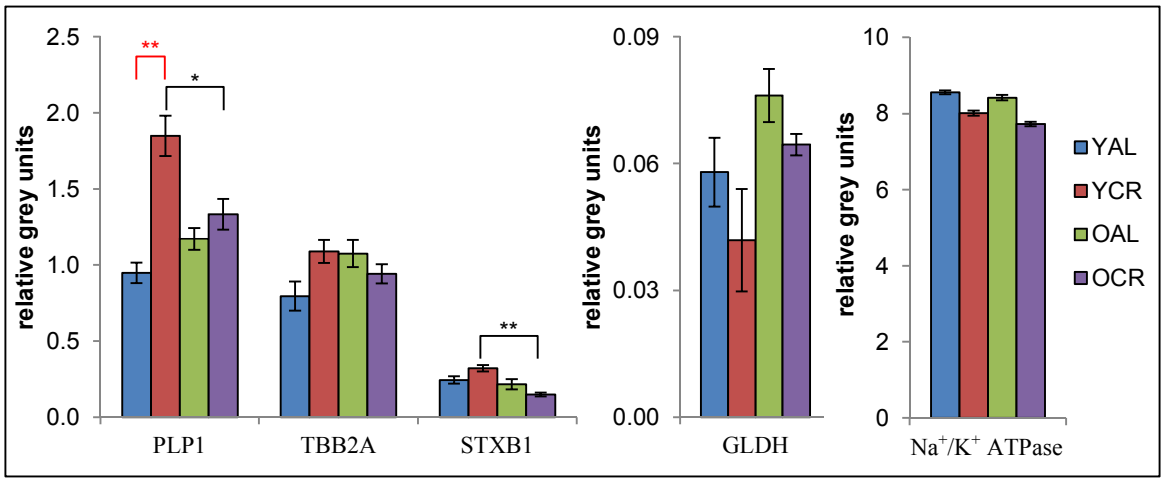

Fig. 4.35: **Cerebellum: protein amount in 2D spots of diverse non-OxPhos proteins.** Intensities (in rel. grey units) of the proteins lipophilin (PLP1), tubulin (TBB2A), syntaxin binding protein (STXB1) and glutamate dehydrogenase (GLDH resp. DHE3) and Na^+/K^+ ATPase from cerebellum are depicted.
bar plots: mean of technical repeats (n=3), error bars: standard error of technical repeats
significance: * = $p < \alpha$ (0.05); ** = $p < \alpha$ (0.01)
asterisks in black: changes caused by ageing, (YAL vs. OAL; YCR vs. OCR)
asterisks in red: changes caused by calorie restriction, (YAL vs. YCR; OAL vs. OCR)

Hippocampus

In Fig. 4.36A for hippocampus of all animal groups (YAL, YCR, OAL, OCR) the sum of the intensities of CI subunits NDUS1, NDUS2 and NDUA9 are plotted for complexes I_1, I_1IV_2, I_1III_2 and $I_1III_2IV_1$. The intensity of the sum of all identified subunits for CI (total CI) is also shown. Ageing (black asterisks) decreases the protein amount of CI for *ad libitum* fed animals (YAL vs. OAL) in complexes I_1 (-32.9 %), I_1III_2 (-11.7 %, both stat. high sig.), for total CI (-20.4 %, stat. sig.) and for I_1IV_2 (-16.6 %) and $I_1III_2IV_1$ (-22.7 %, both not stat. sig.). The protein amount of CI decreases during ageing for animals kept under calorie restriction (YCR vs. OCR) for smaller complexes as I_1 (-22.2 %) and I_1IV_2 (-30.5 %, both not stat. sig.) but rises for supercomplex $I_1III_2IV_1$ (+27.6 %, not stat. sig.).

Short-term calorie restriction (YAL vs. YCR, red asterisks) reduces the CI protein quantity in supercomplexes I_1III_2 (-13.5 %), $I_1III_2IV_1$ (-23.3 %) and total CI (-15.8 %, not stat. sig.). Long-term calorie restriction (OAL vs. OCR, red asterisks) increases the protein amount for I_1III_2 (19.2 %) and total CI (+16.2 %, both not stat. sig.) and for $I_1III_2IV_1$ (26.7 %, stat. sig.).

The spot intensities of the CIII subunit QCR2 for the homooligomeric complexes III_2 and III_4, for the supercomplexes III_2IV_1, I_1III_2 and $I_1III_2IV_1$ and total CIII are shown in Fig. 4.36B. Decreased protein amount in ageing (black asterisks) is observable for *ad libitum* animals (YAL vs. OAL) for III_4 (-63.6 %) and $I_1III_2IV_1$ (-19.9 %, both not stat. sig.), and for III_2IV_1 (-25.5 %) and total CIII (-12.2 %, both stat. sig.). Ageing under calorie restriction (YCR vs. OCR) leads to a declined CIII protein amount for smaller complexes III_2IV_1 (-25.9 %) and III_4 (-31.0 %, both not stat. sig.), and to an increased amount for larger complexes as I_1III_2 (+42.1 %) and $I_1III_2IV_1$ (+43.5 %, both not stat. sig.).

Short-term calorie restriction (YAL vs. YCR) reduces CIII protein amount for super-complexes I_1III_2 (-16.7 %) and $I_1III_2IV_1$ (-21.3 %, both not stat. sig.). Long-term calorie restriction (OAL vs. OCR, red asterisk) increases CIII protein amount in supercomplexes I_1III_2 (+19.4 %, not stat. sig.), $I_1III_2IV_1$ (+40.9 %, stat. sig.) and in total CIII (+7.3 %, not stat. sig.).

Fig. 4.36C shows the effects of ageing and calorie restriction on the subunit COX1 for the individual complex IV_1, the dimer IV_2 and the heteromer III_2IV_1, in comparison to the sum of all identified subunits for CIV (total CIV). Ageing of *ad libitum* fed animals (YAL vs. OAL, black asterisk) lowers CIV protein amount in complexes IV_1 (-9.7 %) and IV_2 (-22.4 %, both not stat. sig.), and in total CIV (-9.3 %, stat. sig.). Ageing decreases the CIV protein quantity in calorie restricted old animals (YCR vs. OCR) for total CIV (-20.6 %, both not stat. sig.).

Short-term (YAL vs. YCR, +8.7 %) and long-term (OAL vs. OCR, +16.6 %) calorie restriction increase the protein amount of the subunit COX1 of complex IV_1 (both not stat. sig., Fig. 4.36C).

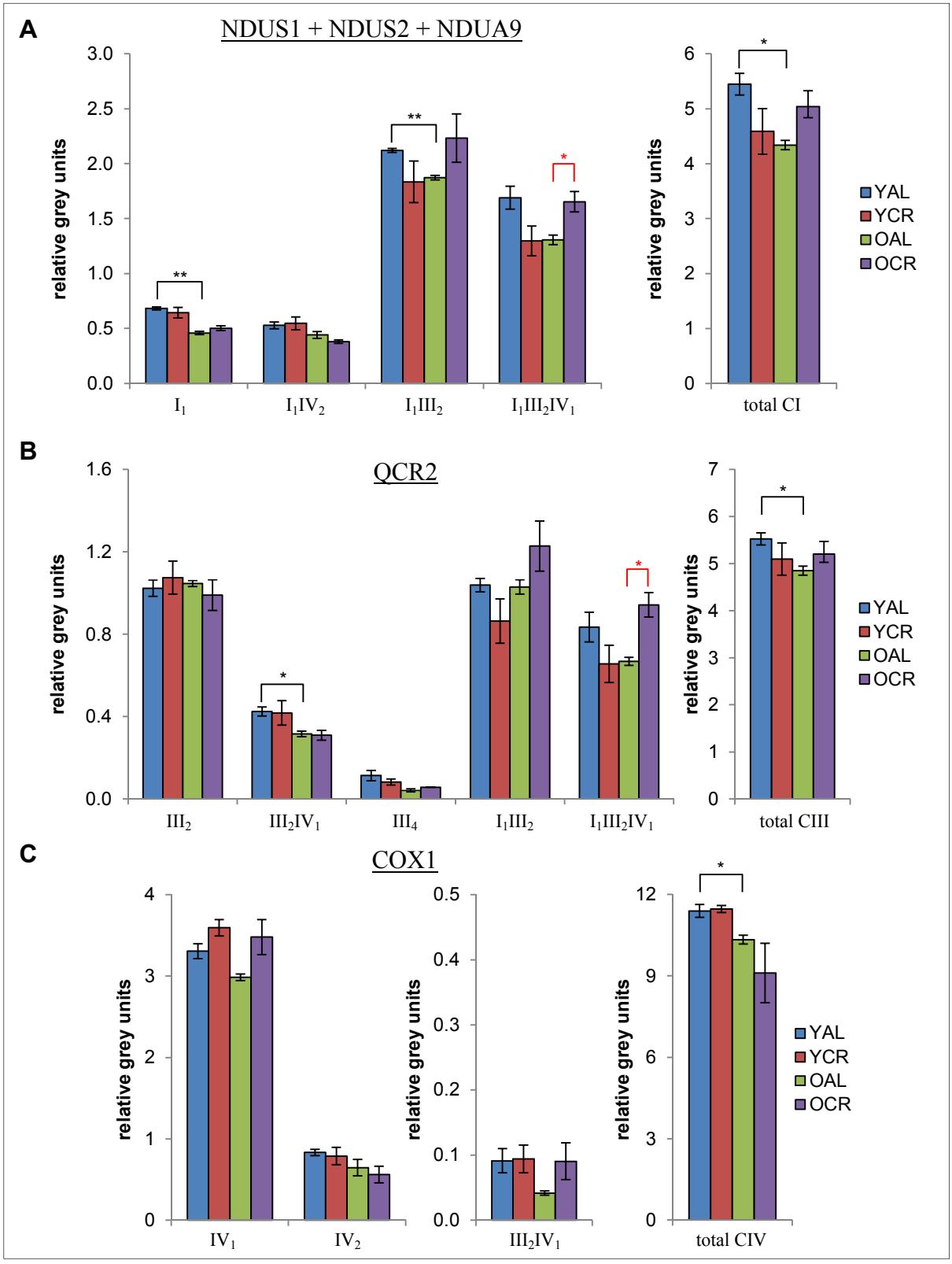

Fig. 4.36: Hippocampus: protein amount in 2D spots for CI, CIII and CIV. A: The sum of the intensities of subunits NDUS1, NDUS2 and NDUA9 for individual complex I_1 and supercomplexes are compared with the sum of the intensities of all identified subunits of CI (total CI); **B:** intensities of subunit QCR2 for complex III_2 and supercomplexes are compared with the sum of the intensities of all identified subunits of total CIII; **C:** intensities of subunit COX1 for homooligomeric complexes IV_1 and IV_2 and supercomplex III_2IV_1 are compared with the sum of the intensities of all identified subunits of total CIV.
bar plots: mean of technical repeats (n=3), error bars: standard error of technical repeats
significance: * = $p < \alpha$ (0.05); ** = $p < \alpha$ (0.01)
asterisks in black: changes caused by ageing, (YAL vs. OAL; YCR vs. OCR)
asterisks in red: changes caused by calorie restriction, (YAL vs. YCR; OAL vs. OCR)

In Fig. 4.37 the sum of the spot intensities in rel. grey units of all identified subunits for the supercomplexes III_2IV_1, I_1III_2 and $I_1III_2IV_1$ are illustrated. Ageing (black asterisks) decreases the protein amount of *ad libitum* nourished rats (YAL vs. OAL) for III_2IV_1 (-31.3 %) and I_1III_2 (-8.1 %, both stat. high sig.) and $I_1III_2IV_1$ (-24.3 %, not stat. sig.). Aged animals under calorie restriction (YCR vs. OCR) show a reduced protein quantity for the smaller complex III_2IV_1 (-21.9 %, not stat. sig.), while for supercomplexes I_1III_2 (+28.2 %) and $I_1III_2IV_1$ (+29.3 %) the amount is raised (both not stat. sig.).

Short-term calorie restriction (YAL vs. YCR, red asterisks) lowers the protein quantity for supercomplexes I_1III_2 (-14.5 %) and $I_1III_2IV_1$ (-24.8 %, both not stat. sig.) while long-term calorie restriction leads to increased protein amount of supercomplexes I_1III_2 (+19.3 %, not stat. sig.) and $I_1III_2IV_1$ (+28.4 %, stat. sig.).

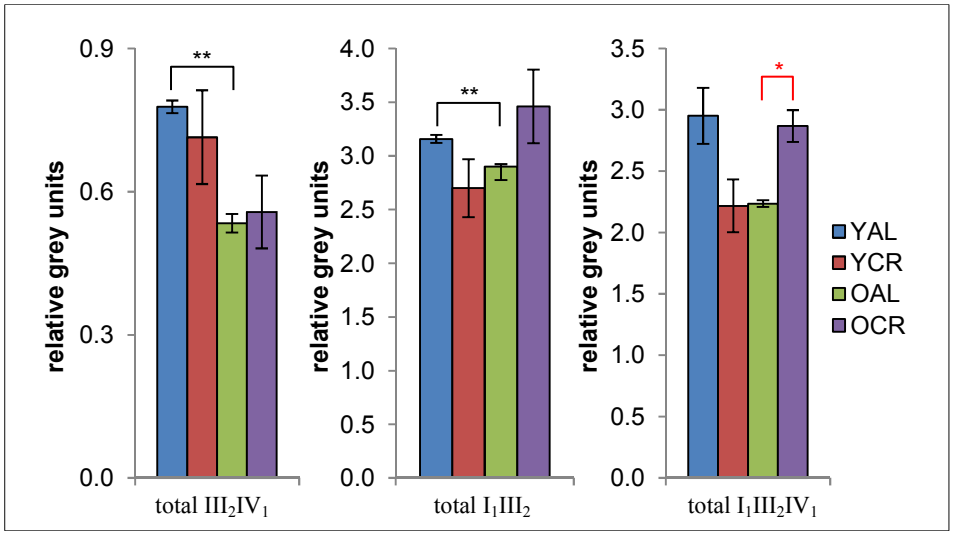

Fig. 4.37: Hippocampus: protein amount in 2D spots for supercomplexes containing CI, CIII and CIV. The sum of intensities (rel. grey units) of all identified spots (=total) for the supercomplexes III_2IV_1, I_1III_2 and $I_1III_2IV_1$ are plotted for each animal group.
bar plots: mean of technical repeats (n=3), error bars: standard error of technical repeats
significance: * = $p < \alpha$ (0.05); ** = $p < \alpha$ (0.01)
asterisks in black: changes caused by ageing, (YAL vs. OAL; YCR vs. OCR)
asterisks in red: changes caused by calorie restriction, (YAL vs. YCR; OAL vs. OCR)

Fig. 4.38 shows the sum of the intensities for all identified subunits of CII for each animal group (YAL, YCR, OAL, OCR) from hippocampus. Ageing leads in both animal groups, *ad libitum* (YAL vs. OAL, -13.3 %) and restricted to food (YCR vs. OCR, -18.4 %), to a decreased protein amount (both not stat. sig.). Short-term calorie restriction (YAL vs. YCR, red

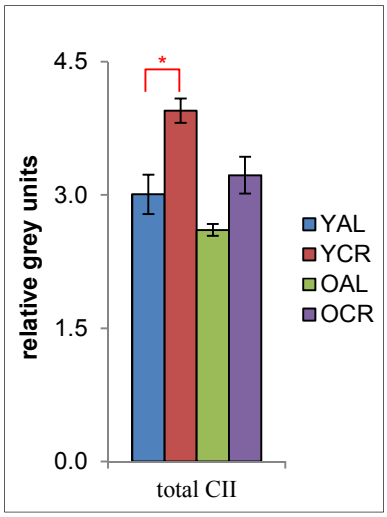

Fig. 4.38: Hippocampus: protein amount in 2D spots for CII.
The sum of the intensities in rel. grey units of total CII are presented for each animal group.
bar plots:
mean of technical repeats (n=3),
error bars:
standard error of technical repeats,
significance:
* = $p < \alpha$ (0.05); ** = $p < \alpha$ (0.01),
asterisks in black:
changes caused by ageing,
(YAL vs. OAL; YCR vs. OCR)
asterisks in red:
changes caused by calorie restriction, (YAL vs. YCR; OAL vs. OCR)

asterisk) increases protein quantity (+31.3 %, stat. sig.), as well as long-term calorie restriction (OAL vs. OCR) (+23.6 %, not stat. sig.).

The spot intensities of ATP synthase subunits are illustrated in Fig. 4.39. Fig. 4.39A indicates all identified subunits of CV (total CV) in comparison with the identified subunits of the monomer V_1, dimer V_2 and the next higher homooligomer V_3 for hippocampus from all animal groups (YAL, YCR, OAL, OCR).

Ageing (black asterisks) of *ad libitum* nourished animals (YAL vs. OAL) decreases the protein amount for total CV (-12.1 %) and complex V_1 (-12.3 %, both stat. sig.) and for V_2 (-13.2 %, not stat. sig.). For aged animals under calorie restriction (YCR vs. OCR), protein quantity is increased for total CV (+15.0 %) and V_2 (+42.6 %, both stat. sig.).

Short-term calorie restriction (YAL vs. YCR) lowers the protein amount for total CV (-9.3 %) and V_2 (-20.3 %, both not stat. sig.), whereas long-term calorie restriction (YAL vs. YCR, red asterisk) increases the amount for total CV (+18.7 %, stat. sig.) and for V_1 (+13.1 %) and V_2 (+30.9 %, not stat. sig.).

In Fig. 4.39B the spot intensities of ATP synthase's subunits α, β and the sum α+β as well as F_o portion and F_1 portion from hippocampus are illustrated. As expected, it is apparent that subunits α and β inhibit similar distribution and intensities.

Ageing (black asterisks) decreases the protein amount for *ad libitum* animals (YAL vs. OAL) for subunit α (-16.6 %) and the sum α+β (-12.8 %, both stat. sig.) and for β (-8.3 %) and F_o portion (-12.6 %, both not stat. sig.). Aged animals grown under calorie restriction (YCR vs. OCR) show an increase of protein amount for α (+33.2%), β (+33.3 %) and α+β (+33.3 %, all stat. sig.), whereas the amount of F_o portion is reduced (-12.9 %, not stat. sig.).

Short-term calorie restriction (YAL vs. YCR) decreases the protein amount of α (-14.4 %), β (-11.6 %) and α+β (-13.1 %, all not stat. sig.). Long-term calorie restriction (OAL vs. OCR, red asterisk) increases the protein amount for α (+36.8 %, stat. sig.) and for β (+28.5 %) and α+β (+32.8 %, both not stat. sig.).

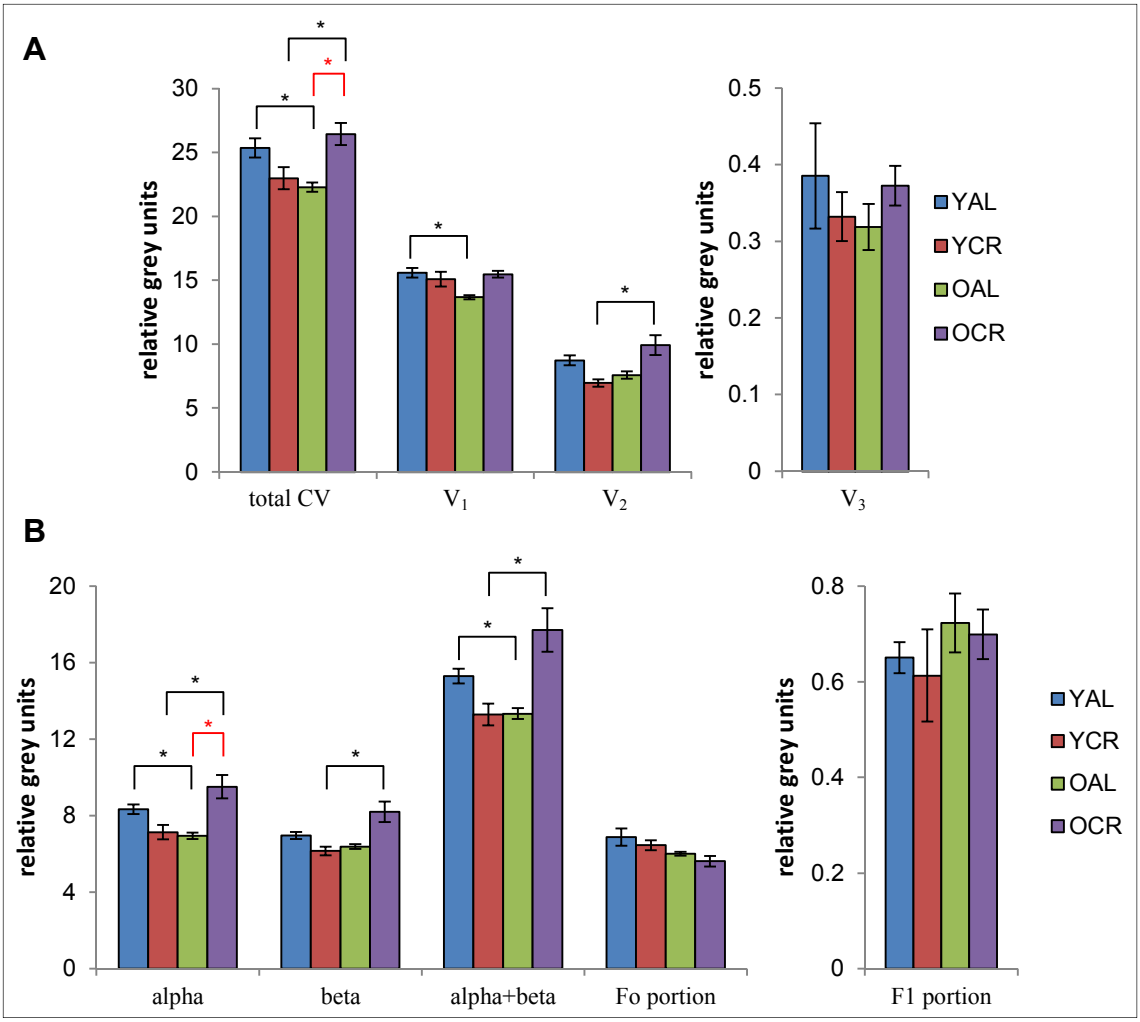

Fig. 4.39: Hippocampus: protein amount in 2D spots for CV. A: intensities of total ATP synthase (total CV) are compared with those of identified subunits of monomer (V_1), dimer (V_2) and next higher homooligomer V_3; **B:** intensities (in rel. grey units) of ATP synthase's subunits α, β and α+β are plotted, as well as F_o and F_1 portion.
bar plots: mean of technical repeats (n=3), error bars: standard error of technical repeats
significance: * = $p < \alpha$ (0.05); ** = $p < \alpha$ (0.01)
asterisks in black: changes caused by ageing, (YAL vs. OAL; YCR vs. OCR)
asterisks in red: changes caused by calorie restriction, (YAL vs. YCR; OAL vs. OCR)

In Fig. 4.40 the protein spot intensities of mtDNA encoded protein subunits CYB (CIII) and COX2 (CIV) of hippocampus are depicted. Due to large error bars, no changes of the amount of CYB based on ageing or calorie restriction are observable. Ageing of calorie restricted animals (YCR vs. OCR) decreases the protein amount for COX2 (-15.9 %, not stat. sig.), as well as long-term calorie restriction (OAL vs. OCR, -14.2 %, not stat. sig.).

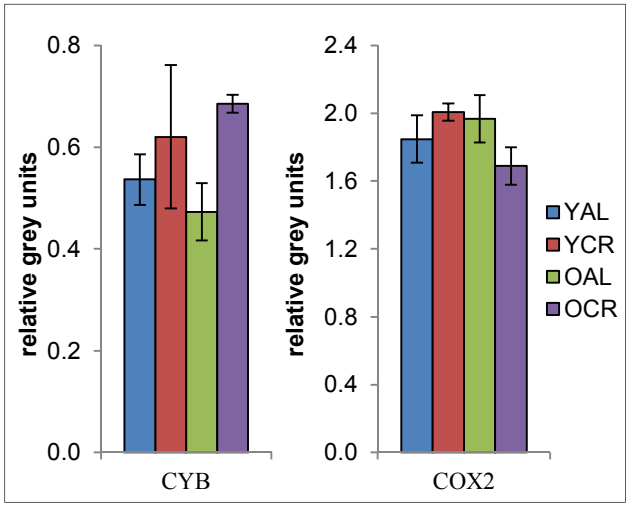

Fig. 4.40: Hippocampus: protein amount in 2D spots for mtDNA encoded OxPhos subunits CYB and COX2. Intensities in rel. grey units of CYB and COX2 are presented for each animal group.
bar plots:
mean of technical repeats (n=3),
error bars:
standard error of technical repeats,
significance:
* = $p < \alpha$ (0.05); ** = $p < \alpha$ (0.01),
asterisks in black:
changes caused by ageing,
(YAL vs. OAL; YCR vs. OCR)
asterisks in red:
changes caused by calorie restriction,
(YAL vs. YCR; OAL vs. OCR)

15 non-OxPhos proteins of hippocampus were analysed and their spot intensities (in rel. grey units) depicted in Fig. 4.41, Fig. 4.42 and Fig. 4.43.

Fig. 4.41 shows the intensities for the mitochondrial 60 kDa heat shock protein (CH60), the protein disulfide-isomerase A4 (PDIA4) and the 78 kDa glucose-regulated protein (GRP78). All of them are involved in cellular stress management. Ageing (black asterisk) of *ad libitum* nourished animals (YAL vs. OAL) reduces the protein amount of PDIA4 only (-17.9 %, not stat. sig.), while in aged animals under calorie restriction (YCR vs. OCR) the amount of CH60 (+40.1 %, stat. sig.) and PDIA4 (+23.1 %, not stat. sig.) is increased.

Short-term calorie restriction (YAL vs. YCR) decreases the protein amount of PDIA4 (-24.7 %, not stat. sig.) only. Long-term calorie restriction (OAL vs. OCR, red asterisk) increases the protein amount of CH60 (+44.5 %, stat. sig.) and PDIA4 (+12.8 %, not stat. sig.).

Due to large error bars, GRP78 of hippocampus does not show any changes in protein amount.

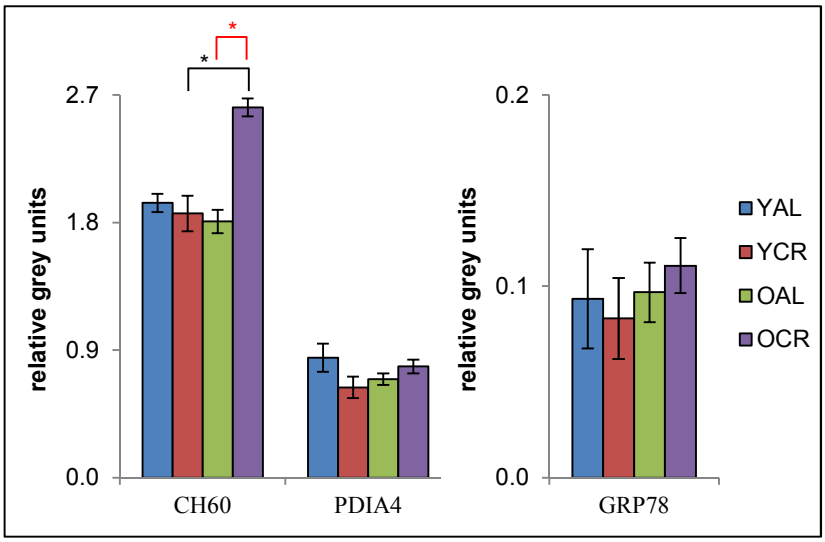

Fig. 4.41: Hippocampus: protein amount in 2D spots of proteins of cellular stress management. Intensities in rel. grey units of diverse stress proteins are presented for each animal group.

bar plots: mean of technical repeats (n=3), error bars: standard error of technical repeats
significance: * = $p < \alpha$ (0.05);
** = $p < \alpha$ (0.01)
asterisks in black: changes caused by ageing, (YAL vs. OAL; YCR vs. OCR)
asterisks in red: changes caused by calorie restriction,
(YAL vs. YCR; OAL vs. OCR)

In Fig. 4.42 spot intensities (in rel. grey units) of proteins involved in TCA cycle and glycolysis are displayed. In Fig. 4.42A the spot intensities of the mitochondrial proteins malate dehydrogenase (MDHM), citrate synthase (CISY), aconitate hydratase (ACON) and 2-oxoglutarate dehydrogenase (ODO1) are depicted. They are proteins involved in the TCA cycle. Ageing (black asterisks) of *ad libitum* fed animals (YAL vs. OAL) increases the protein amount of MDHM (+66.8 %, stat. sig.) and ACON (+12.6 %, not stat. sig.). Aged animals under calorie restriction (YCR vs. OCR) show an increase in protein amount for ACON (+36.9 %, stat. sig.) and a decrease for ODO1 (-40.6 %, not stat. sig.).

Short-term calorie restriction (YAL vs. YCR) reduces the protein amount of CISY (-14.2 %) and ACON (-14.5 %, both not stat. sig.). Long-term calorie restriction (OAL vs. OCR) decreases the amount of MDHM (-30.7 %) and ODO1 (-40.2 %, both not stat. sig.).

Fig. 4.42B shows the spot intensities of the mitochondrial dihydrolipoyl dehydrogenase (DLDH) for the different animal groups, which is involved in TCA cycle and glycolysis. Aged *ad libitum* animals (YAL vs. OAL) show a reduced DLDH amount (-17.5 %, not stat. sig.), as well as animals under the influence of short-term calorie restriction (YAL vs. YCR, -18.0 %, not stat. sig.). Calorie restriction during ageing (YCR vs. OCR, black asterisk) leads to an increased DLDH amount (+24.8 %, stat. sig.), as well as long-term calorie restriction (OAL vs. OCR, red asterisk, +24.0 %, stat. sig.).

In Fig. 4.42C the pyruvate kinase isozymes M1/M2 (KPYM) and fructose-bisphosphate aldolase A/C (ALDOA/C) are depicted. Both are proteins involved in glycolysis. Only for aged animals under calorie restriction (YCR vs. OCR, +62.8 %) and for long-term calorie restriction (OAL vs. OCR, +21.8 %) an increase of protein amount for KPYM is visible (both not stat. sig.). Short-term calorie restriction (YAL vs. YCR) lowers the protein amount of KPYM (-28.2 %, not stat. sig.). The amount of ALDOA/C is reduced under the influence of long-term calorie restriction (OAL vs. OCR, -31.2 %, not stat. sig.).

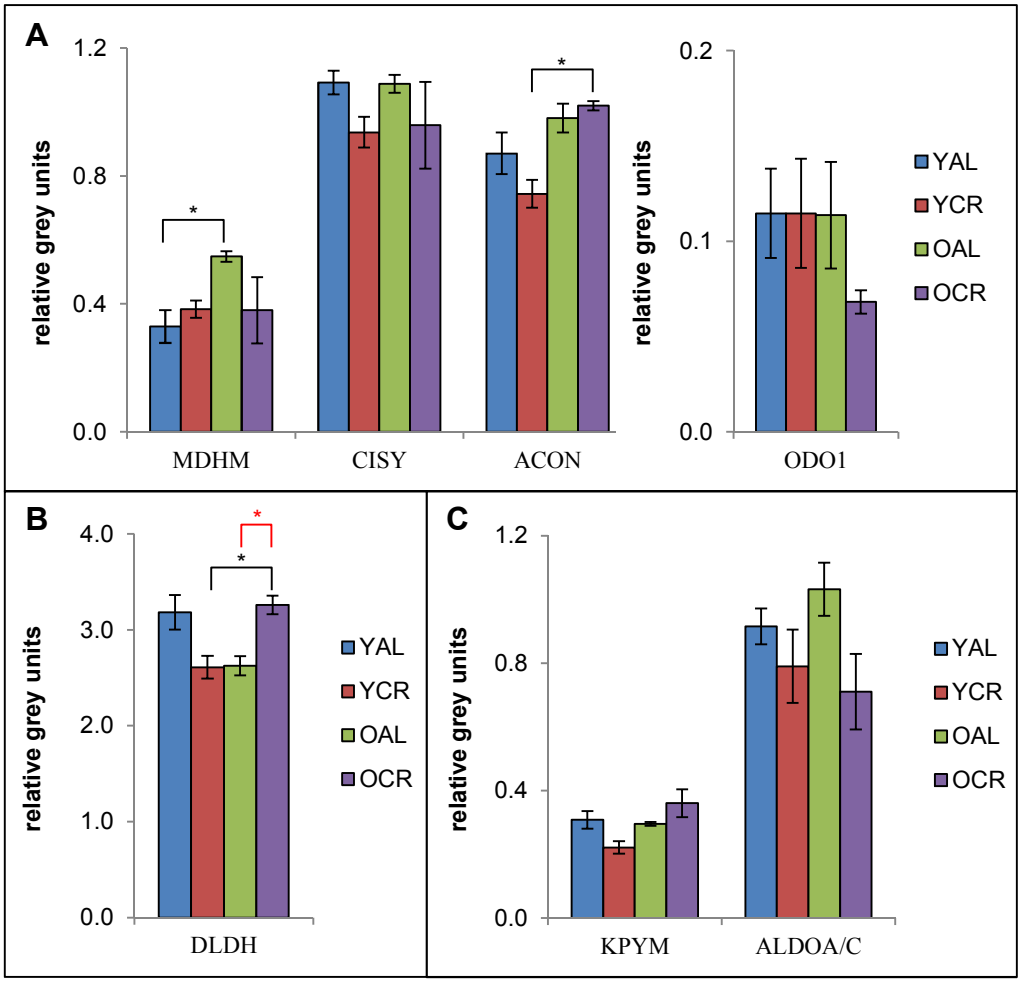

Fig. 4.42: Hippocampus: protein amount in 2D spots of proteins involved in TCA cycle and glycolysis. A: Intensities (in rel. grey units) of proteins from TCA cycle are presented for each animal group. **B:** Intensity (in rel. grey units) of DLDH protein, which is involved in TCA cycle and glycolysis, is depicted for each animal group. **C:** Intensities (in rel. grey units) of proteins involved in glycolysis are depicted for each animal group.
bar plots: mean of technical repeats (n=3), error bars: standard error of technical repeats
significance: * = $p < \alpha$ (0.05); ** = $p < \alpha$ (0.01)
asterisks in black: changes caused by ageing, (YAL vs. OAL; YCR vs. OCR)
asterisks in red: changes caused by calorie restriction, (YAL vs. YCR; OAL vs. OCR)

In Fig. 4.43 the spot intensities (rel. grey units) of the proteins lipophilin (PLP1), tubulin (TBB2A), syntaxin binding protein (STXB1), glutamate dehydrogenase (GLDH) and Na^+/K^+ ATPase from hippocampus are plotted.

Ageing (black asterisks) of *ad libitum* fed animals (YAL vs. OAL) increases the protein amount of PLP1 (+202.3 %, stat. high. sig.) and GLDH (+24.1 %, not stat. sig.). Under the influence of calorie restriction (YCR vs. OCR) the protein amount is increased for TBB2A (+35.4 %) and Na^+/K^+ ATPase (+11.9 %, both not stat. sig.) during ageing, whereas it is declined by the effect of calorie restriction, for PLP1 (-42.6 %, stat. high. sig.) and GLDH (-27.7 %, not stat. sig.).

Short-term calorie restriction (YAL vs. YCR, red asterisks) increases the protein amount of PLP1 (+62.6 %, stat. sig.) and GLDH (+25.4 %, not stat. sig.). Long-term calorie restriction (OAL vs. OCR, red asterisks) reduces the protein amount of PLP1 (-69.1 %, stat. high. sig.) and GLDH (-27.0 %, not stat. sig.), whereas the amount of TBB2A is increased (+29.4 %, stat. sig.). STXB1 of hippocampus is not influenced at all.

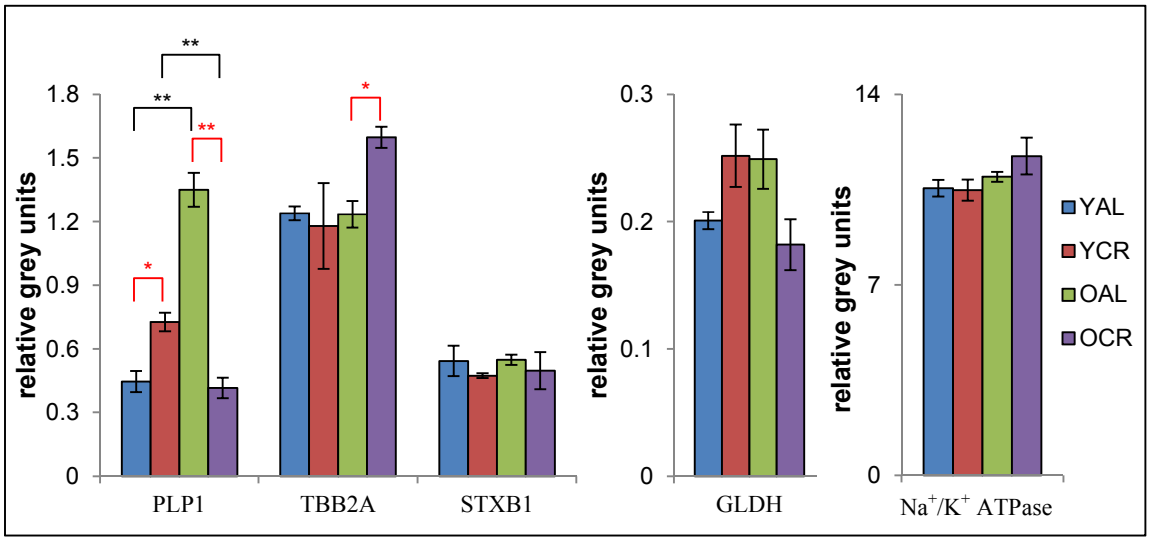

Fig. 4.43: Hippocampus: protein amount in 2D spots of diverse non-OxPhos proteins. Intensities (in rel. grey units) of the proteins lipophilin (PLP1), tubulin (TBB2A), syntaxin binding protein (STXB1) and glutamate dehydrogenase (GLDH resp. DHE3) and Na^+/K^+ ATPase from hippocampus are depicted.
bar plots: mean of technical repeats (n=3), error bars: standard error of technical repeats
significance: * = $p < \alpha$ (0.05); ** = $p < \alpha$ (0.01)
asterisks in black: changes caused by ageing, (YAL vs. OAL; YCR vs. OCR)
asterisks in red: changes caused by calorie restriction, (YAL vs. YCR; OAL vs. OCR)

Cerebrum

In Fig. 4.44A the sum of the intensities (rel. grey units) of CI subunits NDUS1, NDUS2 and NDUA9 are depicted for complexes I_1, I_1IV_2, I_1III_2 and $I_1III_2IV_1$ from all cerebrum animal groups (YAL, YCR, OAL, OCR). The intensities for all identified subunits for CI (total CI) were summed and also plotted in Fig. 4.44A for comparison. This illustration enables to compare the effects on the protein amount of CI as individual complex or in supercomplex assembly.

Ageing (black asterisk) decreases the protein amount of individual complex I_1 (-23.2 %, stat. sig.) in cerebrum of *ad libitum* fed animals (YAL vs. OAL). Ageing of animals kept under calorie restriction (YCR vs. OCR) increases the protein amount of CI in complexes I_1 (+10.8 %), I_1IV_2 (+11.8 %), $I_1III_2IV_1$ (+15.9 %) and total CI (+7.1 %, not stat. sig.), whereas the amount of complex I_1III_2 is decreased (-7.8 %, not stat. sig.).

Short-term calorie restriction (YAL vs. YCR, red asterisks) increases the protein amount for individual complex I_1 (+12.2 %, stat. sig.). Long-term calorie restriction (OAL vs. OCR, red asterisk) raises the protein amount for complex I_1 (+61.9 %, stat. high sig.), and for super-complexes I_1IV_2 (+28.1 %), $I_1III_2IV_1$ (+9.4 %) and total CI (+7.9 %, all not stat. sig.).

The intensities of subunit QCR2 are presented in Fig. 4.44B for complexes III_2, III_2IV_1, III_4, I_1III_2 and $I_1III_2IV_1$. Total CIII represents the sum of the rel. grey units of all identified subunits of CIII. This allows a comparison between homooligomeric and supercomplex assembly of CIII. Ageing (black asterisks) decreases the protein amount of CIII in cerebrum of *ad libitum* nourished rats (YAL vs. OAL) for III_2 (-8.7 %) and III_2IV_1 (-11.9 %, both not stat. sig.), whereas in I_1III_2 the protein amount is increased (+27.4 %, not stat. sig.). Aged calorie restricted animals (YCR vs. OCR) exhibit an increased CIII quantity for all shown complexes except for I_1III_2; for III_2 (+20.0 %, stat. sig.) and III_4 (+36.4 %, stat. high sig.), III_2IV_1 (+7.8 %), $I_1III_2IV_1$ (+14.3 %) and total CIII (+8.5 %, all not stat. sig.). The amount of I_1III_2 is decreased only (-12.3 %, not stat. sig.).

Short-term calorie restriction (YAL vs. YCR) has no effects on CIII. Under conditions of long-term calorie restriction (OAL vs. OCR, red asterisks) the protein amount of CIII is increased for complexes III_2IV_1 (+24.5 %) and III_4 (+47.9 %, both stat. high sig.), for total CIII (+17.9 %, stat. sig.) and for III_2 (+20.5 %) and $I_1III_2IV_1$ (+12.4 %, both not stat. sig.). Only I_1III_2 exhibits a lower CIII protein amount for long-term calorie restriction (-11.5 %, not stat. sig.).

Fig. 4.44C depicts the changes of the protein amount of subunit COX1 of CIV in monomer IV_1, dimer IV_2 and heteromer III_2IV_1 in comparison to the sum of the intensities of all identified subunits of CIV (total CIV). Ageing (black asterisks) of *ad libitum* fed rats (YAL vs. OAL) increases the protein amount of COX1 in IV_1 (+5.9 %, stat. high sig.). But for total CIV the amount is decreased (-21.4 %, stat. sig.). Aged animals under calorie restriction (OAL vs. OCR) show a reduced amount of COX1 in IV_1 (-9.4 %, not stat. sig.).

Short-term calorie restriction (YAL vs. YCR, red asterisks) increases the amount for COX1 in IV_1 (+13.0 %, stat. sig.) and for total CIV (+10.0 %, not stat. sig.). Long-term calorie restriction (OAL vs. OCR) raises the protein amount of total CIV (+29.1 %, not stat. sig.).

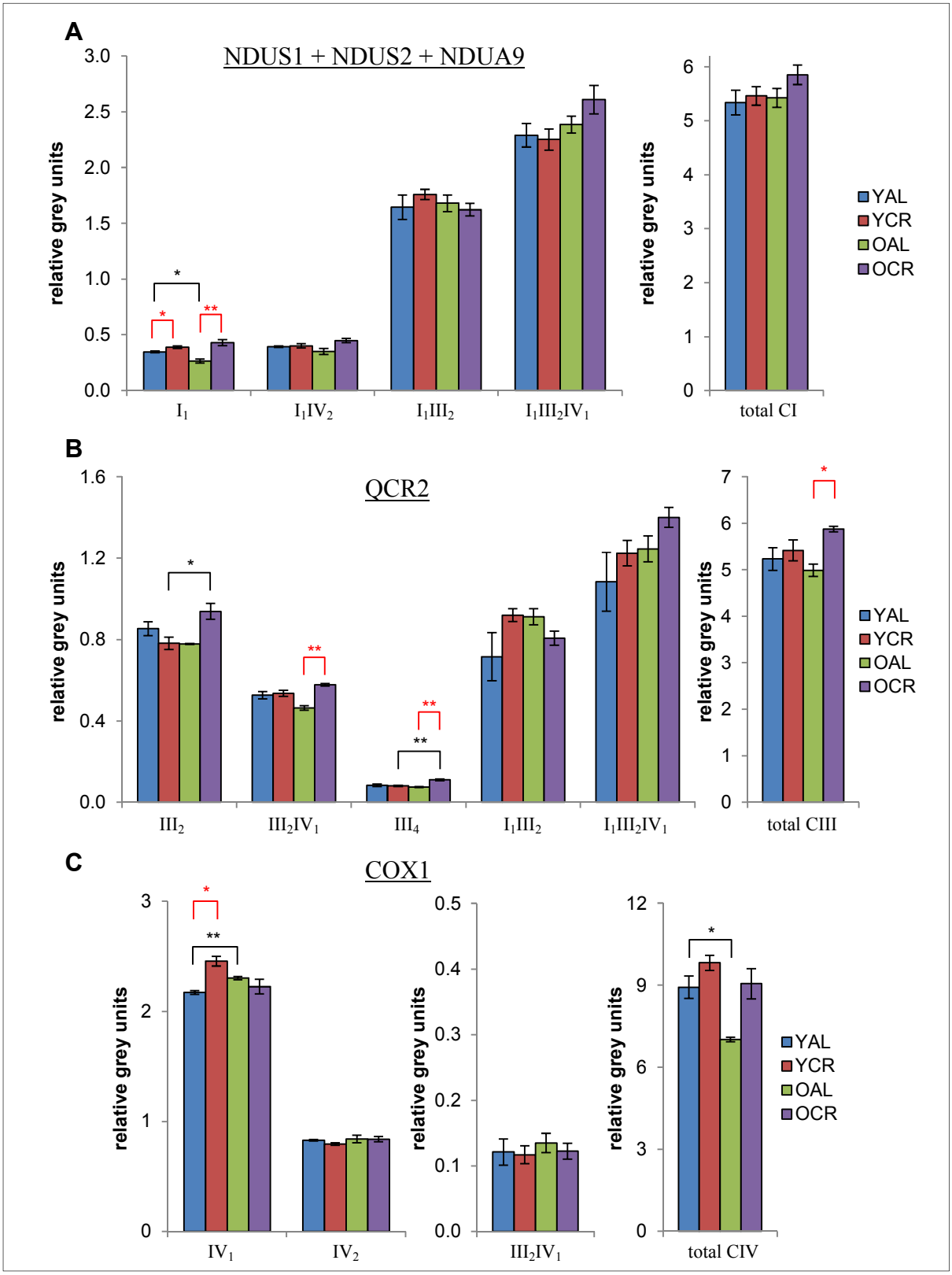

Fig. 4.44: Cerebrum: protein amount in 2D spots for CI, CIII and CIV. A: The sum of intensities of subunits NDUS1, NDUS2 and NDUA9 for individual complex I_1 and supercomplexes are compared with the sum of the intensities of all identified subunits of CI (total CI); **B:** intensities of subunit QCR2 for complex III_2 and supercomplexes are compared with the sum of the intensities of all identified subunits of CIII (total CIII); **C:** intensities of subunit COX1 for homooligomeric complexes IV_1 and IV_2 and supercomplex III_2IV_1 are compared with the sum of the intensities of all identified subunits of CIV (total CIV).
bar plots: mean of technical repeats (n=3), error bars: standard error of technical repeats
significance: * = $p < \alpha$ (0.05); ** = $p < \alpha$ (0.01)
asterisks in black: changes caused by ageing, (YAL vs. OAL; YCR vs. OCR)
asterisks in red: changes caused by calorie restriction, (YAL vs. YCR; OAL vs. OCR)

In Fig. 4.45 the sum of the intensities of all identified spots for the supercomplexes III_2IV_1, I_1III_2 and $I_1III_2IV_1$ is depicted. Ageing (black asterisks) decreases the protein amount in *ad libitum* nourished animals (YAL vs. OAL) for III_2IV_1 (-8.6 %, not stat. sig.). Animals under the condition of calorie restriction (YCR vs. OCR) show an increase of supercomplex $I_1III_2IV_1$ (+14.8 %, stat. sig.) during ageing whereas the protein amount of I_1III_2 decreases (-9.3 %, not stat. sig.).

Short-term calorie restriction (YAL vs. YCR) has no influence on the protein amount, while long-term calorie restriction (OAL vs. OCR, red asterisk) increases the amount of complex $I_1III_2IV_1$ (+8.6 %, stat. high sig., Fig. 4.45).

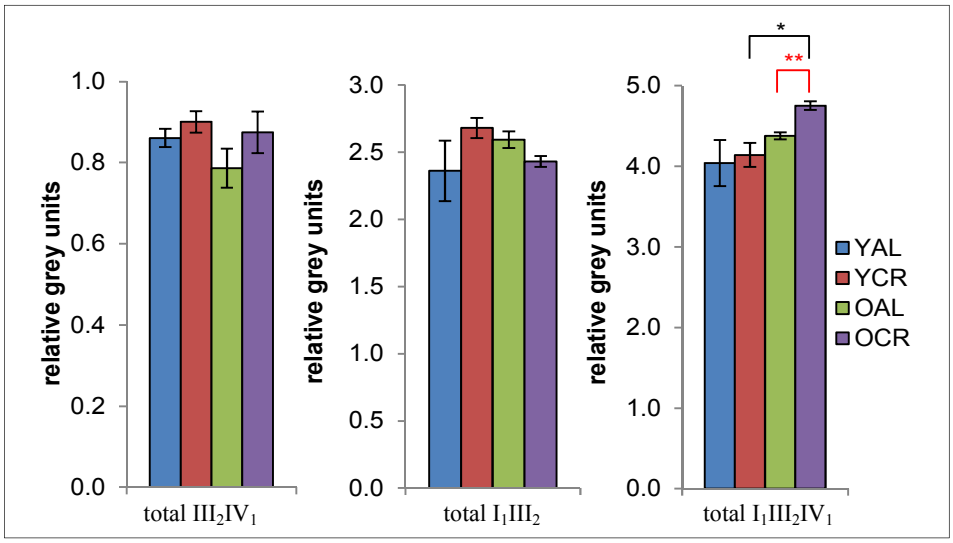

Fig. 4.45: Cerebrum: protein amount in 2D spots for supercomplexes containing CI, CIII and CIV. The sum of intensities (rel. grey units) of all identified spots (=total) for the supercomplexes III_2IV_1, I_1III_2 and $I_1III_2IV_1$ are plotted for each animal group.
bar plots: mean of technical repeats (n=3), error bars: standard error of technical repeats
significance: * = $p < \alpha$ (0.05); ** = $p < \alpha$ (0.01)
asterisks in black: changes caused by ageing, (YAL vs. OAL; YCR vs. OCR)
asterisks in red: changes caused by calorie restriction, (YAL vs. YCR; OAL vs. OCR)

In Fig. 4.46 the sum of the spot intensities of all identified subunits of CII are depicted for cerebrum of all animal groups (YAL, YCR, OAL, OCR). Ageing has no effect on the protein amount of CII. Only for long-term calorie restriction (OAL vs. OCR) a decreased protein amount is observable (-7.7 %, not stat. sig.).

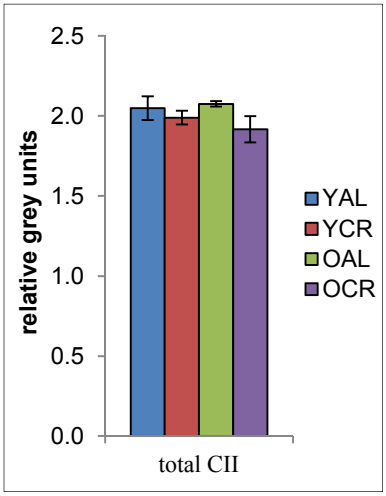

Fig. 4.46: Cerebrum: protein amount in 2D spots for CII. The sum of the intensities in rel. grey units of total CII are presented for each animal group.
bar plots:
mean of technical repeats (n=3),
error bars:
standard error of technical repeats,
significance:
* = $p < \alpha$ (0.05); ** = $p < \alpha$ (0.01),
asterisks in black:
changes caused by ageing,
(YAL vs. OAL; YCR vs. OCR)
asterisks in red:
changes caused by calorie restriction,
(YAL vs. YCR; OAL vs. OCR)

The changes of protein amount of ATP synthase in cerebrum is shown in Fig. 4.47. Fig. 4.47A depicts the sum of the intensities of all identified subunits for CV (total CV) compared with the identified subunits for monomer V_1, dimer V_2 and next higher homooligomer V_3.

Ageing (black asterisks) increases the protein amount of total CV (+7.1 %), V_1 (+6.5 %, Frenzel: -1.5-fold) and V_3 (+26.1 %, all not stat. sig.) in *ad libitum* nourished rats (YAL vs. OAL) as well as for rats grown under calorie restriction (YCR vs. OCR) for total CV (+13.4 %) and V_1 (+13.7 %, both stat. high sig.) and for V_2 (+12.9 %, stat. sig.) and for V_3 (+39.8 %, not stat. sig.). Neither short-term nor long-term calorie restriction has an effect on the protein amount of ATP synthase homooligomers (Fig. 4.47A).

Fig. 4.47B illustrates the spot intensity of the subunits α, β and the sum α+β as well as F_o and F_1 portion of mitochondrial ATP synthase from cerebrum. As expected, it is observable that the intensities, respectively the amounts of the subunits α and β are similar and almost equal in intensity. Ageing (black asterisks) increases the protein amount in both cases, for *ad libitum* fed animals (YAL vs. OAL) and those under conditions of calorie restriction (YCR vs. OCR). This can be observed for *ad libitum* fed animals for α (+11.8 %), β (+13.5 %), α+β (+12.6 %, all not stat. sig.) as well as for F_1 portion (+18.1 %, stat. sig.). For aged calorie restricted rats, the protein amount is enhanced for α (+18.5 %), β (+19.1 %), and α+β (+18.8 %, all stat. high sig.). Long-term calorie restriction (OAL vs. OCR) decreases the amount of F_1 portion (-17.8 %, not stat. sig.).

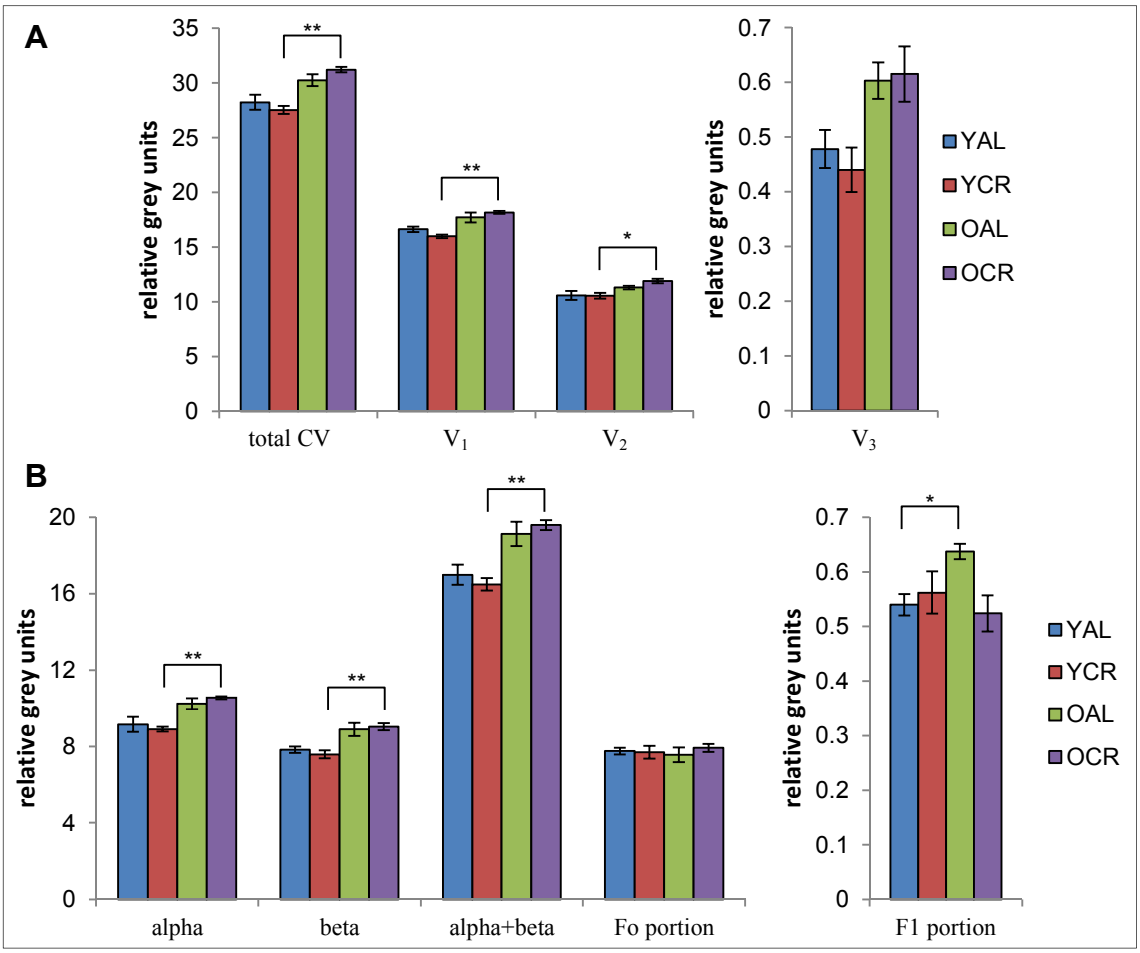

Fig. 4.47: Cerebrum: protein amount in 2D spots for CV. A: The sum of the intensities of all identified subunits of total ATP synthase (CV) are compared with those of identified subunits of monomer (V_1), dimer (V_2) and next higher homooligomer V_3; **B:** intensities (in rel. grey units) of ATP synthase's subunits α, β and α+β are plotted, as well as F_o and F_1 portion.
bar plots: mean of technical repeats (n=3), error bars: standard error of technical repeats
significance: * = $p < \alpha$ (0.05); ** = $p < \alpha$ (0.01)
asterisks in black: changes caused by ageing, (YAL vs. OAL; YCR vs. OCR)
asterisks in red: changes caused by calorie restriction, (YAL vs. YCR; OAL vs. OCR)

In Fig. 4.48 the spot intensities for the mtDNA encoded subunits CYB (CIII) and COX2 (CIV) of cerebrum mitochondria are depicted. The protein amount of the mtDNA encoded subunit CYB is increased with age under *ad libitum* feeding (YAL vs. OAL, +21.9 %, not stat. sig.).

The amount of COX2 is decreased (-15.0 %, stat. sig.) under ageing and *ad libitum* feeding (YAL vs. OAL, black asterisk). Short-term (YAL vs. YCR, red asterisk, +19.0 %, stat. sig.) as well as long-term calorie restriction (OAL vs. OCR, +20.3 %, not stat. sig.) increase the protein amount of COX2.

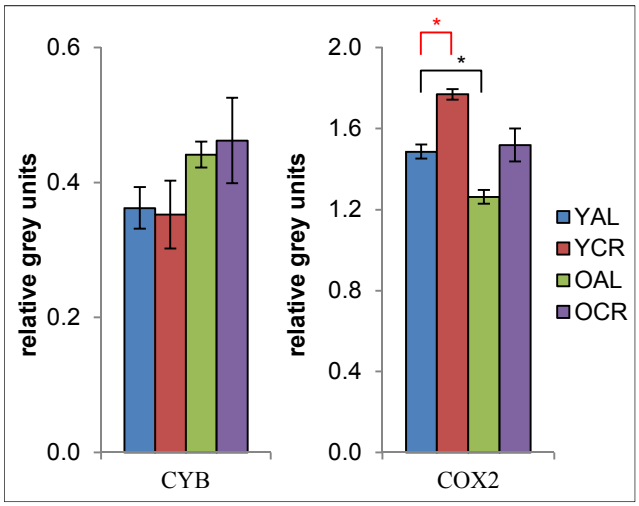

Fig. 4.48: Cerebrum: protein amount in 2D spots for mtDNA encoded OxPhos subunits CYB and COX2. Intensities in rel. grey units of CYB and COX2 are presented for each animal group.
bar plots:
mean of technical repeats (n=3),
error bars:
standard error of technical repeats,
significance:
* = $p < \alpha$ (0.05); ** = $p < \alpha$ (0.01),
asterisks in black:
changes caused by ageing,
(YAL vs. OAL; YCR vs. OCR)
asterisks in red:
changes caused by calorie restriction,
(YAL vs. YCR; OAL vs. OCR)

15 non-OxPhos proteins of cerebrum were analysed and their spot intensities (in rel. grey units) diagrammed in Fig. 4.49, Fig. 4.50 and Fig. 4.51.

In Fig. 4.49 the intensities for three proteins involved in cellular stress management are depicted. These are the mitochondrial 60 kDa heat shock protein (CH60), the protein disulfide-isomerase A4 (PDIA4) and the 78 kDa glucose-regulated protein (GRP78).

Ageing of *ad libitum* fed rats (YAL vs. OAL, +18.5 %) and also of calorie restricted rats (YCR vs. OCR, +11.7 %) increases the protein amount for CH60 (both not stat. sig.). For PDIA4 and GRP78 no changes caused by ageing are visible.

Calorie restriction has no effects on the analysed stress proteins, except a lowered protein amount of GRP78 under the influence of long-term calorie restriction (OAL vs. OCR, -22.6 %, not stat. sig.).

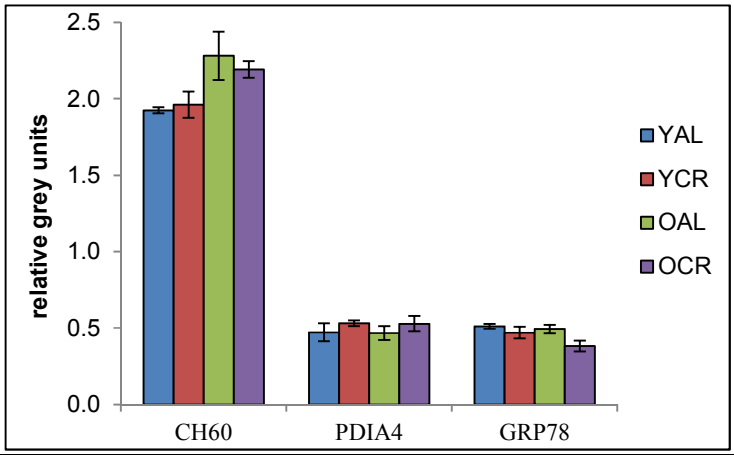

Fig. 4.49: Cerebrum: protein amount in 2D spots of proteins of cellular stress management. Intensities in rel. grey units of diverse stress proteins are presented for each animal group.
bar plots: mean of technical repeats (n=3), error bars: standard error of technical repeats
significance: * = $p < \alpha$ (0.05);
** = $p < \alpha$ (0.01)
asterisks in black: changes caused by ageing, (YAL vs. OAL; YCR vs. OCR)
asterisks in red: changes caused by calorie restriction, (YAL vs. YCR; OAL vs. OCR)

In Fig. 4.50 the changes of the protein amounts of several proteins from cerebrum involved in TCA cycle and glycolysis are displayed. Fig. 4.50A depicts the spot intensities of the mitochondrial proteins: malate dehydrogenase (MDHM), citrate synthase (CISY), aconitate hydratase (ACON) and 2-oxoglutarate dehydrogenase (ODO1).

Ageing (black asterisk) reduces the protein amount of MDHM (-38.4 %, stat. sig.) and ODO1 (-38.0 %, not stat. sig.) for *ad libitum* nourished animals (YAL vs. OAL). The protein amount is also decreased in aged calorie restricted rats (YCR vs. OCR, (black asterisks) for CISY(-15.4 %) and ACON (-19.0 %, both stat. sig.). For MDHM, the protein amount is increased (+60.3 %, stat. sig.) during ageing under calorie restriction (YCR vs. OCR, black asterisk).

Short-term calorie restriction (YAL vs. YCR, red asterisk) decreases the protein amount of MDHM (-47.6 %, stat. sig.) and increases the amount of ACON (+17.2 % not stat. sig.). Long-term calorie restriction (OAL vs. OCR, red asterisks) increases the protein amount of MDHM (+36.5 %, not stat. sig.) and ODO1 (+108.3 %, stat. sig.) and decreases the amount of CISY (-7.1 %, not stat. sig.) and ACON (-13.7 %, stat. sig.).

The mitochondrial dihydrolipoyl dehydrogenase (DLDH) is involved in TCA cycle as well as in glycolysis. The spot intensities are displayed in Fig. 4.50B. Ageing (black asterisk) decreases the DLDH amount (-30.0 %, stat. high sig.) only for animals kept under calorie restriction (YCR vs. OCR). Short-term calorie restriction (YAL vs. YCR, red asterisk) increases the protein amount (+21.5 %, stat. sig.), whereas long-term calorie restriction (OAL vs. OCR, red asterisk) decreases it (-18.0 %, stat. sig.).

In Fig. 4.50C the spot intensities of pyruvate kinase isozymes M1/M2 (KPYM) and fructose-bisphosphate aldolase A/C (ALDOA/C) are shown. Ageing (black asterisk) of animals under calorie restriction (YCR vs. OCR) reduces the protein amount of both, KPYM (-13.8 %, not stat. sig.) and ALDOA/C (-10.8 %, stat. sig.).

Short-term calorie restriction (YAL vs. YCR) causes an increase in amount of KPYM (+21.4 %, not stat. sig.). Animals under the influence of long-term calorie restriction show no changes.

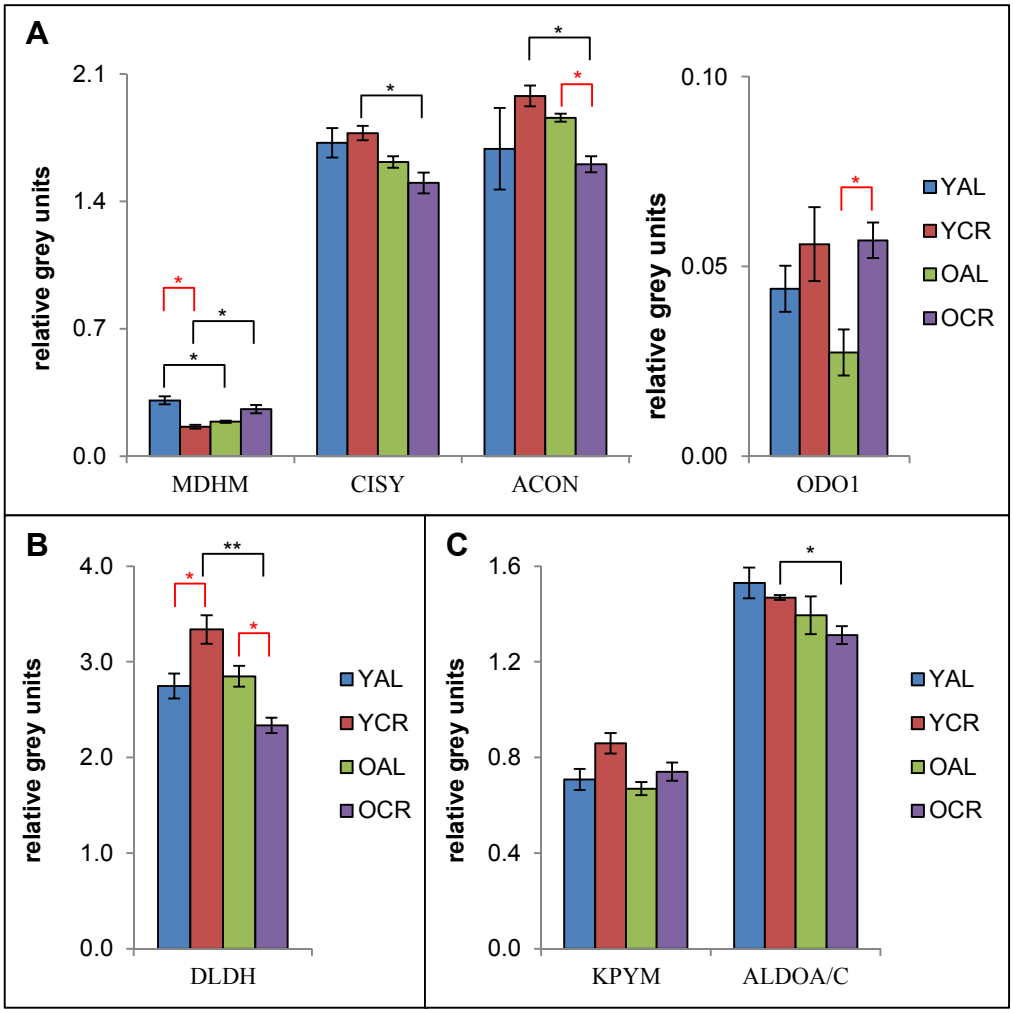

Fig. 4.50: Cerebrum: protein amount in 2D spots of proteins involved in TCA cycle and glycolysis. A: Intensities (in rel. grey units) of proteins from TCA cycle are presented for each animal group. **B:** Intensity (in rel. grey units) of DLDH protein, which is involved in TCA cycle and glycolysis, is depicted for each animal group. **C:** Intensities (in rel. grey units) of proteins involved in glycolysis are depicted for each animal group.
bar plots: mean of technical repeats (n=3), error bars: standard error of technical repeats
significance: * = $p < \alpha$ (0.05); ** = $p < \alpha$ (0.01)
asterisks in black: changes caused by ageing, (YAL vs. OAL; YCR vs. OCR)
asterisks in red: changes caused by calorie restriction, (YAL vs. YCR; OAL vs. OCR)

In Fig. 4.51 the spot intensities (in rel. grey units) of several non-OxPhos proteins from cerebrum are depicted. The changes of lipophilin (PLP1), tubulin (TBB2A), syntaxin binding protein (STXB1), glutamate dehydrogenase (GLDH) and Na^+/K^+ ATPase are shown.

Ageing (black asterisks) of *ad libitum* fed animals (YAL vs. OAL) reduces the protein amount of PLP1 (-39.0 %, stat. high sig.) and of TBB2A (-13.0 %, not stat. sig.), whereas for STXB1 (+22.7 %, not stat. sig.) and Na^+/K^+ ATPase (+10.8 %, stat. sig.) it is increased.

Ageing of calorie restricted animals (YCR vs. OCR) decreases the protein amount of TBB2A (-60.9 %, stat. high sig.) and GLDH (-25.0 %, not stat. sig.), whereas the quantity of PLP1 (+26.5 %, not stat. sig.) and Na^+/K^+ ATPase (+13.5 %, stat. sig.) is increased.

Short-term calorie restriction (YAL vs. YCR, red asterisks) decreases the protein amount of PLP1 (-37.8 %, stat. high sig.) and increases it for TBB2A (+44.2 %, stat. high sig.). Long-term calorie restriction (OAL vs. OCR, red asterisks) increases the amount of PLP1 (+29.2 %, not stat. sig.) and reduces the amount of TBB2A (-35.1 %, stat. high sig.) and STXB1 (-8.8 %, stat. sig.).

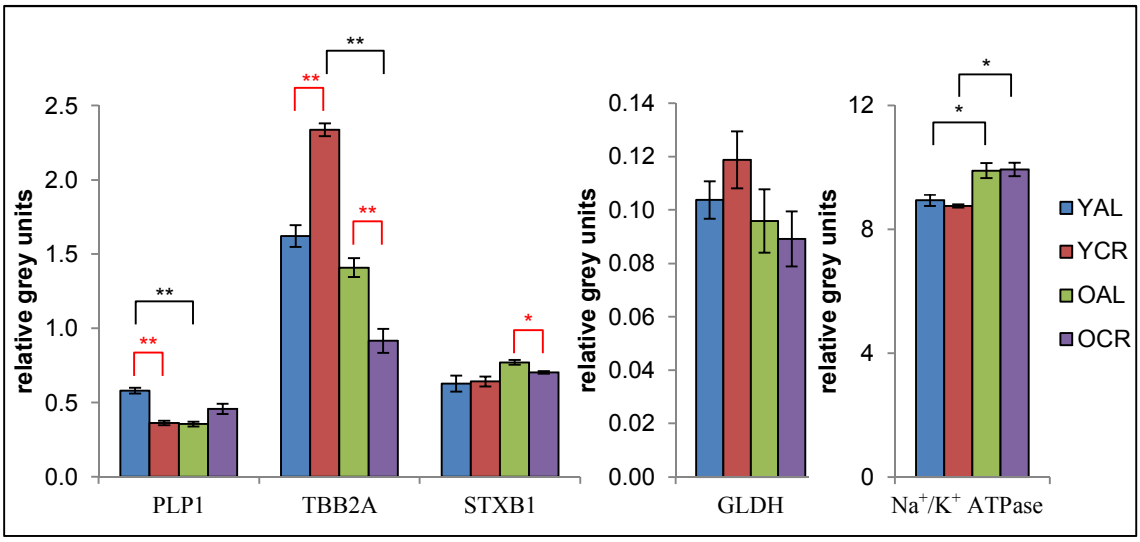

Fig. 4.51: Cerebrum: protein amount in 2D spots of diverse non-OxPhos proteins. Intensities (in rel. grey units) of the proteins lipophilin (PLP1), tubulin (TBB2A), syntaxin binding protein (STXB1) and glutamate dehydrogenase (GLDH resp. DHE3) and Na^+/K^+ ATPase from cerebrum are depicted.
bar plots: mean of technical repeats (n=3), error bars: standard error of technical repeats
significance: * = $p < \alpha$ (0.05); ** = $p < \alpha$ (0.01)
asterisks in black: changes caused by ageing, (YAL vs. OAL; YCR vs. OCR)
asterisks in red: changes caused by calorie restriction, (YAL vs. YCR; OAL vs. OCR)

Summary

A summary of the results from 2D-BN/SDS PAGE analysis is given in Table 4.30. For each tissue sample, the results for changes in age for *ad libitum* fed animals (AL: YAL vs. OAL) and under calorie restriction kept animals (CR: YCR vs. OCR) are presented as well as the effects of short-term (ST: YAL vs. YCR) and long-term (LT: OAL vs. OCR) calorie restriction. An increase of protein amount is marked with an upward-pointing arrow (△), a decrease with a downward-pointing arrow (▽). Both symbols are used in **grey** (**not stat. sig.**), **orange** (**stat. sig.**) and **red** (**stat. high sig.**). Black dashes (▬) were placed, where **no variation** could be examined. Main tendencies are quoted below.

Ageing has no general influence on the protein amount in cerebellum of *ad libitum* nourished rats (AL), while for hippocampus the same group exhibits a predominant decrease of the protein amount, observable also for cerebrum, except for the amount of ATP synthase, which shows an increase of protein quantity.

Aged calorie restricted rats (CR) show a trend for mainly raised protein amount in cerebellum and cerebrum. The protein amount of only some of the non-OxPhos proteins is decreased. For proteins of hippocampus, two trends are observable for the same group: OxPhos complexes I to IV decrease in amount while ATP synthase and the non-OxPhos proteins increase in quantity, as also observed for cerebellum and cerebrum.

Short-term calorie restriction (ST) reduces mainly the protein amount in cerebellum and hippocampus, whereas in cerebrum most of the proteins do not change, only a tendency of enhanced protein quantity prevails.

Long-term calorie restriction (LT) causes no general variation of the protein quantity in cerebellum. In hippocampus and cerebrum the protein amount is mainly increased, but in cerebrum only for OxPhos proteins.

To bring into focus the ATP synthase, ageing under *ad libitum* conditions (AL) reduces its amount in hippocampus only (Table 4.30). The combination of age and calorie restriction leads to an increased ATP synthase amount in cerebellum and cerebrum (CR) and in hippocampus (CR and LT). Short-term calorie restriction (ST) leads to a decreased quantity of ATP synthase in cerebellum and hippocampus.

The mtDNA encoded protein subunits CYB and COX2 do not show specific trends. The changes in amounts seem to follow the trends of total CIII respectively total CIV.

Proteins involved in stress management of the cell are increased in cerebellum during ST and are decreased during ageing under calorie restriction (CR) to the same level as animals aged under *ad libitum* feeding (AL). In hippocampus CR and LT lead to increased amount of stress proteins. In cerebrum, the amount of stress proteins stays at the same level during ageing for AL and CR.

Table 4.30: Summary of the results from 2D-BN/SDS PAGE spot analysis

figures	entity	examined subunits	Cerebellum				Hippocampus				Cerebrum			
			AL	CR	ST	LT	AL	CR	ST	LT	AL	CR	ST	LT
4.28A 4.36A 4.44A	I_1	NDUS1, NDUS2, NDUA9	—	△	▽	—	▽	▽	—	—	▽	△	△	△
	I_1IV_2		—	△	—	△	▽	▽	—	—	—	△	—	△
	I_1III_2		—	△	▽	—	▽	—	▽	△	—	▽	—	—
	$I_1III_2IV_1$		—	—	—	—	▽	△	▽	△	—	△	—	△
	total CI	all	—	△	▽	—	▽	—	▽	△	—	△	—	△
4.28B 4.36B 4.44B	III_2	QCR2	▽	—	▽	—	—	—	—	—	▽	△	—	△
	III_2IV_1		△	△	▽	—	▽	▽	—	—	▽	△	—	▲
	III_4		—	—	—	—	▽	▽	—	—	—	▲	—	▲
	I_1III_2		▽	△	▽	—	—	△	▽	△	△	▽	—	▽
	$I_1III_2IV_1$		—	—	—	—	▽	△	▽	△	—	△	—	△
	total CIII	all	▽	△	▽	—	▽	—	—	△	—	△	—	△
4.28C 4.36C 4.44C	IV_1	COX1	—	▲	▽	▽	▽	—	△	△	▲	▽	△	—
	IV_2		—	—	—	—	▽	—	—	—	—	—	—	—
	III_2IV_1		—	—	—	—	—	—	—	—	—	—	—	—
	total CIV	all	—	—	—	—	▽	▽	—	—	▽	—	△	△
4.29 4.37 4.45	total III_2IV_1	all for III_2IV_1	△	△	▽	—	▽	▽	—	—	▽	—	—	—
	total I_1III_2	all for I_1III_2	—	△	▼	—	▽	△	▽	△	—	▽	—	—
	total $I_1III_2IV_1$	all for $I_1III_2IV_1$	—	—	—	▽	▽	△	▽	△	—	△	—	▲
4.30 4.38 4.46	total CII	all	—	—	—	—	▽	▽	△	△	—	—	—	▽
4.31A 4.39A 4.47A	total CV	all	—	△	▽	—	▽	△	▽	△	△	▲	—	—
	V_1	all for V_1	—	△	▽	—	▽	—	—	△	△	▲	—	—
	V_2	all for V_2	—	△	▽	—	▽	△	▽	△	—	△	—	—
	V_3	all for V_3	—	△	—	—	—	—	—	—	△	△	—	—
4.31B 4.39B 4.47B	alpha	all α	—	△	▽	—	▽	△	▽	△	△	▲	—	—
	beta	all β	—	△	▽	—	▽	△	▽	△	△	▲	—	—
	alpha+beta	all α + all β	—	△	▽	—	▽	△	▽	△	△	▲	—	—
	F_o portion	all for F_o	—	△	▽	—	▽	▽	—	—	—	—	—	—
	F_1 portion	α + β for F_1	—	△	▽	△	—	—	—	—	△	—	—	▽
4.32 4.40 4.48	mtDNA encoded subunits	CYB	—	—	▽	—	—	—	—	—	△	—	—	—
		COX2	—	—	—	—	—	▽	—	▽	▽	—	△	△
4.33 4.41 4.49	Stress proteins	CH60	—	▽	△	—	—	△	—	△	△	△	—	—
		PDIA4	—	▽	△	—	▽	△	▽	△	—	—	—	—
		GRP78	—	▽	△	—	—	—	—	—	—	—	—	▽
4.34A 4.42A 4.50A	TCA cycle	MDHM	—	—	—	—	△	—	—	▽	▽	△	▽	△
		CISY	—	▽	△	—	—	—	▽	—	—	▽	—	▽
		ACON	—	▽	△	—	△	△	▽	—	—	▽	△	▽
		ODO1	—	—	▽	—	—	▽	—	▽	▽	—	—	△
4.34B 4.42B 4.50B	TCA cycle & Glycolysis	DLDH	—	▽	▽	▽	▽	△	▽	△	—	▼	△	▽
4.34C 4.42C 4.50C	Glycolysis	KPYM	—	—	—	—	—	△	▽	△	—	▽	△	—
		ALDOA/C	—	—	—	—	—	—	—	▽	—	▽	—	—
4.35 4.43 4.51	Na^+/K^+ ATPase	AT1A3, AT1B1	—	▽	▽	▽	—	△	—	—	△	△	—	—
	lipophilin	PLP1	△	▽	▲	—	▲	▼	△	▼	▼	△	▼	△
	tubulin	TBB2A	△	▽	△	—	—	△	—	△	▽	▼	▲	▼
	syntaxinBP	STXB1	—	▼	△	▽	—	—	—	—	△	—	—	▽
	GLDH	DHE3	△	△	—	▽	△	▽	△	▽	—	▽	—	—

symbols: "△": increase, "▽": decrease, "—": no change; colours: stat. high sig., stat. sig., not stat. sig.
abbrev.: AL: *ad libitum*, CR: calorie restriction, ST: short-term calorie restriction, LT: long-term calorie restriction

Proteins in energy metabolism (glycolysis and TCA cycle) show in cerebellum the same tendency as the stress proteins. During ST the proteins are increased and decreased during ageing under calorie restriction (CR) to reach the same level after LT as under AL. In hippocampus the proteins of energy metabolism are decreased under ST but during ageing this effect compensates (CR) and is even overcompensated by increased protein amount of DLDK and KPYM (LT). Other changes in hippocampus seem to vary with no specific trend. In cerebrum the amount of two of the TCA cycle proteins is reduced during ageing (AL). ST leads to increased amount of proteins of energy metabolism in cerebrum, are decreased during ageing under CR and remain mainly at a lower level after LT, compared to AL.

Na^+/K^+ ATPase, lipophilin, tubulin, syntaxinBP and glutamate dehydrogenase in the broader sense are all involved in neuronal composition, their function and trafficking at synapses. For cerebellum an age (AL) induced increase of these proteins is visible, which is also present for ST but ageing under CR and LT decreases the amount of these proteins. A loss of neurons or synapses or their activity in cerebellum under calorie restriction could explain these findings. A comparison to the tissue weight or amount of mitochondrial proteins does not correlate. Trends are not pronounced for the same proteins from hippocampus and cerebrum.

For comparison of the results, it is referred to the findings of Olgun et al. (2002), Groebe et al. (2007), Frenzel (2011), Cerqueira et al. (2012) and Thilmany (2013), as they all analysed mitochondria of brain tissue.

Frenzel (2011) analysed the effects of ageing on 5 and 30 months old male Wistar rats. She analysed mitochondria from cerebral cortex, hippocampus and striatum. Cerebral cortex is a large part of cerebrum, therefore it will be compared to cerebrum in this thesis, albeit cerebrum also includes striatum, but the latter is just a little part of cerebrum. In cerebral cortex, ageing decreased amounts of individual complexes (III_2, IV_1, II_1 and V_1) and super-complexes I_1III_2, $I_1III_2IV_1$, and increased the amount of supercomplex III_2IV_1. In hippo-campus, the amount of individual and supercomplexes increased, except for individual IV_1, whereof the quantity decreased. The findings on quantitation of OxPhos (super-) complexes by Frenzel (2011) were mostly contrary to the findings in this thesis. For the F_1 portion she found an increase for both tissues, as found for cerebrum. CH60 (no change) and ACON (increase) showed the same effects for hippocampus, while in cerebral cortex a decrease of CH60 was found by Frenzel (2011) contrary to the increase in cerebrum. ACON in cerebral cortex did not change as in cerebrum. She found the quantity of Na^+/K^+ ATPase increased in hippocampus, which has not changed in this thesis, and decreased in cerebral cortex, contrary to the findings for cerebrum in this thesis. Maybe the findings differ because of the different animal models used as also supposed by Silvestri et al. (2011). Wistar rats are outbred strains and Fischer 344 inbred. Van Der Staay and Blokland (1996) showed differences in behaviour of adult rats from Wistar, Fischer 344, Brown Norway and hybrid Fischer 344 x Brown Norway rats and analysed, whether they are suitable as animal model of ageing. They suggest to favour inbred strains as Fischer 344, Brown Norway and the F1 hybrid Fischer 344 x Brown Norway. Kacew and Festing (1996) note that "[…] Individual samples of rats from an outbred colony may differ markedly in their genetic characteristics […]".

Thilmany (2013) analysed heart mitochondria and, together with her diploma student Michaela Söhn, cerebrum mitochondria from the same animals as used in this thesis. However, problems with the quantitation of the whole mitochondrial protein amount of the cerebrum mitochondria occurred, and that is why these analyses were repeated with a new Bradford quantitation. Deviations to the findings of Söhn (2010) were in average at -33.0 % for single values (maxima: +11.8 % and -62.1 %) (4.2.1). Therefore, it is no wonder that in most cases the changes of ageing and calorie restriction in cerebrum observed in this thesis do not conform with the findings documented by Thilmany (2013) and Söhn (2010).

Cerqueira et al. (2012) analysed the effects of calorie restriction (60 %, supplemented with micronutrients) on brain form mice. They found large increased amounts of cytochrome c oxidase and mitofusin-1, as well as strongly increased activity of citrate synthase, and concluded that mitochondrial mass in the brains of animals under calorie restriction must be increased. Increased amount of CIV was found in this thesis only for individual IV_1 in cerebellum in aged rats under calorie restriction (CR) and in hippocampus for rats under ST and LT as well as for cerebrum under ST. Total CIV is increased under ST and LT in cerebrum.

Olgun et al. (2002) analysed brain mitochondria from mice under calorie restriction (alternate day feeding). They found that the amount of total CI and total CIII did not change, while the quantity of total CIV increased under calorie restriction (+ 16%). The latter is in line with the findings for the amount of total CIV of cerebrum for ST and LT. Cerebrum as the biggest analysed part, could be the most similar to the whole mouse brain.

Groebe et al. (2007) analysed the effects of ageing on rat brain mitochondria from 5-, 17- and 31-months old Fischer rats. They found for several mitochondrial proteins that the amount decreased with age, among them ATP synthase subunit beta (ATPB), tubulin, cytochrome c oxidase subunit Va (COX5A) and malate dehydrogenase (MDHM). These proteins were also analysed in this thesis. COX5A is included in total CIV, of which the amount is decreased due to ageing (AL) in hippocampus and cerebrum, and not changed in cerebellum. ATPB is included in the analysis of all beta subunits of ATP synthase, of which the amount decreased with age (AL) in hippocampus but increased in cerebrum and is not changed in cerebellum. The amount of MDHM is found here to decrease with age (AL) in cerebrum, but increases in hippocampus and is unchanged in cerebellum. Tubulin shows decreased amount in cerebrum, but increased in cerebellum and no change in hippocampus. Mainly the tendency for decreased mitochondrial protein amount is the same in hippocampus and cerebrum. There are obviously differences regarding the analysed single brain parts compared to the whole brain analysed by Groebe et al. (2007).

4.2.6 Quantitation of complex I and IV in-gel activity

Below, the analysis of the results is explained on the basis of the CI in-gel activity test of the hippocampus samples. The procedure is similar for cerebellum and cerebrum samples and likewise CIV in-gel activity.

All animal groups were examined in triplicates. 100 µg (b. sol. d/p: 8g/g, 3.3.1) of RBM proteins were loaded on each lane of an 18 cm by 16 cm sized imidazole BN gel in addition with three lanes of 70 µg (b. sol. d/p: 3g/g) BHM as standard. BN PAGE was performed as described in 3.4, followed by CI in-gel activity test (3.8, respectively CIV in-gel activity test). Images were taken at different time points (see 3.7.3). Evaluation took place as described in 3.11.2. Please keep in mind that printed images differ from evaluated original grey scale images as described in 3.11.

In Fig. 4.52 images of the BN gel with the hippocampus samples (triplicates of YAL, YCR, OAL, OCR) are presented. For one hippocampus sample and for BHM, the complexes and supercomplexes are marked. The abbreviations for the supercomplexes are: a = I_1III_2, b = $I_1III_2IV_1$, c = $I_1III_2IV_2$, d = $I_1III_2IV_3$. An image of the BN gel at time point zero is shown in Fig. 4.52A. In Fig. 4.52B the same BN gel is depicted, but 120 min after start of CI in-gel activity test. The fused image from Delta2D analysis, containing all grey scale images of every time point, is depicted in Fig. 4.52C.

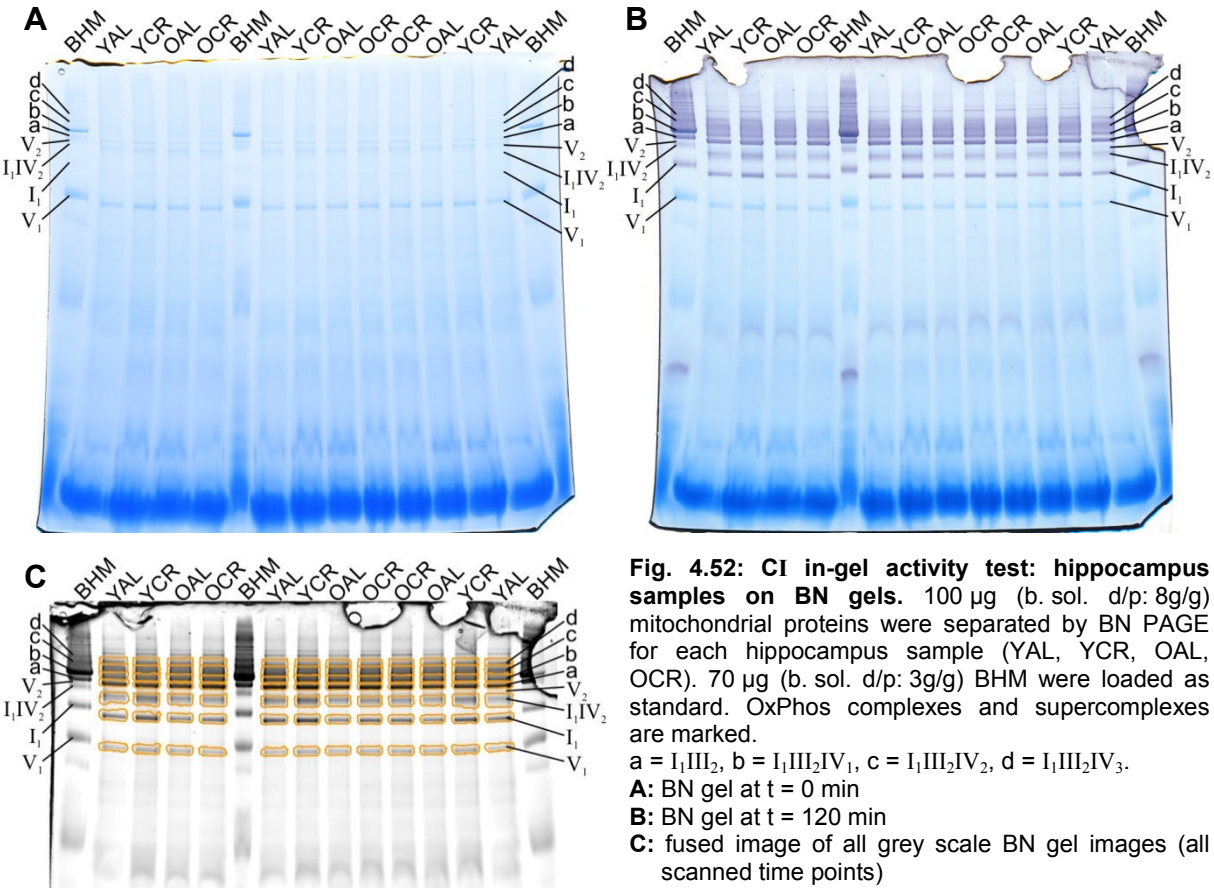

Fig. 4.52: CI in-gel activity test: hippocampus samples on BN gels. 100 µg (b. sol. d/p: 8g/g) mitochondrial proteins were separated by BN PAGE for each hippocampus sample (YAL, YCR, OAL, OCR). 70 µg (b. sol. d/p: 3g/g) BHM were loaded as standard. OxPhos complexes and supercomplexes are marked.
a = I_1III_2, b = $I_1III_2IV_1$, c = $I_1III_2IV_2$, d = $I_1III_2IV_3$.
A: BN gel at t = 0 min
B: BN gel at t = 120 min
C: fused image of all grey scale BN gel images (all scanned time points)

As control for unspecific staining of the bands during time, the intensities of the bands (their grey value pixel volume V [grey units]) of ATP synthase monomer (V_1) are plotted versus time [min] in Fig. 4.53 for all hippocampus samples. It is apparent, that the intensities remain nearly constant between the threshold values ±0.25 for all samples and time points.

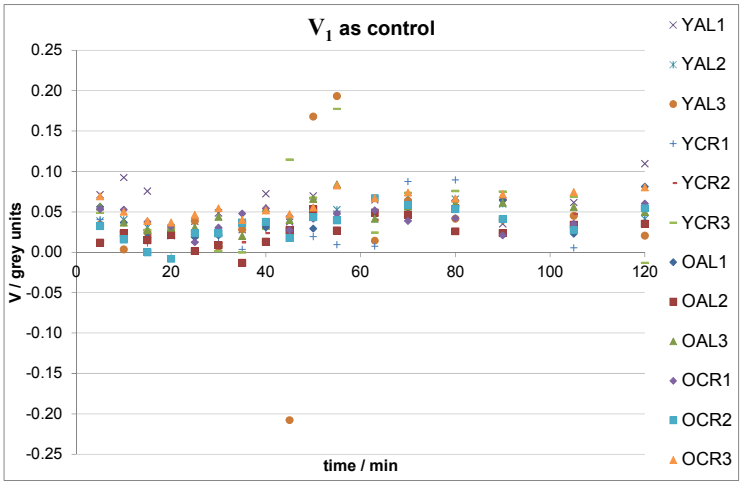

Fig. 4.53: CI in-gel activity test: plot of the intensities of the complex V_1 bands for all time points. All hippocampus samples are shown. The V_1 band serves as a control for unspecific staining during time. Intensities are given in V values (grey units).

For every time point, the intensities of the bands for all hippocampus samples are given in Fig. 4.54 and Fig. 4.55. The figures illustrate plots of the intensities of the bands [grey units] versus time [min]. Lines of best fit, their linear equation and coefficient of determination are given for all triplicates of the samples. The slopes reflect the specific activity in grey units per minute for each band. They were normalised for quantitation as described in 3.11.2.

In Fig. 4.54 the development of the bands of individual complex I_1 and of the CI containing complex I_1IV_2 for duration of the in-gel activity test is presented.

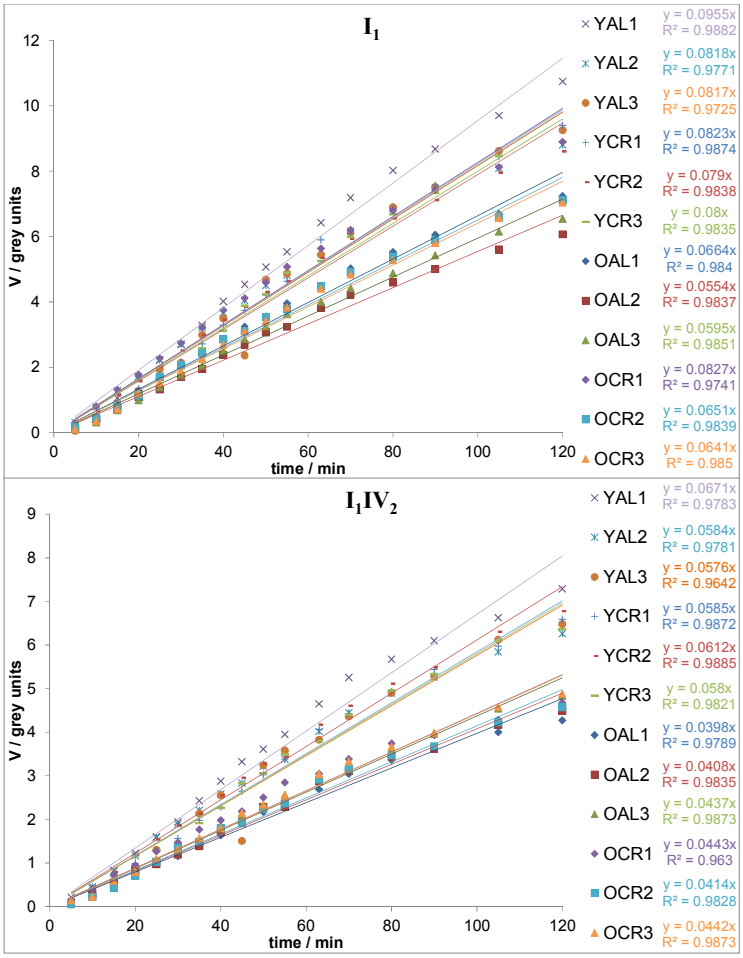

Fig. 4.54: CI in-gel activity test: plots of the intensities of the bands from complex I_1 and I_1IV_2 during time. All hippocampus samples (YAL, YCR, OAL, OCR, three repeats each) are shown for every scanned time point. Lines of best fit, their linear equation and coefficient of determination are given. Slopes are used for quantitation. Intensities are shown in V values [grey units].

Fig. 4.55 depicts similar plots for the development of the CI containing supercomplexes (I_1III_2, $I_1III_2IV_1$, $I_1III_2IV_2$, $I_1III_2IV_3$).

In all plots of Fig. 4.54 and Fig. 4.55, the linear development of the band intensities during time is apparent.

Coefficients of determination show good matches of the lines of best fit with the experimental data. Linear equations display the slopes, which are needed for normalisation and final quantitation of the specific activity (3.11.2).

Normalised specific activities of CI and CIV (in grey units per min) are presented as bar plots (see below). The bars represent the mean of the triplicates. The error bars show the standard errors of the mean. Statistics were performed as described in 3.11.3. Black asterisks indicate changes in ageing and red asterisks in calorie restriction. Significance levels are 0.05 (*) and 0.01 (**).

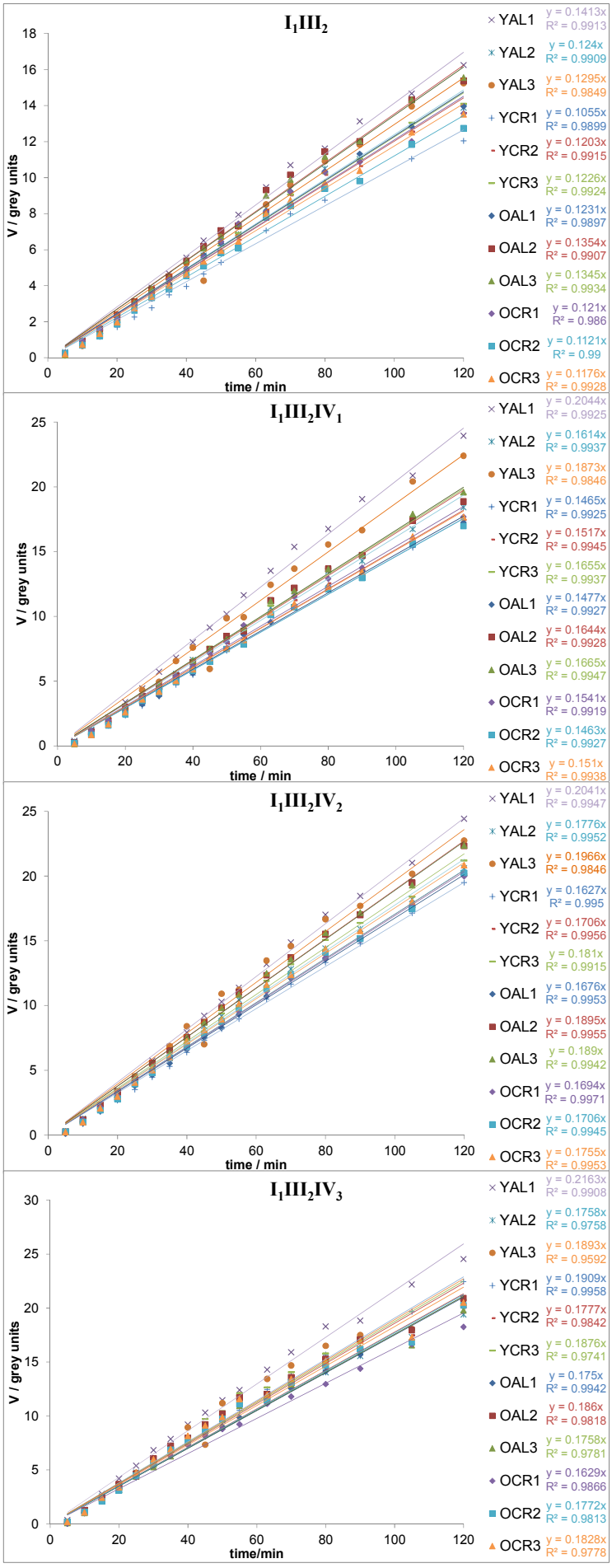

Fig. 4.55: CI in-gel activity test: plots of the band intensities from supercomplexes I_1III_2, $I_1III_2IV_1$, $I_1III_2IV_2$ and $I_1III_2IV_3$ versus time. All hippocampus samples (YAL, YCR, OAL, OCR, three repeats each) are shown for every scanned time point. Intensities are depicted in V values [grey units], time in min. Lines of best fit, their linear equation and coefficient of determination are given. Slopes are used for quantitation.

Cerebellum

CI in-gel activity test was performed (3.8) for cerebellum samples and evaluated quantitatively as described before on the example of hippocampus samples and as outlined in 3.11.2. In Fig. 4.56 the left part of the colour scale image of the BN gel after incubation for 120 min in CI activity test solution is shown. The complete image is attached in "7 Supplements", Fig. 7.10, as well as the analysed fused image in Fig. 7.11. Triplicates of each cerebellum animal group were analysed (not shown in Fig. 4.56). Each sample lane contained 100 µg (b. sol. d/p: 8g/g) RBM protein. An additional lane of 70 µg (b. sol. d/p: 3g/g) of the standard BHM were loaded too. By eye, the blue/purple precipitate of NBT diformazan is visible, which correlates with the activity of CI in individual complex I_1 and in the supercomplexes I_1IV_2, I_1III_2, $I_1III_2IV_1$, $I_1III_2IV_2$ and $I_1III_2IV_3$. Differences between the four animal groups are not observable by eye. Some weak blue/purple bands in the lower area of the gel are also observable, but cannot be related to a specific complex, and are therefore not considered for evaluation. Complexes V_1 and V_2 are visible as CBBG stained bands only, therefore they can be used as control for unspecific background staining (see above). A larger intensity of the CI staining is observable for BHM, although a smaller amount of BHM protein was loaded than of RBM, hence BHM show a higher CI in-gel activity than RBM. The most intense CI staining is observable for BHM in supercomplex $I_1III_2IV_1$ and for RBM in supercomplex I_1III_2.

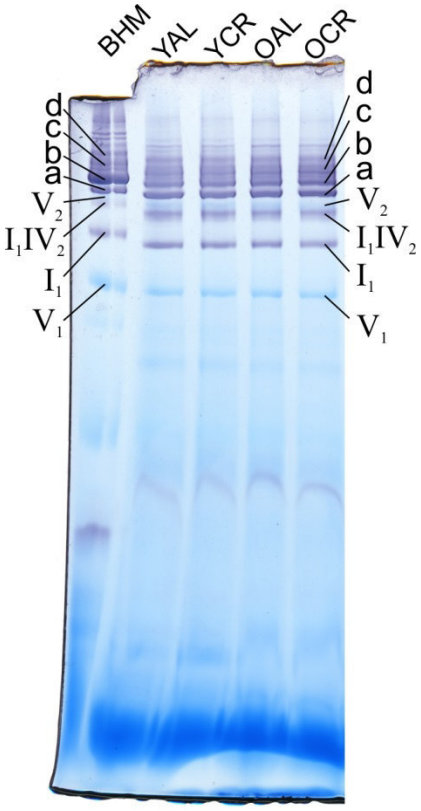

Fig. 4.56: Cerebellum, cut image of BN gel after 120 min in CI activity test solution. From each cerebellum sample (YAL, YCR, OAL, OCR), 100 µg (b. sol. d/p: 8g/g) mitochondrial proteins were separated by BN PAGE, followed by CI in-gel activity test. 70 µg (b. sol. d/p: 3g/g) of BHM were also loaded as standard. CI activity generates blue / purple precipitate of NBT diformazan. OxPhos complexes and supercomplexes are marked. a = I_1III_2, b = $I_1III_2IV_1$, c = $I_1III_2IV_2$, d = $I_1III_2IV_3$.

Fig. 4.57 illustrates the specific activities in grey units per minute for CI in individual complex I_1 and in the supercomplexes I_1IV_2, I_1III_2, $I_1III_2IV_1$, $I_1III_2IV_2$ and $I_1III_2IV_3$. All four animal groups are depicted.

In comparison of the specific activities of CI in all supercomplexes to complex I_1 (Fig. 4.57), an overall trend for all animal groups (YAL, YCR, OAL, OCR) is observable. The specific activity of CI in I_1IV_2 is for all groups smaller (-37 % in average) than for I_1, while for the supercomplexes I_1III_2 (+60 %), $I_1III_2IV_1$ (+114 %), $I_1III_2IV_2$ (+168 %) and $I_1III_2IV_3$ (+190 %, all in average) the specific activity of CI rises with increased mass.

When considering the changes of ageing and calorie restriction in a certain complex, no pronounced changes in specific activity occur. Animals aged under calorie restriction (YCR vs. OCR, black asterisk) show a lower activity of CI in complex I_1IV_2 (-9.3 %, stat. sig.).

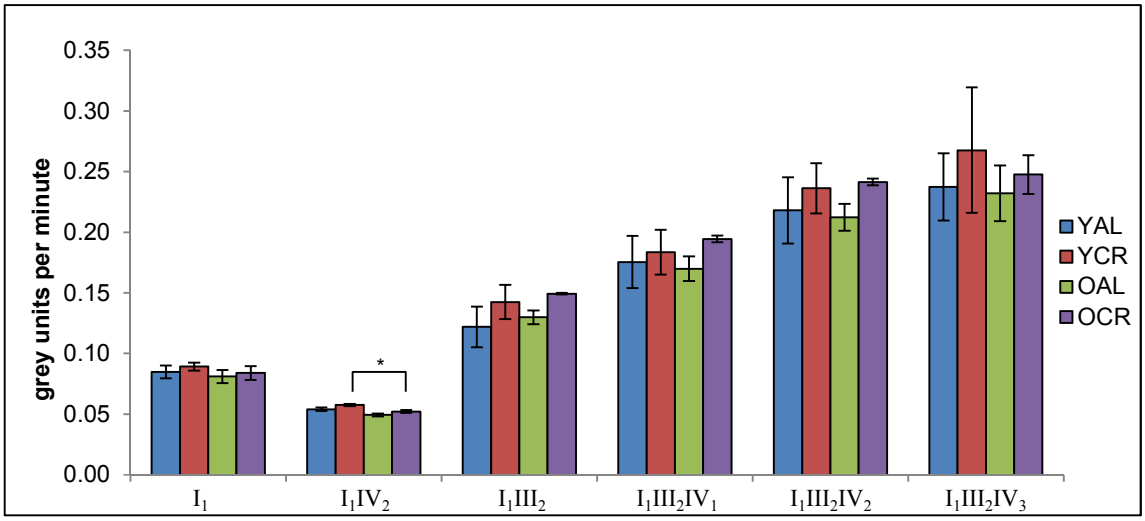

Fig. 4.57: Cerebellum, CI in-gel activity: specific activities of CI in individual and supercomplexes. For each cerebellum animal group (YAL, YCR, OAL, OCR), the specific activity (in grey units per minute) of CI in each analysed gel band is plotted.
bar plots: mean of technical repeats (n=3), error bars: standard error of technical repeats
significance: * = $p < \alpha$ (0.05); ** = $p < \alpha$ (0.01)
asterisks in black: changes caused by ageing, (YAL vs. OAL; YCR vs. OCR)
asterisks in red: changes caused by calorie restriction, (YAL vs. YCR; OAL vs. OCR)

Long-term calorie restriction (OAL vs. OCR) increases the specific CI activity for the supercomplexes I_1III_2 (+15.1 %), $I_1III_2IV_1$ (+14.4 %) and $I_1III_2IV_2$ (+13.7 %, all not stat. sig.).

For CIV in-gel activity test, 100 µg (b. sol. d/p: 8g/g) of RBM proteins were loaded on the BN gel for each cerebellum sample lane (YAL, YCR, OAL, OCR) in triplicates. Lanes of 70 µg (b. sol. d/p: 3g/g) BHM were added as standard. After gel run, CIV in-gel activity test was executed as described in 3.8 and the grey scale images evaluated according to 3.11.2. Fig. 4.58 illustrates the colour scale image of the left part of the BN gel after 150 min of incubation in CIV activity test solution. The entire image is shown in "7 Supplements", Fig. 7.12. The brownish precipitate of polymerised / oxidised DAB on the bands of complexes and supercomplexes is caused by reaction of CIV. Already by eye the precipitate is visible (Fig. 4.58), but variations in activity of the different RBM samples are only apparent, when analysed with the software Delta2D in fused images (Fig. 7.13) on basis of the grey scale images.

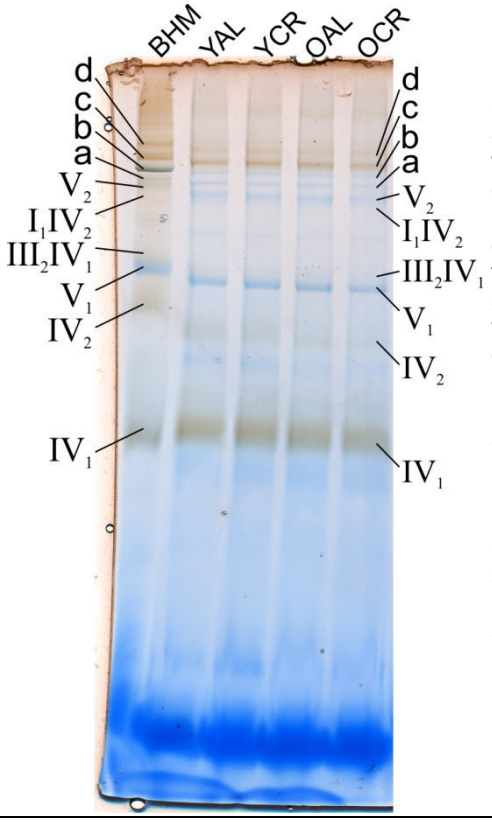

Fig. 4.58: Cerebellum, cut image of BN gel after 150 min in CIV activity test solution. For each sample lane, 100 µg (b. sol. d/p: 8g/g) of mitochondrial protein from every cerebellum sample were loaded on the BN gel. 70 µg (b. sol. d/p: 3g/g) BHM were loaded as standard. Finished gel was put in CIV activity test solution. Brownish precipitate of polymerised / oxidised DAB shows CIV activity. OxPhos complexes and supercomplexes are marked.
a = I_1III_2, b = $I_1III_2IV_1$, c = $I_1III_2IV_2$, d = $I_1III_2IV_3$.

In Fig. 4.58 it is observable that the total CIV activity of the lanes with cerebellum RBM is lower compared to the BHM lane,

although the loaded amount of BHM protein was lower than of RBM, hence the CIV activity of BHM is higher than of RBM. For all RBM samples, complexes IV_1, $I_1III_2IV_2$ and $I_1III_2IV_3$ show the most intense precipitate, whereas it is weak developed for complexes IV_2, III_2IV_1, I_1IV_2 and $I_1III_2IV_1$. Non-active complexes, V_1, V_2 and I_1III_2, exhibit no brownish precipitate, only initial blue CBBG stain is apparent.

The results of quantitative evaluation are depicted as bar plots in Fig. 4.59. Fig. 4.59A expresses the specific activity of CIV in its homooligomeric and heteromeric assemblies. Fig. 4.59B reflects the specific activity, but normalised to one copy of CIV per analysed (super-) complex.

When comparing the specific activity of CIV monomer IV_1 to all other CIV containing complexes, an overall trend is visible for all analysed animal groups. In Fig. 4.59A the specific activity of CIV in the dimer IV_2 (-57 %) and in I_1IV_2 (-34 %, both in average) is lower than in the individual IV_1, approximately on the same level for complex III_2IV_1 (-4 %), and increases with mass of the supercomplexes $I_1III_2IV_1$ (+78 %), $I_1III_2IV_2$ (+367 %) and $I_1III_2IV_3$ (+300 % all in average).

If specific activity is normalised to one copy of CIV, for comparison of the different forms of assembly (Fig. 4.59B), the specific CIV activity of IV_1 equals to the activity of III_2IV_1 (-4 %) and $I_1III_2IV_3$ (+33 %, both in average). The dimer IV_2 (-78 %) and I_1IV_2 (-67 %, both in average) show less than half of the specific CIV activity of the monomer. The specific activity of CIV in the supercomplexes $I_1III_2IV_1$ (+78 %) and $I_1III_2IV_2$ (+133 %, both in average) is raised compared to IV_1. For the old animals (OAL, OCR) the CIV activity of complex $I_1III_2IV_1$ and for all rat groups the activity of CIV in $I_1III_2IV_2$ is even more than doubled.

Concerning the analysis of ageing or calorie restriction, both plots of CIV specific activity (Fig. 4.59) lack stat. sig. differences between the analysed animal groups. Only for the effect of ageing, stat. not sig. tendencies for increased activity of CIV in age are visible, especially for complex I_1IV_2 (+61.9 %, ageing under calorie restriction YCR vs. OCR) and $I_1III_2IV_1$ (+56.8 %, ageing of *ad libitum* fed animals, YAL vs. OAL).

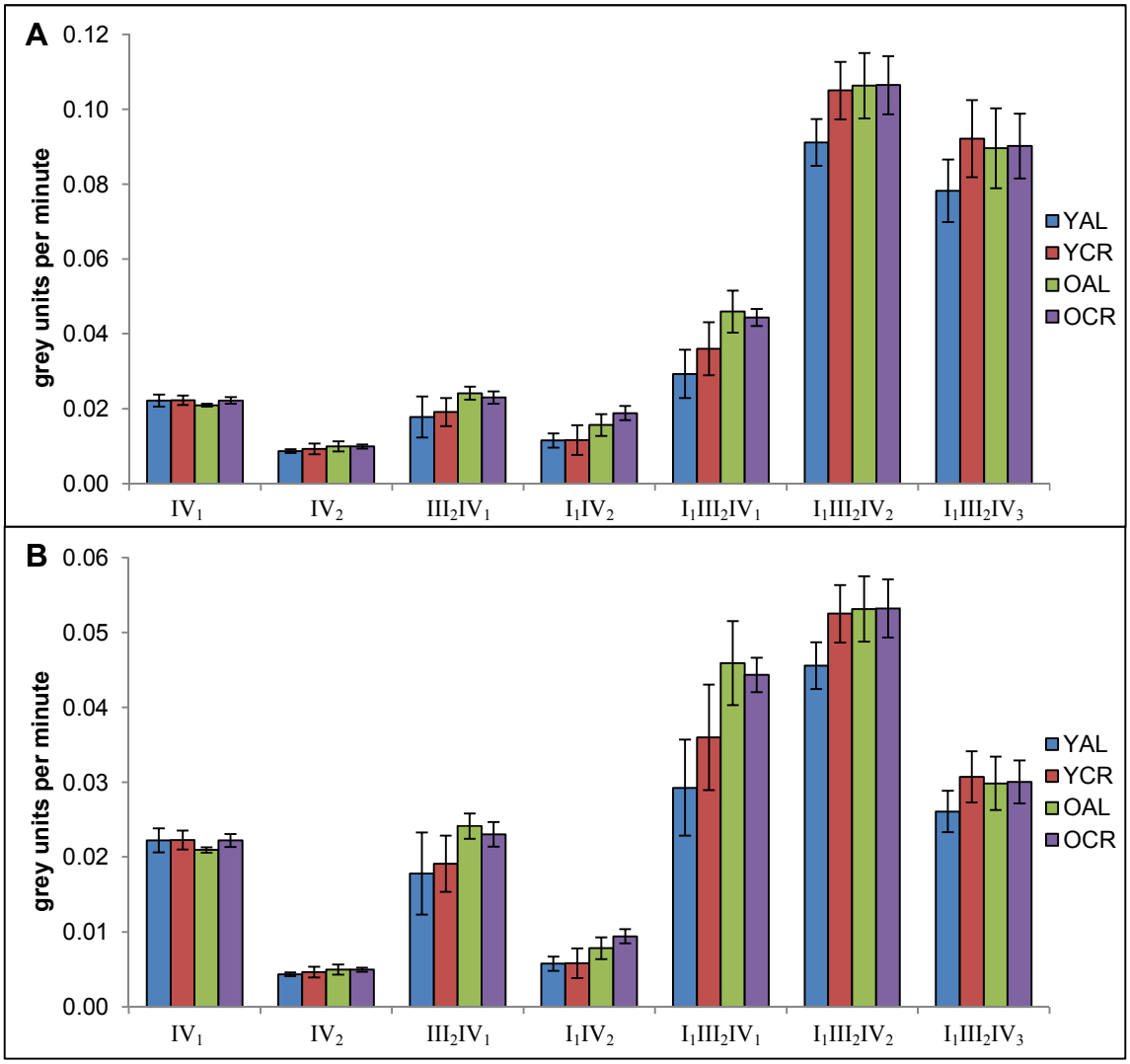

Fig. 4.59: Cerebellum, CIV in-gel activity test, specific activities of CIV in homooligomers and supercomplexes. For each cerebellum animal group (YAL, YCR, OAL, OCR), the specific activity (in grey units per minute) of CIV in each analysed gel band is plotted. **A:** specific activities of total CIV in the visualised complex, **B:** specific activities of CIV, normalised to its portion of the displayed complex.
bar plots: mean of technical repeats (n=3), error bars: standard error of technical repeats
significance: * = $p < \alpha$ (0.05); ** = $p < \alpha$ (0.01)
asterisks in black: changes caused by ageing, (YAL vs. OAL; YCR vs. OCR)
asterisks in red: changes caused by calorie restriction, (YAL vs. YCR; OAL vs. OCR)

Hippocampus

For each hippocampus sample lane, 100 µg (b. sol. d/p: 8g/g) of RBM protein were loaded on the BN gel. The different animal groups (YAL, YCR, OAL, OCR) were triplicated. Additional lanes with 70 µg (b. sol. d/p: 3g/g) BHM were loaded as standard. The gel image in Fig. 4.60 was taken after incubation in CI activity test solution for 120 min. Only the left part of the gel is shown. The entire image is given in Fig. 4.52 and in "7 Supplements", Fig. 7.10. The analysed fused image is depicted in Fig. 7.11. The blue/purple precipitate of NBT diformazan, as a result of CI activity, is apparent for individual complex I_1 and the supercomplexes I_1IV_2, I_1III_2, $I_1III_2IV_1$, $I_1III_2IV_2$ and $I_1III_2IV_3$. By eye, changes between animal groups of hippocampus are not visible. As already seen for cerebellum samples, some weak blue/purple bands in the lower area of the gel appear, but cannot be related to a specific complex, and are therefore not considered for evaluation. As already seen for cerebellum samples, a larger intensity of the CI staining is observable for BHM, although a smaller amount of BHM protein was loaded than of RBM. Therefore, BHM show a higher CI activity than RBM. The most intense CI staining is observable for BHM in supercomplex $I_1III_2IV_1$ and for RBM in supercomplex I_1III_2.

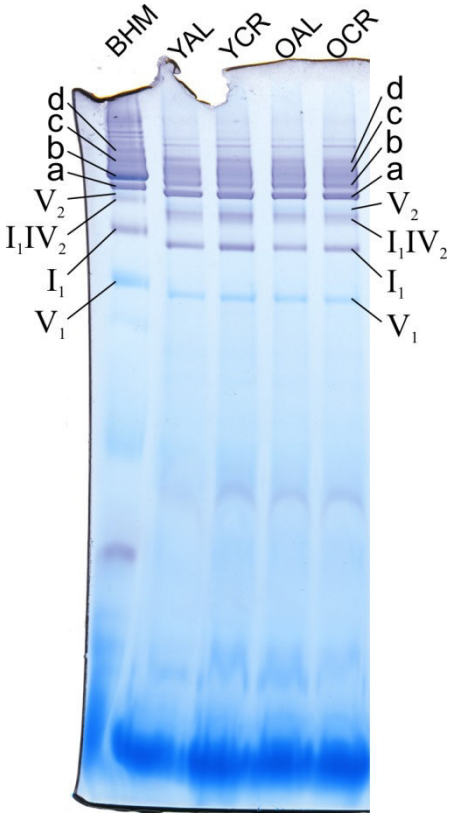

Fig. 4.60: Hippocampus, cut image of BN gel after 120 min in CI activity test solution. From each hippocampus sample (YAL, YCR, OAL, OCR), 100 µg (b. sol. d/p: 8g/g) mitochondrial proteinswere separated by BN PAGE, followed by CI in-gel activity test. 70 µg (b. sol. d/p: 3g/g) of BHM were also loaded as standard. CI activity generates blue / purple precipitate of NBT diformazan. OxPhos complexes and supercomplexes are marked.
a = I_1III_2, b = $I_1III_2IV_1$, c = $I_1III_2IV_2$, d = $I_1III_2IV_3$.

Quantitative evaluation of the formation of the precipitate was performed as described above and in 3.11.2 on the basis of the grey scale images. The results in form of specific activity of CI (in grey units per minute) are given for individual complex I_1 and the supercomplexes I_1IV_2, I_1III_2, $I_1III_2IV_1$, $I_1III_2IV_2$ and $I_1III_2IV_3$ in Fig. 4.61.

An overall trend is visible in Fig. 4.61. When the specific activity of CI for individual complex I_1 is compared to the supercomplexes, it is apparent for each animal group that the specific activity of CI is lower in I_1IV_2 (-31 % in average) than in complex I_1, but higher in the supercomplexes I_1III_2 (+66 %), $I_1III_2IV_1$ (+117 %), $I_1III_2IV_2$ (+140 %) and $I_1III_2IV_3$ (+145 %, all in average). The specific activity of CI rises with increased masses of supercomplexes. This trend is in line with the findings for cerebellum (see above).

Ageing leads to decreased CI activity in *ad libitum* nourished rats (YAL vs. OAL, black asterisks) for individual complex I_1 (-31.1 %) and supercomplex I_1IV_2 (-32.1 %, both stat. sig.), as well as for supercomplex $I_1III_2IV_1$ (-13.5 %, not stat. sig.). Likewise animals aged under calorie restriction (YCR vs. OCR, black asterisk) show decreased CI activity for I_1IV_2 (-26.9 %, stat. high sig.) and individual complex I_1 (-12.2 %, not stat. sig.) (Fig. 4.61).

Short-term calorie restriction (YAL vs. YCR) reduces the specific activity of CI for supercomplexes I_1III_2 (-11.8 %), $I_1III_2IV_1$ (-16.2 %) and $I_1III_2IV_2$ (-11.1 %, all not stat. sig.). Long-term calorie restriction (OAL vs. OCR, red asterisk) decreases the activity of CI in supercomplex I_1III_2 (-10.8 %, stat. sig.).

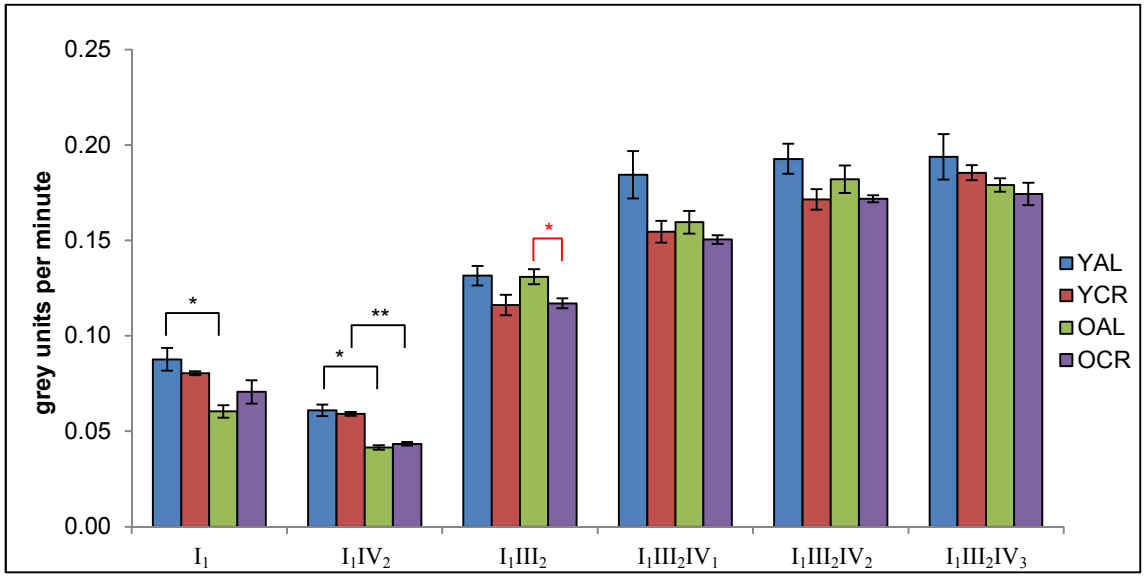

Fig. 4.61: Hippocampus, CI in-gel activity: specific activities of CI in individual and supercomplexes. For each hippocampus animal group (YAL, YCR, OAL, OCR), the specific activity (in grey units per minute) of CI in each analysed gel band is plotted.
bar plots: mean of technical repeats (n=3), error bars: standard error of technical repeats
significance: * = $p < \alpha$ (0.05); ** = $p < \alpha$ (0.01)
asterisks in black: changes caused by ageing, (YAL vs. OAL; YCR vs. OCR)
asterisks in red: changes caused by calorie restriction, (YAL vs. YCR; OAL vs. OCR)

For CIV in-gel activity test, triplicates of 100 µg (b. sol. d/p: 8g/g, 3.3.1) proteins of hippocampus RBM per BN gel lane were separated with additional lanes of 70 µg (b. sol. d/p: 3g/g) BHM as standard on BN PAGE. In-gel activity test was performed as described in 3.8.

In Fig. 4.62 the left side of the coloured image of the BN gel after 150 min of incubation in CIV activity test solution is given. The complete image is attached in "7 Supplements", Fig. 7.12. The analysed fused image is depicted in Fig. 7.13.

Just as shown above for cerebellum samples, lanes with hippocampus RBM have a lower specific activity of CIV than lanes containing BHM, even though the loaded protein amount of BHM was smaller

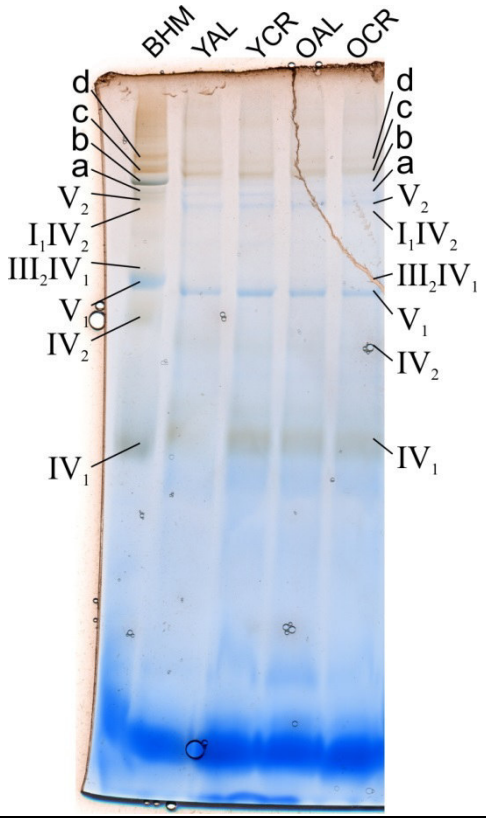

Fig. 4.62: Hippocampus, cut image of BN gel after 150 min in CIV activity test solution. For each sample lane, 100 µg (b. sol. d/p: 8g/g) of mitochondrial protein from every hippocampus sample were loaded on the BN gel. 70 µg BHM (b. sol. d/p: 3g/g) were loaded as standard. Finished gel was put CIV activity test solution. Brownish precipitate of polymerised / oxidised DAB shows CIV activity. OxPhos complexes and supercomplexes are marked.
a = I_1III_2, b = $I_1III_2IV_1$, c = $I_1III_2IV_2$, d = $I_1III_2IV_3$.

than of RBM. This is apparent due to the brownish precipitate of polymerised / oxidised DAB on top of the bands. By eye the brownish precipitate is observable for the complexes IV_1, $I_1III_2IV_2$ and $I_1III_2IV_3$, and only weakly for IV_2, III_2IV_1, I_1IV_2 and $I_1III_2IV_1$. Bands of V_1, V_2 and I_1III_2 exhibit only blue staining, originated from bound CBBG from the cathode buffer.

Quantitative analysis of specific activity of CIV in hippocampus RBM was performed on the basis of grey scale images (see 3.11.2). Results are shown in Fig. 4.63.

Fig. 4.63A displays the specific activity of CIV in its homooligomeric and supercomplex assemblies from hippocampus mitochondria. In Fig. 4.63B, this specific activity is normalised to the number of copies of CIV in each analysed complex. Although large error bars are present, an overall trend is observable for the comparison of the specific activity of individual complex IV_1 to the specific CIV activity from dimer IV_2 or the supercomplexes. As observable in Fig. 4.63A, complex IV_2 (-55 %) and supercomplex I_1IV_2 (-20 %) have lower specific CIV activity than IV_1, while for CIII containing supercomplexes, the CIV activity increases with mass: III_2IV_1 (+34 %) and $I_1III_2IV_1$ (+87 %), $I_1III_2IV_2$ (+280 %) and $I_1III_2IV_3$ (+260 %, all in average).

If normalised to the number of copies of CIV in the analysed (super-)complex (Fig. 4.63B), the differences in specific CIV activities of the supercomplexes become smaller. The CIV activities in the dimer IV_2 (-77 %) and complex I_1IV_2 (-60 %) stay lower compared to IV_1, while CIV activities of supercomplexes III_2IV_1 (+34 %) and $I_1III_2IV_3$ (+20 %) are slightly increased and CIV activity of supercomplexes $I_1III_2IV_1$ (+87 %) and $I_1III_2IV_2$ (+90 %, all in average) are almost double the activity of IV_1. In both plots, the monomer IV_1 of YAL RBM shows a little lower activity than all the others.

Due to the large error bars (Fig. 4.63), observable variations in ageing and calorie restriction have to be taken with caution. In aged *ad libitum* fed animals (YAL vs. OAL) an increase of specific CIV activity in individual complex IV_1 (+54.7 %, not. stat. sig.) is visible. The CIV activity in complex III_2IV_1 is increased (+50.1 %, stat. sig.) for aged animals under calorie restriction (YCR vs. OCR, black asterisk).

Short-term calorie restriction (YAL vs. YCR) increases CIV activity in complex IV_1 (+80.5 %, not stat. sig.), while the CIV activity is decreased for III_2IV_1 (-41.8 %, not stat. sig.). Long-term calorie restriction (OAL vs. OCR) decreases the specific CIV activity in complex III_2IV_1 (-19.7 %, not stat. sig.).

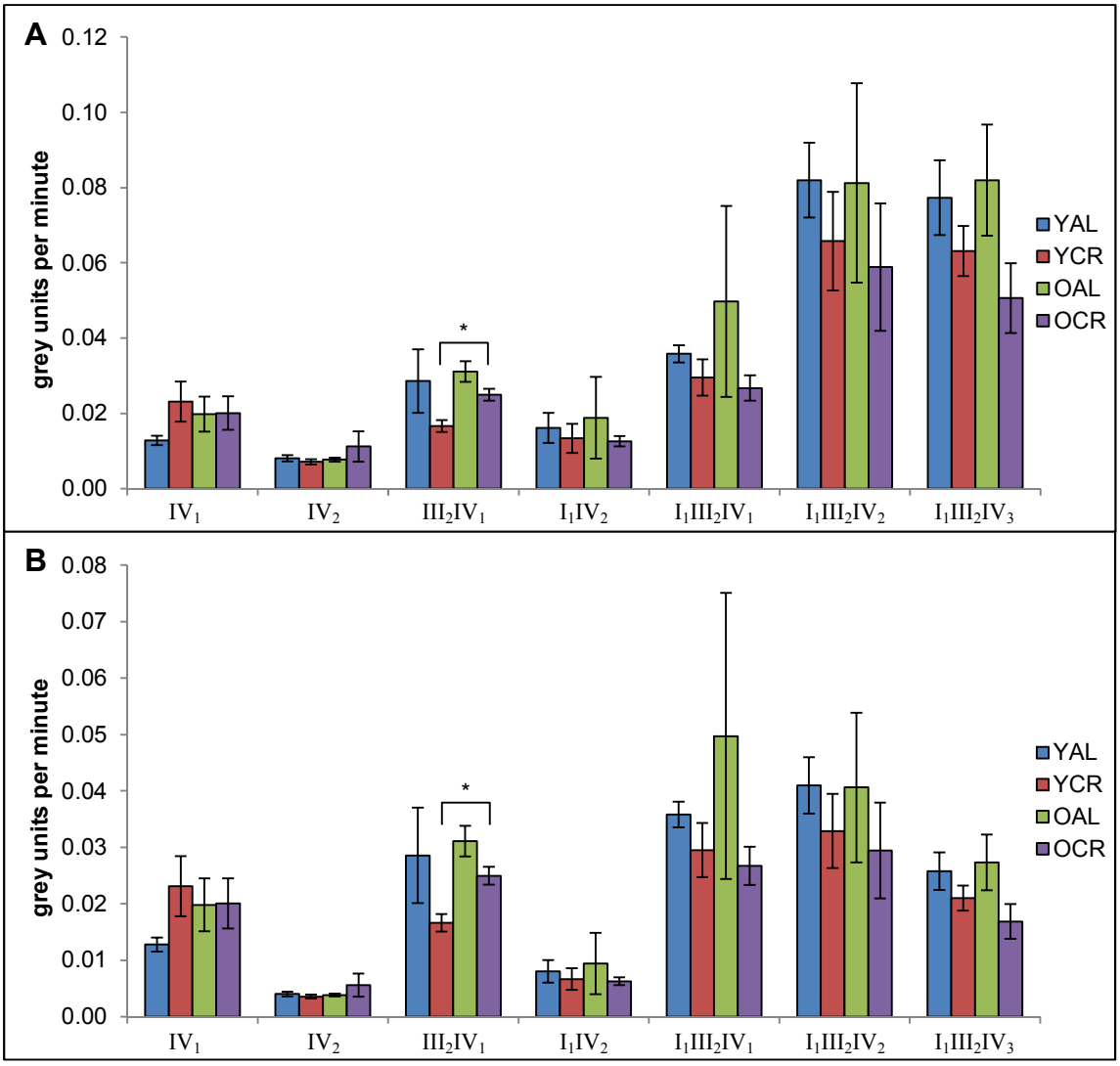

Fig. 4.63: Hippocampus, CIV in-gel activity test, specific activities of CIV in homooligomers and supercomplexes. For each hippocampus animal group (YAL, YCR, OAL, OCR), the specific activity (in grey units per minute) of CIV in each analysed gel band is plotted. **A:** specific activities of total CIV in the visualised complex, **B:** specific activities of CIV, normalised to its portion of the displayed complex.
bar plots: mean of technical repeats (n=3), error bars: standard error of technical repeats
significance: * = $p < \alpha$ (0.05); ** = $p < \alpha$ (0.01)
asterisks in black: changes caused by ageing, (YAL vs. OAL; YCR vs. OCR)
asterisks in red: changes caused by calorie restriction, (YAL vs. YCR; OAL vs. OCR)

Cerebrum

From each cerebrum animal group (YAL, YCR, OAL, OCR) 100 µg (b. sol. d/p: 8g/g) were loaded onto the BN gel in triplicates. Lanes of 70 µg (b. sol. d/p: 3g/g) BHM were added as standard. In Fig. 4.64 the left part of the BN gel image is depicted after incubation in CI activity test solution for 120 min. The entire image is attached in "7 Supplements", Fig. 7.10, and the analysed fused image in Fig. 7.11. CI activity is visible by formation of the blue/purple precipitate of NBT diformazan. Individual complex I_1 and the supercomplexes I_1IV_2, I_1III_2, $I_1III_2IV_1$, $I_1III_2IV_2$ and $I_1III_2IV_3$ can be related. The bands of complexes V_1 and V_2 remained blueish from CBBG, they can be used as control for unspecific activity staining. By eye, no variations between animal groups of cerebrum are visible. Additionally some weak blue/purple bands in the lower area of the gel appear, as already mentioned for cerebellum and hippocampus samples, but they cannot be related to any specific complex, and are therefore not considered for evaluation.

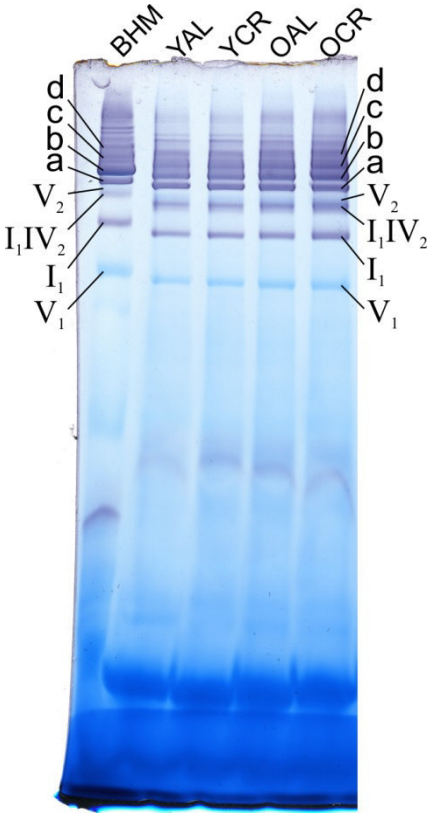

Fig. 4.64: Cerebrum, cut image of BN gel after 120 min in CI activity test solution. From each cerebrum sample (YAL, YCR, OAL, OCR), 100 µg (b. sol. d/p: 8g/g) mitochondrial proteins were separated by BN PAGE, followed by CI in-gel activity test. 70 µg (b. sol. d/p: 3g/g) BHM proteins were also loaded as standard. CI activity generates blue / purple precipitate of NBT diformazan. OxPhos complexes and supercomplexes are marked.
a = I_1III_2, b = $I_1III_2IV_1$, c = $I_1III_2IV_2$, d = $I_1III_2IV_3$.

A larger intensity of the CI staining is observable for BHM, although a smaller amount of BHM protein was loaded than of RBM. Therefore, BHM show a higher CI in-gel activity than RBM. The most intense CI staining is observable for BHM in supercomplex $I_1III_2IV_1$ and for RBM in supercomplex I_1III_2.

Evaluation of results was executed for cerebrum, as exemplified above for the hippocampus samples, and as explained in 3.11.2 on the basis of grey scale images. The resulting specific activity of CI (in grey units per minute) of cerebrum is plotted in Fig. 4.65 for individual complex I_1 and the supercomplexes I_1IV_2, I_1III_2, $I_1III_2IV_1$, $I_1III_2IV_2$ and $I_1III_2IV_3$.

When the specific activity of CI in individual complex I_1 is compared to the CI activity in supercomplexes (Fig. 4.65), the same trend is observable for cerebrum as mentioned above for cerebellum and hippocampus. Specific activity of CI in individual complex I_1 is always higher than in complex I_1IV_2 (-42 % in average), but for the supercomplexes I_1III_2 (+70 %), $I_1III_2IV_1$ (+93 %), $I_1III_2IV_2$ (+166 %) and $I_1III_2IV_3$ (+210 % all in average) enhancement of specific activity becomes apparent with increasing mass of the supercomplex.

In Fig. 4.65 no pronounced changes are observable for the analysis of CI activity in cerebrum during ageing or calorie restriction. Ageing reduces specific CI activity in *ad libitum* nourished animals (YAL vs. OAL) for complex I_1 (-18.6 %, not stat. sig.) and for animals

grown under calorie restriction (YCR vs. OCR) for complexes I_1 (-26.8 %) and I_1IV_2 (-21.7 %, both not stat. sig.).

Long-term calorie restriction (OAL vs. OCR) increases CI specific activity for supercomplex $I_1III_2IV_3$ (+11.5 %, not stat. sig.). No other variations can be examined for cerebrum.

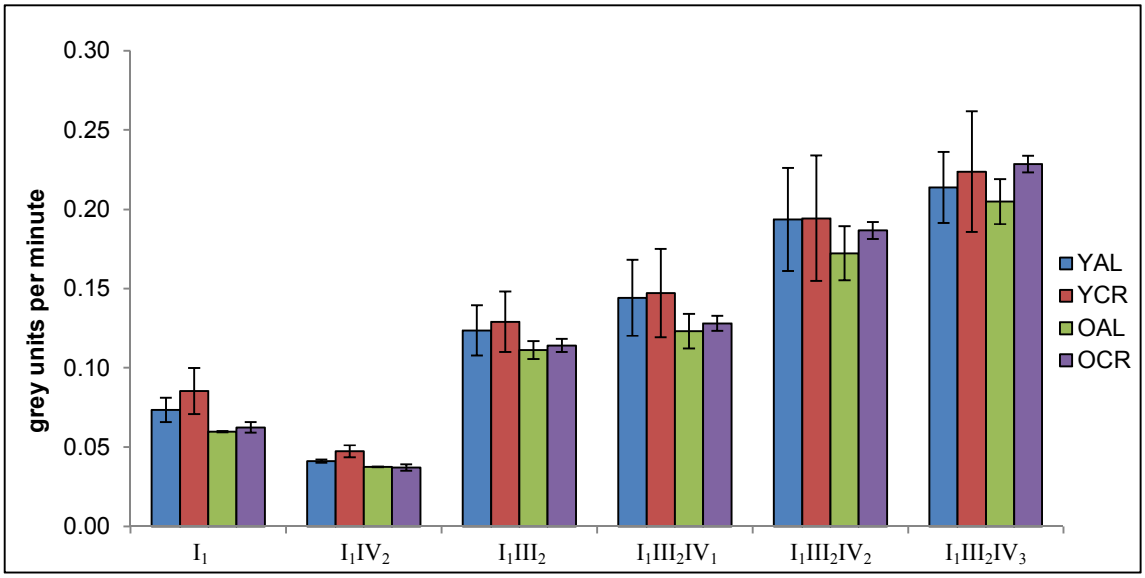

Fig. 4.65: Cerebrum, CI in-gel activity: specific activities of CI in individual and supercomplexes. For each cerebrum animal group (YAL, YCR, OAL, OCR), the specific activity (in grey units per minute) of CI in each analysed gel band is plotted.
bar plots: mean of technical repeats (n=3), error bars: standard error of technical repeats
significance: * = $p < \alpha$ (0.05); ** = $p < \alpha$ (0.01)
asterisks in black: changes caused by ageing, (YAL vs. OAL; YCR vs. OCR)
asterisks in red: changes caused by calorie restriction, (YAL vs. YCR; OAL vs. OCR)

The CIV in-gel activity test was performed on a BN gel with 100 µg (b. sol. d/p: 8g/g) mitochondrial protein per cerebrum sample lane. Each sample (YAL, YCR, OAL, OCR) was triplicated. Lanes with 70 µg (b. sol. d/p: 3g/g) BHM were added as standard. The activity test was conducted for 150 min (3.8.1). The left part of the BN gel, after 150 min incubation time, is shown in Fig. 4.66. The entire image is attached in "7 Supplements", Fig. 7.12.

The amount of the brown precipitate of polymerised / oxidised DAB on top of bands is related to the specific activity of

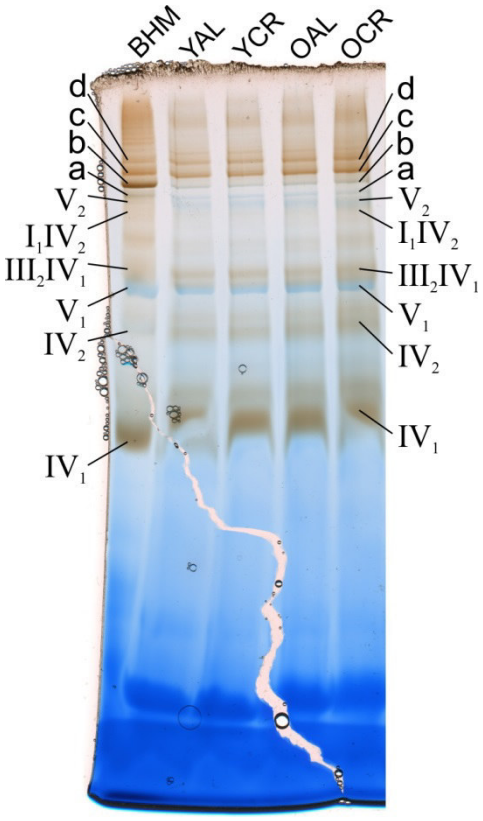

Fig. 4.66: Cerebrum, cut image of BN gel after 150 min in CIV activity test solution. For each sample lane, 100 µg (b. sol. d/p: 8g/g) of mitochondrial protein from every cerebrum sample were loaded on the BN gel. 70 µg BHM (b. sol. d/p: 3g/g) were loaded as standard. Finished gel was put in CIV activity test solution. Brownish precipitate of polymerised / oxidised DAB shows CIV activity. OxPhos complexes and supercomplexes are marked.
a = I_1III_2, b = $I_1III_2IV_1$, c = $I_1III_2IV_2$, d = $I_1III_2IV_3$.

CIV, and can even be allocated by eye, as visible in Fig. 4.66. Homooligomeric complexes IV_1, IV_2, and supercomplexes III_2IV_1, I_1IV_2, $I_1III_2IV_1$, $I_1III_2IV_2$ and $I_1III_2IV_3$ can be assigned. The latter two show the most intensity of brownish precipitate. Bands of V_1, V_2 and I_1III_2 remain blueish from CBBG. The lane of BHM exhibits more precipitate than the RBM sample lanes, which was seen for cerebellum and hippocampus samples, too. Hence the activity of BHM is highter than of RBM, although a smaller amount of BHM was loaded.

For quantitative analysis, the grey scale images were examined as described in 3.11.2, the fused image is depicted in Fig. 7.13. The results are plotted in Fig. 4.67. In Fig. 4.67A, the specific in-gel activity for CIV in its homooligomeric and supercomplex assemblies is plotted. Fig. 4.67B illustrates the specific activity of CIV normalised to its number of copies in the displayed (super-)complexes. By comparison of specific CIV activity of the monomer IV_1 to the activities of the other CIV containing complexes, overall trends are as follows (Fig. 4.67A): the specific CIV activity of complex IV_2 (-32 %, in average) is decreased compared to IV_1, while for all other complexes the CIV activity is increased. The CIV activity of complex I_1IV_2 (+56 %) is slightly increased, while for CIII containing supercomplexes the increase is stronger and increases with mass of the supercomplex: III_2IV_1 (+208 %), $I_1III_2IV_1$ (+218 %), $I_1III_2IV_2$ (+592 %) and $I_1III_2IV_3$ (+497 %, all in average).

After normalisation to the number of copies of CIV in the analysed (super-)complex, the specific CIV activities of complex IV_2 (-66 %) and complex I_1IV_2 (-22 %) are lower than the from IV_1. The specific activity of CIV in supercomplexes III_2IV_1 (+208 %), $I_1III_2IV_1$ (+218 %) and $I_1III_2IV_2$ (+246 %) are approximately at the same level, while the activity of supercomplex $I_1III_2IV_3$ is less increased (+99 %, all in average).

Changes caused by ageing are present for animals under calorie restriction only (YCR vs. OCR, Fig. 4.67). The activity of CIV is statistically non-significantly reduced for the monomer IV_1 (-20.3 %) and supercomplex III_2IV_1 (-22.8 %, both not stat. sig.), whereas for the supercomplexes I_1IV_2 (+66.2 %, not stat. sig.) and $I_1III_2IV_1$ (+60.0 %, stat. sig.) an increase of activity is observable.

Short-term calorie restriction (YAL vs. YCR, red asterisk) increases specific CIV activity, for IV_2 (+48.8 %, stat. sig.) and for III_2IV_1 (+40.5 %, not stat. sig.) and long-term calorie restriction (OAL vs. OCR) for supercomplex $I_1III_2IV_1$ (+27.8 %, not stat. sig.).

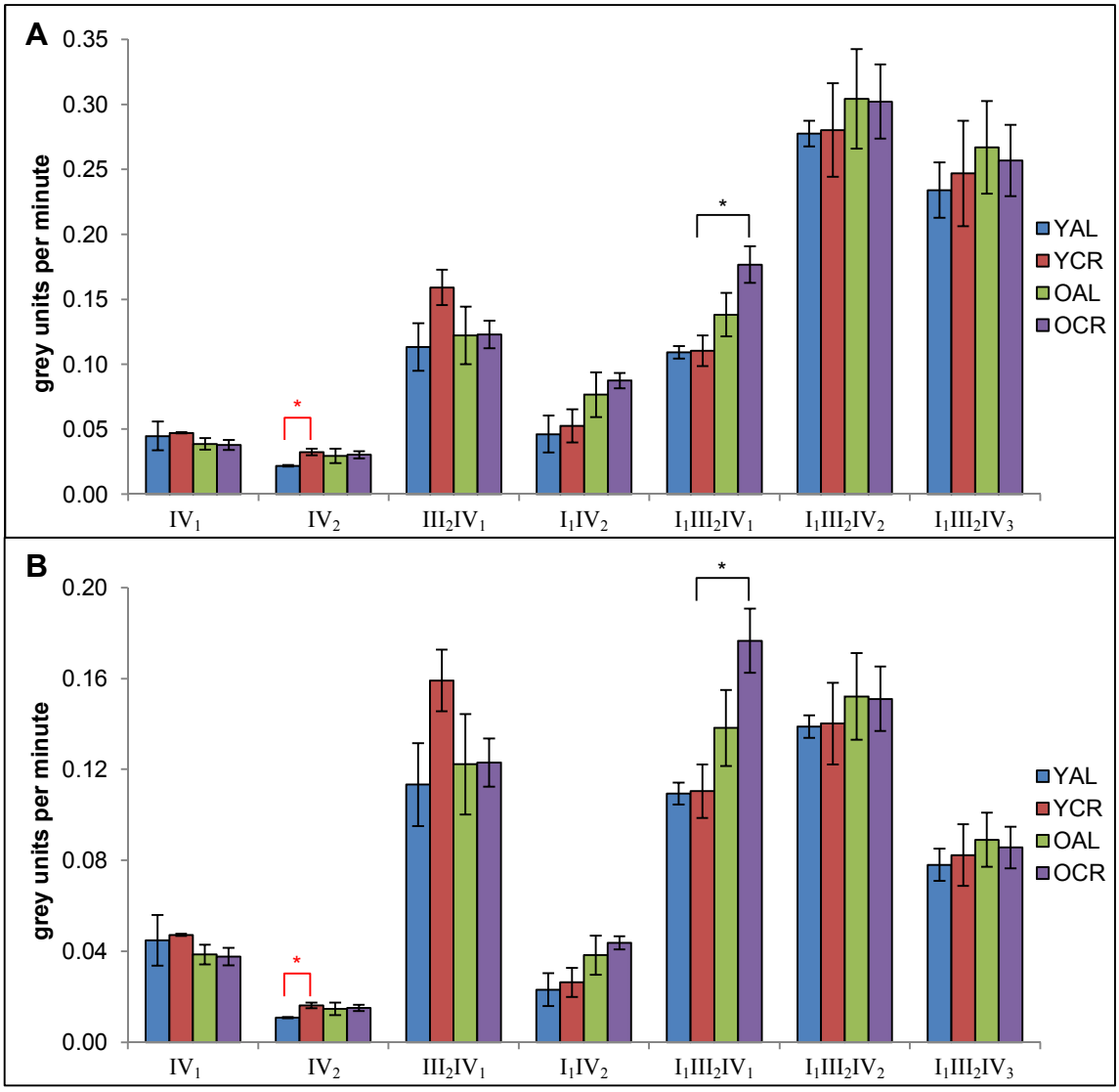

Fig. 4.67: Cerebrum, CIV in-gel activity test, specific activities of complex IV in homooligomers and supercomplexes. For each cerebrum animal group (YAL, YCR, OAL, OCR), the specific activity (in grey units per minute) of CIV in each analysed gel band is plotted. **A:** specific activities of total CIV in the visualised complex, **B:** specific activities of complex IV, normalised to its portion of the displayed complex.
bar plots: mean of technical repeats (n=3), error bars: standard error of technical repeats
significance: * = $p < \alpha$ (0.05); ** = $p < \alpha$ (0.01)
asterisks in black: changes caused by ageing, (YAL vs. OAL; YCR vs. OCR)
asterisks in red: changes caused by calorie restriction, (YAL vs. YCR; OAL vs. OCR)

Summary

The results of the CI and CIV in-gel activity tests are summarised in Table 4.31 and Table 4.32. For comparison of specific CI (or CIV) activity in individual complex I_1 (or IV_1) to (super-)complexes, the changes in specific CI (or CIV) activities normalised to individual complex I_1 (or IV_1) of the analysed (super-)complexes, averaged on the four animal groups, are listed in Table 4.31.

In Table 4.31 it is observable that specific CI activity in complex I_1IV_2 is decreased compared to individual I_1, while for the other supercomplexes I_1III_2, $I_1III_2IV_1$, $I_1III_2IV_2$ and $I_1III_2IV_3$ the specific CI activity increases with mass of the respective supercomplex. The highest activities of CI are found in supercomplex $I_1III_2IV_3$ for all three brain tissues.

Thilmany (2013) found the highest activity of CI in the supercomplexes as well, but the activity of the supercomplexes seems to be tissue specific, as she found the highest CI activities predominantly for $I_1III_2IV_1$ in subsarcolemmal (sub) and predominantly for $I_1III_2IV_2$ in intrafibrillar (int) rat heart mitochondria (RHM).

It seems also to be strain specific, as Frenzel (2011) found in her analysis of cerebral cortex mitochondria from Wistar rats the highest CI activity in $I_1III_2IV_1$.

Table 4.31: Comparison of specific CI and CIV activity
of the respective monomer to the respective (super-) complex

specific CI activity normalised to I_1 [%] (all groups in average)	I_1IV_2	I_1III_2	$I_1III_2IV_1$	$I_1III_2IV_2$	$I_1III_2IV_3$
Cerebellum	-37	+60	+114	+168	+190
Hippocampus	-31	+66	+117	+140	+145
Cerebrum	-42	+70	+93	+166	+210
Mean	-37	+65	+108	+158	+182

specific CIV activity normalised to IV_1 [%] (all groups in average)	IV_2	I_1IV_2	III_2IV_1	$I_1III_2IV_1$	$I_1III_2IV_2$	$I_1III_2IV_3$
Cerebellum	-57	-34	-4	+78	+367	+300
Hippocampus	-55	-20	+34	+87	+280	+260
Cerebrum	-32	+56	+208	+218	+592	+479
Mean	-48	+1	+79	+101	+413	+346
Mean after normalisation to no. of CIV copies	-24	+0	+79	+101	+207	+115

After normalisation to one copy of CIV, it is observable for specific CIV activity, that the dimer IV_2 is less active than the individual IV_1, while specific CIV activity of I_1IV_2 is at the same level as for individual IV_1. For all CIII containing supercomplexes (III_2IV_1, $I_1III_2IV_1$, $I_1III_2IV_2$ and $I_1III_2IV_3$) the CIV activity is increased with mass of the respective supercomplex, only for $I_1III_2IV_3$ the activity is at the same level as $I_1III_2IV_1$. The highest activities of CIV are found in supercomplex $I_1III_2IV_2$ for all three brain tissues (Table 4.31).

Thilmany (2013) found for subsarcolemmal and intrafibrillar rat heart mitochondria the highest CIV activity for $I_1III_2IV_2$. But she analysed only supercomplexes III_2IV_1, $I_1III_2IV_1$ and $I_1III_2IV_2$.

It is remarkable that for CI and CIV activity the presence of CIII increases the activity in such a strong way. This is in line with the finding of Schäfer et al. (2006) that CIII is essential for CI assembly and stability as well as the suggested role of CIV to stabilise the supercomplex formation.

For each tissue sample, the results for changes in age for *ad libitum* fed animals (AL: YAL vs. OAL) and under calorie restriction kept animals (CR: YCR vs. OCR) are presented as well as the effects of short-term (ST: YAL vs. YCR) and long-term (LT: OAL vs. OCR) calorie restriction. The arrows represent the increasing (△) or decreasing (▽) specific activity for CI or CIV of the compared animal groups as a summary of the findings. Both arrows are used in **grey** (not stat. sig.), **orange** (stat. sig.) and **red** (stat. high sig.). Black dashes (▬) were placed, where no variation could be examined. Main tendencies are quoted below. For more details, see the chapters about the different brain parts.

For all analysed tissues, the changes in specific activity of CI and CIV due to ageing or calorie restriction are not very pronounced. Most of the observed variations are statistically non-significant tendencies.

Under the influence of ageing, specific CI activity seems to decrease for complexes I_1 and small supercomplex I_1IV_2 in hippocampus and cerebrum and only under calorie restriction (CR) in cerebellum. Only in hippocampus (AL) the decreasing effect is apparent for the larger supercomplex $I_1III_2IV_1$. Apart from that the CI activity does not change for the CIII containing supercomplexes, $I_1III_2IV_{0\text{-}3}$.

Short-term (ST) and long term (LT) calorie restriction have no influence on the specific CI activity of complexes I_1 and I_1IV_2 in all tissues. LT calorie restriction increases specific CI activity in cerebellum for the supercomplexes $I_1III_2IV_{0\text{-}2}$, whereas in hippocampus ST calorie restriction decreases CI activity for the supercomplexes $I_1III_2IV_{0\text{-}2}$ and likewise for complex I_1III_2 under LT calorie restriction. Specific CI activity in cerebrum causes only one change: activity is increased in complex $I_1III_2IV_3$ under LT calorie restriction.

Just as CI specific activity test does not show large variances for the influences ageing and calorie restriction, CIV activity test does not reveal many changes. Most shown in Table 4.32 are only statistically non-significant tendencies. In cerebellum the effects are marginal. In hippocampus, the CIV activity is not varied for supercomplexes of greater equal mass as I_1IV_2 and $I_1III_2IV_{0\text{-}3}$. For aged animals under calorie restriction (CR), a statistically significant increase in CIV activity for complex III_2IV_1 of hippocampus is observed.

In animals under calorie restriction, only slight tendencies are present for hippocampus. In cerebrum, LT calorie restriction leads to a reduced CIV activity in complexes with lower mass, IV_1 and III_2IV_1, but to an increase of CIV activity in supercomplexes with higher mass, I_1IV_2 and $I_1III_2IV_1$. ST calorie restriction increases the CIV specific activity for the complexes

of lower mass (IV_2 and III_2IV_1) in cerebrum, while supercomplexes of higher mass are not stat. sig. effected.

Table 4.32: Summary of the results from in-gel activity tests for analysis of ageing and calorie restriction

CI in-gel activity	Cerebellum				Hippocampus				Cerebrum			
	AL	CR	ST	LT	AL	CR	ST	LT	AL	CR	ST	LT
I_1	—	—	—	—	▽	▽	—	—	▽	▽	—	—
I_1IV_2	—	▽	—	—	▽	▼	—	—	—	▽	—	—
I_1III_2	—	—	—	△	—	—	▽	▽	—	—	—	—
$I_1III_2IV_1$	—	—	—	△	▽	—	▽	—	—	—	—	—
$I_1III_2IV_2$	—	—	—	△	—	—	▽	—	—	—	—	—
$I_1III_2IV_3$	—	—	—	—	—	—	—	—	—	—	—	△
CIV in-gel activity	**Cerebellum**				**Hippocampus**				**Cerebrum**			
	AL	CR	ST	LT	AL	CR	ST	LT	AL	CR	ST	LT
IV_1	—	—	—	—	△	—	△	—	—	▽	—	—
IV_2	—	—	—	—	—	—	—	—	—	—	△	—
III_2IV_1	—	—	—	—	—	△	▽	▽	—	▽	△	—
I_1IV_2	—	△	—	—	—	—	—	—	—	△	—	—
$I_1III_2IV_1$	△	—	—	—	—	—	—	—	—	△	—	△
$I_1III_2IV_2$	—	—	—	—	—	—	—	—	—	—	—	—
$I_1III_2IV_3$	—	—	—	—	—	—	—	—	—	—	—	—

symbols: "△": increase, "▽": decrease, "—": no change;
colours: red: stat. high sig., orange: stat. sig., grey: not stat. sig.
abbrev.: AL: *ad libitum*, CR: calorie restriction,
ST: short-term calorie restriction, LT: long-term calorie restriction

The results of this thesis are compared to the findings of Thilmany (2013), because she analysed the activity from subsarcolemmal (sub) and intrafibrillar (int) rat heart mitochondria (RHM) of the same animals (Fischer 344 rats), which were used for this thesis. The changes in activities of CI and CIV from RHM for the different (super)complexes were averaged for comparison below.

Dr. Thilmany found increased CI (sub +58 %, int +4 %) and CIV (sub +68 %, int +15 %) activity for aged animals under AL in both types of RHM, contrary to the findings in this thesis for RBM, where the CI and CIV activity is predominantly not changing under AL, with the exception of decreased CI activity in hippocampus under AL.

Ageing under CR decreased CI activity in both types of RHM (sub -14 %, int -32 %), as well as CIV in sub RHM (-22 %), while in int RHM the CIV activity was increased (int +43 %). This is in line with the findings in this thesis for RBM, wherein CI activity in complex I_1 and in the small supercomplex I_1IV_2 is decreasing likewise. However, CIV activity is predominantly not changed in cerebellum and hippocampus of animals aged under CR. In cerebrum, the found decreased CIV activity for smaller complexes as IV_1 and $I_1III_2IV_1$ and the increased CIV activity for supercomplexes I_1IV_2 and $I_1III_2IV_1$ conform with the findings of Thilmany (2013) in int RHM.

ST increased the CI (sub +25 %, int +8 %) and CIV activity (sub +68 %, int +1 %) in both types of RHM, only the activity of supercomplex $I_1III_2IV_1$ was decreased in int RHM. In contrast to that ST showed predominantly no change in CI and CIV activity in RBM. Only in hippocampus the CI activity was decreased for larger supercomplexes.

Under LT the activities of CI (sub -32 %, int -30 %) and CIV (sub -22 %,) were decreased for both types of RHM, only the CIV activity of int RBM (+26 %) was increased. This is in contrast to the predominantly not changed activity of RBM in this thesis and to the increase in CI activity as observable for larger supercomplexes in cerebellum.

Tatarkova et al. (2011) analysed whole Wistar rat heart and found the activities of CI, CII, CIII and CIV decreased under the influence of ageing (AL), likewise Lombardi et al. (2009) found for CI, CII, CIV and CV in skeletal muscle of aged Wistar rats.

Ojaimi et al. (1999) found decreased activities for CI, CII and CIV for aged human brain.

Dani et al. (2010) analysed liver mitochondria from Wistar rats and found increased CIV activity for rats under AL and decreased CIV activity for animals under LT.

Drew et al. (2003) analysed mitochondria from skeletal muscle and from heart of aged Fischer rats kept *ad libitum* and under calorie restriction and found ATP content and rate of ATP production decreased in skeletal muscle while in heart the content and rate were not changed. They found, that calorie restriction has no incluence on the content and rate of ATP production in both tissues. For mitochondria from liver and frontal cortex of brain, they could show just as well, that calorie restriction has no influence on the ATP content and rate of production for these tissues (Drew and Leeuwenburgh 2003).

The findings for other tissues are difficult to compare to the results of rat brain. In summary, a tendency for decreased activity of OxPhos complexes as cause of ageing as well as calorie restriction is found in the other tissues.

For comparison with brain, other studies on rat brain or rat brain areas are of interest. Therefore further comparison refers to publications on changes in brain.

In their analysis of mitochondria from cerebral cortex during ageing (AL) Cocco et al. (2005) and Frenzel et al. (2010) did not find any changes in activity of CI, CIV (both publications) and CII, CII+CIII and CV (Cocco et al.). Gilmer et al. (2010) analysed cerebral cortex too, and found the respiration rates not changed for aged Fischer rats. Cerebral cortex is included in the cerebrum of the studies of this thesis. Cerebrum predominantly did not show any changes in CI or CIV activity under the influence of ageing (AL). This is in line with the findings of Filburn et al. (1996), who analysed whole rat brain homogenates of Wistar rats and found no changes in activity of CI, CIV and CV.

These results are in contrast to the findings of Tian et al. (1998), Haripriya et al. (2004) and Boveris and Navarro (2008). Boveris and Navarro (2008) summarise that decreased electron transfer activity is found for CI and CIV of mitochondria from tissues such as brain, liver, heart and kidney of aged rats and mice, while the activity of CII and CIII remains unchanged. They show in their analyses of whole brain mitochondria from aged mice, kept *ad libitum* or calorie restricted, that CI and CIV activity is decreased with age for both animal groups and that CI and CIV activity is increased in calorie restricted animals compared to *ad libitum* fed ones. Haripriya et al. (2004) found decreased activity of CI and CIV in striatum, cerebral cortex and hippocampus of aged Wistar rats and Tian et al. (1998) decreased activity of CIV in whole brain of aged Fischer rats. Only the trend of decreased CI activity in hippocampus of aged rats (AL) is also observable in this thesis.

4.2.7 Mitochondrial membrane “fluidity”

All steady-state fluorescence anisotropy measurements and evaluations were carried out by M. Sc. Stefanie Kern during and after her master thesis (Kern 2013).

After the intercalation of the membrane probe DPH into the hydrophobic domain of mitochondrial membranes, the steady-state fluorescence anisotropy was measured. Steady state anisotropy measurement provides the information about the order parameter and the rotational dynamics of the membrane (Sugawa et al. 1996). The changes in anisotropy of the probe give information about the surrounding membrane order (Lentz 1993) and its viscosity (Heyn 1979). Membrane viscosity is inversely proportional to the “fluidity” of the membrane (Eckmann et al. (2014), 3.12).

0.01 µg of proteins in their mitochondrial membranes (according to the results of Bradford protein assay, 4.2.1) of each animal sample (YAL, YCR, OAL, OCR) of each tissue (cerebellum, hippocampus, cerebrum) were incubated with 0.02 ng DPH per µL PBS and ten times measured by S. Kern as described in 3.12. The results are illustrated in Fig. 4.68. The bars show the mean of the ten technical repeats for each sample. The error bars represent the standard error of means. Statistics were performed by me as in 3.11.3. Changes in ageing are marked with black asterisks and red asterisks stand for variations based on calorie restriction. Significance levels are 0.05 (*) and 0.01 (**).

As visible in Fig. 4.68, the measured anisotropies of DPH in the mitochondrial membranes of all three analysed tissues are between 0.200 and 0.350. The mitochondrial membrane for cerebellum of young animals (YAL 0.216, YCR 0.256) exhibit much lower anisotropy values of DPH, than all the other analysed samples (mean = 0.330). For YAL RBM of cerebellum the DPH anisotropy is about 35 % smaller and for YCR about 22 % smaller than the mean of the other samples. The changes in anisotropy of the other samples are mainly highly statistically significant, but very small.

Considering Fig. 4.68, ageing of *ad libitum* fed animals (YAL vs. OAL, black asterisks) leads to an increased DPH anisotropy for RBM of cerebellum (+44.7 %) and cerebrum (+3.4 %, both stat. high sig.).

Ageing under calorie restriction (YCR vs. OCR, black asterisks), increases the DPH anisotropy in RBM of cerebellum (+26.4 %, stat. high sig.) and decreases it in hippocampus (-4.7 %, stat. high sig.).

Short-term calorie restriction (YAL vs. YCR, red asterisks) increases the DPH anisotropy in RBM of cerebellum (+18.8 %, stat. high sig.) and hippocampus (+7.5 %, stat. sig.).

Long-term calorie restriction (OAL vs. OCR, red asterisks) increases the DPH anisotropy in RBM of cerebellum (+3.8 %, stat. sig.) and hippocampus (+3.8 %, stat. high sig.), while the DPH anisotropy is reduced in cerebrum (-5.3 %, stat. high sig.).

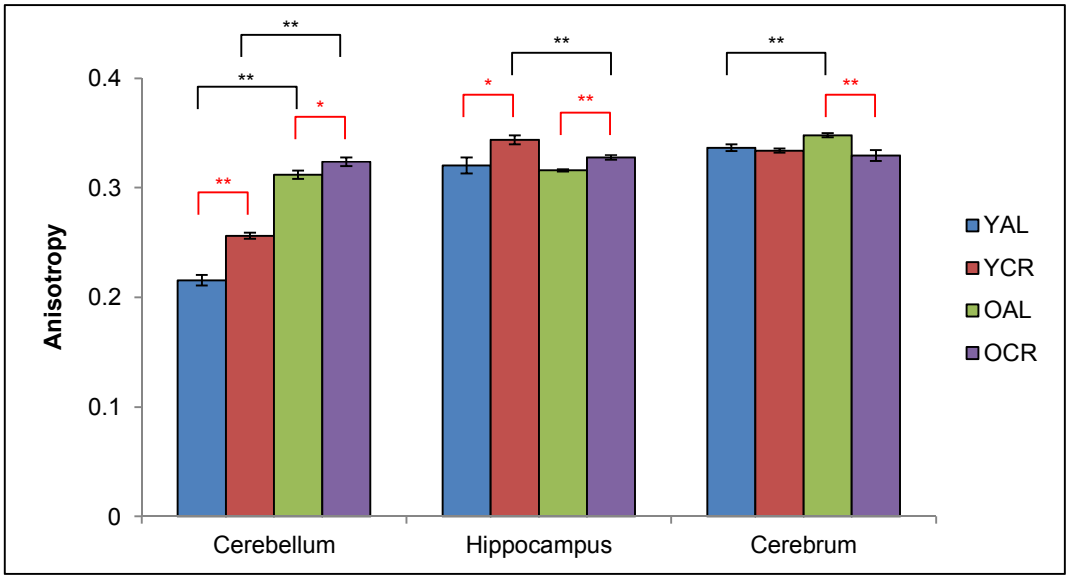

Fig. 4.68: Results of steady-state fluorescence anisotropy measurements of the membrane probe DPH, which was intercalated into the mitochondrial membranes of each animal group (YAL, YCR, OAL, OCR) of each tissue (cerebellum, hippocampus, cerebrum). Anisotropy of DPH is inversely related to the "fluidity" of the surrounding membrane.
bar plots: mean of technical repeats (n=10), error bars: standard error of technical repeats
significance: * = $p < \alpha$ (0.05); ** = $p < \alpha$ (0.01)
asterisks in black: changes caused by ageing, (YAL vs. OAL; YCR vs. OCR)
asterisks in red: changes caused by calorie restriction, (YAL vs. YCR; OAL vs. OCR)

The results of the DPH anisotropy measurements are summarised in Table 4.33. Ageing and calorie restriction decreased in all analysed cases the membrane "fluidity" in cerebellum mitochondria. The "fluidity" of mitochondrial membranes from hippocampus is increased while ageing under calorie restriction (CR) and decreased by the influence of short-term (ST) and long-term (LT) calorie restriction. In cerebrum, the "fluidity" of the mitochondrial membranes is decreased by ageing (*ad libitum*, AL) and increases under long-term calorie restriction.However, all changes were very small.

Table 4.33: Results of steady-state fluorescence anisotropy measurement of DPH

	Cerebellum				Hippocampus				Cerebrum			
	AL	CR	ST	LT	AL	CR	ST	LT	AL	CR	ST	LT
DPH anisotropy	▲	▲	▲	△	—	▼	△	▲	▲	—	—	▼
"fluidity" of membrane	▼	▼	▼	▽	—	▲	▽	▼	▼	—	—	▲

symbols: "△": increase, "▽": decrease, "—": no change;
colours: red: stat. high sig., orange: stat. sig., grey: not stat. sig.
abbrev.: AL: *ad libitum*, CR: calorie restriction,
ST: short-term calorie restriction, LT: long-term calorie restriction

Mitochondrial membranes are maily composed of phospholipids, whereof the most are phosphatidylcholines, phosphatidylethanolamines and cardiolipins. Sterols and sphingolipids are only found in small quantity (Daum 1985). The fatty acid composition of phospholipids in mitochondrial membranes from liver and skeletal muscle varies under the influence of calorie restriction in similar way as from the surrounding tissue (Faulks et al. 2006). Assuming that this is applicable to other tissues, the analyses of synaptosomal plasma membranes from specific parts of the brain can be compared to the findings in this thesis. Increased anisotropy in synaptosomal membranes of cerebellum, cerebral cortex and striatum of very aged Wistar rats (40 months) was found by Sugawa et al. (1996) and explained by increased membrane content of cholesterol. This is in line with the findings by Choi and Yu (1995) for analysis of

cerebral cortex of Fischer rats. They found decreased membrane fluidity for aged rats and no change in membrane fluidity for rats aged under calorie restriction. The membrane fluidity of synaptosomal membranes from calorie restricted animals was usually higher than from *ad libitum* fed animals. They also observed a decreased cholesterol amount in aged CR animals. The findings in this thesis for mitochondria from cerebellum and cerebrum of *ad libitum* fed rats (AL) are in line with these observations, provided that cerebral cortex can be compared to cerebrum in this thesis, which consisted of cerebral cortex, basal ganglia and limbic system, whereof the hippocampus was removed and analysed separately. Wood et al. (2002) detected no change in the fluidity of annular lipids from synaptic plasma membranes of cerebral cortex, cerebellum and hippocampus in aged rats, while in striatum a decreased fluidity of the annular lipids was found. The finding for hippocampus is in line with this thesis, however the findings for cerebellum and cerebral cortex do differ from Choi and Yu (1995), Sugawa et al. (1996) and this thesis.

Mitochondrial membranes are special in their lipid composition. They have a high content of cardiolipin and only small quantity of cholesterol. However in RBM, the amount of cardiolipin is below the amount in liver or heart mitochondria. The brain cardiolipin has a higher content of polyunsaturated fatty acyls such as linoleic (18:2) and linolenic (18:3) acyls as well as arachidonic (20:4) and docosahexanoic (22:6) acyls. Therefore the brain cardiolipin is more sensitive to peroxidation (Paradies et al. 2011). Cardiolipin is of great importance for formation and stability of supercomplexes (Pfeiffer et al. 2003, Acin-Perez and Enriquez 2014) and for activity of OxPhos complexes (Lesnefsky and Hoppel 2006). Therefore, the findings for mitochondrial membranes of RBM in this thesis are compared to analyses on mitochondrial membranes of other tissues from rats:
According to Grinna (1977) the amount of cholesterol is increased (+35 % in liver, +70 % in kidney) and cardiolipin is decreased (about -20 %) in mitochondria from liver and kidney of aged (24 months) Sprague-Dawley rats . She observed an increased rate of oleic acid (18:1) in liver and kidney mitochondria of aged rats as well as of arachadonic acid (20:4) for kidney mitochondria. She concluded that more unsaturated fatty acids would lead to increased fluidity in aged rat mitochondrial membranes, maybe as compensation to the increased amount of cholesterol, which decreases the fluidity. Overall decreased fluidity was observed in kidney and liver mitochondria of aged rats. These findings are in line with the analyses of Vorbeck et al. (1982), who analysed liver mitochondria from Fischer rats under the influence of ageing and found an increase of cholesterol and decreased amount of phospholipids and cardiolipin (-39 %). The anisotropy from steady-state fluorescence polarization measurement of the aged mitochondrial membranes was increased. The findings of Grinna (1977) and Vorbeck et al. (1982) are in line with the results for cerebellum and cerebrum of this thesis.

Lee et al. (1999) analysed heart mitochondria from Fischer rats and found the membrane fluidity decreased under the influence of ageing while calorie restriction had no influence on the fluidity of the mitochondrial membrane. An increase of unsaturated fatty acid (22:4) and a decrease of linoleic acid (18:2) were observed in aged mitochondrial membrane, while calorie restriction did not change both. This seems to be in line with the findings for cerebrum in this thesis.

Frenzel et al. (2010) analysed cerebral cortex from Wistar rats and found a need of a higher detergent to protein ratio for solubilisation of proteins from aged mitochondrial membranes

and concluded that the membrane fluidity is decreased in aged state, in line with the findings of decreased fluidity of membranes from aged cerebrum mitochondria.

Gabbita et al. (1997) observed in mitochondria and synaptosomal membranes of the neocortex of Brown Norway rats an increased membrane rigidity, which was not altered in animals under calorie restriction. But calorie restricted animals showed a lower rigidity of mitochondrial membranes than *ad libitum* fed animals. These findings are in line with the results for cerebrum in this thesis.

Studies of the lipid composition of the same cerebrum samples as used in this thesis were performed by Saager (2010) for her diploma thesis. She found no changes by ageing or calorie restriction in the lipid composition (phosphatidylcholine, phosphatidylinositol, cardiolipin, phosphatidylethanolamine, sphingomyelin and cholesterol) of the mitochondrial membranes. However she observed increased peroxidation in aged membranes for AL and CR. But she did not analyse the saturation level of the acyl chains. According to Choe et al. (1995) peroxidised lipids contribute stronger to the rigidity of membranes than incorporation of cholesterol. It might be that the observed increased membrane viscosity in this thesis is correlated with the stronger peroxidation in aged membranes.

The decrease in fluidity of mitochondrial membranes from cerebellum and hippocampus of short- and long-term calorie restricted animals could not be explained yet. Further analyses are required.

4.3 Influence from NADPH oxidase 4 on mitochondrial function

Late-passage HUVECs (2.6.4) were isolated and treated by Dr. Rafal Koziel as described in our publication (Koziel et al. 2013). Nox4 was knocked down (Nox4 KD) in HUVEC cells by lentiviral shRNA vectors. Control cells were infected with non Nox4 specific shRNA vectors (control). Mitochondria were freshly isolated and shock frozen in liquid nitrogen by Dr. Koziel at IBA. The total protein amount was determined by Bradford protein assay (3.2.1). The comparability of the Bradford results from both laboratories (IBA and TUD) was tested before and gave similar results (data not shown). The frozen mitochondria were transported on dry ice to TUD, where subsequent studies were carried out by me. Solubilisation of mitochondrial protein (3.3) was performed with d/p: 8g/g, final concentration of 1 % (w/v) dig., as described for cell culture by Colindres et al. (2007) and Cavlovic (2015). 120 µg (b. sol. d/p: 8g/g) mitochondrial protein of Nox4 KD and of control were loaded per lane on 18 cm by 16 cm sized BN gels for electrophoretic separation (3.4) and subsequent CBBG staining (3.7.2) as well as CI in-gel activity test (3.8.1). The development of the precipitate was followed in seven time steps up to 80 min. CI in-gel activity was quantitated as in 4.2.6. For CIV in-gel activity test (3.8.1), 50 µg (b. sol. d/p: 8g/g) of mitochondrial protein per lane were separated by BN PAGE (10.0 cm by 10.5 cm sized gel). Additional lanes of 70 µg (b. sol. d/p: 3g/g; 18 cm by 16 cm sized BN gel) respectively 30 µg (b. sol. d/p: 3g/g; 10.0 cm by 10.5 cm sized gel) of BHM were loaded as standard. For analysis of proteins in 2D-BN/SDS (3.5) gels, 150 µg (b. sol. d/p: 8g/g) of mitochondrial protein from Nox4 KD and of control were separated by BN PAGE (3.4), followed by 2D-BN/SDS PAGE (3.5). Gels were stained with SyproRuby (3.7.4) for quantitation and afterwards with silver (3.7.1) for visualisation. Protein spots were assigned referring to Colindres et al. (2007) and Reifschneider et al. (2006).

The results are described in our publication (Koziel et al. 2013), attached below to this chapter. Additional information is presented in Fig. 4.69 and Fig. 4.70. In Fig. 6A (Koziel et al. 2013) the image of the CBBG stained BN gel is depicted for assignment of bands with help of BHM and HWM as standards (compare 4.2.3 in which bands of BHM and RBM where assigned). Control and Nox4 KD showed the same pattern of band migration in BN PAGE. Additional bands were found and assigned as heat shock protein HSP60 and HSP60*, which were also present in the 2D-BN/SDS gel (Fig. 6C, Koziel et al. (2013), purple circles) as two separated protein spots. This was also observed for human fibroblasts by Colindres et al. (2007). They supposed that heptamers and hexamers of HSP60 were found. In tissue such as RBM or BHM the protein band and spots of HSP60* were not observed, only HSP60 (=CH60, 4.2.3).

Fig. 6B (Koziel et al. 2013) depicts an image of the BN gel after 80 min of incubation in CI in-gel activity test solution and a diagram showing the quantified development of the blue/purple precipitate of NBT diformazan (3.8.1), characteristic for CI activity. The activity was normalised to the amount of CI in the respective band (3.11.2). The mean of CI activities of the supercomplexes I_1III_2 and $I_1III_2IV_1$ were diagrammed for seven different timepoints between 0 min and 80. CI activity of control remains below Nox4 KD. The

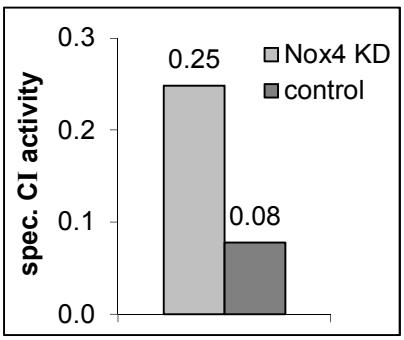

Fig. 4.69: Specific CI activities for Nox4 KD and control were calculated (3.11.2). Specific CI activity of Nox4 KD is higher than of control.

specific CI activity of Nox4 KD is much higher than of the control (+219 %, Fig. 4.69).

Fig. 6C (Koziel et al. 2013) depicts images of silver stained 2D-BN/SDS gels with mitochondrial proteins from Nox4 KD and control. Several spots were marked in colour. Red spots mark CI and CIII subunits of OxPhos supercomplexes. For BHM and RBM they were assigned as NDUS1, QCR2 and NDUS2 (top to bottom, 4.2.3). Orange spots mark subunits of CIV from individual complex IV1. For BHM and RBM they were assigned to COX1 and COX2 (top to bottom, 4.2.3). The subunits were quantified in the grey scale images of the SyproRuby stained gels. The results are depicted in Fig. 4.70. The sum of the subunits NDUS1 & 2, of NDUS1 & 2 + QCR2 and of COX1 & 2 (in grey units) are diagrammed. It is observable that the control cells contain less protein amount in all three bar plots. The relative changes for Nox4 KD compared to the control are +111 % for NDUS1&2, +167 % for NDUS1&2+QCR2 and +17 % for (COX1&2). This shows an increased CI and CIII protein amount for supercomplexes in Nox4 KD, while the protein amount for CIV is only slightly increased. The CIV in-gel acitivity is visible as brownish precipitate in the gel image depicted in Fig. 6D (Koziel et al. 2013). No changes between Nox4 KD and control are observable.

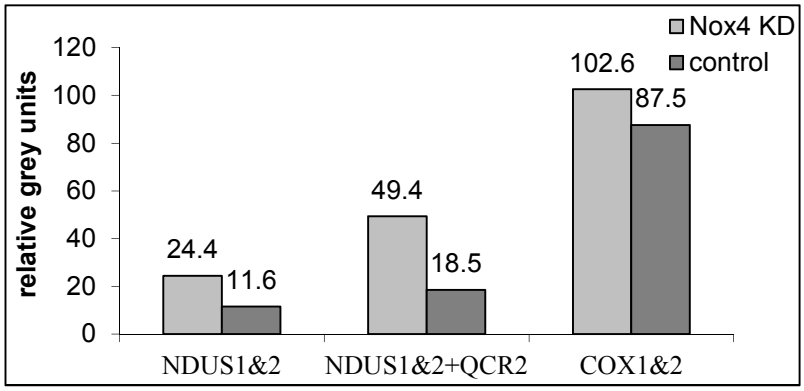

Fig. 4.70: Quantitation of subunits NDUS1&2 and NDUS1&2+QCR2 from supercomplexes and COX1&2 of individual IV_1 for Nox4 KD and control. For Nox4 KD the protein amount of all depicted subunits is higher than for control. The relative ratios are much higher for subunits of CI and CI+CIII than for CIV.

To sum up, the results show that Nox4 KD increased the protein amount and the activity of CI. Additionally mitochondrial morphology was changed, the potential of the inner mitochondrial membrane was stabilised and less H_2O_2 was produced than in control cells (Koziel et al. 2013).

BJ Cell

Biochem. J. (2013) **452**, 231–239 (Printed in Great Britain) doi:10.1042/BJ20121778

View this PDF in Utopia Documents for more interactive functionality
Download FREE software now

Mitochondrial respiratory chain complex I is inactivated by NADPH oxidase Nox4

Rafał KOZIEŁ*, Haymo PIRCHER*, Manuela KRATOCHWIL†, Barbara LENER*‡, Martin HERMANN§, Norbert A. DENCHER† and Pidder JANSEN-DÜRR*‡[1]

*Institute for Biomedical Aging Research, Innsbruck University, Rennweg 10, 6020 Innsbruck, Austria, †Technische Universität Darmstadt, Department of Chemistry, Physical Biochemistry, Petersenstrasse 22, D-64287 Darmstadt, Germany, ‡Tiroler Krebsforschungsinstitut, Innrain 66, 6020 Innsbruck, Austria, and §Department of Anaesthesiology and Critical Care Medicine, Innsbruck Medical University, Innrain 66, 6020 Innsbruck, Austria

ROS (reactive oxygen species) generated by NADPH oxidases play an important role in cellular signal transduction regulating cell proliferation, survival and differentiation. Nox4 (NADPH oxidase 4) induces cellular senescence in human endothelial cells; however, intracellular targets for Nox4 remained elusive. In the present study, we show that Nox4 induces mitochondrial dysfunction in human endothelial cells. Nox4 depletion induced alterations in mitochondrial morphology, stabilized mitochondrial membrane potential and decreased production of H_2O_2 in mitochondria. High-resolution respirometry in permeabilized cells combined with native PAGE demonstrated that Nox4 specifically inhibits the activity of mitochondrial electron transport chain complex I, and this was associated with a decreased concentration of complex I subunits. These data suggest a new pathway by which sustained Nox4 activity decreases mitochondrial function.

Key words: complex I, electron transport chain, mitochondrion, Nox4, oxidative stress, senescence.

INTRODUCTION

NADPH oxidases are membrane-bound enzymes, which reduce molecular oxygen to the superoxide radical anion by electron transfer. So far, five Nox (NADPH oxidase) genes have been identified in the human genome, termed *NOX1–NOX5* [1]. Whereas Nox1–Nox3 require the recruitment of cytosolic regulatory subunits for their activation [2], Nox4 requires only $p22^{phox}$ as a cofactor, as Nox4–$p22^{phox}$ complexes are constitutively active [3]. Several Nox enzymes, including Nox4, contribute to the control of proliferation and survival of different tumour cell types [4]. Nox4 is ubiquitously expressed in a variety of tissues, such as the kidney, lung, heart and the vascular system [1]. Nox4 contains six transmembrane domains and a cytosolic C-terminal domain, which comprises binding sites for FAD and NADPH. Nox4-derived ROS (reactive oxygen species), in particular H_2O_2 [5], were shown to modulate several cellular signal transduction pathways. Signalling through receptor tyrosine kinases, e.g. the EGF (epidermal growth factor) receptor, is positively influenced by Nox4, and this activity has been linked to the ability of Nox4-derived ROS to inactivate protein tyrosine phosphatases, thereby potentiating receptor tyrosine kinase signalling [6]. Nox4 is also required for the activation of several other kinases, such as MAPK (mitogen-activated protein kinase), p38 and JNK (c-Jun N-terminal kinase) [7], and regulates cellular calcium signalling [8]. Nox4-derived ROS play an important role in controlling cell proliferation and cell survival [8,9]. In the human vasculature, SMCs (smooth muscle cells) are known to express Nox1, Nox2 and Nox4, the latter playing a key role in SMC migration [10], in combination with Poldip2 (polymerase δ-interacting protein 2) [11]. Human and murine vascular endothelial cells express Nox2 at relatively low levels, but display a high expression of Nox4 [12], and Nox4 influences cell proliferation and apoptosis in human endothelial cells [13]. The subcellular localization of Nox4 is subject to some debate and may vary between different cell types. Thus Nox4 was found in the endoplasmic reticulum [14], at focal adhesions [15], in mitochondria [16] and in the nucleus [17]. Depletion of Nox4 was found to reduce oxidative damage to nuclear DNA and delay senescence both in human endothelial cells [18] and in H-RasV12-expressing human thyrocytes [19]. Conceivably, nuclear DNA is damaged directly by Nox4-derived H_2O_2, e.g. H_2O_2 produced by Nox4–$p22^{phox}$ complexes in the perinuclear space [19]. In an alternative model, Nox4 localizes to mitochondria where it potentiates mitochondrial production of ROS [16]; however, molecular mechanisms of Nox4 action in the mitochondria have remained elusive. In the present study, we have addressed this question and identified respiratory chain complex I as a previously unreported functional target for Nox4.

EXPERIMENTAL

Cell culture

HUVECs (human umbilical vein endothelial cells) were isolated and propagated as described in [20]. Suitable shRNA (short hairpin RNA) constructs directed to Nox4 were transferred into lentiviral vectors (pLKO, Open Biosystems) and used for gene

Abbreviations used: BHM, bovine heart mitochondria; BN, Blue native; CAT-PEG, catalase conjugated to poly(ethylene glycol); CS, citrate synthase; DHE, dihydroethidium; EGF, epidermal growth factor; FCCP, carbonyl cyanide *p*-trifluoromethoxyphenylhydrazone; HBSS, Hanks balanced salt solution; H_2-DCFDA, 2′,7′-dichlorodihydrofluorescein diacetate; HUVEC, human umbilical vein endothelial cell; IGF, insulin-like growth factor; JNK, c-Jun N-terminal kinase; MAPK, mitogen-activated protein kinase; mPT, mitochondrial permeability transition; NDUFA9, NADH dehydrogenase (ubiquinone) 1 α subcomplex 9; NDUFS4, NADH dehydrogenase (ubiquinone) Fe–S protein 4; Nox, NADPH oxidase; OxPhos, mitochondrial oxidative phosphorylation; ROS, reactive oxygen species; shRNA, short hairpin RNA; SMC, smooth muscle cell; TMPD, *N*,*N*,*N*′,*N*′-tetramethyl-*p*-phenylenediamine; TMRM, tetramethylrhodamine methyl ester.

[1] To whom correspondence should be addressed (email pidder.jansen-duerr@uibk.ac.at).

© The Authors Journal compilation © 2013 Biochemical Society

silencing, as described in [18]. Early-passage (defined herein as cells below passage 12) and late-passage cells (defined herein as cells at or after passage 20, where the senescent phenotype was observed) were used.

Protein detection by immunoblot analysis

Cellular protein lysates were prepared in RIPA buffer (50 mM Tris/HCl, pH 7.4, 150 mM NaCl, 1 mM EDTA, 1 % Triton X-100 and 0.1 % SDS) and subjected to standard immunoblotting, using primary antibodies (Invitrogen) against complex I NDUFA9 [NADH dehydrogenase (ubiquinone) 1 α subcomplex 9] subunit, complex II 70 kDa subunit, complex III UQCRC1 (ubiquinol-cytochrome *c* reductase core protein I) subunit and complex IV subunit IV. Results from three independent experiments were evaluated by densitometry, using an Alpha Innotech FluorChem® HD2 instrument.

Mitochondrial membrane potential ($\Delta\psi_m$)

To determine the electric potential of the inner mitochondrial membrane, cells were suspended in culture medium containing JC-1 (5,5′,6,6′-tetrachloro-1,1′,3,3′-tetraethylbenzimidazolylcarbocyanine iodide) fluorescent dye at 0.5 μg/ml [21], incubated for 30 min at 37 °C, washed and resuspended in PBS containing 1 mM pyruvate and 5 mM glucose. Fluorescence was measured in 10^4 cells using a flow cytometer (FACS Canto II, Becton Dickinson), using a 488 nm laser for excitation and recording emission at wavelength of 530/590 nm. In healthy cells, JC-1 enters the negatively charged mitochondria where it aggregates and fluoresces red. When the mitochondrial potential drops, JC-1 exists as monomers in cytoplasm and fluoresces green. It allows the definition of two populations of cells, with high $\Delta\psi_m$ (high red and low green fluorescence) and low $\Delta\psi_m$ (low red and high green fluorescence). Pre-incubation of the cells with the mitochondrial uncoupler FCCP (carbonyl cyanide *p*-trifluoromethoxyphenylhydrazone) allowed the definition of the cell population with lowered $\Delta\psi_m$. All cells with lower green and higher red fluorescence were counted as the cells with high $\Delta\psi_m$ (as a percentage of the population).

Assessment of ROS

The level of intracellular ROS was measured *in situ* using flow cytometry in cells stained with the DHE (dihydroethidium) or H_2-DCFDA (2′,7′-dichlorodihydrofluorescein diacetate) fluorescent probes (Molecular Probes). The cells (2×10^5) were suspended in 1 ml of the culture medium containing 20 μM DHE or in 1 ml of HBSS (Hanks buffered salt solution) containing 10 μM H_2-DCFDA. The cells were incubated for 30 min at 37 °C, washed twice with PBS and resuspended in PBS. The fluorescence was measured using a flow cytometer (FACS Canto II). The level of ROS was estimated as a mean value of DHE or H_2-DCFDA fluorescence in 10^4 cells. Mitochondrial complex I inhibitor rotenone (1 μM) was added along with DHE as a positive control.

Determination of mitochondrial ROS levels

MitoTracker Red CM-H_2XRos (Molecular Probes) was used to monitor mitochondrial redox state as recommended by the manufacturer. Briefly, cells were incubated with 100 nM MitoTracker Red CM-H_2XRos in culture medium for 15–30 min at 37 °C, washed twice with PBS and measured using a flow cytometer (FACS Canto II) at excitation/emission maxima of 579/599 nm.

Determination of mitochondrial and cytosolic H_2O_2 levels

For the detection of mitochondrial or cytosolic H_2O_2 levels, the cells were transfected with control, pHyPer-dMito/pLenti6/V5-DEST or pHyPer-Cyto/pLenti6/V5-DEST Gateway lentiviral vector and after expansion analysed using confocal fluorescence microscopy. As a positive control, the cells were incubated for 18 h at 37 °C with 200 units/ml CAT-PEG [catalase conjugated to poly(ethylene glycol)].

Analysis of mitochondrial respiratory function

For determination of respiratory activity in intact cells, cells were harvested, and 10^6 cells were resuspended in 3 ml of culture medium and subjected to high-resolution respirometry using an Oxygraph-2k™ machine (OROBOROS Instruments), as described in [22]. After observing steady-state respiratory flux, the ATP synthase (complex V) inhibitor oligomycin (1 μg/ml) was added, followed by uncoupling of oxidative phosphorylation by stepwise titration of FCCP. Finally, respiration was inhibited by the complex I and complex III inhibitors rotenone (0.5 μM) and antimycin A (2.5 μM) respectively. For the detection of respiratory activity of different OxPhos (mitochondrial oxidative phosphorylation) system complexes, oxygen consumption was measured in permeabilized cells. Approximately 10^6 cells were resuspended in 3 ml of mitochondrial respiration medium MiRO5 (OROBOROS Instruments) (0.5 mM EGTA, 3 mM $MgCl_2 \cdot 6H_2O$, 60 mM potassium lactobionate, 20 mM taurine, 10 mM KH_2PO_4, 20 mM Hepes, 110 mM sucrose and 1 g/l BSA, pH 7.1) and subjected to high-resolution respirometry using Oxygraph-2k™ (OROBOROS Instruments). After observing steady-state basal respiratory flux, the cells were permeablized with digitonin (1 mg/ml, 10 μl/10^6 cells) and the rate of respiration was determined after addition of 2 mM malate and 10 mM glutamate for complex I-coupled respiration, 2.5 mM ADP for complex I state III respiration, 10 mM succinate for complex I and complex II state III respiration, 2.5 μM FCCP for complex I and complex II-uncoupled respiration, 0.5 μM rotenone for complex II-uncoupled respiration and finally 2.5 μM antimycin A, 2 mM ascorbate and 20 μM TMPD (*N*,*N*,*N*′,*N*′-tetramethyl-*p*-phenylenediamine) for complex IV-uncoupled respiration. DatLab™ software (OROBOROS Instruments) was used for data analysis. The respirometry data were normalized to CS (citrate synthase) activity, a marker for mitochondrial biomass [23]. Briefly, two portions of 300 μl of the sample were taken from the cell suspension and stirred in the oxygraph chamber before the chamber was closed for recording respiration. Samples were frozen in liquid nitrogen and stored at −80 °C. Total cell lysate (100 μl) was added to 900 μl of medium containing 0.1 mM DTNB [5,5′-dithiobis-(2-nitrobenzoic acid)], 0.5 mM oxaloacetate, 50 μM EDTA, 0.31 mM acetyl-CoA, 5 mM triethanolamine hydrochloride and 0.1 M Tris/HCl (pH 8.1). The activity of CS was measured spectrophotometrically at 412 nm and 30 °C.

Solubilization of membrane proteins

Mitochondria were solubilized for 30 min on ice with a ratio of 8 g of digitonin (Acros Organics)/g of protein at a final detergent concentration of 1 % (w/v), in a buffer containing 30 mM Hepes/KOH (pH 7.4), 150 mM potassium acetate, 10 %

© The Authors Journal compilation © 2013 Biochemical Society

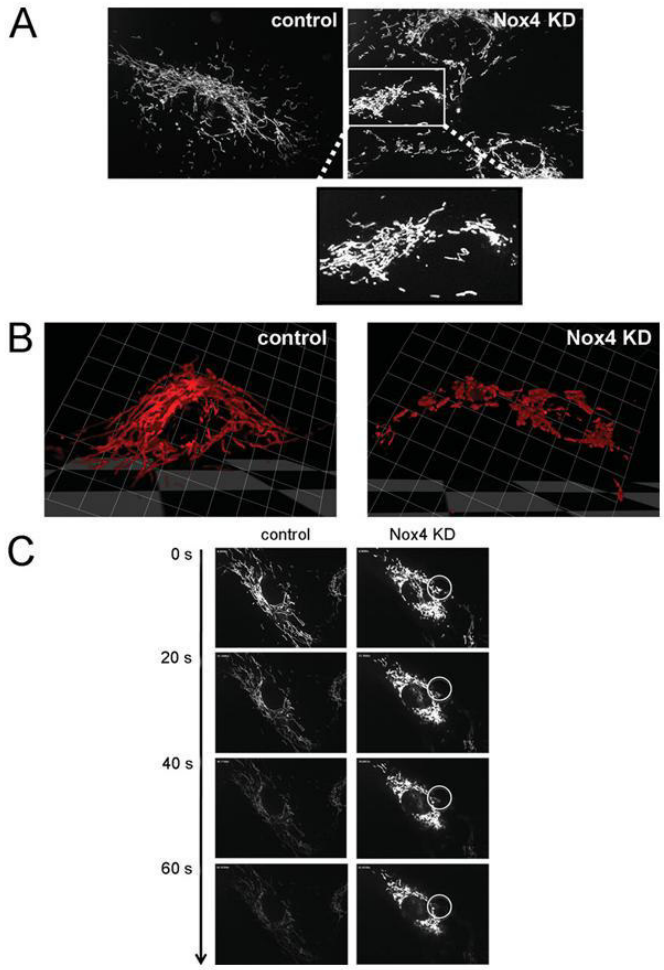

Figure 1 Effects of Nox4 on mitochondrial morphology and stress resistance

(**A**) Late-passage (passage 26) control (shRNA-transfected) and Nox4-depleted (Nox4 KD) HUVECs were stained with TMRM for 15 min, as indicated. Mitochondrial morphology was analysed using confocal microscopy. The lower panel shows an enlargement of the region of interest. (**B**) Following 20 min of incubation with TMRM at 37 °C, *z*-stacks were taken with a Zeiss Observer.Z1 inverted microscope in combination with the UltraView Vox Confocal Imaging System and used to provide a three-dimensional view of mitochondrial networks. For Nox4-depleted (Nox4 KD) and shRNA vector-treated cells, one representative example is shown. (**C**) Control and Nox4-depleted (Nox4 KD) HUVECs were stained with TMRM (100 nM, 15 min in culture medium) and stressed using laser at a wavelength of 561 nm. Changes in $\Delta\psi_m$ were monitored using confocal microscopy at 20 s intervals. Circles highlight selected areas where the decrease in TMRM fluorescence occurred separately in time from different mitochondrial networks in Nox4-depleted cells.

(v/v) glycerol and 0.5 % protease inhibitor cocktail (Sigma, P8340).

BN (Blue native)-PAGE

The solubilized mitochondrial membrane proteins were separated on linear gradient gels at 4 °C. Solubilized BHM (bovine heart mitochondria) prepared from tissue and stored at − 80 °C (3 g of digitonin/g of protein) were loaded as molecular-mass standards for OxPhos (super)complexes. Two types of gels were employed: small gels (10 cm × 10.5 cm × 0.15 cm) with a linear gradient of total acrylamide concentration from 3 to 13 %, overlaid with a 3 % stacking gel (Hoefer Mighty Small II system), and large gels (18 cm × 16 cm × 0.15 cm) with a linear gradient from 4 to 13 %, overlaid with a 3.5 % stacking gel (Hoefer SE 600 system). The electrophoresis was performed essentially as described in [24,25]. For visualization of protein bands, the gels were stained with CBG (Rotiblue, Roth A152.1). For two-dimensional BN/Tricine-SDS/PAGE, lanes of the large BN gel were excised and processed as described in [24,25] using a stacking gel (containing Tricine-SDS gel buffer) with a total acrylamide concentration of 5 % and a separating Tricine-SDS gel with 13 % (Hoefer SE 600 system), followed by electrophoresis. For visualization of protein spots, the gels were stained with silver. Mitochondrial proteins were identified by their characteristic migration behaviour in the BN-PAGE, the specific staining pattern of the activity assays and according to previous protein profiling of rat tissue and cell culture mitochondria by peptide mass fingerprint with MALDI–TOF-MS (matrix-assisted laser-desorption ionization–time-of-flight MS) [25]. For in-gel activity assays, BN-PAGE lanes were

© The Authors Journal compilation © 2013 Biochemical Society

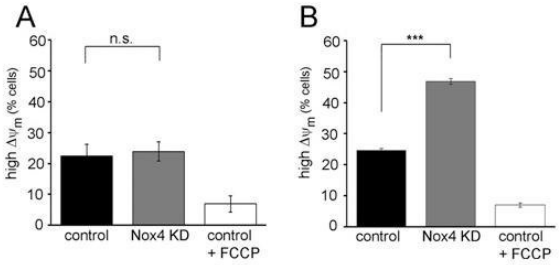

Figure 2 Effects of Nox4 on $\Delta\psi_m$

The electric potential across the inner mitochondrial membrane ($\Delta\psi_m$) was measured with the JC-1 fluorescent probe *in situ*, using flow cytometry in intact Nox4-depleted (Nox4 KD) and shRNA vector-treated cells, as indicated. Measurements were performed in early-passage (before passage 12) cells (**A**) and late-passage (at or after passage 25) cells (**B**). The percentage of cells with high $\Delta\psi_m$ is displayed. Mitochondrial uncoupler FCCP (5 μM) was used during staining as a positive control. Results are means $\pm$ S.E.M. for three independent experiments each. n.s., not significant; $^{***}P < 0.001$.

incubated at room temperature (20°C) in the complex I or complex IV assay solution [50 mM trisodium phosphate, 5 mM reduced cytochrome *c*, 1.58 mM DAB (diaminobenzidine), pH 7.2] [26]. The NADH dehydrogenase activity of complex I was probed by in-gel formazan precipitation using complex I assay solution. The reactions were stopped in 50 % (v/v) methanol and 10 % (v/v) acetic acid for 10 min. Images of the gel lanes were scanned using Epson Biostep. For quantification of complex I activity, images of the gel lane were scanned before ($t = 0$ min) and during ($t = 80$ min) incubation, followed by calculation of the relative activity [26].

Determination of mitochondrial morphology

Cell growth and live confocal imaging were performed in eight-well chambered coverglasses (Nalge Nunc International). The cells were stained for 15 min in 200 μl of culture medium containing 100 μM TMRM (tetramethylrhodamine methyl ester) fluorescent probe (Molecular Probes). After washing cells twice in HBSS, staining of the cells was analysed by confocal microscopy using a microlens-enhanced Nipkow disc-based confocal system UltraView RS (PerkinElmer) mounted on an Olympus IX-70 inverted microscope. Images were acquired using a $\times 100$ oil-immersion objective (Olympus, PlanApo; with a numerical aperture of 1.4). For three-dimensional reconstructions, cells were incubated with TMRM for 20 min at 37 °C, and *z*-stacks were taken with a Zeiss Observer.Z1 inverted microscope in combination with the UltraView Vox Confocal Imaging System (PerkinElmer).

Laser-induced collapse of the mitochondrial potential

The lipophilic cation TMRM accumulates selectively into mitochondria according to their $\Delta\psi_m$. Owing to constant laser illumination of TMRM within the mitochondria, ROS are generated which provoke the mPT (mitochondrial permeability transition). Using this model, induction of the mPT is seen by collapse of the $\Delta\psi_m$. This model represents a widely published and reliable way to reproducibly induce the loss of $\Delta\psi_m$ [27]. For this purpose, we stained the cells with TMRM fluorescent probe as described above. Constant laser illumination at a wavelength of 561 nm was performed for 20 s using the aforementioned settings.

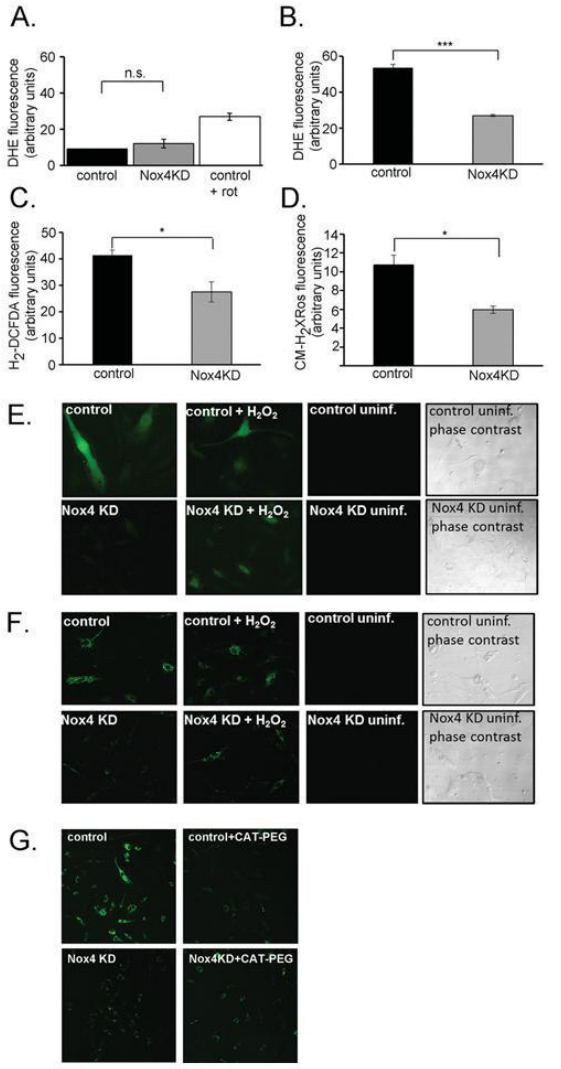

Figure 3 Nox4 induces H_2O_2 production in mitochondria

(**A** and **B**) Intracellular ROS levels were measured *in situ* after staining with DHE using flow cytometry in Nox4-depleted (Nox4KD) and shRNA vector-treated cells, as indicated. Measurements were performed in early-passage (before passage 12) cells (**A**) and late-passage (at or after passage 25) cells (**B**). Results (mean $\pm$ S.E.M. DHE fluorescence of 10^4 cells) were obtained from three independent experiments each. Mitochondrial complex I inhibitor rotenone (rot; 1 μM) was used as a positive control. n.s., not significant; $^{***}P < 0.001$. (**C**) Cellular redox state of Nox4-depleted (Nox4KD) and shRNA vector-treated cells was measured *in situ* using flow cytometry in late-passage cells stained with H_2-DCFDA. Results are means $\pm$ S.E.M. calculated for three independent experiments. $^{*}P < 0.05$. (**D**) Mitochondrion-specific ROS production was determined at late-passage shRNA vector-treated and Nox4-depleted (Nox4KD) HUVECs using MitoTracker Red CM-H_2XRos and analysed using flow cytometry. Results are mean $\pm$ S.E.M. MitoTracker Red CM-H_2XRos fluorescence (arbitrary units) of 10^4 cells. $^{*}P < 0.05$. (**E** and **F**) Mitochondrial (**F**) and cytosolic (**E**) H_2O_2 levels were measured in late-passage Nox4-depleted (Nox4 KD) and shRNA vector-treated HUVECs using compartment-specific HyPer fluorescent sensors. Cells were infected with lentiviral particles harbouring either pHyPer-Cyto or pHyPer-dMito expression vectors, expanded for 2 weeks, and HyPer fluorescence was analysed using confocal microscopy. Uninfected cells (uninf.) were used as a negative control, and cells treated for 1 h with 100 μM H_2O_2 were used as a positive control. (**G**) The late-passage (passage 23) shRNA vector-treated and Nox4-depleted (Nox4 KD) cells expressing pHyPer-dMito were prepared as described in (**F**). The cells were incubated for 18 h with 200 units/ml CAT-PEG as indicated, and mitochondrial H_2O_2 levels were analysed using confocal microscopy.

© The Authors Journal compilation © 2013 Biochemical Society

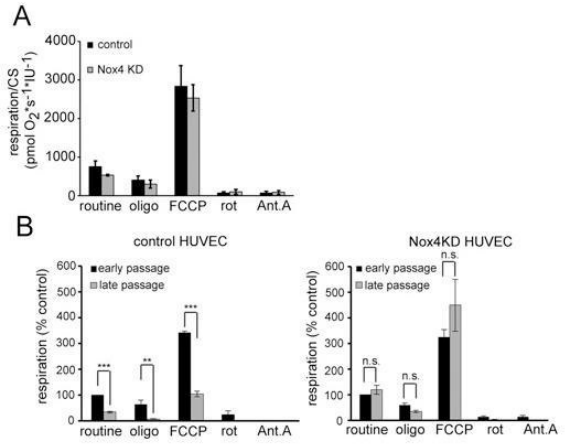

Figure 4 Nox4 reduces mitochondrial respiratory capacity

(**A**) Early-passage (before passage 12) HUVECs were transduced with lentiviral particles harbouring either control or Nox4-specific (Nox4 KD) shRNA, passaged for 3 weeks, and subjected to high-resolution respirometry. The experimental regime started with basal respiration, followed by addition of oligomycin (oligo; 1 μg/ml), followed by stepwise titration of FCCP (2.5–4 μM). Finally, respiration was inhibited by sequential addition of rotenone (rot) at 0.5 μM and antimycin A (Ant.A) at 2.5 μM. Results were normalized to mitochondrial mass marker CS activity and are means $\pm$ S.E.M. for four independent experiments. (**B**) shRNA vector-treated (left-hand panel) and Nox4-deficient (Nox4KD, right-hand panel) HUVECs at early passage (before passage 12) and late passage (at or after passage 25) numbers were subjected to high-resolution respirometry, as indicated. The experimental regime started with basal respiration, followed by addition of oligomycin (oligo; 1 μg/ml), followed by stepwise titration of FCCP (2.5–4 μM). Finally, respiration was inhibited by sequential addition of rotenone (rot) at 0.5 μM and antimycin A (Ant.A) at 2.5 μM. The data were normalized to mitochondrial mass marker CS activity. Basal respiration of untreated cells was set to 100 % in each case. Results are means $\pm$ S.E.M. for three independent experiments. $^{**}P < 0.01$; $^{***}P < 0.001$; n.s., not significant.

The TMRM fluorescence corresponding to $\Delta\psi_m$ was constantly monitored using the UltraView software (PerkinElmer).

RESULTS AND DISCUSSION

Nox4 effects on mitochondrial morphology and stress resistance

Nox4 was knocked down in HUVECs by lentiviral shRNA vectors as described previously [18]. At 3 weeks after infection, both Nox4 mRNA and protein levels were significantly decreased in cells infected with Nox4-specific shRNA vectors, but remained unchanged in cells infected with control shRNA vectors (Supplementary Figure S1 at http://www.biochemj.org/bj/452/bj4520231add.htm). When mitochondrial morphology was analysed by confocal microscopy using the $\Delta\psi_m$-specific dye TMRM, a clear difference in mitochondrial morphology was evident. Thus, in Nox4-depleted HUVECs, mitochondria revealed a feature of highly separated, not interconnected, networks compared with shRNA vector-treated cells (Figure 1A). This was confirmed further by TMRM-based imaging using confocal microscopy, followed by three-dimensional reconstruction (Figure 1B). We also used the Volocity® 3D Image Analysis software (PerkinElmer) to score connectivity of mitochondrial structures. For quantification, mitochondrial networks were divided into four categories, depending on their connectivity, measured as the apparent volume of continuous mitochondrial tubes: large (apparent volume >400 μm^3), intermediate (apparent volume 10–400 μm^3), fragmented (apparent volume 2–10 μm^3) and small (apparent volume <2 μm^3) (Supplementary Figure S2 at http://www.biochemj.org/bj/452/bj4520231add.htm). Subsequently, the percentage of mitochondrial subnetworks of different size categories was determined by counting. In shRNA vector-treated cells, we regularly detected a single highly connected mitochondrial network, along with a few intermediate mitochondrial networks and a few smaller objects. In Nox4-depleted cells, we consistently failed to detect any highly connected mitochondrial networks; instead, such cells contained several intermediate networks and a larger percentage of smaller objects (Supplementary Figure S2). These findings revealed a significantly higher mitochondrial connectivity in shRNA vector-treated compared with Nox4-depleted cells.

To assess effects of Nox4 depletion on mitochondrial stress resistance, Nox4-depleted and shRNA vector-treated HUVECs were laser-irradiated at a wavelength of 561 nm; subsequently, changes in $\Delta\psi_m$ were monitored using TMRM. In these experiments, $\Delta\psi_m$ collapsed after 40 s of irradiation in shRNA vector-treated cells (Figure 1C). In contrast, mitochondria of Nox4-depleted cells were still able to maintain high $\Delta\psi_m$ even after 60 s of irradiation (Figure 1C) with a complete decrease in TMRM fluorescence after 180 s of irradiation. It seems possible that the decreased $\Delta\psi_m$ is due to photoreduction of nitrite to NO [28] which is known to impair mitochondrial function [29]. However, we consider it unlikely that NO production contributes to the differences observed between shRNA vector-treated and Nox4-depleted cells, since the same light energy was applied in both cases.

The disconnection of the mitochondrial network in Nox4-depleted cells was confirmed further by the observation that, in shRNA vector-treated cells, the collapse of $\Delta\psi_m$ occurred in the whole mitochondrial network at once, whereas in Nox4-depleted HUVECs, the decrease in TMRM fluorescence occurred separately in time in different individual mitochondrial subnetworks (Figure 1C, circles). It is known that mitochondrial morphology depends on cell cycle phase and can change in response to various stimuli in a way that is incompletely understood [30]. Mitochondrial fragmentation results from decreased mitochondrial fusion and/or increased mitochondrial fission, and a shift to mitochondrial fragmentation usually correlates with impaired mitochondrial function (reviewed in [31]), opposite to what we observed here for Nox4-depleted HUVECs. However, this correlation is not absolute, and decreases in mitochondrial fission, e.g. by depletion of the fission factor DLP (dynamin-like protein) in human cells, led to mitochondrial hyperfusion, accompanied by decreased mitochondrial function and decreased proliferation rate [32]. The precise molecular alterations leading to altered morphology in Nox4-knockdown cells remain to be identified.

Nox4 activity induces mitochondrial dysfunction

Expression of Nox4 during extended passaging of human endothelial cells is essential for the timing of cellular senescence, since knocking down Nox4 by lentiviral shRNA vectors significantly delayed the senescent phenotype and extended cellular proliferation capacity [18]. Apparently, prolonged activity of Nox4 in such cells leads to the accumulation of molecular damage, in particular DNA damage, which triggers the senescence response [18]. To address molecular mechanisms by which DNA damage is generated, we compared early-passage cells (defined here as cells below passage 12) and late-passage cells (defined here as cells at or after passage 20, where the senescent phenotype was observed). $\Delta\psi_m$ was unaltered by Nox4 depletion in early passage after lentiviral infection (Figure 2A); at late

© The Authors Journal compilation © 2013 Biochemical Society

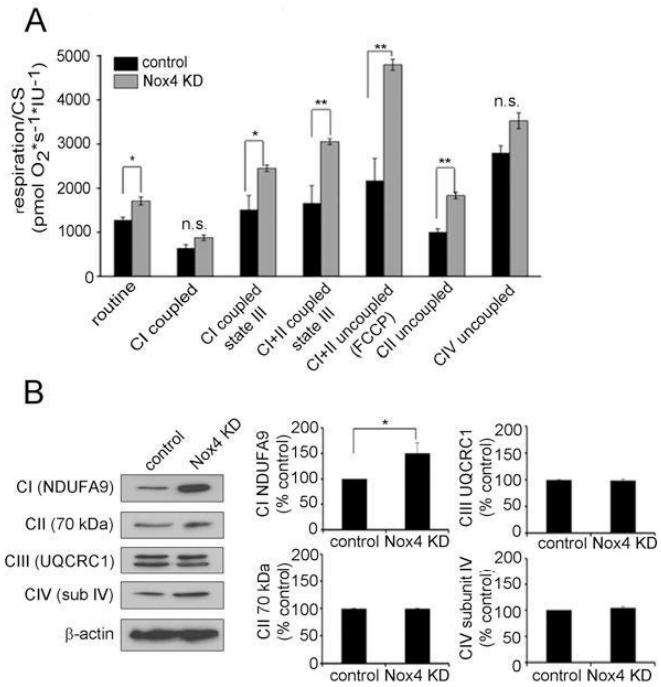

Figure 5 Nox4 reduces mitochondrial OxPhos complex I respiratory activity and protein level

(**A**) Late-passage (at or after passage 25) shRNA vector-treated and Nox4-depleted (Nox4 KD) HUVECs were harvested, and oxygen consumption was determined using an Oxygraph-2k™ instrument in cells permeabilized with digitonin, as described in the Experimental section. The rate of respiration was determined, and the following mitochondrial complexes were targeted by addition of specific substrates: addition of malate and glutamate (complex I-coupled respiration), ADP (complex I state III respiration), succinate (complex I and complex II state III respiration), FCCP (complex I and complex II-uncoupled respiration), rotenone (complex II-uncoupled respiration) and finally antimycin A, ascorbate and TMPD (complex IV-uncoupled respiration). Results were normalized to mitochondrial mass marker CS activity and are means ± S.E.M. obtained from three independent experiments. $^{*}P < 0.05$; $^{**}P < 0.01$; n.s., not significant. (**B**) Late-passage shRNA vector-treated and Nox4-deficient (Nox4 KD) HUVECs were harvested and the expression of selected OxPhos complex I–IV subunits was analysed by Western blotting, as indicated. Left: typical experiment. Right: densitometric analysis obtained from four independent experiments. Results are means ± S.E.M. $^{*}P < 0.05$. C, complex.

passage, Nox4-depleted cells maintained higher $\Delta\psi_m$ relative to shRNA vector-treated cells (Figure 2B). Cellular redox state, probed with the redox-sensitive dyes DHE (Figures 3A and 3B) and H_2-DCFDA (Figure 3C), steadily shifted to pro-oxidant conditions in shRNA vector-treated cells, but not Nox4-depleted cells, at late passage. Similarly, staining with MitoTracker Red CM-H_2XRos, probing selectively the redox state in the mitochondria [33], was significantly decreased in late-passage Nox4-depleted relative to shRNA vector-treated cells (Figure 3D). Whereas collectively these data suggest that Nox4 stimulates ROS production in the mitochondria, other interpretations of these results are possible. Redox-sensitive fluorescence probes such as DHE, H_2-DCFDA and MitoTracker Red CM-H_2XRos do not allow the unambiguous identification of the ROS that are responsible for the observed change in fluorescence and discrimination between redox-regulated effects and effects of specific radicals, e.g. superoxide anion or H_2O_2. Hence the precise nature of changes detected by the fluorescence probes used in the present study is not known.

Nox4 was found to localize within mitochondria in several cell types [16,34], and partial mitochondrial co-localization was also observed in HUVECs (results not shown), raising the possibility that Nox4 enhances the rate of ROS production in this organelle. As H_2O_2 is the main product of Nox4 activity [5], the presence of active Nox4 in mitochondria can be expected to raise mitochondrial H_2O_2 levels. This was confirmed in cells transfected with lentiviral vectors harbouring a mitochondrially expressed protein probe HyPer, allowing specific detection of mitochondrial H_2O_2 [35]. In these experiments, late-passage Nox4-depleted cells revealed a significantly decreased HyPer fluorescence in both cytosol and the mitochondria when compared with shRNA vector-treated cells (Figures 3E and 3F). Collectively, these results suggest a significant decrease in H_2O_2 concentration in the mitochondria of Nox4-depleted cells. Alternatively, the signal output of HyPer sensors used could be influenced by other parameters, e.g. the status of the cellular NAD(P)H-dependent reducing systems. To address further the specific role of H_2O_2 in this process, cells were treated with CAT-PEG, which significantly decreased HyPer fluorescence (Figure 3G), indicating that Nox4 deficiency indeed leads to lower H_2O_2 levels in the mitochondria.

To characterize Nox4 effects on mitochondrial function further, respiratory activity was assessed by high-resolution respirometry. At early passage, mitochondrial respiratory activity was slightly decreased in Nox4-depleted relative to control cells (Figure 4A). The basal respiration rate decreased significantly with extended passaging of shRNA vector-treated HUVECs, whereas it was not affected by extended passaging in the absence of Nox4 (Figure 4B, and Supplementary Figure S3 at http://www.biochemj.org/bj/452/bj4520231add.htm). Similarly, state IV (after oligomycin addition) and maximal state III

© The Authors Journal compilation © 2013 Biochemical Society

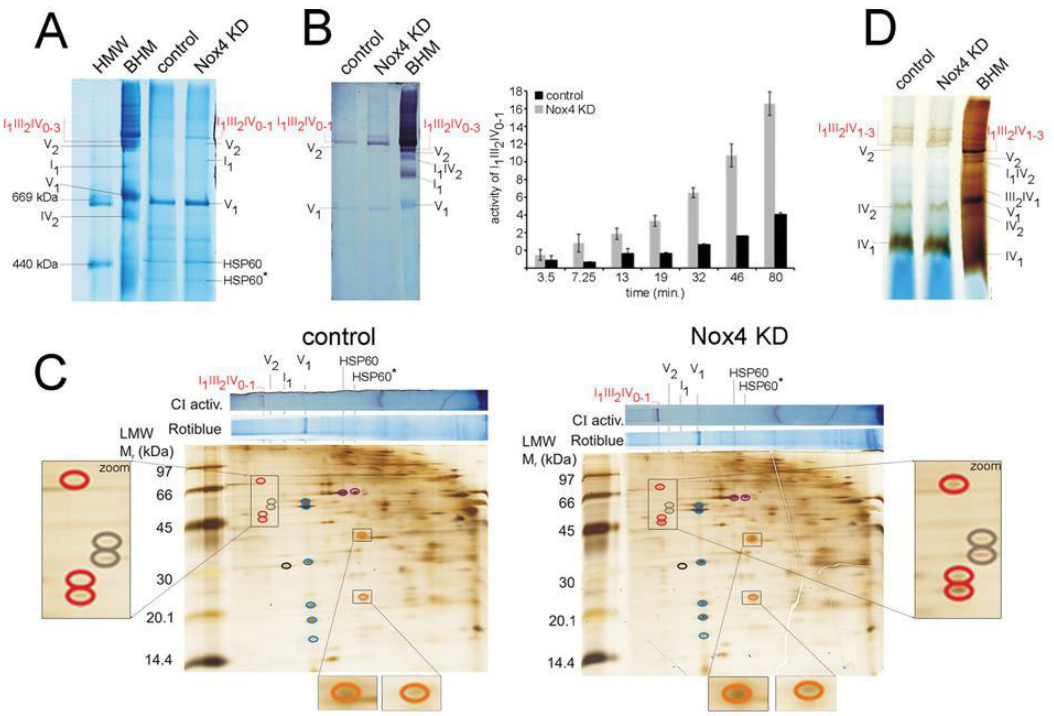

Figure 6 Effects of Nox4 on mitochondrial OxPhos complex I-containing supercomplexes

(**A**) Mitochondria were isolated from late-passage (at or after passage 25) shRNA vector-treated and Nox4-depleted (Nox4 KD) HUVECs as indicated and analysed by separating 120 μg of protein by BN-PAGE. For the detection of mitochondrial OxPhos complexes, the gel was stained in Rotiblue solution overnight. OxPhos complex I monomer (I_1), OxPhos complex I-containing supercomplexes ($I_1III_2IV_{0-1}$) and mitochondrial F_oF_1 ATP synthase monomer (V_1) and dimer (V_2) are shown. High-molecular-mass protein standard (HMW) and 70 μg of solubilized BHM were used as standards. Two oligomeric forms of heat-shock protein 60, HSP60 and HSP60*, probably representing a heptamer and hexamer respectively, are indicated. Molecular masses are indicated in kDa. (**B**) BN-PAGE was performed with 120 μg of protein of shRNA vector-treated and Nox4-depleted (Nox4 KD) HUVEC mitochondria harvested from cells at or after passage 25. Gels were incubated in complex I activity solution and scanned repeatedly for quantification. The image was taken after 80 min of incubation. OxPhos complex I monomer (I_1) and OxPhos complex I-containing supercomplexes (I_1IV_2 and $I_1III_2IV_{0-1}$) are shown. As a standard, 70 μg of BHM was loaded on the gel. Left: typical experimental data for a complex I in-gel activity analysis. Right: analysis of the activity of OxPhos complex I-containing supercomplexes. (**C**) Amounts of 150 μg of shRNA vector-treated and Nox4-depleted (Nox4 KD) HUVEC mitochondrial proteins harvested from cells at passage 27 were separated by BN-PAGE in the first dimension. Subsequently, excised lanes were analysed by Tricine-SDS/PAGE in the second dimension. On the top of each two-dimensional gel image, the images of two differently treated BN gels (complex I activity, and Rotiblue-stained) for each sample are pictured. The spots corresponding to subunits of OxPhos complex I are encircled in black, OxPhos complex I-containing supercomplexes ($I_1III_2IV_{0-1}$) are depicted in red. OxPhos complex IV subunits are presented in orange. Mitochondrial F_oF_1 ATP synthase monomer (V_1, blue) and dimer (V_2, grey) are shown. Protein standards are the same as in (**A**). Molecular masses using the LMW (low-molecular mass) standards are indicated in kDa. (**D**) Amounts of 50 μg of control and Nox4-depleted (Nox4 KD) HUVEC mitochondria harvested from cells at passage 27 were loaded on a small BN gel and incubated in complex IV activity solution for 12 h. OxPhos complex IV monomer (IV_1), OxPhos complex IV dimer (IV_2), and OxPhos complex IV-containing supercomplexes III_2IV_1, I_1IV_2 and $I_1III_2IV_{1-3}$ are shown. As a standard, 30 μg of BHM was used. Molecular masses using the LMW (low-molecular mass) standards are indicated in kDa.

(after FCCP addition) respiration rates were strongly decreased in shRNA vector-treated HUVECs at late passage, but fully preserved in Nox4-depleted cells (Figure 4B). These findings suggest that sustained Nox4 activity decreased both basal respiration and the maximal respiratory capacity of mitochondria.

Mitochondrial activity is regulated by various extracellular and intracellular signalling pathways, including the insulin/IGF (insulin-like growth factor) pathway [36,37], and signalling through Src [38] and Akt [39] kinases. Since Nox4-derived ROS mediate signalling by an overlapping set of kinases, including Src [40], EGF receptor [8], MAPK, p38 and JNK [7], it is conceivable that Nox4 activity triggers specific signalling pathways resulting in decreased mitochondrial activity. However, signalling through JNK, ERK (extracellular-signal-regulated kinase) and p38 was not affected by Nox4 depletion in HUVECs [18], and we did not observe significant changes in Akt phosphorylation in Nox4-depleted relative to shRNA vector-treated cells (results not shown). We cannot, however, exclude the possibility that altered signalling through other pathways, so far not associated with Nox4 activity, may contribute to the differences in mitochondrial activity observed in Nox4-depleted and shRNA vector-treated cells.

Nox4 activity induces dysfunction of mitochondrial OxPhos complex I

To analyse Nox4 effects on the OxPhos system further, shRNA vector-treated and Nox4-depleted cells were permeabilized and subjected to high-resolution respirometry using specific substrates and inhibitors of different mitochondrial OxPhos complexes. Using this approach, we found significantly increased complex I state III as well as complex I-uncoupled respiratory activity in Nox4-depleted HUVECs when compared with shRNA vector-treated cells at late

© The Authors Journal compilation © 2013 Biochemical Society

passage (Figure 5A, and also Supplementary Figure S4 at http://www.biochemj.org/bj/452/bj4520231add.htm). In Nox4-depleted cells, increased protein levels were found for complex I subunits, such as NDUFA9 (Figure 5B), suggesting that Nox4 reduces the abundance of mitochondrial complex I in late-passage HUVECs. Although respirometric data indicated increased complex II respiratory activity in Nox4-depleted cells, complex II protein level was not changed between samples (Figure 5). Neither complex IV activity nor protein levels were changed in Nox4-depleted compared with shRNA vector-treated HUVECs (Figure 5). Similarly, mitochondrial complex III protein levels were not affected by Nox4 depletion (Figure 5B). It is possible that Nox4 affects the synthesis and/or stability of complex I subunits encoded in the mitochondria. Using qRT-PCR (quantitative real-time PCR), we found no significant changes in mRNA concentration of complex I subunits (results not shown), suggesting that transcriptional regulation does not contribute to the altered abundance of complex I subunits in Nox4-depleted cells.

Separation of mitochondrial OxPhos complexes under native conditions revealed a significant increase in both the protein level (Figure 6A) and activity (Figure 6B) of mitochondrial complex I-containing supercomplexes $I_1III_2IV_{0-1}$ in Nox4-depleted HUVECs. Accordingly, our data indicate that Nox4 contributes to a decrease in the protein level of several subunits of the mitochondrial supercomplexes $I_1III_2IV_{0-1}$ (Figure 6C, red circles). Neither complex IV subunit protein levels (Figure 6C, orange circles) nor complex IV in-gel activity (Figure 6D) were changed in these assays, confirming our observation that Nox4 has no influence on mitochondrial complex IV activity and protein level. Inactivation of complex I-containing supercomplexes I_1III_2 and I_1III_2IV in Nox4-expressing cells could reflect molecular damage of such complexes, e.g. by Nox4-derived H_2O_2. Alternatively, Nox4 may affect the assembly of individual complex I into supercomplexes that have much higher enzymatic activity [26,41]. Although more work is required to establish the detailed mechanism of Nox4-mediated inactivation of mitochondrial complex I, the data indicate that Nox4 activity decreases mitochondrial supercomplexes $I_1III_2IV_{0-1}$ protein levels and activity, thereby contributing to mitochondrial dysfunction.

Several previous studies support a role of Nox4 to modulate mitochondrial function in vascular SMCs [42], murine cardiomyocytes [43] and prostate carcinoma cells [34] respectively; however, molecular mechanisms were not experimentally addressed in these studies. The association of electron transport chain complexes to higher-order structures (referred to as supercomplexes) is essential for mitochondrial function, and oxidative stress is known to disassemble supercomplexes, leading to cell damage and disease [44]. In the present paper, we describe for the first time OxPhos complex I and supercomplexes containing complex I as functional targets of Nox4. Several studies suggest possible pathological implications due to changes in mitochondrial supercomplexes. For example, the absence of NDUFS4 [NADH dehydrogenase (ubiquinone) Fe–S protein 4] protein, an accessory subunit of mitochondrial complex I, results in decreased activity and stability of complex I leading to fatal mitochondrial encephalomyopathy in mice, whereas mutations in the *NDUFS4* gene in humans cause a Leigh-like phenotype in humans [45]. Moreover, a deficiency for NDUFA9, the complex I subunit shown in the present study to be targeted by Nox4, has also been described in patients with Leigh syndrome [46]. Whereas these findings raise the possibility that increased Nox4 activity may play a role in Leigh syndrome and related pathologies, more work is required to address this question.

© The Authors Journal compilation © 2013 Biochemical Society

AUTHOR CONTRIBUTION

Rafał Kozieł, Haymo Pircher, Manuela Kratochwil, Barbara Lerner and Martin Hermann performed the experiments and evaluated data. Norbert Dencher, Rafał Kozieł and Pidder Jansen-Dürr designed the experiments and wrote the paper.

ACKNOWLEDGEMENTS

We thank Michael Neuhaus for excellent technical assistance.

FUNDING

This work was supported by the Austrian Science Fund (FWF) [grant number P23742] and the European Union [integrated project MiMAGE grant number LSHM-CT-2004-512020 (to J.P.-D. and N.A.D.)]. M.K. and N.A.D. acknowledge support by the German Federal Ministry for Education and Research (BMBF) through the GerontoMitoSys project [grant number FKZ 0315584] as well as by the Deutsche Forschungsgemeinschaft Graduiertenkolleg (Ph.D. programme) 'Molecular and cellular reaction on ionizing radiation'.

REFERENCES

1 Bedard, K. and Krause, K. H. (2007) The NOX family of ROS-generating NADPH oxidases: physiology and pathophysiology. Physiol. Rev. **87**, 245–313
2 Krause, K. H. (2004) Tissue distribution and putative physiological function of NOX family NADPH oxidases. Jpn. J. Infect. Dis. **57**, S28–S29
3 Nisimoto, Y., Jackson, H. M., Ogawa, H., Kawahara, T. and Lambeth, J. D. (2010) Constitutive NADPH-dependent electron transferase activity of the Nox4 dehydrogenase domain. Biochemistry **49**, 2433–2442
4 Blanchetot, C. and Boonstra, J. (2008) The ROS–NOX connection in cancer and angiogenesis. Crit. Rev. Eukaryotic Gene Expression **18**, 35–45
5 Serrander, L., Cartier, L., Bedard, K., Banfi, B., Lardy, B., Plastre, O., Sienkiewicz, A., Forro, L., Schlegel, W. and Krause, K. H. (2007) NOX4 activity is determined by mRNA levels and reveals a unique pattern of ROS generation. Biochem. J. **406**, 105–114
6 Chen, K., Craige, S. E. and Keaney, Jr, J. F. (2009) Downstream targets and intracellular compartmentalization in Nox signaling. Antioxid. Redox Signaling **11**, 2467–2480
7 Schroder, K., Wandzioch, K., Helmcke, I. and Brandes, R. P. (2008) Nox4 acts as a switch between differentiation and proliferation in preadipocytes. Arterioscler. Thromb. Vasc. Biol. **29**, 239–245
8 Chan, E. C., Jiang, F., Peshavariya, H. M. and Dusting, G. J. (2009) Regulation of cell proliferation by NADPH oxidase-mediated signaling: potential roles in tissue repair, regenerative medicine and tissue engineering. Pharmacol. Ther. **122**, 97–108
9 Lassegue, B. and Griendling, K. K. (2010) NADPH oxidases: functions and pathologies in the vasculature. Arterioscler. Thromb. Vasc. Biol. **30**, 653–661
10 Meng, D., Lv, D. D. and Fang, J. (2008) Insulin-like growth factor-I induces reactive oxygen species production and cell migration through Nox4 and Rac1 in vascular smooth muscle cells. Cardiovasc. Res. **80**, 299–308
11 Lyle, A. N., Deshpande, N. N., Taniyama, Y., Seidel-Rogol, B., Pounkova, L., Du, P., Papaharalambus, C., Lassegue, B. and Griendling, K. K. (2009) Poldip2, a novel regulator of Nox4 and cytoskeletal integrity in vascular smooth muscle cells. Circ. Res. **105**, 249–259
12 Van Buul, J. D., Fernandez-Borja, M., Anthony, E. C. and Hordijk, P. L. (2005) Expression and localization of NOX2 and NOX4 in primary human endothelial cells. Antioxid. Redox Signaling **7**, 308–317
13 Brandes, R. P. and Schroder, K. (2008) Differential vascular functions of Nox family NADPH oxidases. Curr. Opin. Lipidol. **19**, 513–518
14 Chen, K., Kirber, M. T., Xiao, H., Yang, Y. and Keaney, Jr, J. F. (2008) Regulation of ROS signal transduction by NADPH oxidase 4 localization. J. Cell Biol. **181**, 1129–1139
15 Hilenski, L. L., Clempus, R. E., Quinn, M. T., Lambeth, J. D. and Griendling, K. K. (2004) Distinct subcellular localizations of Nox1 and Nox4 in vascular smooth muscle cells. Arterioscler. Thromb. Vasc. Biol. **24**, 677–683
16 Block, K., Gorin, Y. and Abboud, H. E. (2009) Subcellular localization of Nox4 and regulation in diabetes. Proc. Natl. Acad. Sci. U.S.A. **106**, 14385–14390
17 Kuroda, J., Nakagawa, K., Yamasaki, T., Nakamura, K., Takeya, R., Kuribayashi, F., Imajoh-Ohmi, S., Igarashi, K., Shibata, Y., Sueishi, K. and Sumimoto, H. (2005) The superoxide-producing NAD(P)H oxidase Nox4 in the nucleus of human vascular endothelial cells. Genes Cells **10**, 1139–1151

18 Lener, B., Koziel, R., Pircher, H., Hutter, E., Greussing, R., Herndler-Brandstetter, D., Hermann, M., Unterluggauer, H. and Jansen-Dürr, P. (2009) The NADPH oxidase Nox4 restricts the replicative lifespan of human endothelial cells. Biochem. J. **423**, 363–374
19 Weyemi, U., Lagente-Chevallier, O., Boufraqech, M., Prenois, F., Courtin, F., Caillou, B., Talbot, M., Dardalhon, M., Al Ghuzlan, A., Bidart, J. M. et al. (2012) ROS-generating NADPH oxidase NOX4 is a critical mediator in oncogenic H-Ras-induced DNA damage and subsequent senescence. Oncogene **31**, 1117–1129
20 Wagner, M., Hampel, B., Bernhard, D., Hala, M., Zwerschke, W. and Jansen-Dürr, P. (2001) Replicative senescence of human endothelial cells *in vitro* involves G1 arrest, polyploidization and senescence-associated apoptosis. Exp. Gerontol. **36**, 1327–1347
21 Cossarizza, A., Baccarani-Contri, M., Kalashnikova, G. and Franceschi, C. (1993) A new method for the cytofluorimetric analysis of mitochondrial membrane potential using the J-aggregate forming lipophilic cation 5,5′,6,6′-tetrachloro-1,1′,3,3′-tetraethylbenzimidazolcarbocyanine iodide (JC-1). Biochem. Biophys. Res. Commun. **197**, 40–45
22 Hutter, E., Renner, K., Pfister, G., Stockl, P., Jansen-Dürr, P. and Gnaiger, E. (2004) Senescence-associated changes in respiration and oxidative phosphorylation in primary human fibroblasts. Biochem. J. **380**, 919–928
23 Hutter, E., Skovbro, M., Lener, B., Prats, C., Rabol, R., Dela, F. and Jansen-Dürr, P. (2007) Oxidative stress and mitochondrial impairment can be separated from lipofuscin accumulation in aged human skeletal muscle. Aging Cell **6**, 245–256
24 Schagger, H. (2001) Blue-native gels to isolate protein complexes from mitochondria. Methods Cell Biol. **65**, 231–244
25 Reifschneider, N. H., Goto, S., Nakamoto, H., Takahashi, R., Sugawa, M., Dencher, N. A. and Krause, F. (2006) Defining the mitochondrial proteomes from five rat organs in a physiologically significant context using 2D blue-native/SDS-PAGE. J. Proteome Res. **5**, 1117–1132
26 Frenzel, M., Rommelspacher, H., Sugawa, M. D. and Dencher, N. A. (2010) Ageing alters the supramolecular architecture of OxPhos complexes in rat brain cortex. Exp. Gerontol. **45**, 563–572
27 Hausenloy, D. J., Yellon, D. M., Mani-Babu, S. and Duchen, M. R. (2004) Preconditioning protects by inhibiting the mitochondrial permeability transition. Am. J. Physiol. Heart Circ. Physiol. **287**, H841–H849
28 Lundberg, J. O., Weitzberg, E. and Gladwin, M. T. (2008) The nitrate–nitrite–nitric oxide pathway in physiology and therapeutics. Nat. Rev. Drug Discovery **7**, 156–167
29 Shiva, S., Huang, Z., Grubina, R., Sun, J., Ringwood, L. A., MacArthur, P. H., Xu, X., Murphy, E., Darley-Usmar, V. M. and Gladwin, M. T. (2007) Deoxymyoglobin is a nitrite reductase that generates nitric oxide and regulates mitochondrial respiration. Circ. Res. **100**, 654–661
30 Wasilewski, M. and Scorrano, L. (2009) The changing shape of mitochondrial apoptosis. Trends Endocrinol. Metab. **20**, 287–294
31 Galloway, C. A., Lee, H. and Yoon, Y. (2012) Mitochondrial morphology-emerging role in bioenergetics. Free Radical Biol. Med. **53**, 2218–2228
32 Parone, P. A., Da Cruz, S., Tondera, D., Mattenberger, Y., James, D. I., Maechler, P., Barja, F. and Martinou, J. C. (2008) Preventing mitochondrial fission impairs mitochondrial function and leads to loss of mitochondrial DNA. PLoS ONE **3**, e3257
33 Kuznetsov, A. V., Kehrer, I., Kozlov, A. V., Haller, M., Redl, H., Hermann, M., Grimm, M. and Troppmair, J. (2011) Mitochondrial ROS production under cellular stress: comparison of different detection methods. Anal. Bioanal. Chem. **400**, 2383–2390
34 Graham, K. A., Kulawiec, M., Owens, K. M., Li, X., Desouki, M. M., Chandra, D. and Singh, K. K. (2010) NADPH oxidase 4 is an oncoprotein localized to mitochondria. Cancer Biol. Ther. **10**, 223–231
35 Belousov, V. V., Fradkov, A. F., Lukyanov, K. A., Staroverov, D. B., Shakhbazov, K. S., Terskikh, A. V. and Lukyanov, S. (2006) Genetically encoded fluorescent indicator for intracellular hydrogen peroxide. Nat. Methods **3**, 281–286
36 Stump, C. S., Short, K. R., Bigelow, M. L., Schimke, J. M. and Nair, K. S. (2003) Effect of insulin on human skeletal muscle mitochondrial ATP production, protein synthesis, and mRNA transcripts. Proc. Natl. Acad. Sci. U.S.A. **100**, 7996–8001
37 Yu, T., Robotham, J. L. and Yoon, Y. (2006) Increased production of reactive oxygen species in hyperglycemic conditions requires dynamic change of mitochondrial morphology. Proc. Natl. Acad. Sci. U.S.A. **103**, 2653–2658
38 Arachiche, A., Augereau, O., Decossas, M., Pertuiset, C., Gontier, E., Letellier, T. and Dachary-Prigent, J. (2008) Localization of PTP-1B, SHP-2, and Src exclusively in rat brain mitochondria and functional consequences. J. Biol. Chem. **283**, 24406–24411
39 Lai, H. C., Liu, T. J., Ting, C. T., Sharma, P. M. and Wang, P. H. (2003) Insulin-like growth factor-1 prevents loss of electrochemical gradient in cardiac muscle mitochondria via activation of PI 3 kinase/Akt pathway. Mol. Cell. Endocrinol. **205**, 99–106
40 Block, K., Eid, A., Griendling, K. K., Lee, D. Y., Wittrant, Y. and Gorin, Y. (2008) Nox4 NAD(P)H oxidase mediates Src-dependent tyrosine phosphorylation of PDK-1 in response to angiotensin II: role in mesangial cell hypertrophy and fibronectin expression. J. Biol. Chem. **283**, 24061–24076
41 Schafer, E., Seelert, H., Reifschneider, N. H., Krause, F., Dencher, N. A. and Vonck, J. (2006) Architecture of active mammalian respiratory chain supercomplexes. J. Biol. Chem. **281**, 15370–15375
42 Wosniak, Jr, J., Santos, C. X., Kowaltowski, A. J. and Laurindo, F. R. (2009) Cross-talk between mitochondria and NADPH oxidase: effects of mild mitochondrial dysfunction on angiotensin II-mediated increase in Nox isoform expression and activity in vascular smooth muscle cells. Antioxid. Redox Signaling **11**, 1265–1278
43 Ago, T., Kuroda, J., Pain, J., Fu, C., Li, H. and Sadoshima, J. (2010) Upregulation of Nox4 by hypertrophic stimuli promotes apoptosis and mitochondrial dysfunction in cardiac myocytes. Circ. Res. **106**, 1253–1264
44 Lenaz, G. and Genova, M. L. (2012) Supramolecular organisation of the mitochondrial respiratory chain: a new challenge for the mechanism and control of oxidative phosphorylation. Adv. Exp. Med. Biol. **748**, 107–144
45 Calvaruso, M. A., Willems, P., van den Brand, M., Valsecchi, F., Kruse, S., Palmiter, R., Smeitink, J. and Nijtmans, L. (2012) Mitochondrial complex III stabilizes complex I in the absence of NDUFS4 to provide partial activity. Hum. Mol. Genet. **21**, 115–120
46 Leshinsky-Silver, E., Lev, D., Tzofi-Berman, Z., Cohen, S., Saada, A., Yanoov-Sharav, M., Gilad, E. and Lerman-Sagie, T. (2005) Fulminant neurological deterioration in a neonate with Leigh syndrome due to a maternally transmitted missense mutation in the mitochondrial *ND3* gene. Biochem. Biophys. Res. Commun. **334**, 582–587

Received 27 November 2012/11 March 2013; accepted 20 March 2013
Published as BJ Immediate Publication 20 March 2013, doi:10.1042/BJ20121778

© The Authors Journal compilation © 2013 Biochemical Society

4.4 Changes of the mitochondrial proteome in an animal model of early Parkinson's disease

Proteome studies were performed on male Wistar rats. Substantia nigra (SN) and striatum (STR) of both hemispheres from six animals each, sham operated (SH) as control, four days after injection with 6-OHDA (4DL) and four weeks after injection with 6-OHDA (4WL), were dissected, frozen in liquid nitrogen and stored at -80°C by Dr. Kuter at IF-PAN, Krakow (2.6.2). Frozen tissues were transported by her on dry ice to our institute (TUD).

I introduced Dr. Kuter to the methods of our laboratory by performing the proteome analyses on SN together with her. Together we isolated the mitochondria (3.1), determined the total protein content by Bradford protein assay in wellplates (3.2.2), solubilised mitochondrial proteins with d/p: 8g/g (3.3.1, 3.3.2), performed BN PAGE on 10.0 cm by 10.5 cm sized gels for separation of proteins (3.4) and subsequent CI in-gel acitivity test (3.8.1), DIGE labelling (3.7.5) and subsequent 2D-BN/SDS PAGE on 18 cm by 16 cm sized gels (3.5.3), as well as staining of gels (3.7), and PMF for identification of protein spots on 2D-BN/SDS gels (3.9). I also introduced her to the methods for evaluation of the data (3.11). Thereafter Dr. Kuter performed CIV in-gel activity and all proteome studies on STR by herself under my mentorship.

We chose the Bradford protein assay in wellplates, BN PAGE on 10.0 cm by 10.5 cm sized gels and DIGE labelling and subsequent 2D-BN/SDS PAGE as methods for analyses of SN and STR, because of the small SN tissue size and therefore the resulting low total mitochondrial protein amount. For example, for one DIGE gel 52.5 µg (b. sol.) of RBM protein of one sample was used, while for one SyproRuby stained gel of the same size 120 µg (b. sol.) would have been needed. Additional amount of samples is saved because of application of the internal standard (IS) is supposed to diminish the differences between the different gels, from this follows that less number of gels (technical repeats) is needed.

In total, 18 DIGE-gels of the six animals per group were performed for quantitative analysis of the mitochondrial proteins from SN. Because of dye-swap (3.7.5) two technical repeats of each animal sample, stained with two different G-dyes (G-Dye200 and G-Dye300), were included. The IS consisted of a mixture of all animal samples, labelled with another G-Dye (G-Dye100, 3.7.5). One DIGE gel contained three different samples labelled with G-Dye100, G-Dye200 and G-Dye300 respectively. Therefore, from these 18 gels, the information of 54 images was obtained. For each sample the labelled mitochondrial protein amount was 35 µg (b. sol. d/p: 8g/g) for each dye, in total 105 µg were used of each animal sample for the DIGE experiment.
16 DIGE gels were performed by Dr. Kuter for the quantitative analysis of mitochondrial proteins from STR, resulting in 48 images for quantitation.
The evaluation of the results of the DIGE gel experiments is still in progress and a publication is planned.

For identification of protein spots, PMF (3.9) of SN and STR was performed. 300 µg mitochondrial protein of each tissue sample were solubilised (d/p: 8g/g, 3.3.1) and 2D-BN/SDS gels were performed (3.5). Gels were stained with silver (3.7.1), and protein spots were cut and destained (3.9.2) at our institute (TUD) by Dr. Kuter and me. The subsequent preparation of the samples and measurements of MALDI-MS-MS spectra as well as

evaluation was performed by Dr. S. Hartwig, Dipl. Ing. S. H. Marx and me at the Proteome Analysis Unit of Dr. S. Lehr at DDZ.
The manuscript containing this data is in preparation together with results from PMF identification from other samples of this thesis (cerebellum, cerebrum, hippocampus of rat 2.6.1 and BHM 2.6.3) as well as samples from Dipl. Ing. S. H. Marx (heart mitochondria of house pig, wild boar, deer, mouse, and kidney of deer) and the data for cell culture from Dr. L. Cavlovic (OLN-93) and Dipl. Biochem. V. Decker (SH-SY5Y). This manuscript will also include Western blot analyses of the OxPhos complexes in 2D-BN/SDS PAGE from most of these samples.

The results of the in-gel activity tests (CI and CIV) are described in our manuscript (Kuter et al. submitted: September 2015), which was submitted and is currently under review. It is not attached for copyright reasons but the abstract below in this chapter. CI and CIV in-gel activities of SN and STR were analysed. STR of all six individual animals were analysed separately, while for SN tissues from three animals were pooled, because of the small amount of mitochondria from this brain structure, in addition to one lane of mitochondria from one individual animal sample.

Dr. Kuter performed additional studies on this animal model. Together with M.Sc. S. Kern she analysed the membrane fluidity of the mitochondria of SN and STR at our institute (TUD). Besides the proteome investigations at our institute, Dr. Kuter performed additional analyses at IF-PAN: behavioural analyses of the rats, HPLC analyses of the dopamine concentration and its metabolites as well as immunohistochemical staining of brain sections and stereological counting of dopaminergic and non-dopaminergic neurons.

For copyright reasons the data obtained is not shown here, but the abstract of the submitted manuscript (Kuter et al. submitted: September 2015) is attached below.

Manuscript submitted:

K. Kuter, **M. Kratochwil**, K. Berghauzen-Maciejewska, U. Głowacka, M. D. Sugawa, K. Ossowska, N. A. Dencher

Adaptation within mitochondrial oxidative phosphorylation supercomplexes and membranes viscosity during degeneration of dopaminergic neurons in an animal model of early Parkinson's Disease.

Journal of Molecular Biology

Abstract:

In Parkinson's disease (PD) motor symptoms are not observed until the loss of approx. 70 % of dopaminergic neurons in substantia nigra (SN). Mitochondrial dysfunction has been indicated in the neuropathological process already at the early PD stages.

In presented 6-OHDA rat model, selective, medium-sized dopaminergic lesion was used to study mitochondrial membrane adaptations at the level of oxidative phosphorylation complexes (Cxs) and their higher assembled states - supercomplexes (SCxs), during the early degeneration processes and after it. We observed loss of dopaminergic phenotype in SN and decreased dopamine level in striatum (STR) before actual death of neurons in SN. Interestingly, behavioural deficits induced by lesion were reversed despite progressing neurodegeneration.

Along with degeneration process in STR, mitochondrial Cx I performance and amount decreased after 6-OHDA toxin injection in almost all analysed SCxs. Also, progressing decrease of Cx IV performance in few forms of SCxs ($I_1III_2IV_{3-1}$, I_1IV_{2-1}) in STR was observed during degeneration. In SN, SCxs containing Cx I showed significant increase in protein amount and a shift of individual Cx I_1 into superassembled states. Importantly, mitochondrial membrane viscosity changed in parallel with altered SCxs performance in dopaminergic structures. These results show for the first time adaptations at the level of mitochondrial membranes viscosity corresponding to SCxs function after dopaminergic system degeneration. It implicates that altered mitochondrial membrane viscosity, could play an important role in pathomechanisms of PD. The data obtained are also discussed in relationship to compensatory processes observed.

5 Conclusions

5.1 Methodical aspects

5.1.1 Identification of proteins in BN gels and 2D-BN/SDS gels

The migration pattern in BN-PAGE and 2D-BN/SDS-PAGE of mitochondrial proteins from whole rat brain is highly comparable to the pattern of proteins from the rat brain areas cerebellum, hippocampus and cerebrum, especially when the same detergent, in this thesis digitonin, is used for solubilisation of proteins in the same detergent to protein ratio (8 g / g for brain mitochondria).

The migration pattern of BHM proteins is highly comparable to the pattern of proteins from RBM. In the first dimension (BN) a difference in migration pattern is visible, caused by the different applied detergent to protein ratios (3 g / g for BHM and 8 g / g for RBM). This leads to the conclusion that mitochondrial proteins are highly conserved in mammals although little differences in molecular weight or posttranslational modifications occur. The band and spot pattern are mainly transferable between samples of mammals.

5.1.2 Comparison of different methods for protein visualisation and quantitation in 2D-BN/SDS gels

In general, which method is the appropriate to visualise the protein spots in 2D gels depends on the experimental setup, the available budget and the samples themselves, especially on the available amount of analysable protein. Each stain or label has its own characteristics for protein binding and visualising. Certainly, the staining has to be reproducible and to provide a sufficient linear range as well as enough sensitivity, especially when quantitation is planned. For this purpose DIGE-labelling or SyproRuby staining are the appropriate methods from the ones tested in this thesis. In any case, it is important to stay with the same method for conclusions about compared analyses.

5.1.3 Comparison of methods for quantitation of proteins

Quantitation of proteins in bands on CBBG stained BN gels is less accurate and can give varying result in comparison to the analysis of protein spots in 2D-BN/SDS gels. Protein bands in BN gels could overlay and make it impossible to distinguish between the different proteins. Applied SyproRuby staining of 2D-BN/SDS gels is more sensitive than CBBG staining. Therefore the results of 2D-BN/SDS PAGE are regarded as more trustworthy and used for evaluation of the changes by ageing and calorie restriction in this thesis.

5.2 Effects of ageing and calorie restriction on the mitochondrial proteome

5.2.1 Cerebellum

Ageing of *ad libitum* fed rats reduced the tissue weight and the average total protein content of mitochondria from cerebellum. The amount of proteins involved in neuronal composition increased, while for all other analysed proteins no changes were observed. The activities of CI and CIV were not altered. The membrane fluidity decreased with ageing.

The reduced tissue weight correlates with the decreased total protein content. The not changed amount of OxPhos (incl. CV) complexes and not changed activity indicate an ongoing compensation, as well as the fact, that the decreased fluidity seems to have no influence on the activity.

Ageing under calorie restriction (CR) reduced the average total protein content of cerebellum mitochondria, while the tissue weight was not changed. The amount of OxPhos proteins inclusive CV increased, while the amount of proteins of stress management, energy metabolism and those involved in neuronal composition decreased. The activities of CI and CIV were predominantly not altered under calorie restriction (CR) in cerebellum. The membrane fluidity decreased with ageing under CR.

CR seems to compensate the age dependent decline of the tissue weight. It is interesting that aged animals under CR show a lower total protein content while the amount of OxPhos complexes (incl. CV) increases in a tissue, of which the weight stays the same. This might be a compensation process to eliminate the effects of lower membrane fluidity and for the not altered CI and CIV activity.

ST decreased the tissue weight of cerebellum while the average total protein content of mitochondria increased. The amount of OxPhos proteins inclusive CV decreased, while the amount of proteins of stress management, energy metabolism and those involved in neuronal composition increased. The activities of CI and CIV were not changed. The fluidity of cerebral mitochondrial membranes decreased under ST.

The tissue weight of cerebellum was not changed under LT. LT increased the average total protein content of mitochondria from cerebellum. The amount of OxPhos complexes inclusive CV, as well as proteins of stress management and energy metabolism did not change. Proteins involved in neuronal composition decreased. LT increased the specific CI activity for the supercomplexes $I_1III_2IV_{0\text{-}2}$. A decrease in fluidity of mitochondrial membranes was observed under LT.

ST and LT show the differences compared to animals kept *ad libitum* which occur during time. An increased total protein content is observeable in ST, maybe caused by the increased amounts of proteins of stress management, energy metabolism (which could compensate for the decreased OxPhos protein amount) and the proteins for neuronal composition.

Under LT the total protein content is still increased but the amount of OxPhos complexes increased again to the normal level and the proteins of stress management, energy metabolism and those involved in neuronal composition decreased to their normal level.

Ageing leads to decreased cerebellum weight independently from nutrition. Calorie restriction seems to stress the body in the beginning, observable by increased amounts for proteins of stress management and energy metabolism and maybe also in later phase, as a higher total protein content is visible for ST and LT. The decrease in fluidity of mitochondrial membranes under ST and LT would also support this theory.

It is of interest, whether the functions of cerebellum, such as balance and spatial orientation, fine motor skills and planning movement, remained unaltered under these conditions.

5.2.2 Hippocampus

Ageing of *ad libitum* fed animals (AL) decreased the tissue weight and the average total protein content of mitochondria from hippocampus. This is in line with the finding that the amount of all analysed proteins decreased. Remarkable is the decrease of CV amount. The specific CI activity decreased in hippocampus. The fluidity of the membrane did not change.

Ageing under calorie restriction (CR) decreased the average total protein content of mitochondria from hippocampus as well as slightly the tissue weight. Mainly the amount of OxPhos proteins inclusive CV and proteins of energy metabolism and stress management were increased. The specific CI activity was decreased for smaller complexes. CR increased the fluidity of the mitochondrial membrane.

Calorie restriction reduced heavily the tissue weight already in young animals (ST). Also, the average total protein content of mitochondria from hippocampus decreased, likewise mainly all proteins of hippocampus mitochondria. ST decreased CI activity for the larger supercomplexes $I_1III_2IV_{0-2}$, as well as the fluidity of the membranes.

LT decreased the tissue weight and the average total protein content of mitochondria from hippocampus, however the amount of almost all analysed proteins was increased. LT decreased CI activity for complex I_1III_2, as well as the fluidity of the membranes.

Hippocampus tissue is decreased by ageing and the total protein content too, both independently from type of feeding. The protein amount of OxPhos complexes is decreased during ageing and ST, but increased under CR and LT. CI activity decreased in hippocampus for all analysed states but differed in the affected (super-)complexes. CIV activity was not changed in any state. As expected, the fluidity of the membranes decreased with age under *ad libitum* feeding as well as under ST and LT. Only when the calorie restricted animals were compared, the fluidity increased with age (CR). It is remarkable, that all measured parameters such as tissue weight, total protein content, amounts of single proteins, CI activity and the fluidity of the membranes are decreased in ST rats. Maybe ST calorie restriction has a strong negative influence on hippocampus mitochondria and hippocampus content.

The decreased tissue weight, amount of total protein, the loss in CI activity and the decreased fluidity of the membranes indicate that destructive processes seem to occur in the aged rats independently from nutrition. The increased amount of OxPhos and proteins of energy metabolism and stress management under CR could be part of compensation processes.

It would be of interest, whether hippocampus still was able to perform in an appropriate way, as it is known to transfer short-term into long-term memory and the disorder of this function is a characteristic symptom for age-associated diseases like dementia.

5.2.3 Cerebrum

Ageing reduced the tissue weight of cerebrum from rats under *ad libitum* feeding. A decrease in protein amount of OxPhos complexes (excl. CV) as well as for several proteins of energy metabolism was observed. Only the amount of CV increased. The proteins of stress management showed no change. The activities of CI and CIV were predominantly not altered. The fluidity of the mitochondrial membrane decreased.

Ageing under calorie restriction (CR) decreased the tissue weight slightly and increased the protein amount of OxPhos complexes inclusive CV. The amount of proteins of energy metabolism was partly decreased and increased. The activities of CI and CIV were decreased for smaller (super-)complexes and CIV activity increased for supercomplexes I_1IV_2 and $I_1III_2IV_1$. The fluidity of the mitochondrial membrane did not change under CR.

ST reduced the tissue weight. No changes of protein amount except for some increased proteins of energy metabolism were observed for ST. The specific CIV activity was increased for smaller complexes. The fluidity of the mitochondrial membrane did not change.

Under LT the tissue weight was slightly decreased and the amount of OxPhos complexes (excl. CV) increased, while some proteins of energy metabolism and some of those involved in neuronal composition decreased. The specific activities of CI and CIV were predominantly not changed under LT. The fluidity of mitochondrial membranes was increased.

Under ST only the CIV activity is changed (increased) and all the other measured parameters remained on the same level as in *ad libitum* fed animals. Therefore ST seems to have no influence on the cerebrum mitochondria. An increase of the amount of the OxPhos complexes under LT and CR while the activity of CI and CIV nearly remains at the same level as before / as in *ad libitum* rats indicates a compensation process. Although the fluidity of the mitochondrial membrane is decreased in aged *ad libitum* fed animals and a lower amount of OxPhos protein is available, the activity of CI and CIV is maintained.

5.2.4 Additonal common changes

Young animals under calorie restriction (YCR) compared to young *ad libitum* (YAL) ones developed a smaller body weight. Ageing under CR increased the body weight to the same extent as under AL.

The mtDNA encoded protein subunits CYB (CIII) and COX2 (CIV) do not show specific trends. The changes in amounts seem to follow the trends of total CIII respectively total CIV.

The highest activities of CI are found in supercomplex $I_1III_2IV_3$ and for CIV in supercomplex $I_1III_2IV_2$ for all three brain tissues. It is observable that for CI and CIV activity the presence of CIII increases the activity in a strong way. For all analysed tissues, the changes in specific activity of CI and CIV due to ageing or calorie restriction are not very pronounced. Therefore the activity of the respiratory chain is maintained while ageing under both types of nutrition.

5.2.5 Remarks and outlook

Present results demonstrate how important studies of separate brain areas are. Each brain tissue has a different function and therefore the mitochondria differ as well. Additional criteria, which are important to consider for comparison of results, are the differences of analysed rat strains like Fischer, Wistar, Brown-Dawley amongst others. Of course, the comparability of different animal models is also important. But even methodical aspects, which could influence the results, have to be considered, such as the method for isolation of mitochondria. For example, in this thesis crude mitochondrial fraction as yielded from differential centrifugation was used and in other works isopycnic density gradient centrifugation is applied. Both lead to different ratios of purities and application of the gradient could even discard not fully intact mitochondria, which are important to analyse if in research for affected mitochondria. More examples are the chosen method of the subsequent protein determination or the detergent to protein ratio for solubilisation, which could influence strongly the results of the whole experiment, and of course the influence of freezing on the activity of enzymes.

According to the results in this thesis for brain ageing, calorie restriction, as a tool to live a longer and healthier life, cannot be recommended, because of the destructive impact on the brain tissues, especially of hippocampus.

It has to be analysed in the future, why the increased total protein amounts are necessary for the tissue under calorie restriction and which proteins are those increased ones. It is also of interest to study the lipid composition of the membranes to understand the changes in fluidity. And behavioural studies would also be interesting, to find out, how much the specific brain tissue is affected and to see differences between calorie restriction and *ad libitum* nutrition.

Finally the transfer of results from animal studies to human models is not even trivial. Volunteers would be needed and because of the long lifespan of humans, results cannot be expected in short time.

6 References

Acin-Perez, R. and Enriquez, J. A. (2014) "The function of the respiratory supercomplexes: The plasticity model" *Biochimica et Biophysica Acta (BBA) - Bioenergetics* **1837**: 444-450.

Andringa, K. K., King, A. L., Eccleston, H. B., Mantena, S. K., Landar, A., Jhala, N. C., Dickinson, D. A., Squadrito, G. L. and Bailey, S. M. (2010) "Analysis of the liver mitochondrial proteome in response to ethanol and S-adenosylmethionine treatments: novel molecular targets of disease and hepatoprotection" *Am J Physiol Gastrointest Liver Physiol* **298**: G732-745.

Basso, M., Giraudo, S., Corpillo, D., Bergamasco, B., Lopiano, L. and Fasano, M. (2004) "Proteome analysis of human substantia nigra in Parkinson's disease" *Proteomics* **4**: 3943-3952.

Bedard, K. and Krause, K. H. (2007) "The NOX family of ROS-generating NADPH oxidases: physiology and pathophysiology" *Physiol Rev* **87**: 245-313.

Berggren, K., Chernokalskaya, E., Steinberg, T. H., C., K., Lopez, M. F., Diwu, Z., Haugland, R. P. and Patton, W. F. (2000) "Background-free, high sensitivity staining of proteins in one- and two-dimensional sodium dodecyl sulfate-polyacrylamide gels using a luminescent ruthenium complex" *Electrophoresis* **21**: 2509-2521.

Bevilacqua, L., Ramsey, J. J., Hagopian, K., Weindruch, R. and Harper, M. E. (2005) "Long-term caloric restriction increases UCP3 content but decreases proton leak and reactive oxygen species production in rat skeletal muscle mitochondria" *Am J Physiol Endocrinol Metab* **289**: 429-438.

Bio-Rad (2000) "SYPRO® Ruby Protein Stains, Instruction Manual".

Blum, H., Beier, H. and Gross, H. J. (1987) "Improved silver staining of plant proteins, RNA and DNA in polyacrylamide gels" *Electrophoresis* **8**: 93-99.

Boveris, A. and Navarro, A. (2008) "Brain mitochondrial dysfunction in aging" *IUBMB Life* **60**: 308-314.

Breton, S., Milani, L., Ghiselli, F., Guerra, D., Stewart, D. T. and Passamonti, M. (2014) "A resourceful genome: updating the functional repertoire and evolutionary role of animal mitochondrial DNAs" *Trends in Genetics* **30**: 555-564.

Brown Rodgers, A. (2008). "Alzheimer's disease, Unraveling the mystery". Silver Spring, National institute on aging, U.S. Department of Health and Human Services.

Bruker Daltonik (2012) "Instructions for use, Prespotted AnchorChip PAC II 384 / 96 HCCA".

Buratovich, M.,Spring Arbor University, (access date: 15.07.2015, https://beyondthedish.files.wordpress.com/2014/09/basal-ganglia.jpg.

Carl Roth (2011) "Roti®-Blue, Instructions for use".

Carothers, D. J., Pons, G. and Patel, M. S. (1989) "Dihydrolipoamide dehydrogenase: functional similarities and divergent evolution of the pyridine nucleotide-disulfide oxidoreductases" *Arch Biochem Biophys* **268**: 409-425.

Cavlovic, L. (2015) "Wirkung von ionisierender Strahlung auf Proteom und Lipidom sowie auf zelluläre und mitochondriale Aktivität" Doctoral thesis, Technische Universität Darmstadt.

Cerqueira, F. M., Cunha, F. M., Laurindo, F. R. M. and Kowaltowski, A. J. (2012) "Calorie restriction increases cerebral mitochondrial respiratory capacity in a NO•-mediated mechanism: Impact on neuronal survival" *Free Radical Biology and Medicine* **52**: 1236-1241.

Chan, D. C. (2006) "Mitochondria: Dynamic Organelles in Disease, Aging, and Development" *Cell* **125**: 1241-1252.

Cheung, T. H. and Cardinal, R. N. (2005) "Hippocampal lesions facilitate instrumental learning with delayed reinforcement but induce impulsive choice in rats" *BMC Neurosci* **6**: 36.

Choe, M., Jackson, C. and Yu, B. P. (1995) "Lipid peroxidation contributes to age-related membrane rigidity" *Free Radical Biology and Medicine* **18**: 977-984.

Choi, J.-H. and Yu, B. P. (1995) "Brain synaptosomal aging: Free radicals and membrane fluidity" *Free Radical Biology and Medicine* **18**: 133-139.

Cocco, T., Sgobbo, P., Clemente, M., Lopriore, B., Grattagliano, I., Di Paola, M. and Villani, G. (2005) "Tissue-specific changes of mitochondrial functions in aged rats: effect of a long-term dietary treatment with N-acetylcysteine" *Free Radic Biol Med* **38**: 796-805.

Coffey, C. E., Wilkinson, W. E., Parashos, I. A., Soady, S. A., Sullivan, R. J., Patterson, L. J., Figiel, G. S., Webb, M. C., Spritzer, C. E. and Djang, W. T. (1992) "Quantitative cerebral anatomy of the aging human brain: a cross-sectional study using magnetic resonance imaging" *Neurology* **42**: 527-536.

Colindres, M., Fournier, C., Ritter, S., Zahnreich, S., Decker, H., Dencher, N. A. and Frenzel, M. (2007) "Increase of oxidative stress in normal human fibroblasts after irradiation" *RADIATION-BIOPHYSICS* **11**: 365.

Colman, R. J., Beasley, T. M., Kemnitz, J. W., Johnson, S. C., Weindruch, R. and Anderson, R. M. (2014) "Caloric restriction reduces age-related and all-cause mortality in rhesus monkeys" *Nat Commun* **5**.

Columbia University, (access date: 15.07.2015, www.columbia.edu/cu/psycology/courses/1010/mangels/neuro/anatomy/structure.html.

Cumming, G., Fidler, F. and Vaux, D. L. (2007) "Error bars in experimental biology" *J Cell Biol* **177**: 7-11.

Dai, D. F., Karunadharma, P. P., Chiao, Y. A., Basisty, N., Crispin, D., Hsieh, E. J., Chen, T., Gu, H., Djukovic, D., Raftery, D., Beyer, R. P., MacCoss, M. J. and Rabinovitch, P. S. (2014) "Altered proteome turnover and remodeling by short-term caloric restriction or rapamycin rejuvenate the aging heart" *Aging Cell* **13**: 529-539.

Dani, D., Shimokawa, I., Komatsu, T., Higami, Y., Warnken, U., Schokraie, E., Schnolzer, M., Krause, F., Sugawa, M. D. and Dencher, N. A. (2010) "Modulation of oxidative phosphorylation machinery signifies a prime mode of anti-ageing mechanism of calorie restriction in male rat liver mitochondria" *Biogerontology* **11**: 321-334.

Daum, G. (1985) "Lipids of mitochondria" *Biochim Biophys Acta* **822**: 1-42.

de Winter, J. C. F. (2013) "Using the Student's t-test with extremely small sample sizes" *Practical Assessment, Research & Evaluation* **18**: 1-12.

Decker, V. (presumably 2016) Doctoral thesis, Technische Universität Darmstadt.

Decodon (2011a) "Delta2D 4.3 GettingStarted".

Decodon (2011b) "Delta2D 4.3 GettingStarted DIGE".

Destatis Statistisches Bundesamt, (access date: 18.07.2015)"13. koordinierte Bevölkerungsvorausberechnung für Deutschland", https://www.destatis.de/bevoelkerungspyramide/#!y=2015&o=2050v1, Wiesbaden.

Destatis Statistisches Bundesamt, (access date: 19.07.2015)"Krankheitskosten: Deutschland, Jahre, Krankheitsdiagnosen (ICD-10), Geschlecht, Altersgruppen (2008)", https://www-genesis.destatis.de/genesis/online/logon?sequenz=tabelleErgebnis&selectionname=23631-0003&sachmerkmal=ICD10Y&sachschluessel=ICD10-F00-F03&transponieren=true, Wiesbaden.

Deutsche Alzheimer Gesellschaft e.V. Selbsthilfe Demenz (2014) "Das Wichtigste 1 Die Häufigkeit von Demenzerkrankungen". Berlin.

Drew, B. and Leeuwenburgh, C. (2003) "Method for measuring ATP production in isolated mitochondria: ATP production in brain and liver mitochondria of Fischer-344 rats with age

and caloric restriction" *American Journal of Physiology - Regulatory, Integrative and Comparative Physiology* **285**: R1259-R1267.
Drew, B., Phaneuf, S., Dirks, A., Selman, C., Gredilla, R., Lezza, A., Barja, G. and Leeuwenburgh, C. (2003) "Effects of aging and caloric restriction on mitochondrial energy production in gastrocnemius muscle and heart" *American Journal of Physiology - Regulatory, Integrative and Comparative Physiology* **284**: R474-R480.
Dudkina, N. V., Kouril, R., Peters, K., Braun, H. P. and Boekema, E. J. (2010) "Structure and function of mitochondrial supercomplexes" *Biochim Biophys Acta* **1797**: 664-670.
E, L. and Swerdlow, R. H. (2012). "Mitochondria in Neurodegeneration". Scatena, R., Bottoni, P. and Giardina, B. *Advances in mitochondrial medicine*. Dordrecht Heidelberg London New York, Springer. **12:** 269-286.
Eckmann, J., Clemens, L. E., Eckert, S. H., Hagl, S., Yu-Taeger, L., Bordet, T., Pruss, R. M., Muller, W. E., Leuner, K., Nguyen, H. P. and Eckert, G. P. (2014) "Mitochondrial membrane fluidity is consistently increased in different models of Huntington disease: restorative effects of olesoxime" *Mol Neurobiol* **50**: 107-118.
Efremov, R. G., Baradaran, R. and Sazanov, L. A. (2010) "The architecture of respiratory complex I" *Nature* **465**: 441-445.
Faulks, S. C., Turner, N., Else, P. L. and Hulbert, A. J. (2006) "Calorie restriction in mice: effects on body composition, daily activity, metabolic rate, mitochondrial reactive oxygen species production, and membrane fatty acid composition" *J Gerontol A Biol Sci Med Sci* **61**: 781-794.
Ferri, C., Piovezan, R. D., Padilla, I., Prince, M., Albanese, E. and Prina, M. (2014). "Lifestyle". *World Alzheimer Report 2014, Dementia and Risk Reduction, An analysis of protective and modifiable factors*. London, Alzheimer's Disease International (ADI). **4:** 42-65.
Filburn, C. R., Edris, W., Tamatani, M., Hogue, B., Kudryashova, I. and Hansford, R. G. (1996) "Mitochondrial electron transport chain activities and DNA deletions in regions of the rat brain" *Mech Ageing Dev* **87**: 35-46.
Fontana, L., Partridge, L. and Longo, V. D. (2010) "Dietary Restriction, Growth Factors and Aging: from yeast to humans" *Science (New York, N.Y.)* **328**: 321-326.
Frenzel, M. (2006) "Altersabhängige Untersuchung des Proteoms von Rattus norvegicus." Diploma Thesis, Technische Universität Darmstadt.
Frenzel, M. (2011) "Mitochondrial ageing in rat brain areas and human fibroblasts" Doctoral Thesis, Technische Universität Darmstadt.
Frenzel, M., Rommelspacher, H., Sugawa, M. D. and Dencher, N. A. (2010) "Ageing alters the supramolecular architecture of OxPhos complexes in rat brain cortex" *Exp Gerontol* **45**: 563-572.
Gabbita, S. P., Butterfield, D. A., Hensley, K., Shaw, W. and Carney, J. M. (1997) "Aging and Caloric Restriction Affect Mitochondrial Respiration and Lipid Membrane Status: An Electron Paramagnetic Resonance Investigation" *Free Radical Biology and Medicine* **23**: 191-201.
Gaenslen, A. and Berg, D. (2010). "Early Diagnosis of Parkinson's Disease". Daniela, B. and Uwe, W. *International Review of Neurobiology*. Waltham, Massachusetts, Academic Press. **90:** 81-92.
GE Healthcare (2005) "Ettan DIGE System, User Manual".
GE Healthcare (2006) "Typhoon, Users Guide Version 3.0".
GE Healthcare Amersham (2006a) "High Molecular Weight Calibration Kit for native electrophoresis".
GE Healthcare Amersham (2006b) "Low Molecular Weight Calibration Kit for SDS Electrophoresis".

Gerlach, M., Reichmann, H. and Riederer, P. (2007). "Die Parkinson-Krankheit, Grundlagen, Klinik, Therapie". Wien, Springer-Verlag.
Gilmer, L. K., Ansari, M. A., Roberts, K. N. and Scheff, S. W. (2010) "Age-related Changes in Mitochondrial Respiration and Oxidative Damage in the Cerebral Cortex of the Fischer 344 Rat" *Mechanisms of ageing and development* **131**: 133-143.
Gómez, L. A., Monette, J. S., Chavez, J. D., Maier, C. S. and Hagen, T. M. (2009) "Supercomplexes of the mitochondrial electron transport chain decline in the aging rat heart" *Archives of Biochemistry and Biophysics* **490**: 30-35.
Grandier-Vazeille, X. and Guérin, M. (1996) "Separation by Blue Native and Colorless Native Polyacrylamide Gel Electrophoresis of the Oxidative Phosphorylation Complexes of Yeast Mitochondria Solubilized by Different Detergents: Specific Staining of the Different Complexes" *Analytical Biochemistry* **242**: 248-254.
GraphPad Software Inc. (1995-2014) "GraphPad Statistics Guide, The unequal variance Welch t test".
Grinna, L. S. (1977) "Age related changes in the lipids of the microsomal and the mitochondrial membranes of rat liver and kidney" *Mech Ageing Dev* **6**: 197-205.
Groebe, K., Krause, F., Kunstmann, B., Unterluggauer, H., Reifschneider, N. H., Scheckhuber, C. Q., Sastri, C., Stegmann, W., Wozny, W., Schwall, G. P., Poznanovic, S., Dencher, N. A., Jansen-Durr, P., Osiewacz, H. D. and Schrattenholz, A. (2007) "Differential proteomic profiling of mitochondria from Podospora anserina, rat and human reveals distinct patterns of age-related oxidative changes" *Exp Gerontol* **42**: 887-898.
Haan, C. and Behrmann, I. (2007) "A cost effective non-commercial ECL-solution for Western blot detections yielding strong signals and low background" *J Immunol Methods* **318**: 11-19.
Hamanaka, R. B. and Chandel, N. S. (2010) "Mitochondrial reactive oxygen species regulate cellular signaling and dictate biological outcomes" *Trends Biochem Sci* **35**: 505-513.
Hancock, J. T., Desikan, R. and Neill, S. J. (2001) "Role of reactive oxygen species in cell signalling pathways" *Biochem Soc Trans* **29**: 345-350.
Haripriya, D., Devi, M. A., Kokilavani, V., Sangeetha, P. and Panneerselvam, C. (2004) "Age-dependent alterations in mitochondrial enzymes in cortex, striatum and hippocampus of rat brain -- potential role of L-Carnitine" *Biogerontology* **5**: 355-364.
Harman, D. (1956) "Aging: a theory based on free radical and radiation chemistry" *J Gerontol* **11**: 298-300.
Harman, D. (1972) "The biologic clock: the mitochondria?" *J Am Geriatr Soc* **20**: 145-147.
Heidrich, N. G. (2011) "Superkomplexe aus Algen und Cyanobakterien." Doctoral Thesis, Technische Universität Darmstadt.
Heyn, M. P. (1979) "Determination of lipid order parameters and rotational correlation times from fluorescence depolarization experiments" *FEBS Lett* **108**: 359-364.
Jo, S.-H., Son, M.-K., Koh, H.-J., Lee, S.-M., Song, I.-H., Kim, Y.-O., Lee, Y.-S., Jeong, K.-S., Kim, W. B., Park, J.-W., Song, B. J. and Huhe, T.-L. (2001) "Control of Mitochondrial Redox Balance and Cellular Defense against Oxidative Damage by Mitochondrial NADP+-dependent Isocitrate Dehydrogenase" *Journal of Biological Chemistry* **276**: 16168-16176.
Kacew, S. and Festing, M. F. W. (1996) "Invited Review: ROLE OF RAT STRAIN IN THE DIFFERENTIAL SENSITIVITY TO PHARMACEUTICAL AGENTS AND NATURALLY OCCURRING SUBSTANCES" *Journal of Toxicology and Environmental Health* **47**: 1-30.
Karp, N. A., Kreil, D. P. and Lilley, K. S. (2004) "Determining a significant change in protein expression with DeCyder during a pair-wise comparison using two-dimensional difference gel electrophoresis" *Proteomics* **4**: 1421-1432.

Kern, S. (2013) "Biochemical and biophysical characterization of biological membranes." Master Thesis, Technische Universität Darmstadt.

Kolasiewicz, W., Kuter, K., Berghauzen, K., Nowak, P., Schulze, G. and Ossowska, K. (2012) "6-OHDA injections into A8-A9 dopaminergic neurons modelling early stages of Parkinson's disease increase the harmaline-induced tremor in rats" *Brain Res* **1477**: 59-73.

Koolman, J., Röhm, K.-H. and Wirth, J. (2003). "Taschenatlas der Biochemie". Stuttgart, Georg Thieme Verlag.

Koziel, R., Pircher, H., Kratochwil, M., Lener, B., Hermann, M., Dencher, N. A. and Jansen-Dürr, P. (2013) "Mitochondrial respiratory chain complex I is inactivated by NADPH oxidase Nox4" *Biochem J* **452**: 231-239.

Krause, F. (2004) "Biochemische Charakterisierung der supramolekularen Organisation der mitochondrialen OXPHOS-Komplexe von Säugern, Pilzen und Pflanzen" Doctoral Thesis, Technische Universität Darmstadt.

Krause, F., Reifschneider, N. H., Goto, S. and Dencher, N. A. (2005) "Active oligomeric ATP synthases in mammalian mitochondria" *Biochem Biophys Res Commun* **329**: 583-590.

Krause, F. and Seelert, H. (2008) "Detection and analysis of protein-protein interactions of organellar and prokaryotic proteomes by blue native and colorless native gel electrophoresis" *Curr Protoc Protein Sci* **Chapter 14**: Unit 14 11.

Kuter, K., Kratochwil, M., Berghauzen-Maciejewska, K., Głowacka, U., Sugawa, M. D., Ossowska, K. and Dencher, N. A. (submitted: September 2015) "Adaptation within mitochondrial oxidative phosphorylation supercomplexes and membranes viscosity during degeneration of dopaminergic neurons in an animal model of early Parkinson's Disease." *Journal of Molecular Biology*.

Laemmli, U. K. (1970) "Cleavage of structural proteins during the assembly of the head of bacteriophage T4" *Nature* **227**: 680-685.

Lee, J., Yu, B. and Herlihy, J. (1999) "Modulation of cardiac mitochondrial membrane fluidity by age and calorie intake" *Free Radical Biology and Medicine* **26**: 260-265.

Lenaz, G. (2012). "Mitochondria and Reactive Oxygen Species. Which Role in Physiology and Pathology?". Scatena, R., Bottoni, P. and Giardina, B. *Advances in mitochondrial medicine*. Dordrecht Heidelberg London New York, Springer. **5:** 93-136.

Lentz, B. R. (1993) "Use of fluorescent probes to monitor molecular order and motions within liposome bilayers" *Chem Phys Lipids* **64**: 99-116.

Lesnefsky, E. J. and Hoppel, C. L. (2006) "Oxidative phosphorylation and aging" *Ageing Res Rev* **5**: 402-433.

Li, H., Liu, D., Lu, J. and Bai, Y. (2012). "Physiology and Pathophysiology of Mitochondrial DNA". Scatena, R., Bottoni, P. and Giardina, B. *Advances in mitochondrial medicine*. Dordrecht Heidelberg London New York, Springer. **2:** 39-52.

Liang, C.-L., Wang, T. T., Luby-Phelps, K. and German, D. C. (2007) "Mitochondria mass is low in mouse substantia nigra dopamine neurons: Implications for Parkinson's disease" *Experimental Neurology* **203**: 370-380.

Lombardi, A., Silvestri, E., Cioffi, F., Senese, R., Lanni, A., Goglia, F., de Lange, P. and Moreno, M. (2009) "Defining the transcriptomic and proteomic profiles of rat ageing skeletal muscle by the use of a cDNA array, 2D- and Blue native-PAGE approach" *J Proteomics* **72**: 708-721.

Lottspeich, F. and Engels, J. W. (2012). "Bioanalytik". Berlin-Heidelberg, Springer Spektrum.

Marshall, T. and Williams, K. M. (2004) "Interference in the Coomassie Brilliant Blue and Pyrogallol Red protein dye-binding assays is increased by the addition of sodium dodecyl sulfate to the dye reagents." *Analytical Biochemistry* **331**: 255-259.

Matsuo, M., Gomi, F., Kuramoto, K. and Sagai, M. (1993) "Food restriction suppresses an age-dependent increase in the exhalation rate of pentane from rats: a longitudinal study" *J Gerontol* **48**: B133-136.

Mattison, J. A., Roth, G. S., Beasley, T. M., Tilmont, E. M., Handy, A. M., Herbert, R. L., Longo, D. L., Allison, D. B., Young, J. E., Bryant, M., Barnard, D., Ward, W. F., Qi, W., Ingram, D. K. and de Cabo, R. (2012) "Impact of caloric restriction on health and survival in rhesus monkeys from the NIA study" *Nature* **489**: 318-321.

McCay, C. M., Crowell, M. F. and Maynard, L. A. (1935) "The Effect of Retarded Growth Upon the Length of Life Span and Upon the Ultimate Body Size: One Figure" *The Journal of Nutrition* **10**: 63-79.

Michaelis, E. K., Wang, X., Pal, R., Bao, X., Hascup, K. N., Wang, Y., Wang, W. T., Hui, D., Agbas, A., Choi, I. Y., Belousov, A. and Gerhardt, G. A. (2011) "Neuronal Glud1 (glutamate dehydrogenase 1) over-expressing mice: increased glutamate formation and synaptic release, loss of synaptic activity, and adaptive changes in genomic expression" *Neurochem Int* **59**: 473-481.

Molecular Probes Invitrogen detection technologies (2007) "SYPRO® Ruby Protein Gel Stain, Product information".

Moser, B. K. and Stevens, G. R. (1992) "Homogeneity of Variance in the Two-Sample Means Test" *The American Statistician* **46**: 19-21.

Murphy, Michael P. (2009) "How mitochondria produce reactive oxygen species" *Biochemical Journal* **417**: 1-13.

^{NH}*Dye*AGNOSTICS (2011) "G-Dye Imaging Properties".

^{NH}*Dye*AGNOSTICS (2012) "Refraction-2D™-Produkt-Guide".

^{NH}*Dye*AGNOSTICS (2012-2013) "Protein Labeling Kits eBrochure".

Ojaimi, J., Masters, C. L., Opeskin, K., McKelvie, P. and Byrne, E. (1999) "Mitochondrial respiratory chain activity in the human brain as a function of age" *Mech Ageing Dev* **111**: 39-47.

Olgun, A., Akman, S., Serdar, M. A. and Kutluay, T. (2002) "Oxidative phosphorylation enzyme complexes in caloric restriction" *Experimental Gerontology* **37**: 639-645.

Omodei, D. and Fontana, L. (2011) "Calorie restriction and prevention of age-associated chronic disease" *FEBS Lett* **585**: 1537-1542.

Omodei, D., Pucino, V., Labruna, G., Procaccini, C., Galgani, M., Perna, F., Pirozzi, D., De Caprio, C., Marone, G., Fontana, L., Contaldo, F., Pasanisi, F., Matarese, G. and Sacchetti, L. (2015) "Immune-metabolic profiling of anorexic patients reveals an anti-oxidant and anti-inflammatory phenotype" *Metabolism* **64**: 396-405.

Ott, A., Breteler, M. M., van Harskamp, F., Claus, J. J., van der Cammen, T. J., Grobbee, D. E. and Hofman, A. (1995) "Prevalence of Alzheimer's disease and vascular dementia: association with education. The Rotterdam study" *BMJ : British Medical Journal* **310**: 970-973.

Papa, S., Martino, P. L., Capitanio, G., Gaballo, A., Rasmo, D. D., Signorile, A. and Petruzzella, V. (2012). "The Oxidative Phosphorylation System in Mammalian Mitochondria". Scatena, R., Bottoni, P. and Giardina, B. *Advances in mitochondrial medicine*. Dordrecht Heidelberg London New York, Springer. **1:** 3-38.

Paradies, G., Petrosillo, G., Paradies, V. and Ruggiero, F. M. (2011) "Mitochondrial dysfunction in brain aging: role of oxidative stress and cardiolipin" *Neurochem Int* **58**: 447-457.

Pfeiffer, K., Gohil, V., Stuart, R. A., Hunte, C., Brandt, U., Greenberg, M. L. and Schägger, H. (2003) "Cardiolipin Stabilizes Respiratory Chain Supercomplexes" *Journal of Biological Chemistry* **278**: 52873-52880.

Plum, S., Steinbach, S., Abel, L., Marcus, K., Helling, S. and May, C. (2014) "Proteomics in neurodegenerative diseases: Methods for obtaining a closer look at the neuronal proteome" *Proteomics Clin Appl*.

Rabilloud, T., Vuillard, L., Gilly, C. and Lawrence, J. J. (1994) "Silver-staining of proteins in polyacrylamide gels: a general overview" *Cell Mol Biol (Noisy-le-grand)* **40**: 57-75.

Reifschneider, N. H. (2006) "Elektrophoretische und massenspektrometrische Analyse des mitochondrialen Proteoms von Eukaryonten" Doctoral Thesis, Technische Universität Darmstadt.
Reifschneider, N. H., Goto, S., Nakamoto, H., Takahashi, R., Sugawa, M., Dencher, N. A. and Krause, F. (2006) "Defining the Mitochondrial Proteomes from Five Rat Organs in a Physiologically Significant Context Using 2D Blue-Native/SDS-PAGE" *J Proteome Research* **5**: 1117-1132.
Reisinger, V. and Eichacker, L. A. (2007) "How to analyze protein complexes by 2D blue native SDS-PAGE" *Proteomics* **7 Suppl 1**: 6-16.
Ribeiro, L. C., Rodrigues, L., Quincozes-Santos, A., Tramontina, A. C., Bambini-Junior, V., Zanotto, C., Diehl, L. A., Biasibetti, R., Kleinkauf-Rocha, J., Dalmaz, C., Goncalves, C.-A. and Gottfried, C. (2012) "Caloric restriction improves basal redox parameters in hippocampus and cerebral cortex of Wistar rats" *Brain Research* **1472**: 11-19.
Roth, L., Daunderer, M. and Kormann, K. (1988). "Giftpflanzen - Pflanzengifte". Landsberg/München, ecomed Verlagsgesellschaft mbH.
Saager, M. (2010) "Abhängigkeit des Lipidmusters in biologischen Membranen vom physiologischen Zustand" Diploma Thesis, Technische Universität Darmstadt.
Sabar, M., Balk, J. and Leaver, C. J. (2005) "Histochemical staining and quantification of plant mitochondrial respiratory chain complexes using blue-native polyacrylamide gel electrophoresis" *Plant J* **44**: 893-901.
Schäfer, E., Seelert, H., Reifschneider, N. H., Krause, F., Dencher, N. A. and Vonck, J. (2006) "Architecture of active mammalian respiratory chain supercomplexes" *J Biol Chem* **281**: 15370-15375.
Schagger, H. (1995) "Quantification of oxidative phosphorylation enzymes after blue native electrophoresis and two-dimensional resolution: normal complex I protein amounts in Parkinson's disease conflict with reduced catalytic activities" *Electrophoresis* **16**: 763-770.
Schägger, H. and Pfeiffer, K. (2000) "Supercomplexes in the respiratory chain of yeast and mammalian mitochondria" *The EMBO Journal* **19**: 1777-1783.
Schägger, H. and von Jagow, G. (1987) "Tricine-sodium dodecyl sulfate-polyacrylamide gel electrophoresis for the separation of proteins in the range from 1 to 100 kDa" *Anal Biochem* **166**: 368-379.
Schon, E. A. and Area-Gomez, E. (2013) "Mitochondria-associated ER membranes in Alzheimer disease" *Molecular and Cellular Neuroscience* **55**: 26-36.
Schrattenholz, A. (2001). "Methoden der Proteomforschung: Molekulare Analyse der Proteinexpression", Spektrum Akademischer Verlag.
Schwarz, T. L. (2013) "Mitochondrial Trafficking in Neurons" *Cold Spring Harbor Perspectives in Biology* **5**.
Shinitzky, M. and Barenholz, Y. (1978) "Fluidity parameters of lipid regions determined by fluorescence polarization" *Biochimica Biophysica Acta* **515**: 367-394.
Shokolenko, I. N., Ledoux, S. P. and Wilson, G. L. (2007). "Mitochondrial DNA Damage and Repair". Schaffer, S. W. and Suleiman, M.-S. *Mitochondria - The Dynamic Organelle*. New York, Springer. **15:** 323-347.
Siegel, M. P., Kruse, S. E., Percival, J. M., Goh, J., White, C. C., Hopkins, H. C., Kavanagh, T. J., Szeto, H. H., Rabinovitch, P. S. and Marcinek, D. J. (2013) "Mitochondrial-targeted peptide rapidly improves mitochondrial energetics and skeletal muscle performance in aged mice" *Aging Cell* **12**: 763-771.
Sigma-Aldrich (2008) "Colorimetric Alkaline Phosphatase and Peroxidase Substrate Detection Systems" *Biofiles* **3.4**.
Sigma-Aldrich (2014a) structure of "1,6-Diphenyl-1,3,5-hexatriene", CAS-no. 1720-32-7.
Sigma-Aldrich (2014b) structure of "Coomassie Brilliant Blue G-250", CAS-no. 6104-58-1.
Sigma-Aldrich (2014c) structure of "SDS", CAS-no. 151-21-3.

Silvestri, E., Lombardi, A., Cioffi, F. and Goglia, F. (2015) "BN-PAGE-based approach to study thyroid hormones and mitochondrial function" *Methods Mol Biol* **1241**: 111-122.
Silvestri, E., Lombardi, A., Glinni, D., Coelho, C., Senese, R., Cioffi, F., Lanni, A., Goglia, F., Moreno, M. and de Lange, P. (2011) "Mammalian mitochondrial proteome and its functions: current investigative techniques and future perspectives on ageing and diabetes." *Journal of Integrated Omics* **1**: 17-27.
Smejkal, G. B., Robinson, M. H. and Lazarev, A. (2004) "Comparison of fluorescent stains: Relative photostability and differential staining of proteins in two-dimensional gels" *ELECTROPHORESIS* **25**: 2511-2519.
Sohal, R. S., Mockett, R. J. and Orr, W. C. (2002) "Mechanisms of aging: an appraisal of the oxidative stress hypothesis" *Free Radic Biol Med* **33**: 575-586.
Söhn, M. (2010) "Der Einfluss von Altern und Kalorienreduktion auf das mitochondriale Proteom des Rattenhirns." Diploma Thesis, Technische Universität Darmstadt.
Song, D. D. and Haber, S. N. (2000) "Striatal Responses to Partial Dopaminergic Lesion: Evidence for Compensatory Sprouting" *The Journal of Neuroscience* **20**: 5102-5114.
Speakman, J. R. (2005) "Body size, energy metabolism and lifespan" *J Exp Biol* **208**: 1717-1730.
Speakman, J. R., Talbot, D. A., Selman, C., Snart, S., McLaren, J. S., Redman, P., Krol, E., Jackson, D. M., Johnson, M. S. and Brand, M. D. (2004) "Uncoupled and surviving: individual mice with high metabolism have greater mitochondrial uncoupling and live longer" *Aging Cell* **3**: 87-95.
Spillantini, M. G., Schmidt, M. L., Lee, V. M. Y., Trojanowski, J. Q., Jakes, R. and Goedert, M. (1997) "[alpha]-Synuclein in Lewy bodies" *Nature* **388**: 839-840.
Storck, T., Schulte, S., Hofmann, K. and Stoffel, W. (1992) "Structure, expression, and functional analysis of a Na(+)-dependent glutamate/aspartate transporter from rat brain" *Proc Natl Acad Sci U S A* **89**: 10955-10959.
Sugawa, M., Coper, H., Schulze, G., Yamashina, I., Krause, F. and Dencher, N. A. (1996) "Impaired plasticity of neurons in aging. Biochemical, biophysical, and behavioral studies" *Ann N Y Acad Sci* **786**: 274-282.
Tatarkova, Z., Kuka, S., Racay, P., Lehotsky, J., Dobrota, D., Mistuna, D. and Kaplan, P. (2011) "Effects of aging on activities of mitochondrial electron transport chain complexes and oxidative damage in rat heart" *Physiol Res* **60**: 281-289.
The Lancet (2015) "Global, regional, and national age-sex specific all-cause and cause-specific mortality for 240 causes of death, 1990-2013: a systematic analysis for the Global Burden of Disease Study 2013" *Lancet* **385**: 117-171.
Thews, G., Mutschler, E. and Vaupel, P. (1999). "Anatomie, Physiologie, Pathophysiologie des Menschen". Stuttgart, Wissenschaftliche Verlagsgesellschaft mbH Stuttgart.
Thilmany, S. C. (2013) "Das mitochondriale Proteom von Rattus norvegicus in Abhängigkeit von Alter und Kalorienrestriktion." Doctoral Thesis, Technische Universität Darmstadt.
Tian, L., Cai, Q. and Wei, H. (1998) "Alterations of antioxidant enzymes and oxidative damage to macromolecules in different organs of rats during aging" *Free Radic Biol Med* **24**: 1477-1484.
Tsukihara, T., Aoyama, H., Yamashita, E., Tomizaki, T., Yamaguchi, H., Shinzawa-Itoh, K., Nakashima, R., Yaono, R. and Yoshikawa, S. (1996) "The Whole Structure of the 13-Subunit Oxidized Cytochrome c Oxidase at 2.8A" *Science* **272**: 1136-1144.
Van Der Staay, F. J. and Blokland, A. (1996) "Behavioral differences between outbred Wistar, inbred Fischer 344, Brown Norway, and hybrid Fischer 344 × Brown Norway rats" *Physiology & Behavior* **60**: 97-109.
Verma, N., Pink, M., Petrat, F., Rettenmeier, A. W. and Schmitz-Spanke, S. (2015) "Proteomic analysis of human bladder epithelial cells by 2D blue native SDS-PAGE

reveals TCDD-induced alterations of calcium and iron homeostasis possibly mediated by nitric oxide" *J Proteome Res* **14**: 202-213.
Voet, D., Voet, J. G. and Pratt, C. W. (2002). "Lehrbuch der Biochemie". Weinheim, Wiley-VCH Verlag GmbH & Co. KGaA.
Vorbeck, M. L., Martin, A. P., Long, J. W., Jr., Smith, J. M. and Orr, R. R., Jr. (1982) "Aging-dependent modification of lipid composition and lipid structural order parameter of hepatic mitochondria" *Arch Biochem Biophys* **217**: 351-361.
Wallace, D. C. (2010) "Mitochondrial DNA mutations in disease and aging" *Environ Mol Mutagen* **51**: 440-450.
Watt, I. N., Montgomery, M. G., Runswick, M. J., Leslie, A. G. and Walker, J. E. (2010) "Bioenergetic cost of making an adenosine triphosphate molecule in animal mitochondria" *Proc Natl Acad Sci U S A* **107**: 16823-16827.
Weiß, C. (2013). "Basiswissen Medizinische Statistik". Berlin-Heidelberg, Springer-Verlag.
Weyerer, S. (2005). "Gesundheitsberichterstattung des Bundes Heft 28 "Altersdemenz"". Berlin, Robert Koch-Institut.
Wittig, I. (2008) "Native Elektrophorese von Membranproteinen" *BioSpektrum* **05**: 499-501.
Wittig, I., Carrozzo, R., Santorelli, F. M. and Schagger, H. (2007) "Functional assays in high-resolution clear native gels to quantify mitochondrial complexes in human biopsies and cell lines" *Electrophoresis* **28**: 3811-3820.
Wittig, I. and Schagger, H. (2008) "Structural organization of mitochondrial ATP synthase" *Biochim Biophys Acta* **1777**: 592-598.
Wood, W. G., Schroeder, F., Igbavboa, U., Avdulov, N. A. and Chochina, S. V. (2002) "Brain membrane cholesterol domains, aging and amyloid beta-peptides" *Neurobiology of Aging* **23**: 685-694.
Wortmann, M., Fletcher, S. and Gillings, D. (2014). "Foreword". *World Alzheimer Report 2014, Dementia and Risk Reduction, An analysis of protective and modifiable factors*. London, Alzheimer's Disease International (ADI) 1-3.
Zigmond, M. J. (1997) "Do Compensatory Processes Underlie the Preclinical Phase of Neurodegenerative Disease? Insights from an Animal Model of Parkinsonism" *Neurobiology of Disease* **4**: 247-253.

7 Supplements

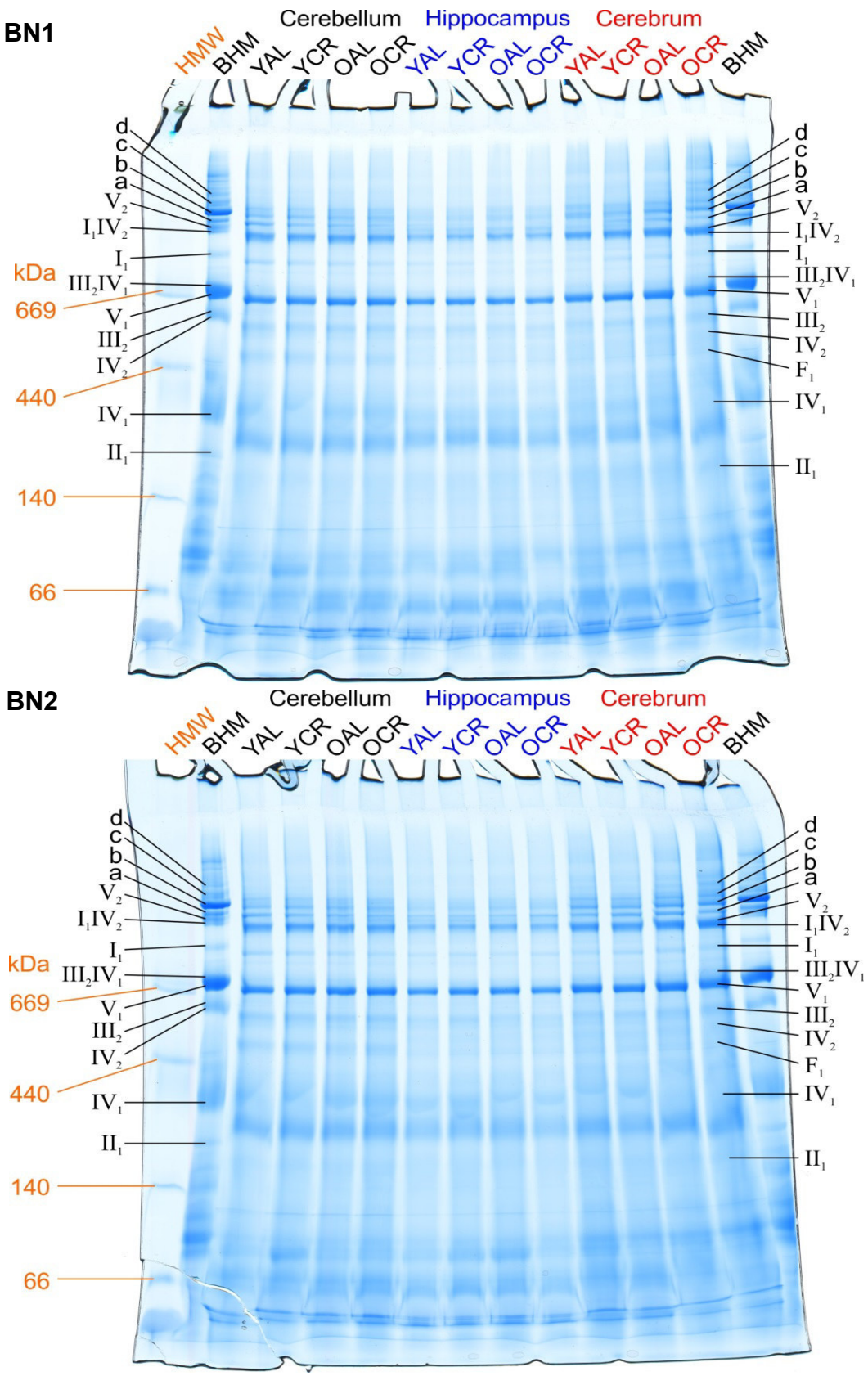

Fig. 7.1: Images BN1 and BN2 of CBBG stained BN gels. For each brain area, and each animal group (YAL, YCR, OAL, OCR) 100 µg proteins were solubilised with 8 g dig. / g and separated by BN PAGE, followed by CBBG staining. 70 µg BHM (b. sol. d/p: 3g/g) and HMW (marked in orange) served as standard, OxPhos complexes and supercomplexes are marked. a = I_1III_2, b = $I_1III_2IV_1$, c = $I_1III_2IV_2$, d = $I_1III_2IV_3$.

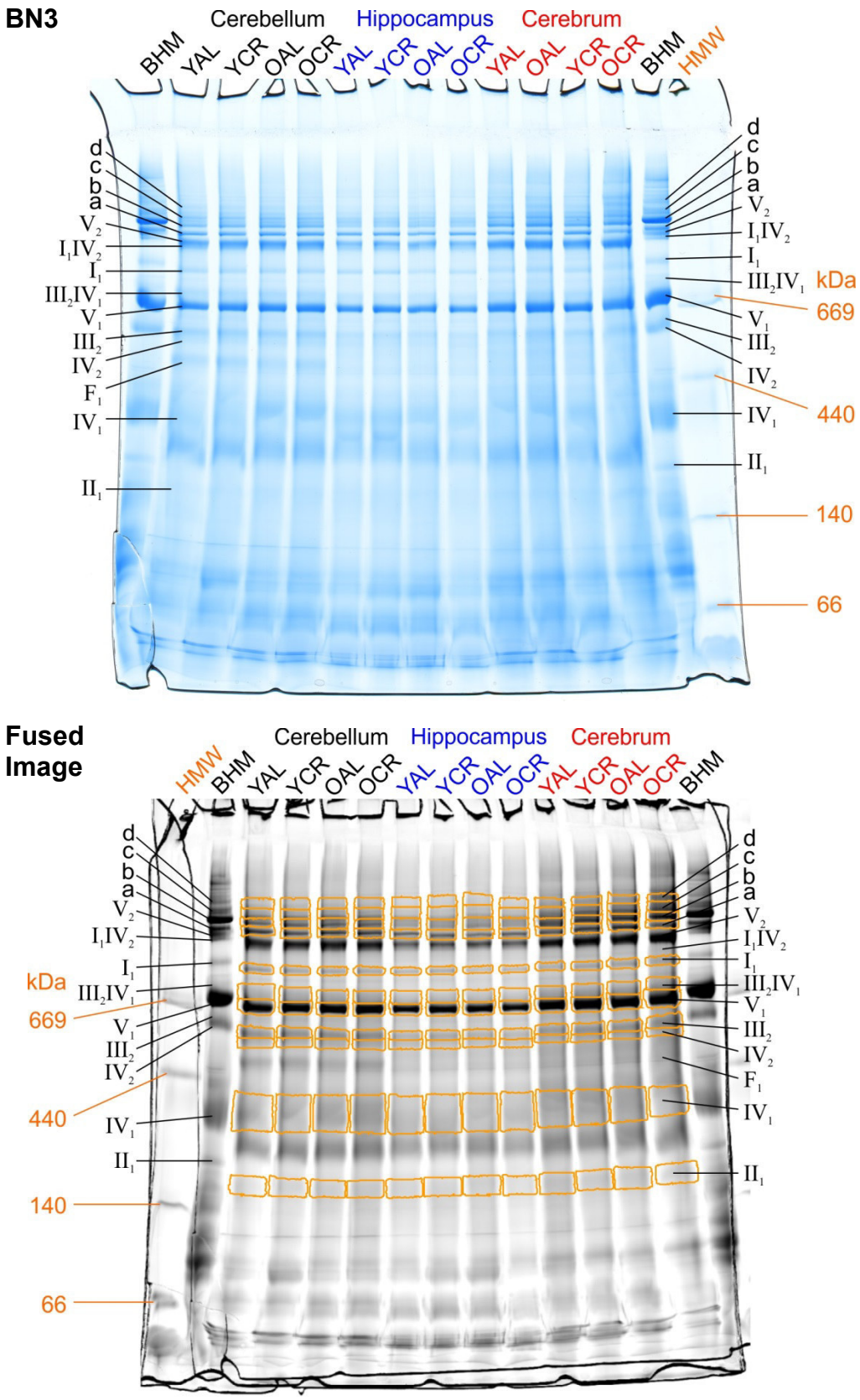

Fig. 7.2: Image BN3 of CBBG stained BN gel and fused image of grey scale images BN1-3. BN1: For each brain area, and each animal group (YAL, YCR, OAL, OCR) 100 µg proteins were solubilised with 8 g dig. / g and separated by BN PAGE, followed by CBBG staining. 70 µg BHM (b. sol. d/p: 3g/g) and HMW (marked in orange) served as standard. **Fused image:** Grey scale images of BN gels (BN1, BN2 and BN3) were fused and analysed in Delta2D for quantitation of protein amount. OxPhos complexes and supercomplexes are marked. a = I_1III_2, b = $I_1III_2IV_1$, c = $I_1III_2IV_2$, d = $I_1III_2IV_3$.

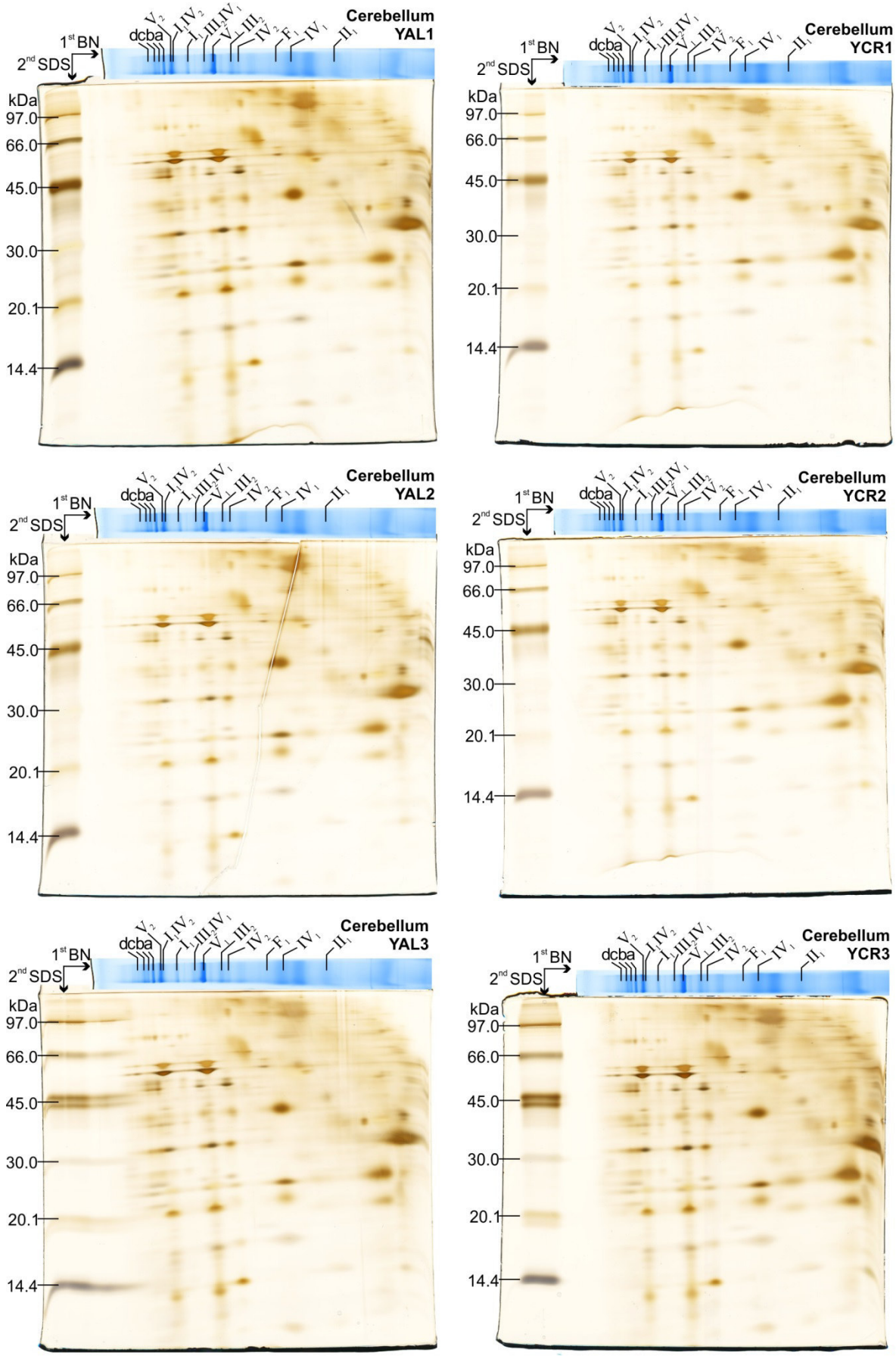

Fig. 7.3: Cerebellum, YAL and YCR: Images of silver stained2D-BN/SDS gels. 120 µg mitochondrial proteins (b. sol. d/p: 8g/g) of each sample were separated by 2D-BN/SDS PAGE. The image of the CBBG stained BN gel lane was arranged horizontally above the image of the silver stained SDS gel, for assignment of bands. Masses of LMW were marked. a = I_1III_2, b = $I_1III_2IV_1$, c = $I_1III_2IV_2$, d = $I_1III_2IV_3$

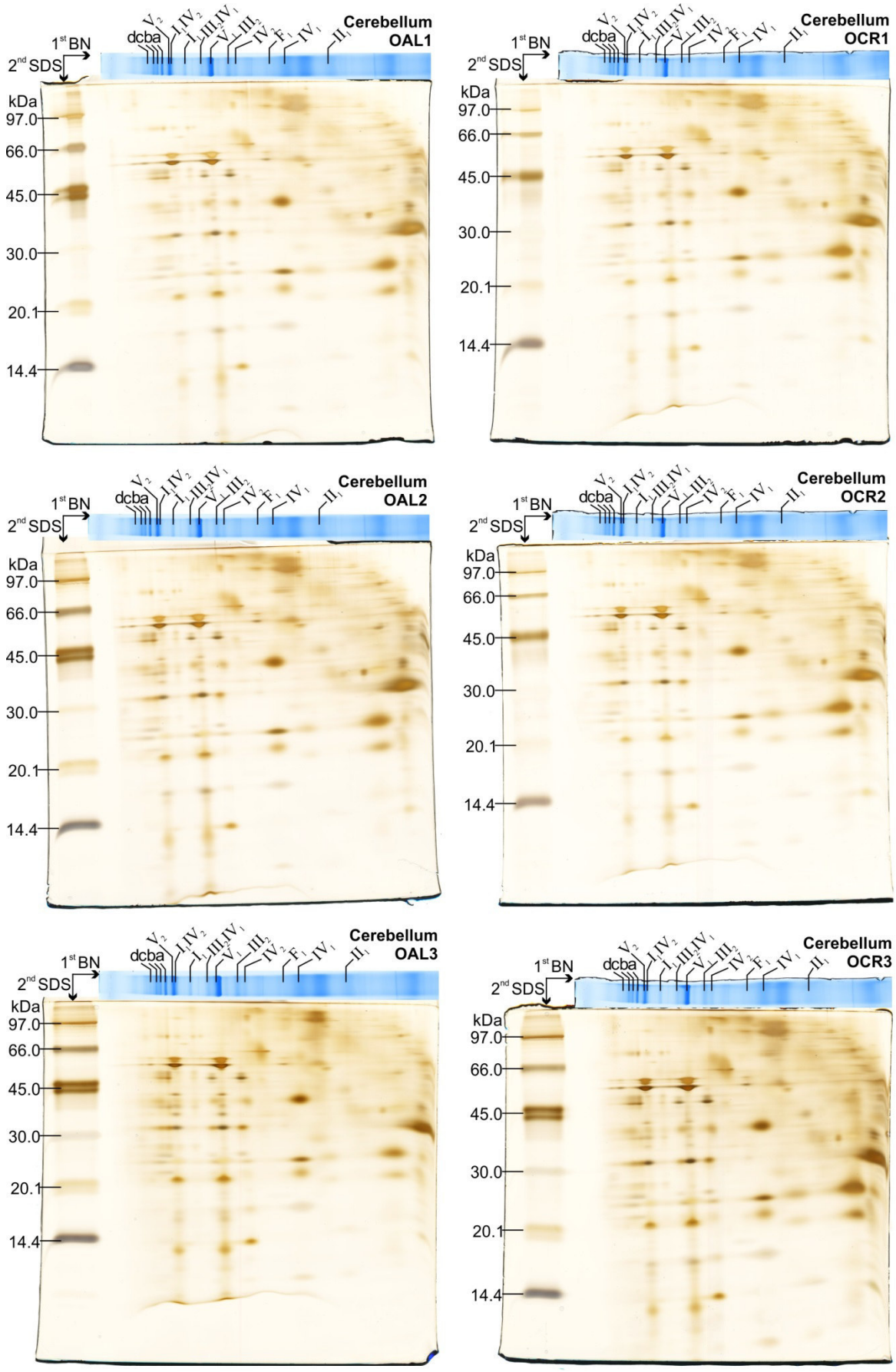

Fig. 7.4: Cerebellum, OAL and OCR: Images of silver stained2D-BN/SDS gels. 120 µg mitochondrial proteins (b. sol. d/p: 8g/g) of each sample were separated by 2D-BN/SDS PAGE. The image of the CBBG stained BN gel lane was arranged horizontally above the image of the silver stained SDS gel, for assignment of bands. Masses of LMW were marked. a = I_1III_2, b = $I_1III_2IV_1$, c = $I_1III_2IV_2$, d = $I_1III_2IV_3$

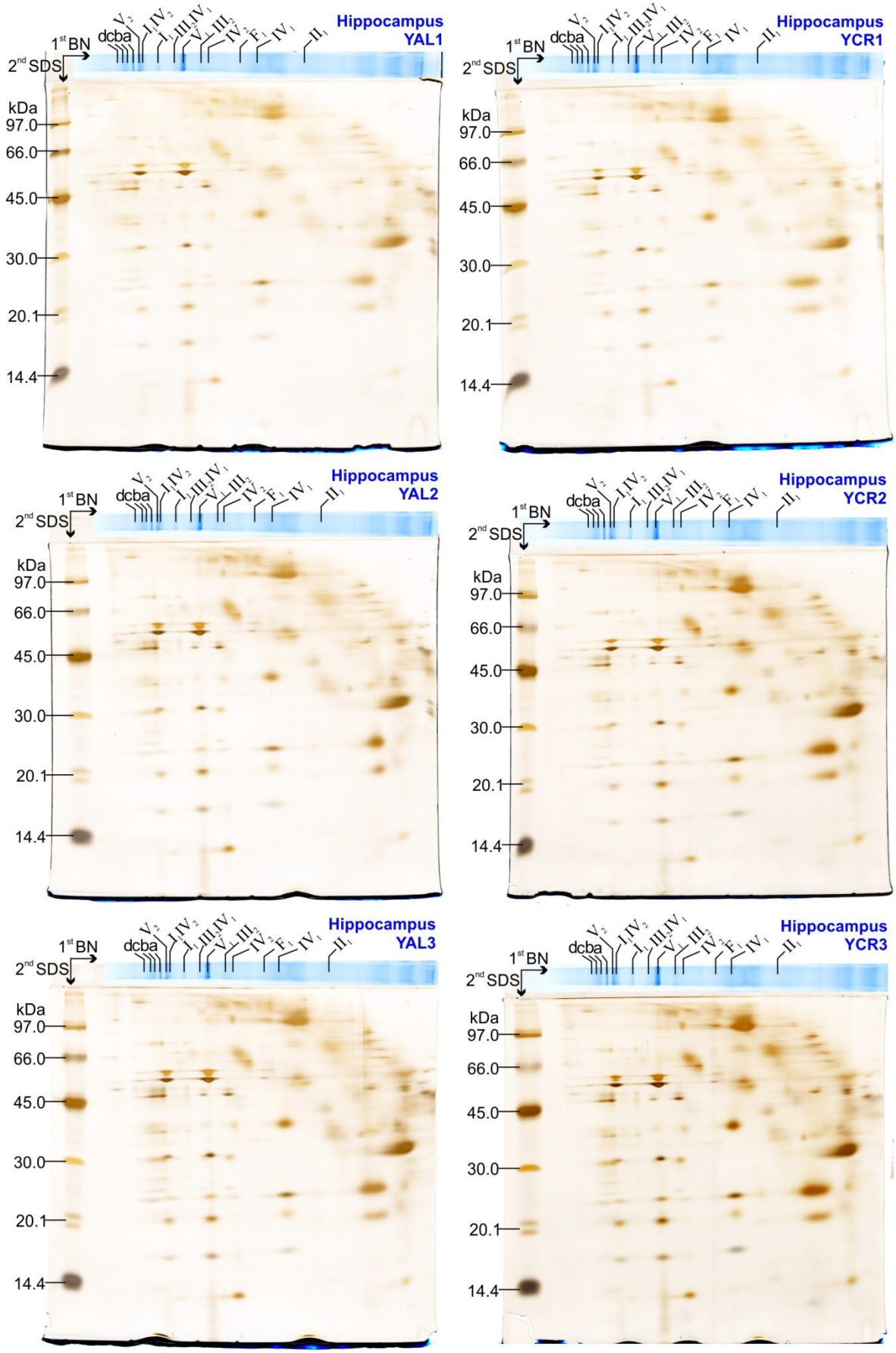

Fig. 7.5: Hippocampus, YAL and YCR: Images of silver stained2D-BN/SDS gels. 120 µg mitochondrial proteins (b. sol. d/p: 8g/g) of each sample were separated by 2D-BN/SDS PAGE. The image of the CBBG stained BN gel lane was arranged horizontally above the image of the silver stained SDS gel, for assignment of bands. Masses of LMW were marked. a = I_1III_2, b = $I_1III_2IV_1$, c = $I_1III_2IV_2$, d = $I_1III_2IV_3$

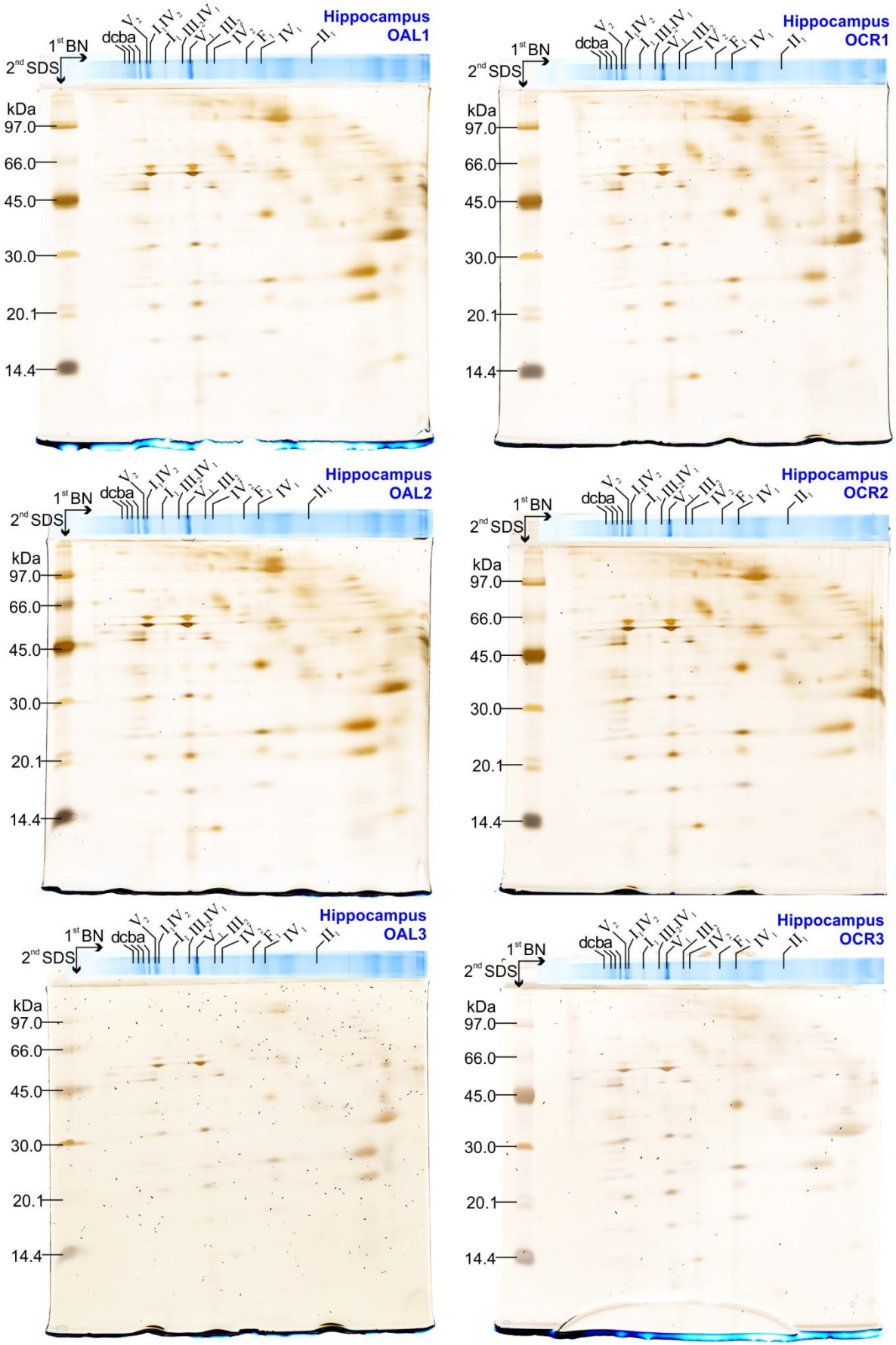

Fig. 7.6: Hippocampus, OAL and OCR: Images of silver stained2D-BN/SDS gels. 120 µg mitochondrial proteins (b. sol. d/p: 8g/g) of each sample were separated by 2D-BN/SDS PAGE. The image of the CBBG stained BN gel lane was arranged horizontally above the image of the silver stained SDS gel, for assignment of bands. Masses of LMW were marked. a = I_1III_2, b = $I_1III_2IV_1$, c = $I_1III_2IV_2$, d = $I_1III_2IV_3$

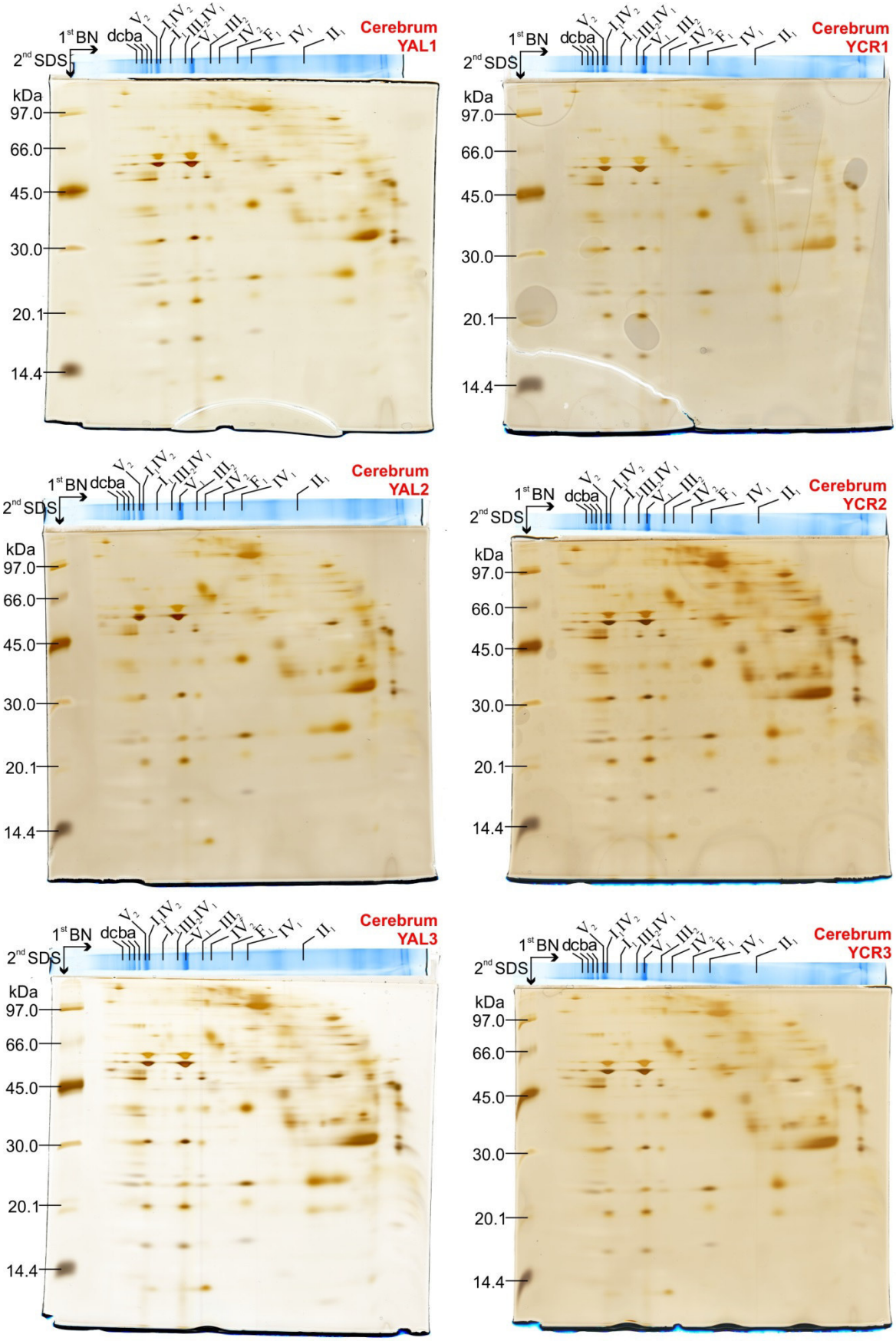

Fig. 7.7: Cerebrum, YAL and YCR: Images of silver stained2D-BN/SDS gels. 120 µg mitochondrial proteins (b. sol. d/p: 8g/g) of each sample were separated by 2D-BN/SDS PAGE. The image of the CBBG stained BN gel lane was arranged horizontally above the image of the silver stained SDS gel, for assignment of bands. Masses of LMW were marked. a = I_1III_2, b = $I_1III_2IV_1$, c = $I_1III_2IV_2$, d = $I_1III_2IV_3$

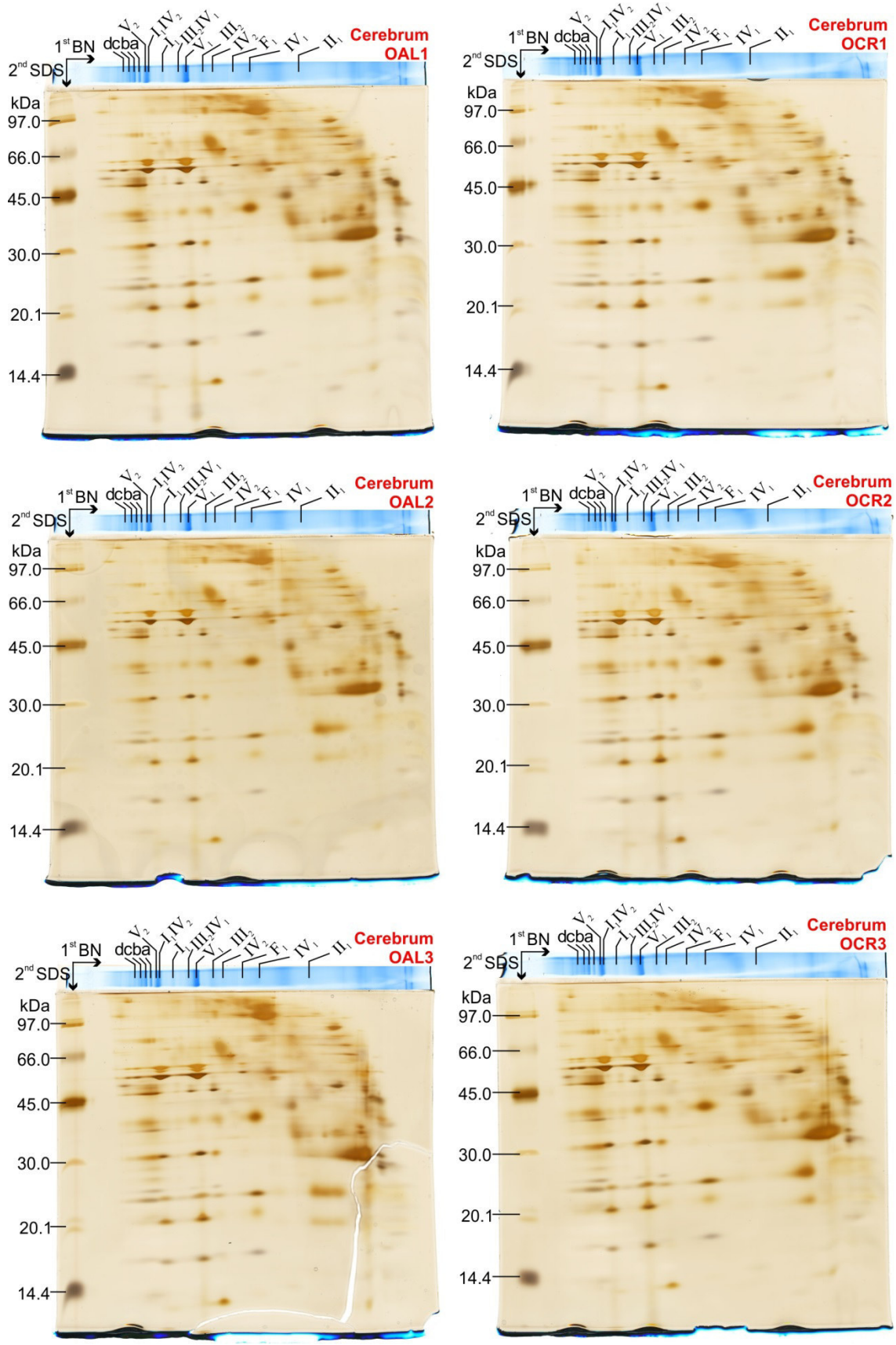

Fig. 7.8: Cerebrum, OAL and OCR: Images of silver stained2D-BN/SDS gels. 120 µg mitochondrial proteins (b. sol. d/p: 8g/g) of each sample were separated by 2D-BN/SDS PAGE. The image of the CBBG stained BN gel lane was arranged horizontally above the image of the silver stained SDS gel, for assignment of bands. Masses of LMW were marked. a = I_1III_2, b = $I_1III_2IV_1$, c = $I_1III_2IV_2$, d = $I_1III_2IV_3$

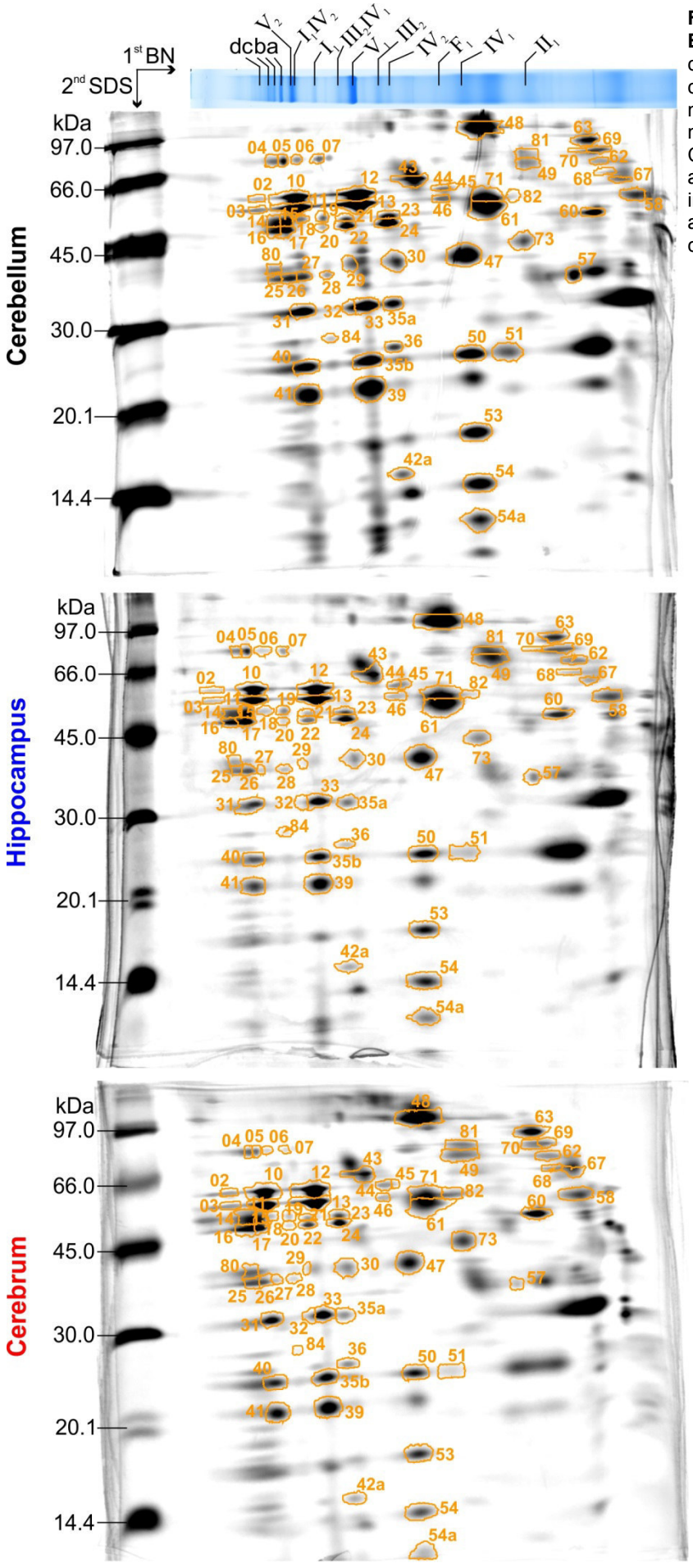

Fig. 7.9: Fused images of 2D-BN/SDS grey scale images for cerebellum, hippocampus and cerebrum. Protein spots were marked as well as the protein marker LMW. The image of the CBBG stained BN gel lane was arranged horizontally above the image of the first fused image. a = I_1III_2, b = $I_1III_2IV_1$, c = $I_1III_2IV_2$, d = $I_1III_2IV_3$

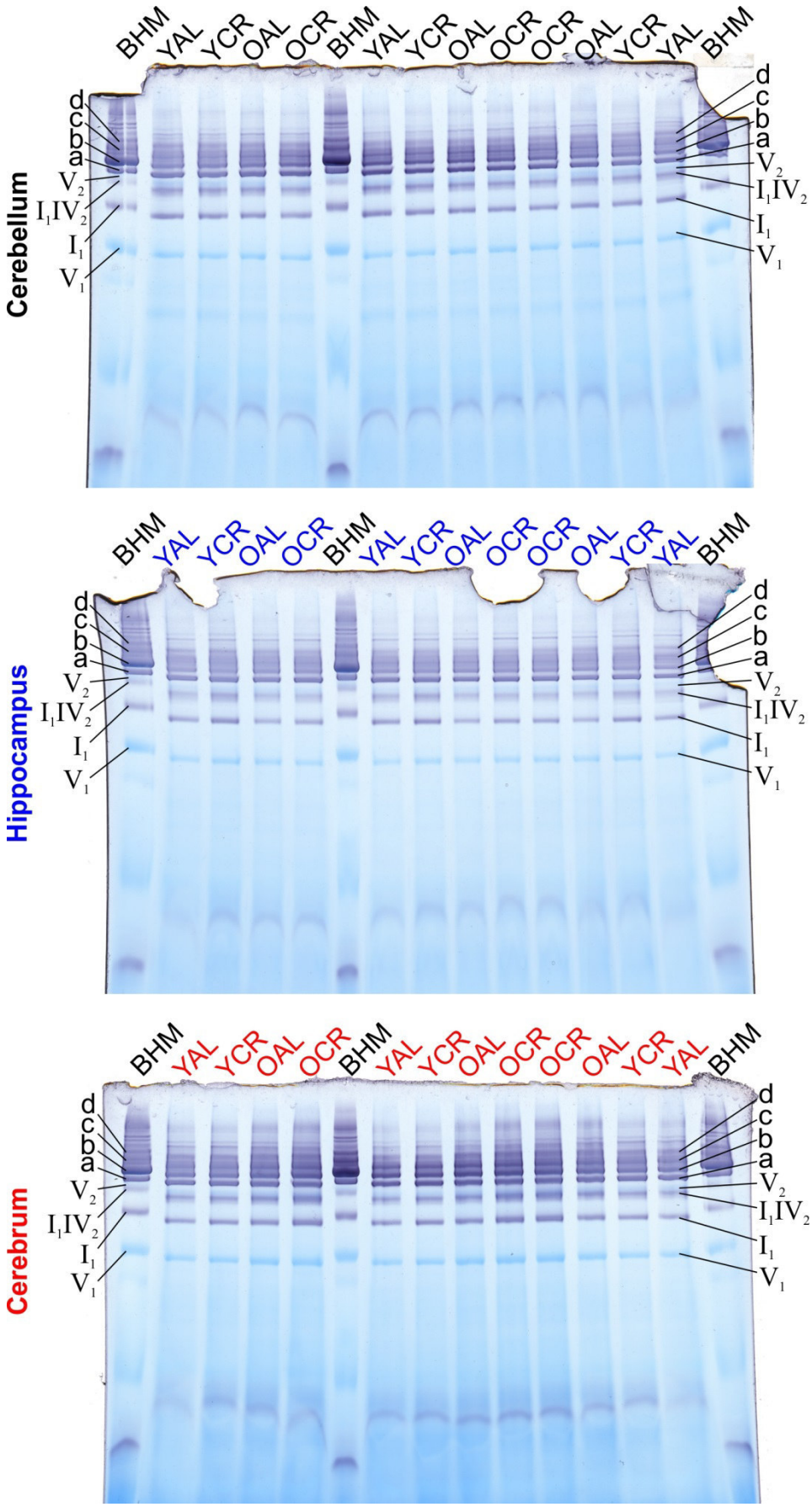

Fig. 7.10: Images of BN gels, stained in complex I in-gel activity test solution for each brain tissue. Each lane contained 100 µg of RBM proteins (b. sol. d/p: 8g/g). Three lanes of 70 µg (b. sol. d/p: 3g/g) BHM each served as standard.

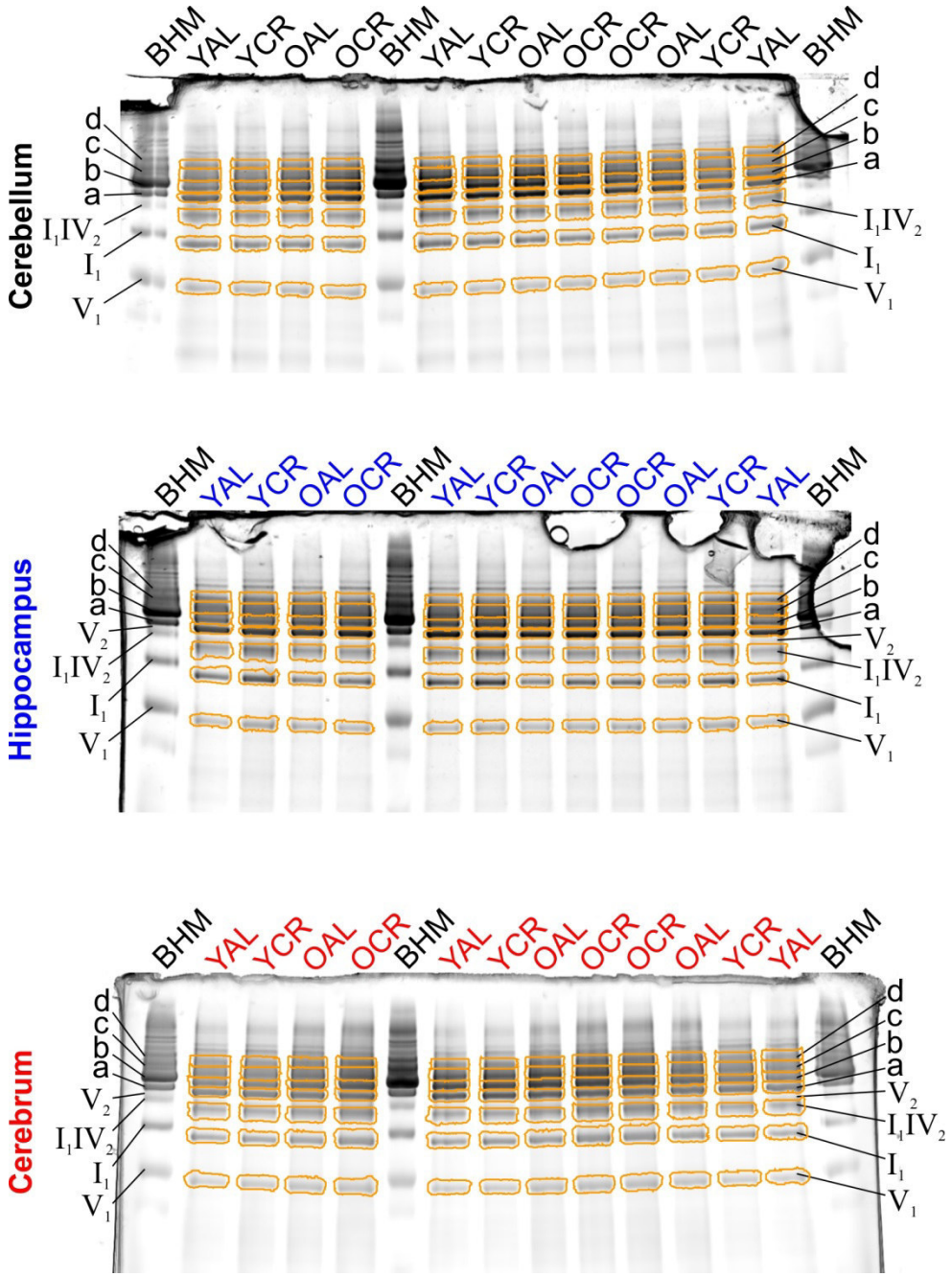

Fig. 7.11: Fused images of grey scale images from CI in-gel activity test for cerebellum, hippocampus and cerebrum.

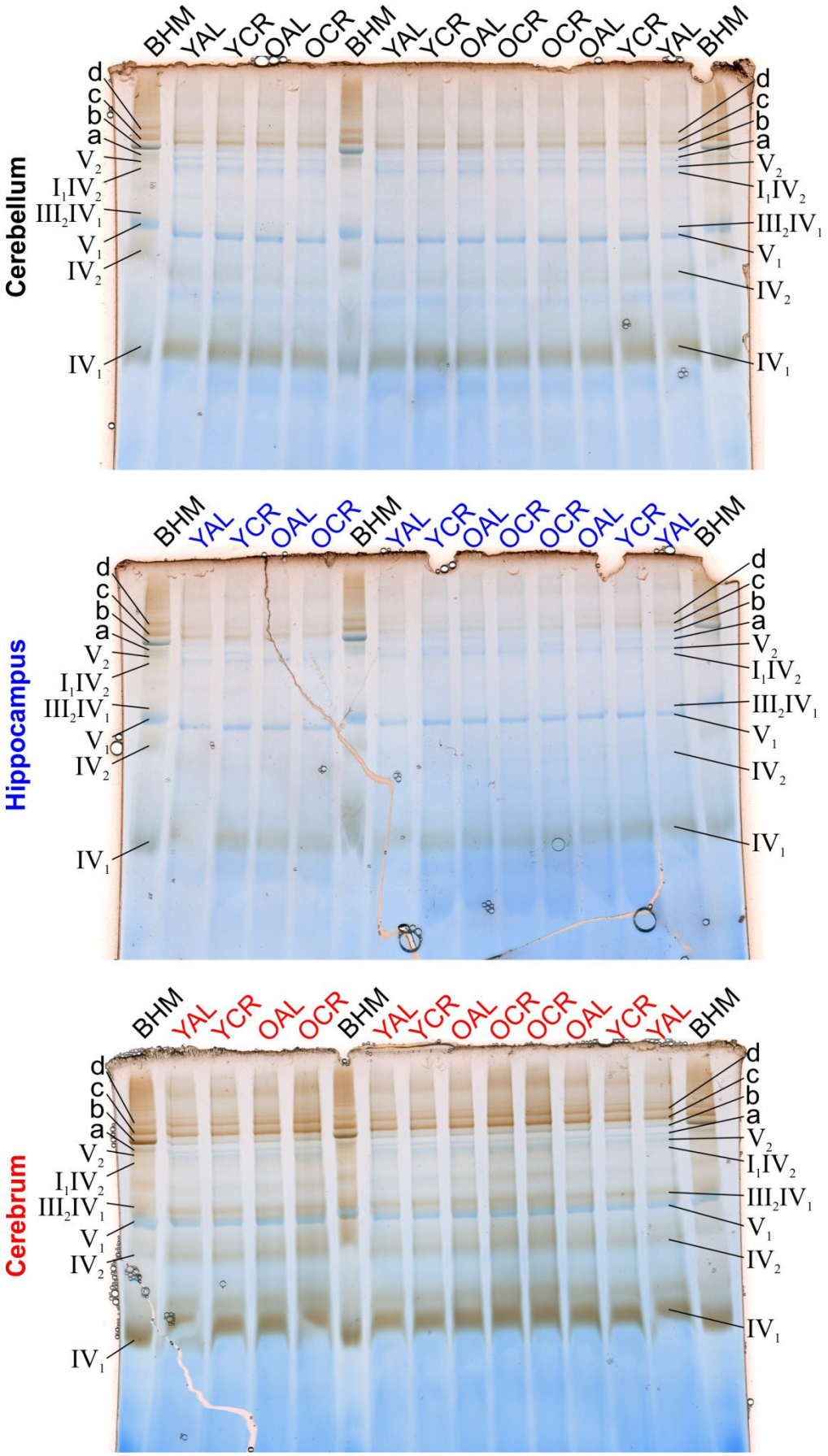

Fig. 7.12: Images of BN gels, stained in complex IV in-gel activity test solution for each brain tissue. Each lane contained 100 µg of RBM proteins (b. sol. d/p: 8g/g). Three lanes of 70 µg (b. sol. d/p: 3g/g) BHM each served as standard.

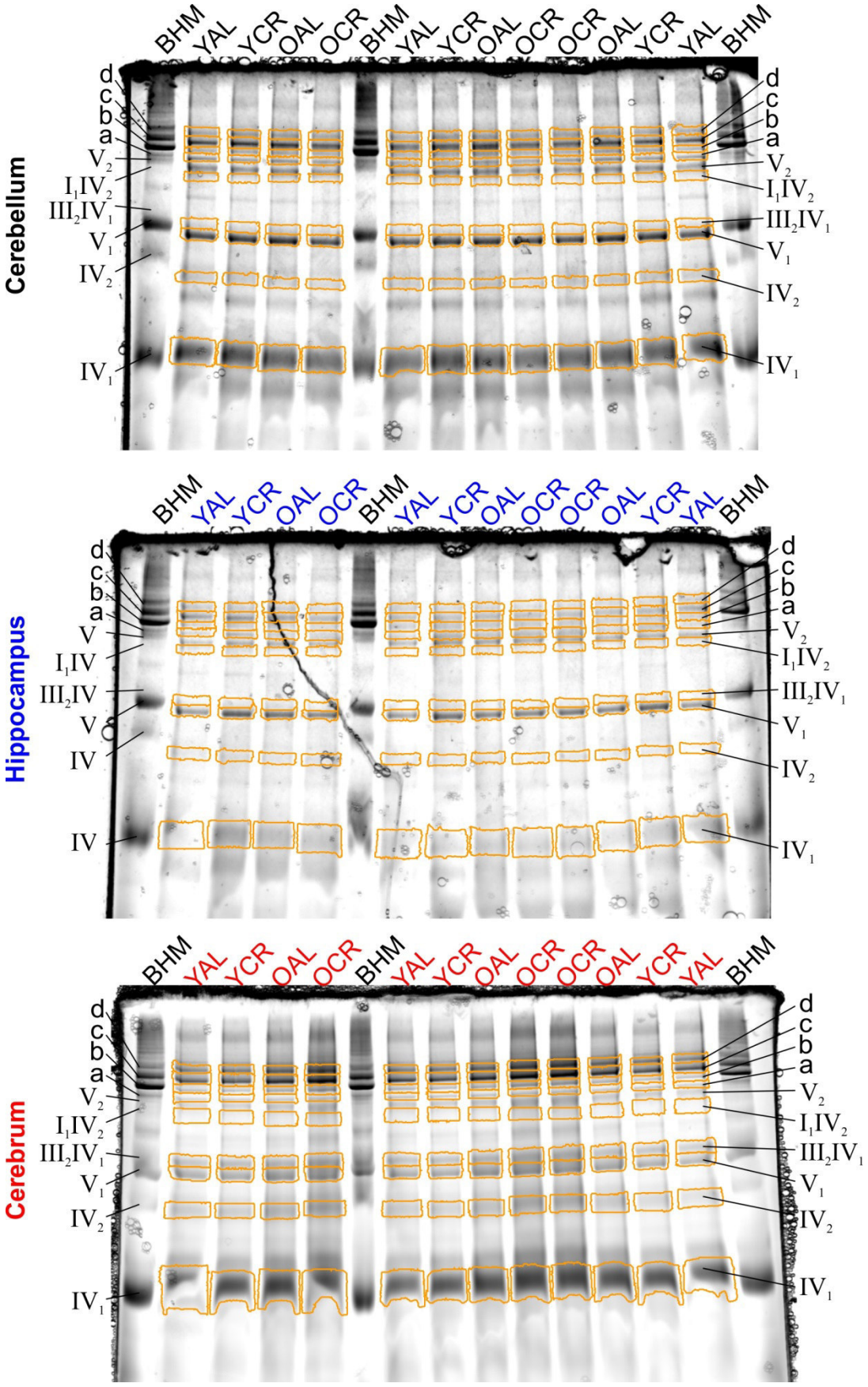

Fig. 7.13: Fused images of grey scale images from CIV in-gel activity test for cerebellum, hippocampus and cerebrum.

Curriculum Vitae

Personal details

Name	Manuela Kratochwil
Academic title	Dipl. Chem. / graduate chemist
Place of Residence	Potsdamer Str. 2, D-64372 Ober-Ramstadt, Germany
Date, Place of Birth	19.09.1980, Wiesbaden, Germany
Nationality	German

Academic program

Aug. 2010 - Sept. 2015	Research Assistant and PhD student at research group of Prof. Dr. N. A. Dencher, Clemens-Schöpf-Institute for Biochemistry, Technische Universität Darmstadt, Germany Research topics: analysis of ageing processes, age related diseases and effects of calorie restriction by membrane and proteome research Methods: 1D- and 2D-BN/SDS-PAGE, staining and labelling techniques, e.g. DIGE, Western Blot, MALDI-MS, UV/Vis- and fluorescence spectroscopy Further duties: responsible for international guest scientists, students, practical courses and tutorials
July 2011 - June 2014	Member of DFG-funded Graduate College 1657 of TU Darmstadt: “Molecular and cellular responses to ionizing radiation”
Jan. 2010 - June 2010	Guest scientist at research group of Dr. I. Köper, School of Chemical and Physical Sciences, Flinders University of South Australia, Adelaide, Australia Methods: buildup of tethered bilayer lipid membranes and integration of proteins, impedance- and surface plasmon resonance spectroscopy Further duties: organisation of laboratory startup, communications and collaboration with other departments of the university, teaching of students
Oct. 2009	Diploma Examination with the overall grade: good (2.0)
Jan. - Oct. 2009	Student Research Assistant and Diploma Thesis with the title: Synthesis and Properties of Two- and Threefold Triazolo-annulated Azines, grade: very good (1.3), at the research group of Prof. Dr. H. Detert, Institute for Organic Chemistry, Johannes Gutenberg-Universität Mainz, Germany Methods: multi-step organic synthesis of potential liquid crystalline fluorescent dyes, thinlayer and column chromatography, IR- and NMR-spectroscopy, UV/Vis- and fluorescence spectroscopy
Apr. 2003 - Oct. 2009	German Diploma studies Biomedical Chemistry at Universität Mainz, Germany Main subjects of advanced study period: Analytical Chemistry, Biochemistry, Biophysics, Organic Chemistry

Employment history

Nov. - Dec. 2009 and during Semester Breaks	Full time reserve pool employee as Bank Business Management Assistant at Nassauische Sparkasse Wiesbaden, Germany Duties: Customer service, handling of the cash, training of apprentice and temporary personnel
Jan. 2003 - Mar. 2003	Full time position as Bank Business Management Assistant at branch Waldems/Idstein of Nassauische Sparkasse, Germany
Aug. 2000 - Jan. 2003	Apprenticeship as Bank Business Management Assistant at Nassauische Sparkasse Wiesbaden, Germany Final Examination at Chamber of Commerce Wiesbaden, Germany, grade good (2.0)

School education

Aug. 1987 - July 2000	General qualification for university entrance (Abitur), grade good (2.0) at Gymnasiale Oberstufe of Gesamtschule Obere Aar, Taunusstein, Germany Majors: Biology and Chemistry

Additional knowledge

publication	*"Mitochondrial respiratory chain complex I is inactivated by NADPH oxidase Nox4."*, Koziel R. et al., Biochem. J., 2013; 452(2), 231-239.
Languages	German (native speaker) English fluent (spoken and written) French (fair)
IT-knowledge	very good knowledge in: MS Office-products, Corel Draw, internet applications, database research, various laboratory equipment software
additional functions	Company safety officer at TU Darmstadt, first-aider
fellowship	GDCH, VAA, GBM
advanced training	poster presentations at diverse conferences summer school "Proteomic Basics", Brixen, Italy 4th, 5th and 7th Protein Rainbow Workshops, Düsseldorf, Germany several workshops and lectures, e.g. project management and leadership competencies

Extracurricular interests

Hobbies	active member of gospel choir "popCHORn", repairing my car

Ober-Ramstadt, 14th, September, 2015 

Manuela Kratochwil

Potsdamer Str. 2

64372 Ober-Ramstadt

Ober-Ramstadt, 14.09.2015

Erklärung

Ich erkläre hiermit, dass ich meine Dissertation selbstständig und nur mit den angegebenen Hilfsmitteln angefertigt habe.

Manuela Kratochwil

Manuela Kratochwil

Potsdamer Str. 2

64372 Ober-Ramstadt

Ober-Ramstadt, 14.09.2015

Erklärung

Ich erkläre hiermit, noch keinen Promotionsversuch unternommen zu haben.

Manuela Kratochwil